DEVELOPMENT OF THULIUM-DOPED AND CO-DOPED FIBER LASERS USING GRAPHENE AND GRAPHENE RELATED SATURABLE ABSORBER

HANAFIAH SHAMSUDIN

INSTITUTE OF GRADUATE STUDIES
UNIVERSITY OF MALAYA
KUALA LUMPUR

2017

DEVELOPMENT OF THULIUM-DOPED AND CO-DOPED FIBER LASERS USING GRAPHENE AND GRAPHENE RELATED SATURABLE ABSORBER

HANAFIAH SHAMSUDIN

THESIS SUBMITTED IN FULFILLMENT OF THE REQUIREMENT FOR THE DEGREE OF DOCTOR OF PHILOSOPHY

INSTITUTE OF GRADUATE STUDIES
UNIVERSITY OF MALAYA
KUALA LUMPUR

2017

UNIVERSITY OF MALAYA

ORIGINAL LITERARY WORK DECLARATION

Name of Candidate: **HANAFIAH SHAMSUDIN**

Registration/Matric No: **HHE 140001**

Name of Degree: **DOCTOR OF PHILOSOPHY (PHOTONICS)**

Title of Thesis ("this Work"):

Development of Thulium-Doped and Co-Doped Fiber Lasers Using Graphene and Graphene Related Saturable Absorber

Field of Study: **PHOTONICS ENGINEERING**

I do solemnly and sincerely declare that:

(1) I am the sole author/writer of this Work;
(2) This Work is original;
(3) Any use of any work in which copyright exists was done by way of fair dealing and for permitted purposes and any excerpt or extract from, or reference to or reproduction of any copyright work has been disclosed expressly and sufficiently and the title of the Work and its authorship have been acknowledged in this Work;
(4) I do not have any actual knowledge nor do I ought reasonably to know that the making of this work constitutes an infringement of any copyright work;
(5) I hereby assign all and every rights in the copyright to this Work to the University of Malaya ("UM"), who henceforth shall be owner of the copyright in this Work and that any reproduction or use in any form or by any means whatsoever is prohibited without the written consent of UM having been first had and obtained;
(6) I am fully aware that if in the course of making this Work I have infringed any copyright whether intentionally or otherwise, I may be subject to legal action or any other action as may be determined by UM.

Candidate's Signature Date

Subscribed and solemnly declared before,

Witness's Signature Date

Name:

Designate

ABSTRACT

Two-micron pulsed fiber lasers offer numerous applications in various fields such as high-precision material processing, bio-medicine and ranging. This thesis focuses on the development of fiber lasers that emit longer wavelength beams utilizing thulium-doped fiber (TDF), thulium-ytterbium co-doped fiber (TYDF) and thulium-holmium co-doped fiber (THDF) as the gain medium in conjunction with a carbon-based saturable absorber (SA). Various SA based on graphite, carbon nanotubes and graphene were fabricated for use in generating both Q-switching and mode-locking pulse train in 2-micron region. TDF lasers (TDFLs) operating in multi-wavelength, Q-switching and mode-locking modes have been successfully demonstrated. For instance, the mode-locked TDFL operating at 1901.6 nm was demonstrated using a graphene oxide (GO) paper as SA. It generates 82.4 MHz pulse train with the estimated pulse width of 12.66 ps, and the pulse energy of 83.1 pJ at the 1552 nm pump power of 1052 mW. The TYDF laser (TYDFL) provides an efficient lasing at 1950 nm region based on energy transfer from ytterbium to thulium ions. A mode-locked TYDFL is also successfully demonstrated using a GO-based SA. The laser operates at 1942.0 nm with a threshold pump power as low as 1.8 W, a repetition rate of 22.32 MHz and calculated pulse duration of 1.1 ns. Continuous wave (CW), Q-switched and mode-locked THDF laser (THDFL) have also been successfully demonstrated using THDF as the gain medium in conjunction with 1552 nm pumping. The CW THDFL operates at around 1980 nm region with an efficiency of 5.78 % with the use of 5 m long gain medium due to Ho^{3+} transition ($^5I_7 \rightarrow {}^5I_8$). Q-switched and mode-locked THDFL were realized using GO embedded in polyvinyl alcohol (PVA) film as a passive SA. The self-started Q-switching pulse train was realized with the repetition rate, pulse width, output power, and pulse energy of 54.43 kHz, 2.44 μs, 8 mW, and 0.146 nJ, respectively at the maximum pump power of 1151

mW. By adding 10 m long highly nonlinear scandium doped fiber (ScDF) inside the similar THDFL cavity, the laser can be transformed into the mode-locking mode with the repetition rate of 9 MHz and an estimated minimum possible pulse width of 10.29 ps.

ABSTRAK

Laser fiber berdenyut julat dua-mikron menawarkan pelbagai aplikasi dalam pelbagai bidang seperti pemprosesan bahan berketepatan tinggi, bio-perubatan dan pengukuran jarak. Tesis ini memberi tumpuan kepada pembangunan laser fiber yang mengeluarkan pancaran jarak gelombang yang lebih panjang menggunakan fiber thulium-didopkan (TDF), thulium-ytterbium didopkan bersama (TYDF) dan thulium holmium didopkan bersama (THDF) sebagai medium gandaan dengan penyerap mudah tepu berasaskan karbon (SA). Pelbagai SA berasaskan grafit, tiub nano karbon dan graphene telah direka untuk digunakan dalam menjana siri denyut dalam kedua-dua teknik Q-switching dan mod terkunci dalam julat 2-mikron. Laser TDF (TDFLs) yang beroperasi di pelbagai jarak gelombang, Q-switching dan mod terkunci telah berjaya dibangunkan. Sebagai contoh, TDFL mod dikunci beroperasi pada 1901.6 nm dibangunkan menggunakan SA oksida graphene (GO) jenis kertas. Ia menjana siri denyut 82.4 MHz dengan lebar denyut anggaran 12.66 ps, dan tenaga denyut daripada 83.1 pJ dengan pam 1552 nm berkuasa 1052 mW. Laser TYDF (TYDFL) menyediakan pelaseran yang cekap di julat 1950 nm berdasarkan pemindahan tenaga dari ytterbium kepada ion thulium. Laser TYDFL mod dikunci juga berjaya dihasilkan dengan menggunakan SA berasaskan GO. Laser beroperasi pada 1942.0 nm dengan pam berkuasa pada ambang serendah 1.8 W, kadar pengulangan 22.32 MHz dan tempoh denyutan dikira sebanyak 1.1 ns. Gelombang berterusan (CW), Q-switched dan mod dikunci laser THDF (THDFL) juga telah berjaya dihasilkan menggunakan THDF sebagai medium gandaan dengan menggunakan pam 1552 nm. CW THDFL beroperasi pada julat 1980 nm dengan kecekapan 5.78 % dengan penggunaan medium gandaan yang panjangnya 5 m disebabkan peralihan Ho^{3+} ($^5I_7$ - $^5I_8$). Q-switched dan mod dikunci THDFL direalisasikan menggunakan GO tertanam dalam filem polyvinyl alkohol (PVA) sebagai SA pasif. Siri

denyut kendali sendiri Q-switching mula aktif dengan kadar pengulangan, lebar denyutan, kuasa output, dan tenaga nadi, 54.43 kHz, 2.44 μs, 8 mW, dan 0.146 nJ, masing-masing pada pam berkuasa 1151 mW. Dengan menambah 10 m panjang fiber nonlinear yang sangat tinggi scandium doped (ScDF) dalam rongga THDFL yang sama, laser boleh berubah ke mod terkunci dengan kadar pengulangan 9 MHz dan anggaran minimum lebar nadi 10.29 ps.

ACKNOWLEDGEMENTS

All Praise and Thanks be to Allah SWT, the Almighty for leading me to a successful completion of the programme of Doctor of Philosophy (PhD) in 31 months. I would like to express my sincere and deepest gratitude to my supervisors, **Prof. Dr. Sulaiman Wadi Harun** and **Prof. Dato' Dr. Harith Ahmad** for their support, help and guidance throughout my research works which were conducted in Optical Fibre Devices Laboratory, Photonics Research Centre (PRC) in the Department of Physics, Faculty of Science, University of Malaya.

My sincere and heartfelt gratitude goes to my great mentor **Engr. Anas Abdul Latiff** for his selflessness and generous help in doing laboratory works and precious discussions throughout our studies. My appreciation also goes to the members of the PRC especially **Nadia, Aisyah, Badrol, Farid**, and **Haziq**. They have made the laboratory most enjoyable place to work despite many challenges. We have gone through the hard and good times together.

I am also extremely indebted to the Thesis Unit, Institute of Graduate Studies, University of Malaya for providing help to check on the style of writing and formatting of my thesis before binding. Also, to those who have directly or indirectly contributed to the completion of this thesis.

My entire study is sponsored by the Malaysian Ministry of Higher Education through a special initiative MyBrain15 (MyPhD). I thank them for their generosity, which helped me to pursue the PhD programme and to be commemorated in a Convocation Ceremony of the University of Malaya in October 2018.

Last but not least, to my families and friends in Lurah Bilut, Bentong, Kuantan, Kuala Lumpur and Parit Buntar, for their encouragement, support and prays for me. Most of all, to my soulmate **Ir. Raja Zaimas Rosdin** for her companionship and supportive during the remaining days of my studies.

Ir. HANAFIAH SHAMSUDIN

Institute of Graduate Studies	Optical Fibre Devices Laboratory
University of Malaya	Photonics Research Centre,
50603 Kuala Lumpur	University of Malaya,
MALAYSIA.	50603 Kuala Lumpur.

17th April 2017

TABLE OF CONTENTS

LIST OF FIGURES

LIST OF TABLES

LIST OF SYMBOLS AND ABBREVIATIONS

d_{core}	Diameter of a fiber's core
d_{clad}	Diameter of a fiber's cladding
A_{core}	Core area
A_{clad}	Inner cladding area
θ_i	Maximum acceptance angle
n	Refractive index
E_0	Energy of a ground state
h	Plank's constant
v_{10}	Frequency of the incoming photon for level 0 and 1
N	Ion populations
W_{ij}	Stimulated absorption and emission rate
A_{ij}	Spontaneous decay rate for the radiative and non-radiative decay
A_i^{nr}	Spontaneous decay rate for the non-radiative decay
L	Cavity length
γ	Measured loss in a single passage
β	Amplification coefficient
P_{out}	Output power of the laser
P_{in}	Absorbed pump power
η_s	Slope efficiency
Q	Quality of the laser resonator
τ_p	Pulse width
P_{avg}	Average power
f_{rep}	Repetition rate
E_p	Pulse energy

ACCVD	Alcohol catalytic CVD
ASE	Amplified spontaneous emission
CCD	Charge-coupled device
CNTs	Carbon nanotubes
CVD	Chemical vapour deposition
CW	Continuous wave
EDX	Electron diffraction X-ray
EDFL	Er^{3+}-doped fiber laser
EPMA	Electron probe microscopic analysis
Er	Erbium
ET	Energy transfer
FBG	Fiber Bragg grating
FWHM	Full-width at half-maximum
GSA	Graphene saturable absorber
GO	Graphene oxide
GOSA	Graphene oxide saturable absorber
GOSA-PVA	Graphene oxide saturable absorber – polyvinyl alcohol
HeNe	Helium neon
Ho	Holmium
IR	Infrared
LAGS	Lithium-alumino-germano-silicate
LIDAR	Light detection and ranging
MCVD	Modified chemical vapour deposition
MMC	Multimode combiner
MOPA	Master oscillator/power amplifier
MWCNTs	Multi-walled carbon nanotubes

MWCNT-PVA	Multi-walled carbon nanotube – polyvinyl alcohol
NA	Numerical aperture
OPM	Optical power meter
OSA	Optical spectrum analyzer
OSNR	Optical signal to noise ratio
PEO	Polyethylene oxide
PM	Power meter
PVA	Polyvinyl alcohol
RF	Radio frequency
RI	Refractive index
SA	Saturable absorber
SD	Solution doping
SDS	Sodium dodecyl sulphate
SESAM	Semiconductor saturable-absorber mirror
SEM	Scanning electron microscopy
SNR	Signal to noise ratio
SPM	Self-phase modulation
TDF	Thulium-doped fiber
TDFL	Thulium doped fiber laser
TEM	Transmission electron microscopy
THF	Thulium-holmium co-doped fiber
THFL	Thulium-holmium co-doped fiber laser
TYF	Thulium-ytterbium co-doped fiber
TYDFL	Thulium ytterbium co-doped fiber laser
Tm	Thulium
WDM	Wavelength division multiplexing

XPM	Cross-phase modulation
YAS	yttria-alumino-silicate
YAS-RE	yttria-alumino-silicate –rare earth
Yb	Ytterbium
YDFL	Ytterbium-doped fiber lasers
YTDFL	Yb^{3+} / Tm^{3+} co-doped fiber lasers

CHAPTER 1 : INTRODUCTION

1.1 Introduction to Fiber Laser

A laser is a landmark invention of the mid-20th century, which has triggered the explosive progress in optics (Hecht, 2010). The invention of the laser has opened several new scientific fields such as photonics, fiber-optics, opto-electronics and nonlinear optics. The development of the photonics technologies has been affecting almost every aspect of our life and has been pushing forward the progress of other scientific fields, such as medical research, information technology, biological science, etc.

The term "laser" originated as an acronym for "light amplification by stimulated emission of radiation". It is a device that emits photons through a process of optical amplification based on the stimulated emission of electromagnetic radiation. In 1917, Albert Einstein described the theory of "stimulated emission" in which, the matter may lose energy by emitting an exactly same photon when it encounters a photon. This is the initial idea for the laser operation. However, it was not until 1960 that the first laser was demonstrated by Theodore Maiman (Maiman, 1960). This laser was built based on a ruby crystal that was pumped by a flash lamp in a Fabry-Perot cavity. After that, a large variety of lasers were demonstrated using different types of materials including helium neon (Javan et al., 1961), neodymium crystal (Johnson, 1962), semiconductor (Hall et al., 1962), CO_2 (Patel, 1964), Nd:YAG (Geusic et al., 1964), dye (Sorokin & Lankard, 1966), titanium sapphire (Moulton, 1986), etc. The earliest form of fiber laser was also developed by E. Snitzer and his colleagues in 1964 (Koester & Snitzer, 1964).

The first optical fiber was proposed and fabricated by Charles K. Kao in 1965 (Kao & Hockham, 1966), where he discovered that the high losses were due to impurities in the glass rather than the technology itself. After that, the optical fiber fabrication technology has rapidly progressed where the optical fiber losses have improved significantly from many dB/m to losses below 1 dB/km. To date, it is used in a vast amount of applications mainly within the fields of communication and sensors. In communication applications, the deteriorated optical signals as they travel along the transmission lines, are needed to be amplified. In the late 1980's, David N. Payne has pioneered the fiber amplifier by using an erbium-doped fiber (EDF) as the gain medium (Mears et al., 1987). The success of EDF amplifier has led to the rapid development of fiber lasers, which used the similar concept of doping active ions in optical fibers.

A fiber laser is an oscillator using an optical fiber, which is doped with rare-earth (RE) ions as the active medium in the cavity. Erbium (Er), ytterbium (Yb), neodymium (Nd), thulium (Tm), and holmium (Ho) are the most commonly used rare earth ions for fiber lasers. Compared with the conventional bulk lasers, fiber laser has a lot of attractive advantages, including good beam quality, outstanding heat-dissipating capability, compactness, robust operation and free of alignment, etc. Fiber lasers have been investigated and developed for more than fifty years. To date, many works have been devoted to build and develop cheaper and better fiber lasers in terms of new operating wavelength, narrower linewidth (single frequency), shorter pulse duration, higher power/energy, etc.

Ytterbium-doped fiber laser (YDFL) is the most successful fiber lasers so far due to its low quantum defect and high pump absorption per unit length (Richardson et al., 2010). They are, to this day, still the record-holder in terms of power scaling and laser performance with up to 10 kW in the single-mode (SM) regime in continuous wave (CW) operation (Stiles, 2009). On the other hand, Yb has an emission around 1 μm and is thus

limited to only a few applications. Therefore, there is an increased interest in other RE elements such as thulium (Tm) and holmium (Ho), in order to realize high-power sources in the 2 μm range. This thesis aims to develop 2-micron fiber lasers using three different gain media; thulium singly doped (TDF), thulium-ytterbium co-doped (TYDF) and thulium-holmium co-doped fiber (THDF).

1.2 Pulsed Lasers

Many applications require the use of modulated lasers or in other words pulsed lasers. There is a variety of pulsed laser applications in the area of optical communication, range finding, spectroscopy, and micromachining. The pulsed laser has been proposed soon after the first demonstration of a single-mode CW fiber laser. The first Q-switched and mode-locked fiber lasers were reported by Alcock et al., (1986). The pulsed formation has been realized by using an acousto-optic modulator which generated a pulse width of 200 ns and ~1 ns for Q-switching and mode-locking, respectively. The pulsed formation can be achieved using several techniques and the simplest way is to directly modulate the CW lasers. Light can escape from the cavity for a very short period of time by placing the fast modulator into the cavity. However, by using this method, the loss of the produced light is high when the modulator is in a closed state. Thus, more sophisticated techniques have been used such as cavity dumping, gain switching, mode-locking, and Q-switching. The two latter techniques provide more reliable, robust and superior technique for pulsing the lasers.

The Q-switched and mode-locked fiber lasers have been demonstrated based on various host media such as silica, tellurite (Richards et al., 2008), germanate (Fang et al., 2012) and fluoride (Yang et al., 1996) fibers. Among the host materials used, silica is preferred because of its compatibility with standard optical components. The use of passive elements to generate pulse lasers are favourable due to their flexibility of

configurations. The lasers have been successfully demonstrated using different kinds of saturable absorbers (SA), such as semiconductor saturable absorber mirrors (SESAMs), nonlinear polarization rotation (NPR), carbon nanotubes, graphene, and graphene oxide. In this thesis, Q-switched and mode-locked fiber lasers operating in 2-micron region are demonstrated using carbon-based materials such as carbon nanotubes and graphene as the SA.

1.3 2 μm Pulsed Fiber Laser

Recently a lot of researches on 2 μm laser have been conducted in both solid-state laser and fiber laser field because of its wide applications in medicine, remote sensing, LIDAR, range finder, and molecular spectroscopy (Damanhuri et al., 2013; Tao et al., 2013). The strong absorption by water and the weak absorption by human tissues at 2 μm also nominate it as an ideal wavelength for biological and medical applications including laser angioplasty in the coronary arteries, ophthalmic procedures, arthroscopy, laparoscopic cholecystectomy and refractive surgeries. In addition, other features of 2 μm laser such as the lower atmospheric absorption, smaller scattering and "eye-safe" property make the wavelength desirable for material processing, ranging, low-altitude wind shear and remote sensing, which includes Doppler LIDAR wind sensing and water vapour profiling by differential absorption LIDAR (DIAL). Such wavelength is also an ideal pump source for mid-infrared optical material.

The 2 μm laser can be realized using a thulium-doped fiber as the gain medium. The TDF laser (TDFL) was firstly discovered by Hanna et al., in 1988 with a 797 nm dye laser as the pump source. Meanwhile, the first 2 μm Q-switched TDFL was carried out in 1993 by using an acousto-optic modulator (Myslinski et al., 1993). The pulsed laser has many potential applications such as in pumping 2-4 μm and medical applications (Scholle et al., 2010). However, to date, few works on the generation of Q-switched and mode-

locked fiber lasers near the 2 μm wavelength region have been reported. For instance, Wang et al., (Wang et al., 2012) reported on the Q-switched generation with maximum pulse energy of 69 nJ and a repetition rate of 26 kHz using a 1560 nm CW laser source as pump laser and graphene saturable absorber (GSA). More recently, Jiang et al., (Jiang et al., 2013) achieved laser with a short pulse duration of 760 ns and the repetition rate of 202 kHz using graphene that is being transferred to the high reflectivity (HR) mirror to function as SA. Works on graphene saturable absorber (GSA) based Q-switched TDFLs are mostly related to the free-space arrangement (Wang et al., 2012) and linear configuration (Lu et al., 2013).

The Q-switched TDFL can be realized by either active or passive techniques. The active Q-switching is based on an active loss modulation with a Q-switcher and thus its pulse repetition rate can be externally controlled. Normally, active Q-switches are mechanical Q-switches, electro-optical Q-switches, and acousto-optic Q-switches. Besides that, as an alternative to the active Q-switched laser, the passively Q-switched laser gives a low cost, reliable operation without high voltages. In this thesis, Q-switched 2-micron fiber lasers are proposed using a passive saturable absorber and TDF or TYDF or THDF as the gain medium.

1.4 Research Objectives

The principal objective of this thesis and its chapter are to develop an efficient 2-micron fiber lasers operating in both CW and pulsed regimes. This work also aims to evaluate the effect of co-doping ytterbium and holmium to the thulium ions in order to enhance the performance at 2 μm region for CW, Q-switched and mode-locked fiber lasers. Carbon-based saturable absorbers such as graphite, carbon nanotubes and graphene are explored for Q-switching and mode-locking applications in the 2 μm region. To achieve this, few objectives have been proposed to guide the research direction, i.e.:

1. To demonstrate a fiber laser operating in 2 μm region using a commercial thulium doped fiber (TDF), a homemade thulium-ytterbium co-doped fiber (TYDF) and a commercial thulium-holmium co-doped fiber (THDF) as the gain mediums.

2. To develop new saturable absorbers (SAs) based on carbon materials such as graphite, multi-walled carbon nanotubes (MWCNTs) and graphene oxide for Q-switching and mode-locking applications in 2 μm region.

3. To generate Q-switching and mode-locking pulse train in TDF lasers (TDFL), TYDF lasers (TYDFL) and THDF lasers (THDFL) cavities.

1.5 Outline of the Thesis

This thesis consists of six chapters including this chapter which serves as an introduction. This current chapter presents an introduction to fiber laser, pulsed lasers, and 2 μm pulsed fiber laser. The research objectives, outline of the thesis and achievement of the research works are briefly presented in this chapter.

Chapter 2 explains the theoretical background on fiber optics, a concept of total internal reflection (TIR) that relate to pumping the light into fiber's core. This chapter also describes the fundamental of fiber lasers, stimulated emission and spontaneous emission and population inversion. The rate equations for the generation of CW and Q-switched fiber lasers, literature on the thulium energy transitions, gain characteristics and basic rate equations which serve as a key element in this thesis. It is then followed by the literature on the cladding pumping technique involved in this work. Moreover, the 2D nanomaterials used as saturable absorbers in generating of Q-switched and mode-locked fiber lasers are briefly discussed.

Chapter 3 describes the demonstrations of CW, Q-switched and mode-locked TDF lasers (TDFLs) operating at around 1.9 micron region. The multi-wavelength CW TDFL is demonstrated using a linear cavity consisting of a broadband mirror and a flat-cleaved fiber end in conjunction with 1552 nm pumping. Q-switched and mode-locked TDFLs are demonstrated using a pencil-core and graphene oxide (GO) paper based SA, respectively. The pencil-core based SA was prepared by cleaving its flakes onto adhesive surface of tape, which is then repeatedly folded over to homogeneously distribute the graphite layer on the tape. A small piece of the tape was sandwiched in between two ferrules to act as all-fiber SA device. GO paper is obtained using modified Hummer's method.

Chapter 4 proposes new, efficient fiber lasers operating at 2 μm based on cladding-pumping approach using a newly developed double-clad TYDF as the gain medium. The TYDF laser (TYDFL) provides an efficient lasing at 1950 nm region based on energy transfer from ytterbium to thulium ions. The Q-switched TYDFL laser is obtained by exploiting a multi-walled carbon nanotubes (MWCNTs) embedded in polymer composite film as a SA. On the other hand, the mode-locked operation is obtained by a GO based SA.

In **Chapter 5,** the performances of the CW, Q-switched and mode-locked THDF lasers (THDFL) with a 1552 nm pumping in ring configuration are investigated. Graphene oxide (GO) embedded in polyvinyl alcohol (PVA) film is used as a passive SA in generating both Q-switched and mode-locked pulse train. A GOSA-PVA is integrated into a ring laser cavity by sandwiching it between two fiber connectors. The mode-locking operation is realized by adding a 10-m long highly nonlinear scandium-doped fiber (ScDF) inside the THDFL cavity.

The findings in this thesis are summarized and concluded in **Chapter 6**. Future work suggestions are also provided as an extension of the work presented in this thesis.

1.6 Achievement of the Research Works.

Some of the contributions of this thesis works are highlighted below:

1. Development of TDFL, TYDFL and THDFL using home-made 2D nanomaterials comprise graphite (pencil-core), graphene oxide (GO), GO-PVA and MWCNT-PVA as saturable absorbers exhibit efficient threshold pump power, pulse energy, slope efficiencies and output power in conjunction with appropriate pumping wavelengths (800, 1552 nm for TDFL; 905, 927 and 980 nm for TYDFL and 1552 nm for THDFL).

2. Demonstration of broadband ASE generation in the 2 μm region using a new commercial thulium-doped and thulium-holmium co-doped fiber as the gain mediums. The 10 dB bandwidth of the broad ASE spectrum covers from 1720 nm to 2010 nm for TDFL using the 800 nm pump and from 1790 nm to 2200 nm for THDFL using the 1552 nm pump.

3. To the best of our knowledge, the generation of mode-locked THDFL using GO-PVA SA in conjunction with a new commercial highly nonlinear scandium doped fiber (ScDF) in a ring cavity for the first time.

4. TDFL exhibits the highest laser efficiency of 16.57 % from single-mode fibers and comparatively low threshold pump power of 500 mW in multi-wavelength lasers with the assistance from active thulium ions.

5. Development of Q-switched THDFL using GO-PVA SA in which core-pumped by a laboratory-made 1552 nm fiber laser via fused WDM and passively Q-switched at two lasing wavelengths of 1910.7 and 1980.7 nm. Stable pulsing with a threshold pump power of 968 mW, a maximum repetition rate of 54.43 kHz, the highest pulse energy of 0.166 nJ and the smallest pulse width of 2.28 μs.

6. The generated Q-switched fiber laser is the first reported at 2 μm region using MWCNT-PVA SA in conjunction with a newly fabricated TYDF as the gain medium. The pulse has been observed to generate a wide pump power range of 440 mW to 528 mW with the highest repetition rate and the lowest pulse duration of 35.1 kHz and 1.52 μs, respectively using a 980 nm pump wavelength.

7. The use of passive elements comprise graphite (pencil-core), graphene oxide (GO), GO-PVA SA and MWCNT-PVA SA proposed in this work are simpler, cost-effective and more compact due to the all-fiber linear and ring configurations compared to the previous research work that used the active elements.

CHAPTER 2 : LITERATURE REVIEW OF FIBER OPTICS AND LASERS

2.1 Fundamental of Fiber Optics

An optical fiber is a cylindrical dielectric waveguide composed of an inner core and an outer cladding. It is made mainly of an optical low-loss material, such as silica glass. Light is guided in a central core, embedded inside a cladding, made of a material with slightly lower refraction index than the core. In terms of ray optics, every incident ray on the boundary between core and cladding at angles greater than critical angle undergoes a total internal reflection. Those rays are guided through the core without refraction into the cladding. **Figure 2.1** shows different modes of light propagation in the core of fiber optic for the step-index multi-mode, graded-index multi-mode and step-index single-mode fiber which have its refractive index profile. Light propagates in the core of fiber in the form of modes. Each mode travels along the axis of the waveguide with its characteristic propagation constant and group velocity. The fiber optic with a small diameter can supports a straight of light propagation is called single-mode. One of the difficulties with controlled light propagation inside a multi-mode fiber is due to modal dispersion. Different group velocities result in a spread of travel times and a light pulse traveling through the fiber is broadened. The graded-index multi-mode fibers able to provide this solution for overcoming the modal dispersion of the propagation of light. Normally rays with a greater inclination and longer path, travel faster in areas closer to the cladding. Therefore, travel times of different modes can be equalized.

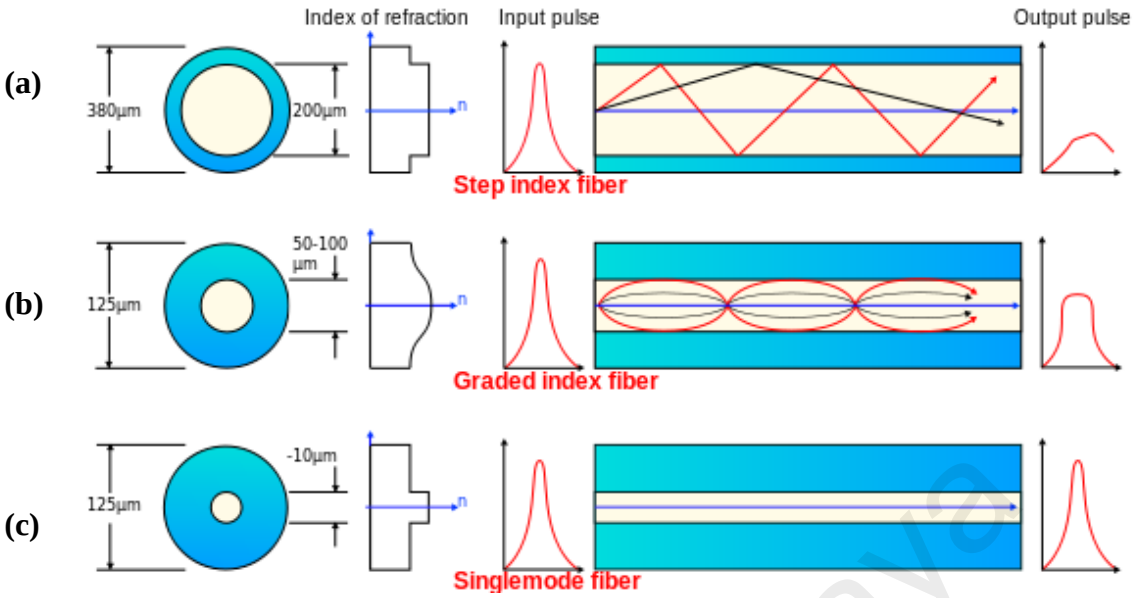

Figure 2.1: Refractive index profile and typical rays in **(a)** a step-index multi-mode fiber (MMF); **(b)** graded-index multi-mode fiber (GRIN MMF) and **(c)** a step-index single mode fiber (SMF) ("Wikipedia," 2016).

Currently, the fiber optics available in the world market are made of different host glass like silica, tellurite and alumina and different host plastic. For glass optical fibers, the diameter of the core ranges between 10-600 µm, the cladding thickness is between 125-630 µm, and that of the jacket varies between 250-1040 µm. For plastic optical fibers, all diameters range between 750-2000 µm. **Figure 2.2** depicts a basic structure of the fiber optics made of glass and plastic that available on the world market with different diameter of the core and cladding. One of the main differences between glass and plastic optical fibers is their diameter. Fiber optics basically applied a principle of total internal refraction in which resulting in guiding of light inside a medium with higher index of refraction than surrounding medium. The total internal reflection principle was proven scientifically by a Swiss physicist Jean-Daniel Colladon and a French physicist Jacques Babinet who have conducted an experiment of guiding light inside a thin stream of water in 1842.

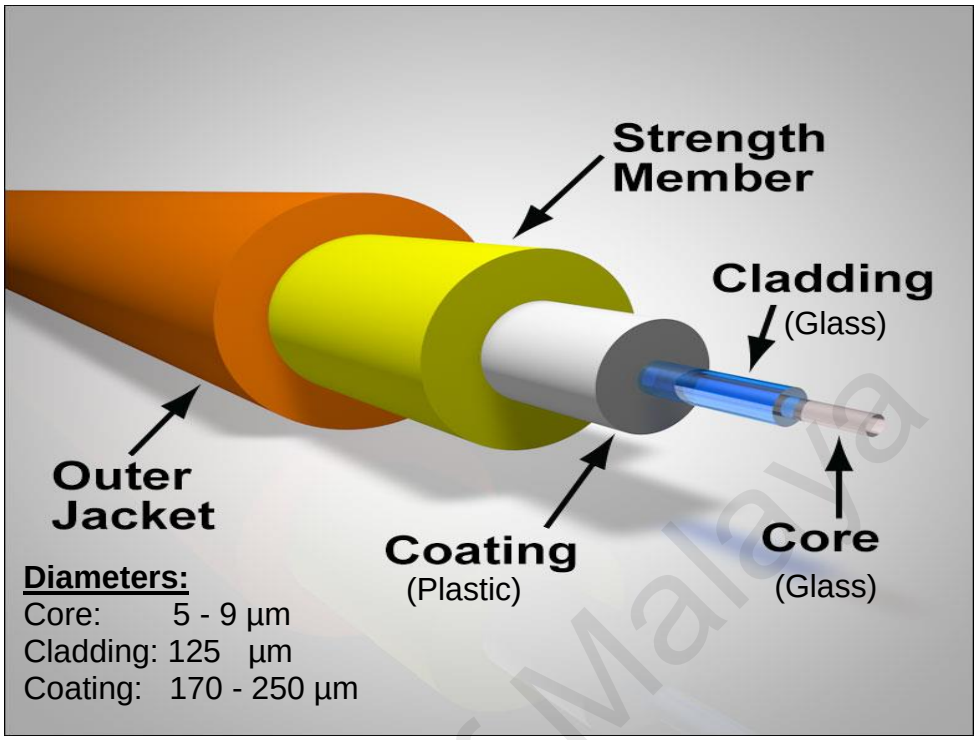

Figure 2.2: A basic structure of fiber optics (source: www.thorlabs.com).

2.1.1 Total Internal Reflection

Figure 2.3 depicts an illustration of total internal reflection where the refractive index n_1, n_2 and n_4, degree of acceptance θ_1, reflection angle θ_2 and critical angle θ_3 and propagation of light in the core of fiber optics. As light travels from the core into the cladding of different refractive index at a normal angle, part of light is reflected back into the core. However if the light enters the cladding at certain angle larger than critical angle θ_c , light will bounce back into the core. This phenomenon is known as total internal reflection (TIR) and becomes a fundamental of guiding operation to allow light to be transmitted and received in an optical fiber. Critical angle can be calculated using Equation (2.1) below;

$$\theta_c = sin^{-1} \frac{n_4}{n_2} \tag{2-1}$$

where θ_c is the critical angle, n_2 and n_4 are the refractive index of the core and the cladding, respectively. Refractive index n is a dimensionless unit which representing the speed of light c in the vacuum condition, to the speed of light v in the medium itself , and it can be calculated using Equation (2-2);

$$n = \frac{c}{v} \tag{2-2}$$

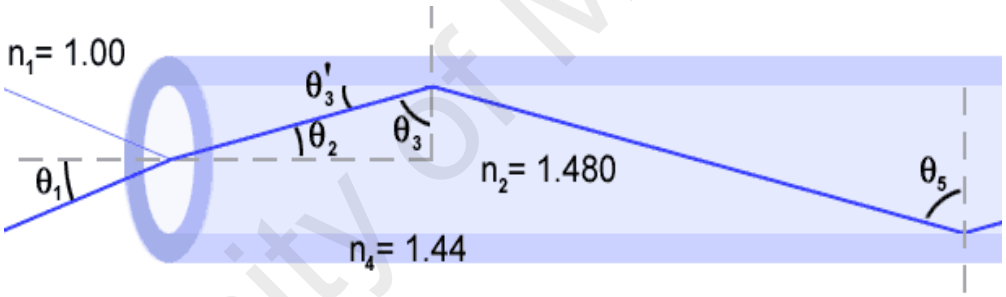

Figure 2.3: Illustration of a total internal reflection of the fiber optic with propagation of light, degree of acceptance θ_1 and reflection angle θ_2, refractive index n_1, n_2 and n_4 (Wagner, 1999).

The TIR principle works whenever light travelling from the first medium of high refractive index into the second medium with lower refractive index while the incident angle is larger than the critical angle to ensure the light is tightly confine in the first medium. The **Figure 2.3** shows the propagation of light as it travels from air which its refractive index is n_1 into the core of fiber made of silica glass which is refractive index labeled as n_2. The TIR is portrayed by the propagation of light where the light is

reflected back perfectly in the silica glass. Theoretically the TIR allows light stay in the fiber. However, practically as light propagates in the fiber it may hit random boundary between the core and the cladding at an angle less than the critical angle θ_c. This will cause leakage into the cladding hence reduce output efficiency. Light in the same mode must have hit the core-cladding boundary at a certain angle. This particular angle is well known as a numerical aperture (NA) of the fiber. The NA can be calculated from acceptance angle $2\theta_c$ or from the refractive index of the core and cladding using equations;

$$NA = n\ sin\ \theta'_m = n_2 \sin \theta_c \tag{2-3}$$

$$= \sqrt{n_2^2 - n_4^2} = n_2 \sqrt{2\Delta} \tag{2-4}$$

where n, n_2 and n_4 are the refractive index of the medium, the core and the cladding, and θ_m is acceptance angle. The θ'_m is the total reflection complimentary angle and Δ is the relative refractive index different given by:

$$\Delta = \frac{{n_2}^2 - {n_4}^2}{2{n_2}^2} = \frac{{n_2}^2 - {n_4}^2}{n_2} \tag{2-5}$$

2.2 Fundamental of Fiber Lasers

Light Amplification by Stimulated Emission of Radiation is an abbrevation for LASER. The word laser discussed here is only for electromagnetic radiation-emitting devices based on light amplification by stimulated emission of radiation. The electromagnetic (EM) spectrum includes range from gamma rays to long radio waves.

The EM spectrum in **Figure 2.4** illustrates the various types of EM waves and their respective wavelength regions.

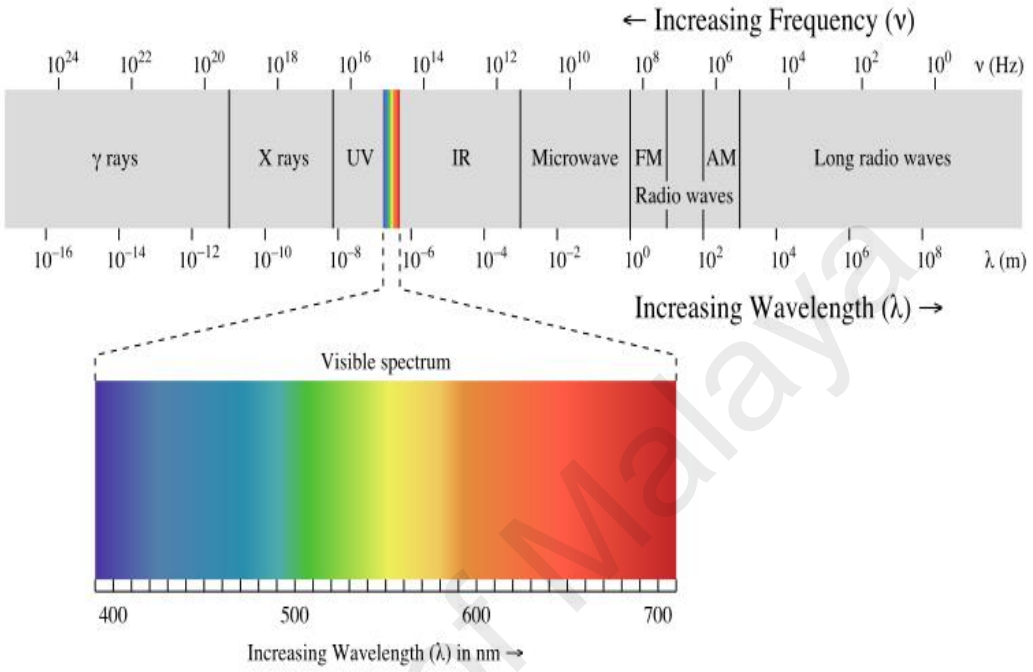

Figure 2.4: Illustration of electromagnetic spectrum ("Wikipedia," 2016).

The primary wavelengths for lasers include the ultraviolet, visible and infrared regions of the spectrum. The ultraviolet light region consists of wavelength between 180 nm and 400 nm, while the visible light region consists of radiation with wavelengths between 400 nm and 700 nm. The wavelength of light being emitted depends on the type of lasing material used. For thulium-doped, thulium-ytterbium co-doped and thulium-holmium co-doped fiber, the lasing wavelength emitted is 2 μm.

The terms fiber lasers are usually associated with the gain media of optical fibers. The active gain medium is an optical fiber core doped with one or more rare-earth ions, precisely known as lanthanides in the periodic table (but not restricted to the lanthanide, other samples includes ytterbium, holmium, erbium) (Digonnet, 2002). A Fabry-Perot (FP) resonator is an example of simple fiber laser setup as depicted in **Figure 2.5**. The FP

consists of the optical laser cavity which is formed by the input and output coupler which provides feedback to form a standing wave for light amplification that produced by the gain medium.

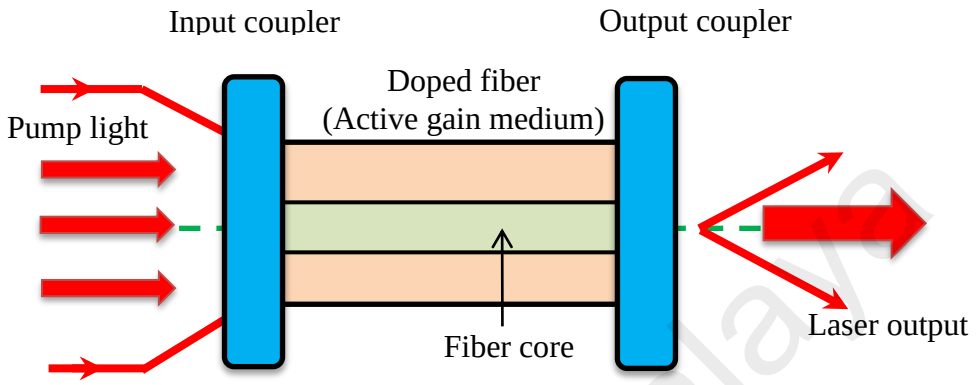

Figure 2.5: A basic schematic diagram of the simplest fiber laser with Fabry-Perot resonator.

The light confinement and low propagation loss in optical fibers are an advantage for the use of longer active gain medium which can provide higher gain. Nevertheless, the higher dopant concentration of the active gain medium as short as 2 cm long can produce laser using the erbium-concentration of 2500 ppm (Zyskind et al., 1992). Generally, for the short cavity length of the FP, a high concentration of active ions must be introduced into the fiber core to facilitate sufficient pump power to reach threshold.

2.3 Stimulated Emission and Spontaneous Emission

The quantum theory suggests that atoms exist only in certain discrete energy states and the absorption and emission of light cause them to make transitions from one discrete energy state to another. The frequency of the absorbed or emitted radiation f_{21} or v is

related to difference in energy ΔE between the higher energy state E_2 and the lower energy level state E_1 and is given by Equation (2-6);

$$\Delta E = E_2 - E_1 = hv \tag{2-6}$$

where h = 6.626 x 10^{-34} Js is Planck's constant.

An incident light of energy hv cause absorption of light which excites atoms from level E_1 to level E_2, while emission of light occurs when atoms from energy level E_2 fall to level E_1, releasing a photon. This phenomenon is shown in **Figure 2.6**. The red dot indicates the state of the atom before and after transition take place. Emission can occur in two ways:

(i) **Spontaneous Emission** is produced when atoms return to the lower energy level in random manner. According to quantum mechanics theory, spontaneous emission always involves transition from a higher energy level state to a lower energy state. The spontaneous emission produced is amplified by an active medium thus is known as amplified spontaneous emission (ASE) and is a major noise factor in optical amplifier.

(ii) **Stimulated Emission** is produced when a signal stimulates an atom in a higher state drop to a lower state by emission of photon identical to the signal. The stimulated photon is of the same frequency, phase and polarization as the stimulating signal. Therefore when an atom is stimulated to emit light energy by an incident wave, the liberated energy could add to the wave in a constructive manner, providing amplification.

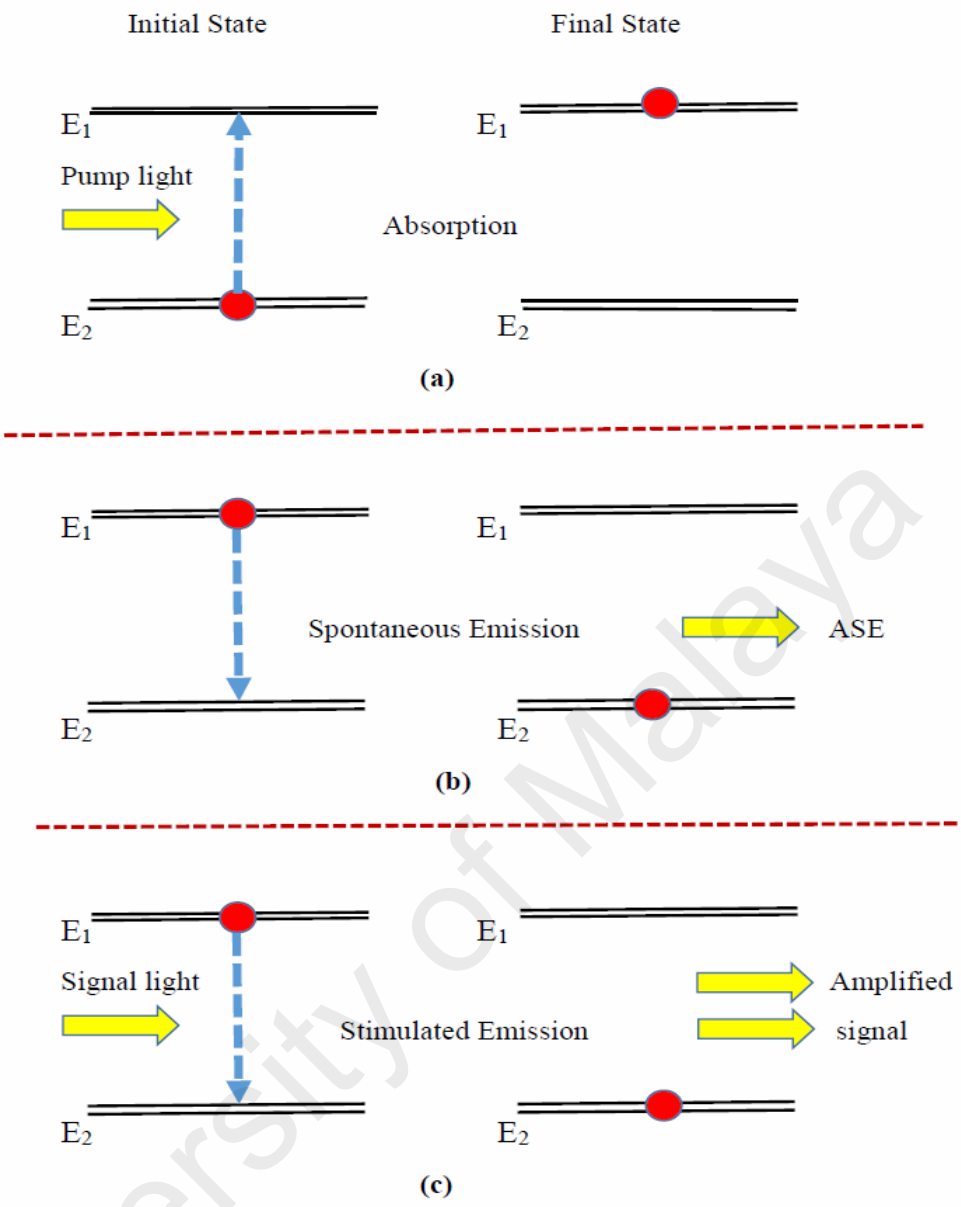

Figure 2.6: Schematic represents light absorption and emission between two energy levels: **(a)** absorption; **(b)** spontaneous emission; **(c)** stimulated emission.

2.4 Population Inversion

The population inversion is state where N_2 becomes much larger than N_1 thus increasing the stimulated emission rate. This can be achieved by injecting power into the system through an external energy source also knowns as pumping source. This mechanism is to excite atoms into the upper energy level E_2 from ground or lower level

E_1. In atomic system with thermal equilibrium, the atom density in each energy level obeys the Boltzmann distribution given by Equations (2-7) and (2-8);

$$\frac{N_2}{N_1} = \exp\left[-\frac{(E_2 - E_1)}{kT}\right] \tag{2-7}$$

$$= \exp\left[-\frac{hv}{kT}\right] \tag{2-8}$$

where N_1 and N_2 are atom densities for the energy level E_1 and E_2 respectively;

k is the Boltzmann constant

T is the absolute temperature in Kelvin

h is Planck's constant

According to Equation (2-8), a normal atomic system at thermal equilibrium, N_2 is much smaller than N_1. Therefore stimulated absorption is dominant compared to stimulated emission. There is a need to reverse this effect and this is achieved through population inversion.

2.6 Fiber Lasers System in 2 μm Region

In the wavelength range around 2 μm the most interesting transitions for high power continuous wave (CW) and pulsed laser operation exist in the trivalent rare earth ions Tm^{3+} and Ho^{3+}. Using these ions laser emission was achieved in many different host crystals and glass fibers. For CW operation the thulium lasers are most interesting; however, for pulsed and Q-switched operation holmium lasers are more attractive due to the higher gain of the holmium doped crystals. The first experiments with Tm^{3+} and Ho^{3+} doped crystals were already carried out in the 1960s (Johnson, 1963). For both ions, the

relevant laser transition for the 2 μm emission ends in the upper Stark levels of the ground state. Therefore both lasers can be described as quasi-three level lasers with a thermally populated ground state (Svelto, 1998; Koechner, 2006). Thulium lasers have the great advantage that the Tm^{3+} ions can be directly excited with commercially available laser diodes/pump around 800 nm. To achieve efficient laser operation at 2.1 μm, holmium can only be excited directly around 2 μm or by exploiting an energy transfer process from thulium or holmium. Thulium is one of the rare earth ions which provide a lot of interesting applications based on fiber lasers. Its broad emission ranging from 1400 nm to 2400 nm make it possible to be used in spectroscopy, military, and medical field (Scholle et al., 2010). Interestingly, its emission at the 2 μm region has strong water and biological tissue absorption coefficients, thus making it possible for the medical application. Several works on thulium-doped fiber laser (TDFL) has been demonstrated using different glass host such as ZBLAN (Allain et al., 1989), tellurite (Wu et al., 2005), germanate (Wu et al., 2007) and silica (Hanna et al., 1990; Jackson & King, 1998).

Thulium-doped fiber with silica based glass exhibit higher non-radiative decay (Layne et al., 1975; Layne et al., 1977). The high phonon energy in silica fiber limits the quantum efficiency of the respective level which leads to low efficiency. Yet, silica based materials are needed for the integration into standard communication systems as well as for robustness in applications. Nevertheless, the use of other glasses to avoid high phonon energy such as fluoride or tellurite glass gives some disadvantages in terms of low melting temperature; low durability and strength thus contribute to the problem in splicing. Another problem associated with thulium ions is the lack of pumping source at their high absorption band of 1.2 μm, thus several works have reported on the sensitization of ytterbium ion in thulium-doped fiber to realize the absorption at this wavelength. In this work, two different co-doping elements which are thulium-ytterbium co-doped fiber (TYDF) and thulium-holmium co-doped fiber (THDF) are used as gain mediums. The

TYDF is a newly fabricated fiber and the THDF is a new commercial fiber which their spectroscopic properties as well as energy transfer processes and lasing performances have been investigated.

Thulium-ytterbium co-doped fiber lasers (TYDFLs) rely on the indirect pumping from the Yb^{3+} usually over the wavelength region from 910 nm to 980 nm to allow the energy transfer between the Yb^{3+} to Tm^{3+} (Jackson, 2003). Ytterbium co-doping enhanced the pump absorption and could facilitate population inversion between the energy level. Spectroscopic properties, namely up-conversion (UC) has also been extensively studied for TYDF since the 90's in order to realize the laser emission at the visible wavelength (Hanna et al., 1990; Zhang et al., 1995). In this work, the lasing performances at 2 μm region of TYDFL on various length, doping concentration and pump wavelength will be investigated and discussed.

A study of thulium-holmium co-doped fiber laser (THFL) for operation in 2 μm region seems limited in terms of publications and research works. The most common reported works usually focus on the broadband light sources based on the emission properties from the energy structure of dopant ions in the glass host that are thulium and holmium (Zhou et al., 2011). The amplified spontaneous emission (ASE) sources operating around the 2000 nm spectral region have gained tremendous interest for possible applications in spectroscopy, gas sensing, low coherence interferometer and medical imaging via optical coherence tomography. Tm^{3+} has a broad ASE between 1650 nm to 2100 nm (Agger & Povlsen, 2006) and therefore, is suitable to be a broadband ASE source which is doped with active holmium ions to realize broad emission wavelength via energy transfer (Ruan et al., 2009). Based on previously reported work, countless publications have been reported on the high output power using double-clad fiber. However, considerable amounts of output power, as well as laser efficiency at 2 μm

regions is suitable for some applications, such as a sensor, where the only low amount of energy and power are needed (Coté, 2001) owing to their specific infra-red (IR) absorption at the 2000 nm region. The use of a single-mode fiber instead of double-clad fiber brings significant advantages in term of laser performance such as low threshold power. There is a few research works have been done to investigate the 2 μm emission from thulium rare earth ions using the single-mode silica fiber with comparatively high laser efficiency and low threshold power.

2.7 Reviews in Related Areas

Following sub-section in this chapter reviews briefly on rare earth (RE) dopant and materials, transition energy for cross-relaxation and energy level. The term ‘rare earth’ is derived from the word ‘rare’ which refers to the idea that only a small amount of the discovered element was present in the Earth’s crust. In the Earth's crust, oxygen (47 %) is the most abundant element, followed by silicon (28 %) and aluminum (8 %). There are millions of different compounds but only 118 different types of elements. These 118 elements are listed in a well-known Periodic Table of Elements which include the RE elements such as thulium, ytterbium and holmium.

2.7.1 Rare Earth Dopant and Material

The first invention to apply rare earth was suggested in the late 19th century by an Austrian scientist, Carl Auer von Welsbach. He discovered a useful development in the production of light by generating white light (gas lamp) when heated by a flame (Greinacher, 1980) which is still being used today as a lantern. Nowadays, rare earth elements become an important role in various fields. Most lanthanides are widely used in lasers, and as co-dopants in doped-fiber optical amplifiers and lasers as well as in life science applications (Bünzli & Piguet, 2005). The rare earth elements when embedded in

the host glass forms trivalent (+3) rare earth ionization state of these elements, which has an electronic configuration of xenon plus a certain number; $[Xe]4f^N5s^25p^66s^0$, where $N = 1 \ldots 14$ (Digonnet, 2002). All existing trivalent rare earth elements are 4-level lasers. Its N inner electrons of $4f$ shell are shielded from the external electromagnetic field by the outmost shell $5s$ and $5p$. Since the optically active electrons in rare earths are well shielded, the energy levels remain fairly constant when comparing the levels in different hosts.

2.7.2 Energy Transition and Gain Characteristic in Tm^{3+} Ions for 2 μm Lasers

Thulium has an atomic number of 69 discovered by Per Theodor Cleve in 1879. He found that the residue from erbia; the oxide of erbium (Er_2O_3) varies in weight, thus it contains other elements which are found to be holmium and thulium (James, 1911). Like the other lanthanides, the most common oxidation state is +3, seen in its oxide and other compounds. The energy level diagram of Tm^{3+} is shown in **Figure 2.7**. Thulium presents three major absorption bands in the infrared region from the ground state absorption (GSA) shown in **Figure 2.7** which are $^3H_6$ to $^3F_4$ (~1550 nm), $^3H_5$ (~1210 nm) and $^3H_4$ (~790 nm) (Moulton et al., 2009b). Other possible transitions are provided in the figure which consists of GSA and excited state absorption (ESA). The electronic transition of $^3F_4 \rightarrow {}^3H_6$ is a well-known energy transition of Tm^{3+} ions used for 2 μm light emission. The transition of $^3H_6 \rightarrow {}^3H_4$ exhibits broad emission, ~130 nm.

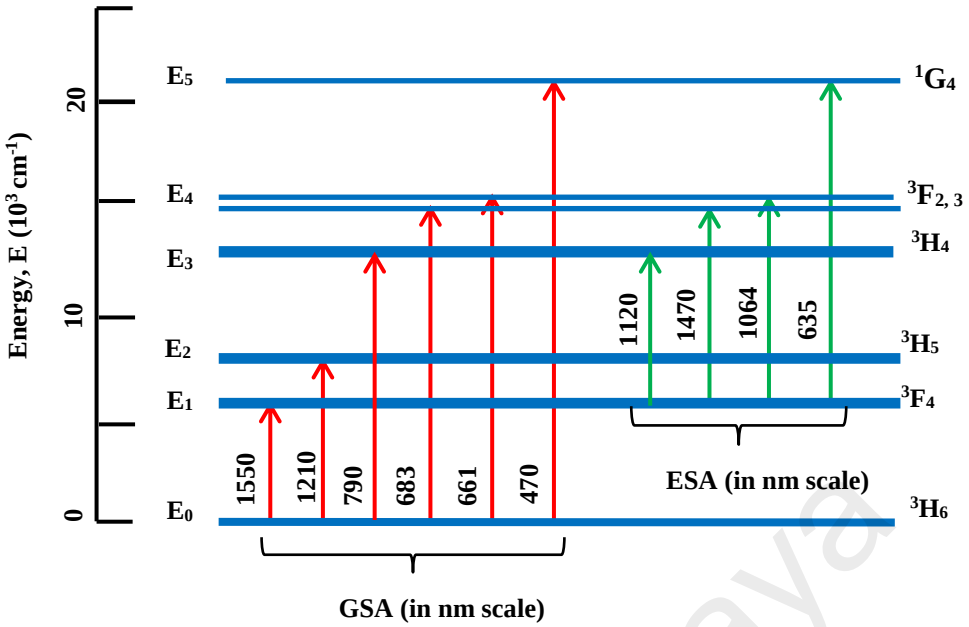

Figure 2.7: Possible ground state absorption (GSA) and excited state absorption (ESA) of Tm^{3+} ions.

This is due to the fiber absorption peak which coincides with the laser diode operating wavelength of 790 nm. Therefore, it is suitable to be used in tunable laser source for broadband application. The gain of the Tm^{3+} ions can be modelled in terms of an atomic rate equation depending on their respective energy level of transitions. **Figure 2.8** denotes the possible Tm^{3+} ions transition according to Moulton et al., (Peterka et al., 2011). The left hand side shows the energy level of thulium while the right hand side indicates the number of levels associated with it. The energy level diagram shown in **Figure 2.8** includes some of the transitions involved in the thulium-doped fiber. This thesis emphasizes on the 800 nm and 1552 nm pumping mechanism, thus certain energy levels have been omitted for simplicity, and only a three-level system is considered.

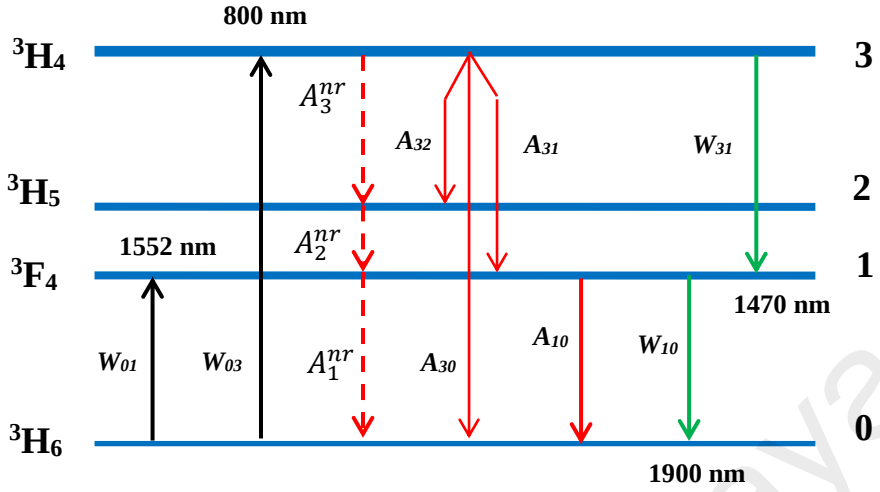

Figure 2.8: The possible laser transition of Tm^{3+} ions in a silica based fiber.

The population density at $^3H_5$ level is neglected because of the high non-radiative decay rates ($\gg 10^5 s^{-1}$) transition of $^3H_5 \rightarrow {}^3F_4$ (Peterka et al., 2011). The rate equations for the ion populations, *N* at each level are expressed as follows:

$$\frac{dN_0}{dt} = -(W_{01} + W_{03})N_0 + (W_{10} + A_1^{nr} + A_{10})N_1 + A_{30}N_3 \quad (2\text{-}9)$$

$$\frac{dN_1}{dt} = W_{01}N_0 - (W_{10} + A_{10})N_1 + (W_{31} + A_3^{nr} + A_{31} + A_{32})N_3 \quad (2\text{-}10)$$

$$\frac{dN_3}{dt} = W_{03}N_0 - (W_{31} + A_3^{\mathrm{nr}} + A_{30} + A_{31} + A_{32})N_3 \quad (2\text{-}11)$$

$$\sum_{i=0}^{3} N_i = N_t \quad (2\text{-}12)$$

where W_{ij} is the stimulated absorption and emission rate accounts for amplified spontaneous emission (ASE), A_{ij} and A_i^{nr} are the spontaneous decay rate for the radiative and non-radiative decay rates from level i to j, and N_t is the total thulium dopant concentration.

Another special feature of Tm^{3+} is the cross relaxation (CR) between Tm^{3+} pairs. This process allows the two Tm^{3+} ions occupy $^3F_4$ level. When two Tm^{3+} are close enough to each other, with a separation distance lower than that of the emission wavelength, the CR energy transfer ($^3H_4$,$^3H_6 \rightarrow {}^3F_4$,$^3F_4$) will be triggered. **Figure 2.9** shows the schematic diagram for the CR process between two Tm^{3+} ions. The thulium ion (donor ion) in the ground state absorbs photon from the 790 nm pump thus elevated to $^3H_4$ level. When the ion in this level de-excites to $^3F_4$, instead of emitting at 1.47 µm, the energy is transferred to a nearby thulium ion (acceptor ion). The ion that resides in the ground state absorbs the transferred energy to occupy the upper laser level, $^3F_4$. Both ions then drop to the ground state and emit at 1.9 µm photons. With each absorbed pump photon at 790 nm, two 1.9 µm photons are produced.

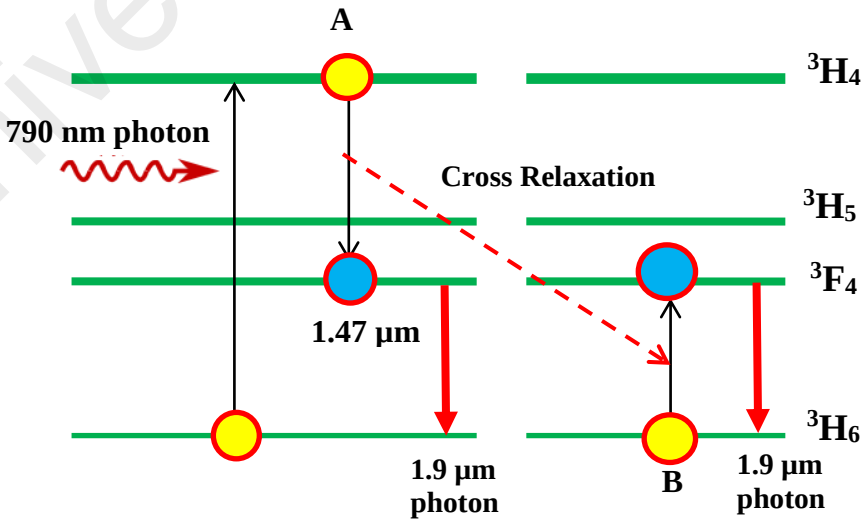

Figure 2.9: The cross relaxation process between donor ion, A and acceptor ion, B.

Therefore, higher quantum efficiency is attainable under the above condition for thulium operating at the 2 μm emission region. The amount of CR can be calculated according to Taher et al., (2011). The following is a rate-equation system in which considering empty $^3H_5$ level to analyze the cross-relaxation CR ;

$$\frac{dN_0}{dt} = -W_{03}N_0 + \frac{N_3}{\tau_{30}} + \frac{N_1}{\tau_1} - C_R N_3 N_1 \quad (2\text{-}13)$$

$$\frac{dN_1}{dt} = \frac{N_3}{\tau_{31}} - \frac{N_1}{\tau_1} + 2C_R N_3 N_0 \quad (2\text{-}14)$$

$$\frac{dN_3}{dt} = W_{03}N_0 + \frac{N_3}{\tau_{30}} + \frac{N_3}{\tau_{31}} - C_R N_3 N_1 \quad (2\text{-}15)$$

where N_0, N_1 and N_3 are the populations of Tm^{3+} ions in the $^3H_6$, $^3F_4$, and $^3H_4$ levels respectively. W_{03} is the pump rate (s^{-1}), C_R is the cross relaxation parameter, τ_{xy} is the lifetime of the x to y transition and τ_x is the lifetime of level x. Note that $\tau_3 = ({\tau_{31}}^{-1} + {\tau_{30}}^{-1})^{-1}$. The C_R parameter is a function of the Tm doping level. At steady state, the time derivatives in the rate equations are equal to zero. Considering the conservation law of Tm^{3+} ions populations, we can also write $N_t = N_0 + N_1 + N_3$. The methods based on fluorescence lifetime measurements (De Camargo et al., 2002; Petrin et al., 1992) uses Equation 2.13 and calculate the cross relaxation parameter from level 3 lifetime quenching. However lifetime values falls below 1 μm for highly-doped samples and measurements of low level signals is difficult. To overcome the limitation of previous methods, Taher et al., proposed to investigate the steady-state emission from $^3H_4$ and the $^3F_4$ levels (Taher et al., 2012).

In steady-state condition from Equation 2.14, C_R follows:

$$C_R = \frac{1}{2N_0}\left[-\frac{1}{\tau_{31}} + \frac{N_1}{N_3\,\tau_1}\right] \tag{2-16}$$

2.8 Optical Fiber Lasers

In this subsection, we are providing description of the optical fiber lasers comprises laser cavity and laser parameters. The optical fiber lasers defined in this subsection is refer to a device that allows the amplification of light in a coherent, monochromatic and unidirectional manner in the optical spectrum region. The common characteristic of all types of laser devices is the population inversion of the active gain medium in a laser cavity. In order to generate laser, three basic conditions must be satisfied. First, the laser should have an active gain medium. Secondly, the gain medium should be placed in between the reflective optical cavity to allow circulation of photons. Finally, the external pump source is needed to generate population inversion. All optical fiber lasers are built with these three basic elements. Several configurations of laser cavity will be discussed afterwards.

2.8.1 Laser Cavity

A fiber lasers devices or system must have some conditions for amplification of light within the input and output couplers or laser cavity. The most common laser cavity used for optical fiber laser is a Fabry-Perot resonator as shown in **Figure 2.10 (a)**. The Fabry-Perot resonator is typically constructed by placing an active gain medium in between two planar dielectric mirrors. The mirrors serve as an input and output coupler. Both ends of the fiber are either perpendicularly cleaved or polished flat. The pump power provided by the pump source is directly coupled into the fiber by splicing or by high

transmittance mirror through the input coupler (mirror), which is transparent to the pump light and highly reflective to the generated light emission. The mirrors introduce optical feedback to the laser beam in the cavity, therefore causes a population inversion. The laser beam that propagates back and forth in the cavity enables amplification due to stimulated emission. The generated light leaves the laser cavity through the output coupler (mirror).

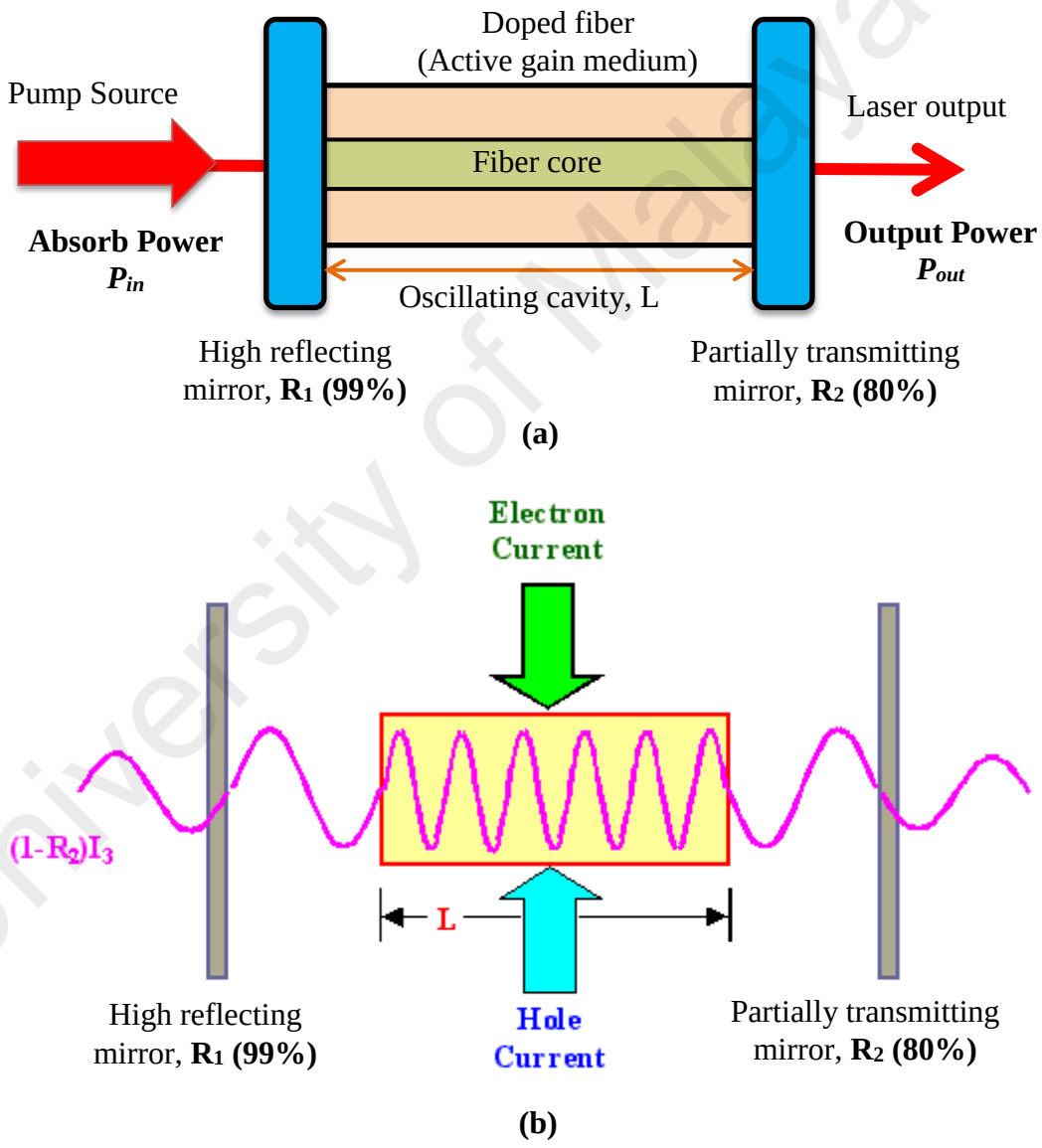

Figure 2.10: Schematic diagram of **(a)** a basic Fabry-Perot (FP) fiber resonator and **(b)** the FP fiber resonator with detail of electron current and hole current in gain medium.

To ensure that the laser can be realized, the population inversion which produces the gain within the cavity must be sufficient to compensate for the fraction of energy loss due to all causes. Several reflecting elements such as fiber Bragg grating (FBG), selective wavelength filter and injection locking can also be used to replace the dielectric mirror. The all-fiber laser resonator setup can also be configured in a ring cavity as shown in **Figure 2.11**. The cavity allows light to oscillate in both directions thus generates bidirectional output which limits the efficiency of the laser. The constructive interference between the counterpropagating signals produce a standing wave which induces the spatial hole burning. This effect allows the oscillation of several longitudinal modes in the laser cavity (Digonnet, 2002). The bidirectional signal light travelling in the cavity can be eliminated using an optical isolator by forcing the light travel in a unidirectional operation.

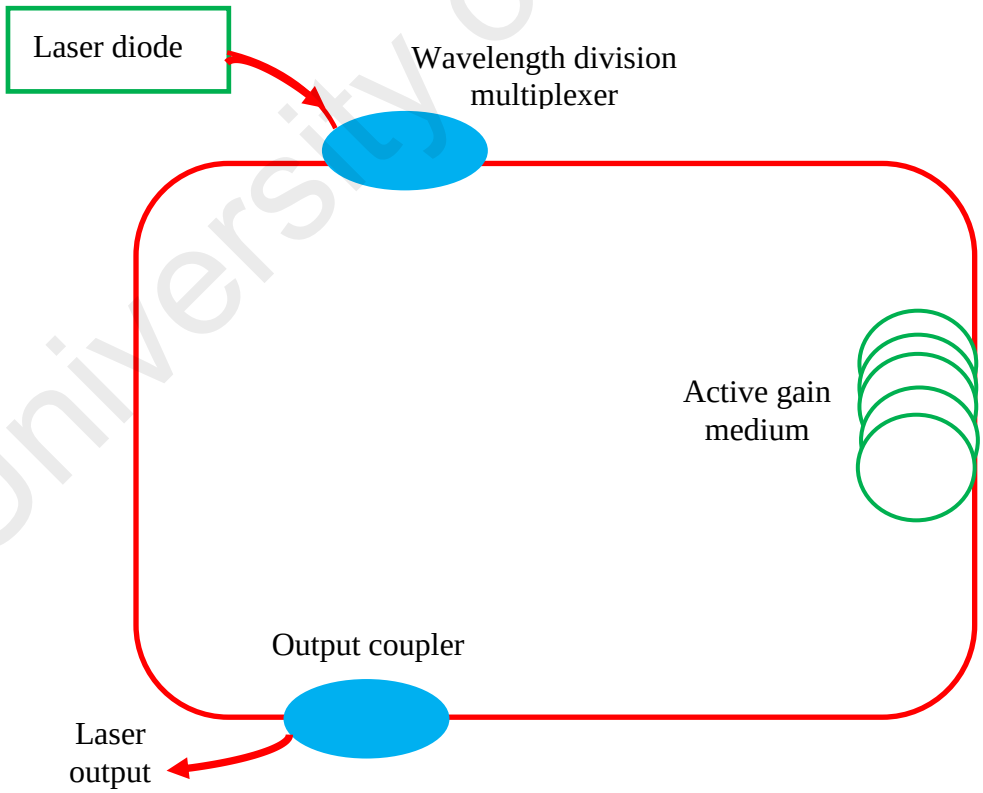

Figure 2.11: Schematic diagram of all-fiber ring cavity configuration.

However, the small amount of loss introduced by the isolator will increase the threshold of the laser. Another method to reduce the effect of spatial hole burning is to introduce the polarization controller (PC) that modifies the polarization state of light and allows continuous adjustment of the birefringence within the cavity to balance the gain and loss. The ring laser cavity offers the advantages of simplicity in design, low cost and low threshold operation. Ring cavities are commonly designed for pulse laser applications (Nelson et al., 1997; Panasenko et al., 2006).

2.9 Q-Switched Fiber Lasers

Q-switching is a simple and well-known technique for achieving energetic and nanosecond pulses in a laser system. In 1962, Hellwarth together with Fred J. McClung, proved their laser theory and generated peak powers 100 times than that of ordinary ruby laser by using electrically switched Kerr cell shutters (McClung & Hellwarth, 1963). The invented pulse produces fast, intense and controllable 'giant' laser pulses by 'Q-modulation'. Nowadays, the generated pulse is called Q-switching. Generally, the fiber laser can be designed to operate either in CW or pulsed mode. **Figure 2.12 (a)** shows the continuous output powers by CW lasers with constant time while **Figure 2.12 (b)** shows the pulsed laser which generates the output power with constant repetition frequency.

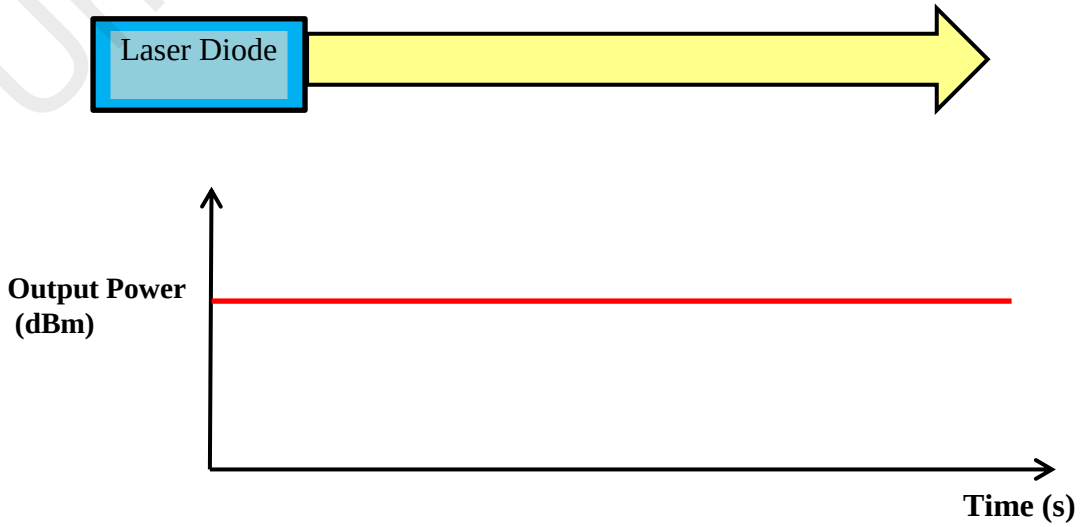

(a) Continuous wave laser

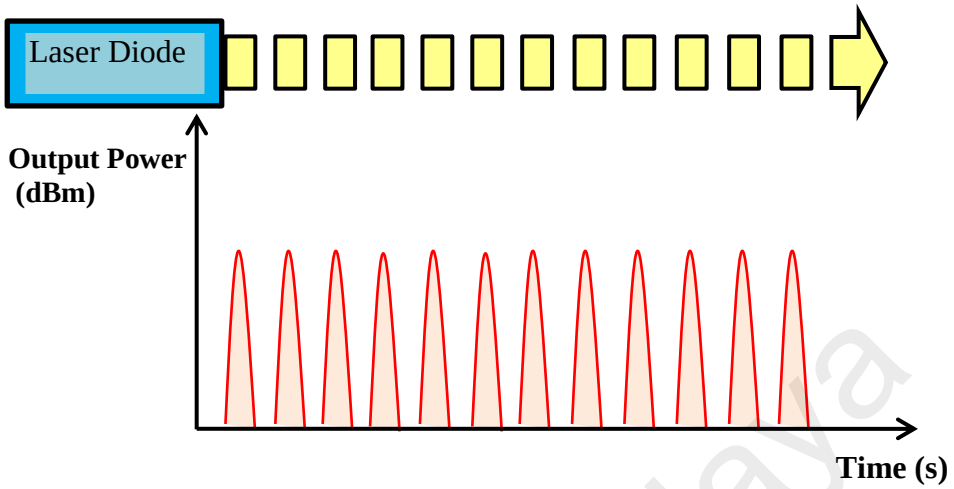

(b) Pulsed laser

Figure 2.12: The operation of **(a)** continuous wave laser and **(b)** pulsed laser.

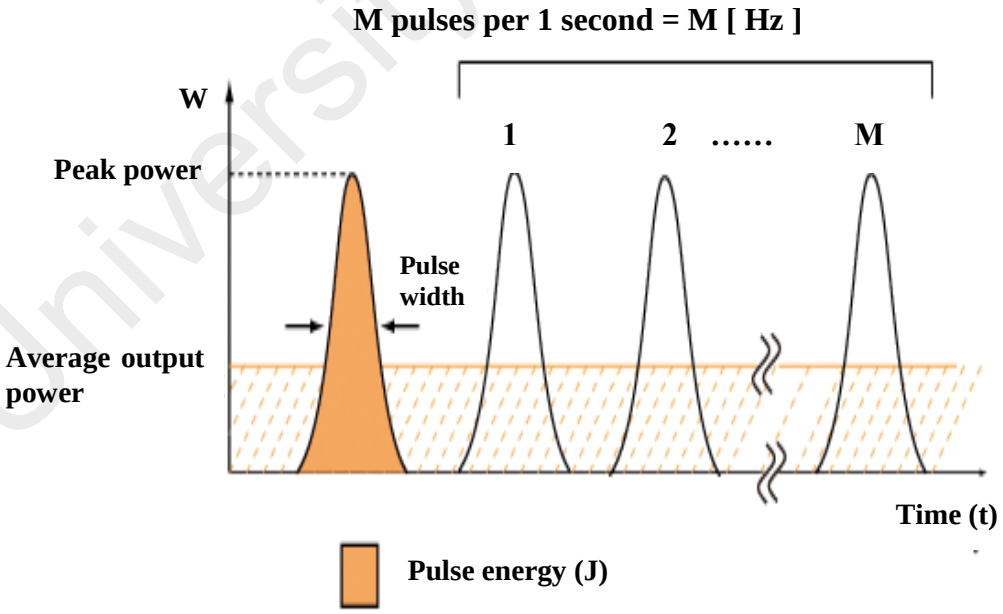

Figure 2.13: Relationship among all sorts of parameters of pulsed laser ("Wikipedia," 2016).

A CW laser is characterized by an average power in watt (W). A pulsed laser is generally characterized by a pulse duration in second (s), a repetition rate is denoted in hertz (Hz), a pulse energy in joule (J), and a peak power in watt (W) as depicted in **Figure 2.13**.

2.9.1 Q-Switching Technique

Q-switching laser involves the technique of modulating the losses of the laser resonator by any method. The term Q represents the quality of the laser resonator which contains information regarding the cavity losses. The quality factor (Q-factor) portrays the ability of a laser cavity to preserve its energy. A higher Q indicates a lower intracavity loss. The Q-switching phrase describes the idea of switching the laser configuration from a low to high Q to create short pulse duration. Originally, the Q-factor is kept at low level (i.e. high losses), preventing any potential for lasing. The gain medium provides an accumulation of spontaneous emission in the cavity by constant pumping; thus energy is stored. At the moment that the Q-factor is suddenly switched to a high level and the desired amount of energy is stored, spontaneous emission grows into lasing and a laser pulse starts to build up in the laser cavity. The pulse grows stronger until the gain equals the losses. When the pulse peak power is reached and depletes the gain completely, the laser is no longer able to oscillate. The Q-switched is open again (low Q), and the process starts from the beginning to build up more inversion for the next consecutive pulse. It is useful to have a long upper state lifetime of a gain medium in order to store gain, therefore it does not disappear as fluorescence emission before the Q-switched is opened (Digonnet, 2002).

A Q-switched laser can be realized using active and passive means. The common devices of active Q-switching are electro-optic and acousto-optic modulators.

Additionally, the rotating mirror or a prism can also be used. In active Q-switching, the repetition rate can be controlled and exhibit low timing jitter due to the exemption of movable parts in the cavity (Hjelme & Mickelson, 1992; Zayhowski & Dill, 1995). Basically, timing jitter cannot be avoided due to the oscillating photon originating from spontaneous emission from the gain medium. Typically, the pulse width in active Q-switching reduces and the pulse energy rises with the increase in pump power (Eichhorn & Jackson, 2007b). The pulse width depends on the two factors which are the gain and the cavity round trip time whereas the pulse energy depends on the repetition rate (Zayhowski & Kelley, 1991). Since the repetition rate in the active Q-switched can be controlled by driving the modulator with different seed signal, increasing the pulse energy to a certain rate reduces, the gain will be divided by fewer pulses, thus individual pulses will receive more gain.

A passive Q-switching offers a simpler method in providing a compact setup and is more cost-effective. It does not need external modulation incorporated in the setup, thus the saturable absorber has been used to self-modulate the cavity losses and the gain. Saturable absorbers are made up of materials and methods such as semiconductor compounds (Spühler et al., 1999) and crystal doped (Chen et al., 2000; Tsai & Birnbaum, 2000). Other reported works focused on the generation of Q-switching using doped fiber (Jackson, 2007; Kurkov, 2011). The transmission and reflection of the saturable absorber are based on the light intensity. It absorbs the light up to a certain limit which is determined by the absorber saturation fluence (Keller, 2003). When the energy reaches the limit, pulse is released.

In this thesis, passively Q-switched fiber laser has been demonstrated in conjunction with a graphene oxide and multi-walled carbon nanotubes (MWCNTs) based saturable absorber (SA). Graphene oxide and carbon nanotubes are allotropes of carbon

with a cylindrical nanostructure, which has been observed by previous scientists in 1991 for (CNTs) and 2004 for (graphene). The tremendous growth of these materials was due to their unique structure and physical properties (Hasan et al., 2009; Sun et al., 2010). The characteristic of 2D nanomaterials such as carbon nanotubes, graphene, and graphene oxide will be discussed in section 2.12.1, 2.12.2, and 2.12.3 respectively.

2.9.2 Parameter of Passive Q-Switching

Figure 2.14 shows the formation of the Q-switched fiber laser of one pulse cycle (Spühler et al., 1999). The saturable absorber with bleach, '**0**', unbleached conditions 'q_0' and a saturable absorber loss coefficient $q(t)$, have been considered and **the total cavity loss** within one cavity round trip is l. As can be seen in the figure, in **Phase 1**, the pulse starts to emerge when the gain, $\mathbf{g(t)}$ reaches the total cavity loss condition (low Q) at the saturable absorber unbleached conditions.

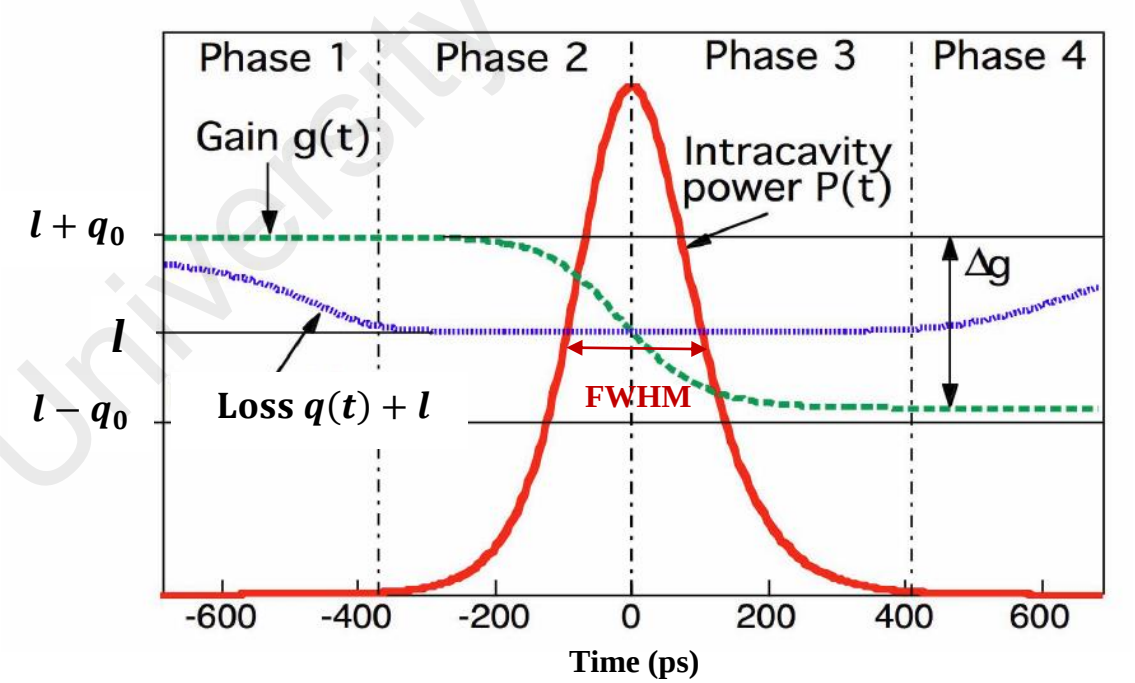

Figure 2.14: The formation of Q-switched fiber laser ("Wikipedia," 2016).

At this point, the power increases until the gain is capable to bleach the absorber. The intracavity power **P(t)** grows when gain **g(t)** reaches ***l*** in which saturable absorber is saturated before grows significantly. **Phase 2**, when the induced power causes the absorber to totally bleach, the gain **g(t)** is at the high Q until the gain starts to deplete to the loss level ***q(t) + l***. The maximum pulse occurs when the gain **g(t)** is equal to the total cavity loss ***l*** at the bleach condition. Then in **Phase 3**, the gain **g(t)** depletion continues and reaches the negative value, therefore the intracavity power **P(t)** decreases. Finally, in **Phase 4**, the absorber restores its unbleached state due to the shorter absorber's recovery time as compared to the gain **g(t)**. The continuous pumping of the gain medium will provide sufficient gain to attain the threshold level to start over for the next consecutive pulse which is going back to **Phase 1.** The **Phase 1** starts when gain **g(t)** reaches the unsaturated loss as shown in **Figure 2.15**.

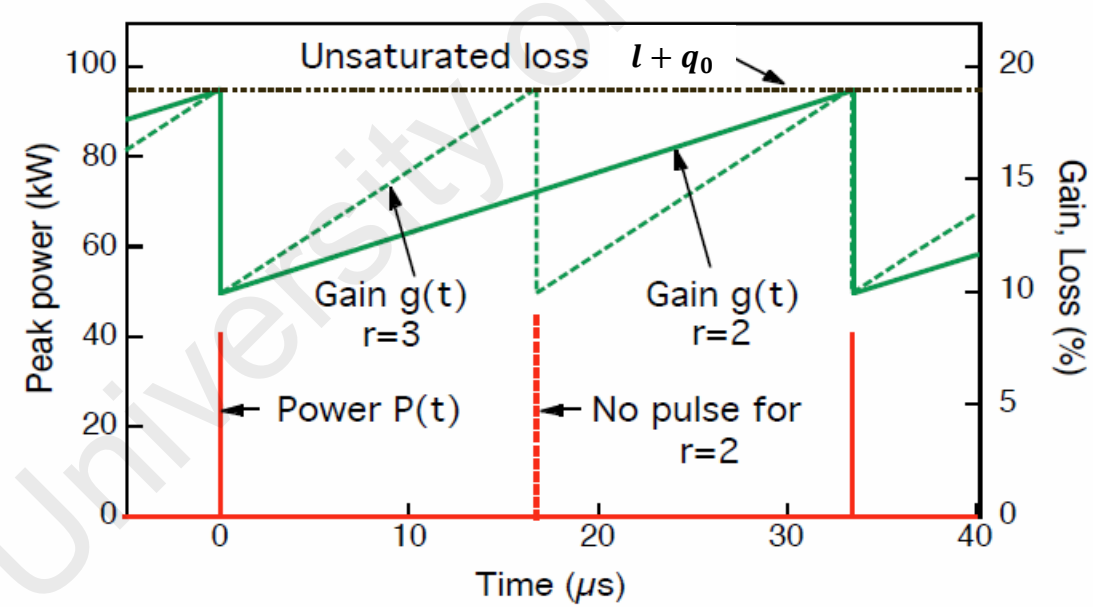

Figure 2.15: The cycle of the formation of Q-switched fiber laser("Wikipedia," 2016).

The stored energy in the gain medium for optical pumping or formation in Q-switching can be defined as;

$$E_{stored} = AL_G N_2 \, hv_1 \tag{2-17}$$

where N_2 is excitation energy, hv_1 is photon energy at the pumping wavelength, AL_G is pumped gain volume.

Pulse Width

In passive Q-switching, pulse width and pulse energy are independent of the pump power (Spühler et al., 1999). However, the pulse width usually decreased as the pump power increased as explained by (Herda et al., 2008). The pulse width (which is sometimes called pulse duration) of the Q-switching can also be observed in **Figure 2.14**. The FWHM of the pulse determines the pulse width. According to (Zayhowski & Dill, 1994) and based on **Figure 2.14**, the pulse width can be expressed as:

$$\tau_p = \frac{S_p T_r}{q_0}\left[\frac{\delta(1+\delta)\eta}{\Delta - ln(1+\delta)}\right] \tag{2-18}$$

where $S_p \sim 0.88$ is the pulse shape factor, T_r is the cavity round-trip time, η is the energy extraction efficiency of a light pulse and δ is the ratio between saturable and unsaturable cavity loss. It can be seen that the pulse width is proportional to the cavity round-trip time and inversely proportional to the saturable losses of the cavity.

Repetition Rate

The repetition rate is defined as a number of emitted pulses per second or the inverse of adjacent pulse. It can be measured directly from the oscilloscope by observing the duration between the output pulse trains. The repetition rate is commonly observed to be linearly dependent on the pump power and normally in the range of 1–100 kHz. This has also been confirmed by various experiments using fiber lasers (Jackson, 2007).

Pulse Energy

The average power of the Q-switched laser is measured directly from the power meter. Since average power is measured while the laser is Q-switching, the repetition rate at which the measurement was taken should be considered to calculate the pulse energy. An equation for the pulse energy is determined by dividing the average power, P_{avg} by repetition rate, f_{rep}:

$$E_p = \frac{P_{avg}}{f_{rep}} \tag{2-19}$$

According to (Spühler et al., 1999), the pulse energy depends on the amount of energy stored in the gain medium. Therefore, the lifetime of the gain medium and the absorber saturation loss are crucial. This is due to their relation as shown in **Figure 2.14**. Nevertheless, passive Q-switching suffers from the timing jitter (Huang et al., 1999). This is due to the fluctuations in pump power, temperature, losses and many more. In a fiber laser, the large amount of intracavity spontaneous emission is significant to produce jitter in a pulse.

Peak Power

The peak power of an optical pulse is defined as the maximum occurring optical power of a pulse. For long pulse duration, the peak power can be measured directly from the oscilloscope (OSC) with a photodiode. For short pulse duration in picosecond and femtosecond region, the peak power of a pulse can be calculated by the following equation where E_p is the pulse energy and τ_p is the pulse width:

$$P_{peak} = \frac{E_p}{\tau_p} \tag{2-20}$$

2.10 Mode-Locked Fiber Lasers

In 1989, the first mode locked fiber laser based on soliton pulse shaping was reported (Kafka et al., 1989) which demonstrate ~4 ps pulses. A year later, sub-picosecond pulses shorter than 500 fs were reported from Nd^{3+}-doped fiber laser by pulse compression mode-locking. In contrast with mode-locking, Q-switching typically produces a giant pulse formation which is high in pulse energy and peak powers while the repetition rate is in the range of hertz to kilohertz. One of a few best Q-switching performances was indicated in 1999 by Paschotta et al., (1999) generating pulses with as much as 0.1 mJ pulse energy at 1.53 μm and a repetition rate of higher than 1 kHz using a semiconductor saturable-absorber mirror (SESAM). In the following year, (Alvarez-Chavez et al., 2000) reported on the actively Q-switched Yb^{3+}-doped fiber laser which is capable of generating a 2.3 mJ of output pulse energy at a 500 Hz repetition rate and more than 5 W of average output power at higher repetition rates. In 2007, Schmidt et al., demonstrated a Q-switched employing a short-length Yb-doped photonic crystal fiber producing 100 W of average output power with up to 2 mJ of pulse energy and a sub-10 ns pulse duration was extracted at lower repetition rates (Schmidt et al., 2007).

2.10.1 Mode-Locking Technique

Mode-locking is a technique of generating an ultra-short pulse laser. The pulse duration range can be between picoseconds (10^{-12} s) to femtoseconds (10^{-15} s). An ultra-short pulse can be generated when all the longitudinal modes have a fixed phase relationship, hence the term “mode-locking” or “phase-locking”. The fixed phase superposition between all the modes oscillating inside a laser cavity causes the cw laser to be transformed into a train of pulse. The number of longitudinal mode that can simultaneously lase are dependent on the gain linewidth, Δv_g and the frequency

separation between modes. Under sufficiently strong pumping, we can expect that the number of modes, *M* oscillating in the cavity is given by

$$M = \frac{\Delta v_g}{c/2L} = \frac{2L}{c}\Delta v_g \tag{2-21}$$

where *c* is the speed of light and *L* is the length of a linear cavity. The shortest pulse duration that we can expect to obtain by a given gain linewidth is

$$\tau_{min} = \tau_M = \frac{2L}{cM} = \frac{1}{v_g} \tag{2-22}$$

From Equation (2.22), we can conclude that the shortest pulse that can be obtained is a reciprocal of gain linewidth (in Hz) (Milonni & Eberly, 2010).

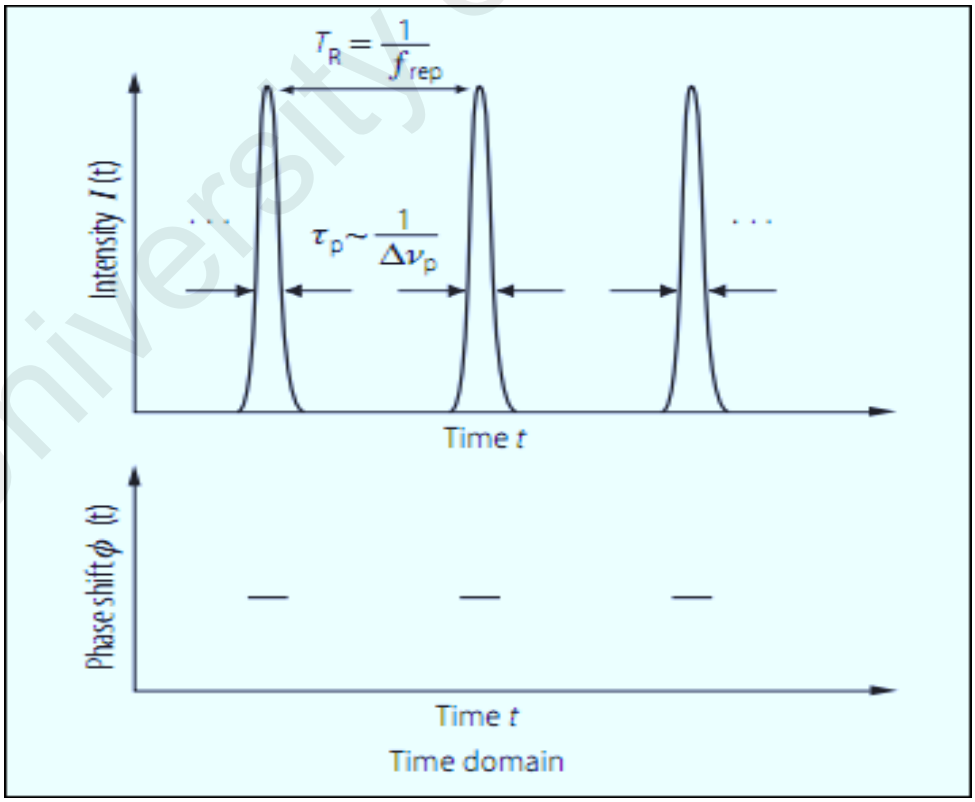

(a)

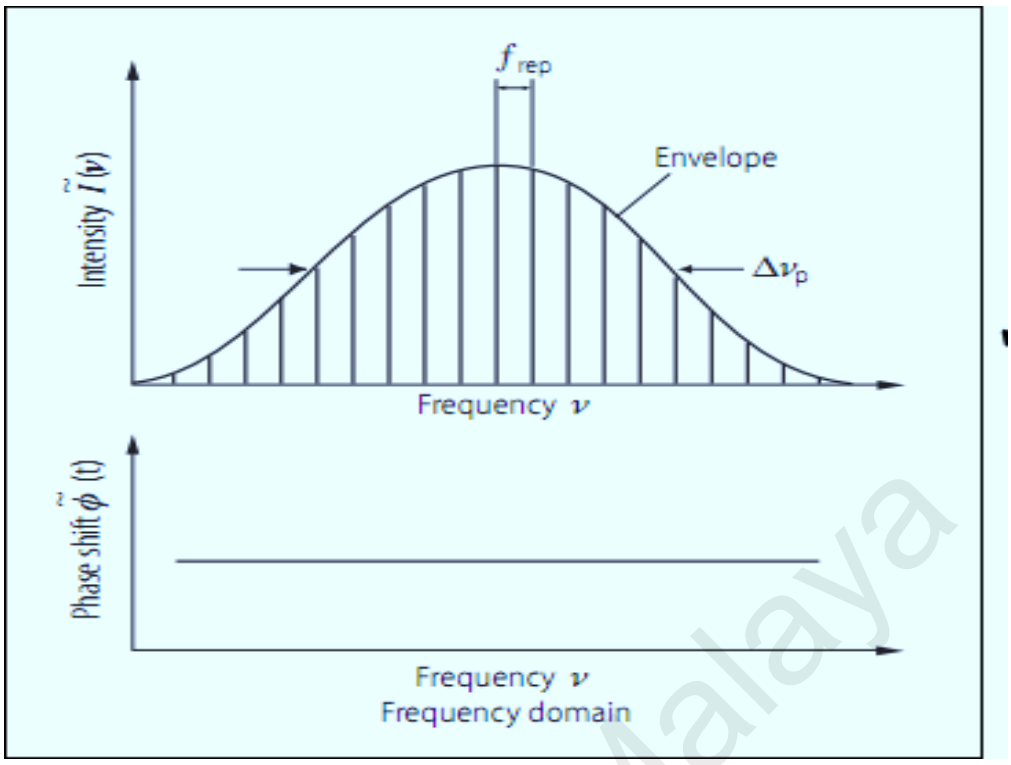

(b)

Figure 2.16: Mode-locked pulse in **(a)** the time domain and **(b)** frequency domain (Keller, 2004).

Mode-locking involves periodic modulation of resonator loss. Once the resonator loss is modulated, all the laser modes phase can easily be fixed. In the time domain, a mode-locked laser generates an equidistance pulse train, with T_R defines the round-trip time of a pulse inside the laser cavity while pulse duration is indicated by τ_p. In the frequency domain, this resulted in a phase-locked frequency comb with constant mode-spacing, ν_R, that is equal to $1 / T_R$. The pulse duration, τ_p, is inversely proportional to the spectral width of the envelope of the frequency comb, $\Delta\nu_g$. Mode-locking in a frequency domain is homogeneously broadened laser normally lases at one axial mode at the peak of the gain. However, the periodic loss modulation transfers additional energy phase-locked to adjacent mode separated by the modulation frequency. This modulation frequency is normally referring to the cavity round-trip frequency. Consequently, the frequency comb has an equidistance axial modes locked together in phase forms a short

pulse in the time domain. Mode-locked pulse in the time and frequency domains are depicted in **Figure 2.16**. The fundamental repetition rate of a mode-locked laser is determined by its cavity length, as shown in the equations below.

$$\text{Repetition rate (for linear cavity)} = \frac{c}{2Ln} \tag{2-23}$$

$$\text{Repetition rate (for ring cavity)} = \frac{c}{Ln} \tag{2-24}$$

L, *c* and *n* denotes the length of the cavity, speed of light and refractive index respectively. As the round-trip time, T_R, is the inverse of repetition rate, therefore;

$$T_R = \frac{Ln \text{ (for ring cavity) or } 2Ln \text{ (for linear cavity)}}{c} \tag{2-25}$$

2.11 Double-Clad Fiber

Despite the tremendous advances in fiber lasers, the output power was still limited by the availability of single transverse mode pump power launched into the single mode fiber core. Owing to this limitation, E. Snitzer et al., found a way to overcome this limitation (Snitzer et al., 1988) by allowing the use of a double-clad fiber in order to inject the high-power pump light (in a kilowatt based) to the doped fiber. They designed a fiber with two types of cladding consisting of the inner cladding and outer cladding. Mostly, the inner cladding was not round in shape in order to improve pump absorption (Muendel, 1996). The new invention has led to the increase in the laser's output power which is typically limited by the power level of the laser diode. As mentioned earlier, the pioneering work of double-clad fiber was proposed by E. Snitzer in late 80s (Po et al., 1989). The gain medium used in this work was neodynium-doped fiber pumped by the

GaAIAs phased array. The development of cladding pumping ytterbium-doped fiber lasers (YDFL) followed slightly after. The demonstration of YDFL has been proposed by Hanna and co-worker in the 90s (Hanna et al., 1990; Pask et al., 1995). The accelerating pace can be seen in successive publications afterwards. The use of double clad fiber has successfully achieved a continuous wave (CW) output power of several kW level (Jeong et al., 2004) which was generated from the 12-m length of double-clad ytterbium-doped fiber. Due to the high achievement of fiber lasers in terms of its output power and efficiency, interest was then focused on the erbium-doped fiber laser (EDFL) which has an operating wavelength of 1550 nm that falls within the low-loss telecommunication window. Since the introduction of double clad fibers, the maximum reported output power of a CW EYDFL has reached 297 W at wavelength of 1567 nm using a 6-m long Er-Yb co-doped double-clad fiber (Jeong et al., 2007) within a very short time span.

2.11.1 Cladding Pumping Technique

The drastic improvement in fiber lasers performance has been realized with the enhancement in various approaches. One of the famous approaches is the novel design of double clad fibers and cladding pumping scheme (Mears et al., 1985; Poole et al., 1986). The cladding pumping technique makes use of a double-clad fiber with a rare-earth-doped core that is designed to be single-mode at the relevant lasing wavelength. The core is surrounded by a cladding layer heavily multimode at the pump wavelength, which is itself surrounded by an outer cladding layer of still lower refractive index as depicted by **Figure 2.17**. The inner cladding layer is adapted in shape and dimensions to allow efficient end-coupling of the output from high-power semiconductor diode stripes and arrays.

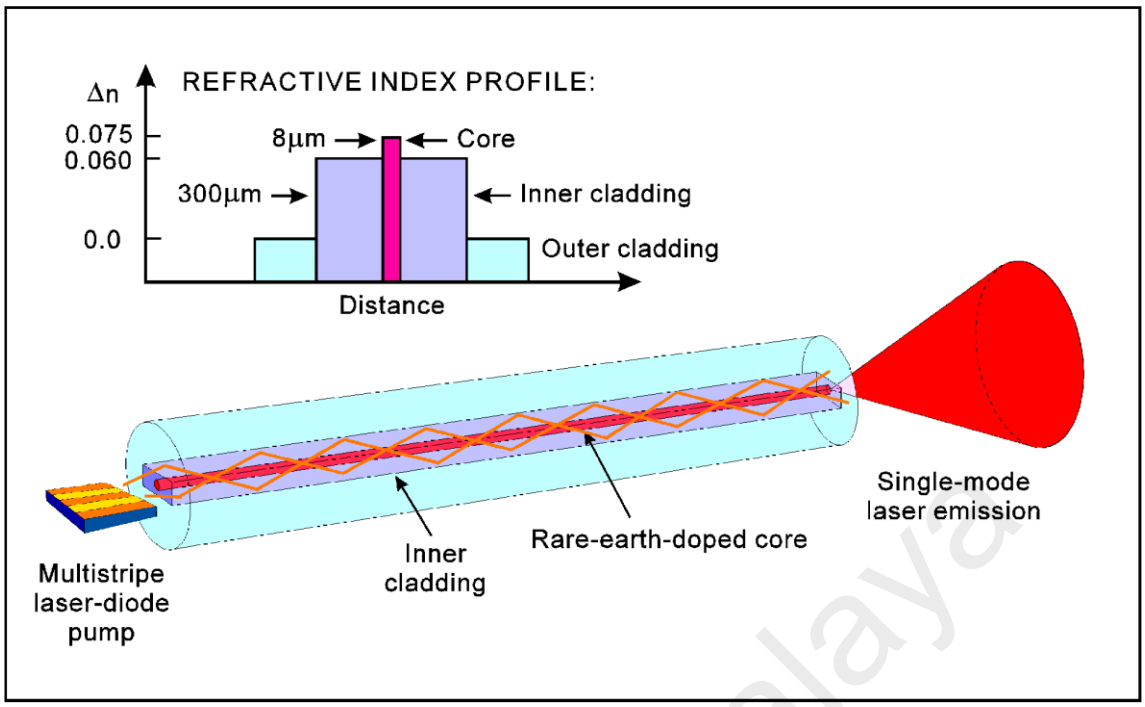

Figure 2.17: Double-clad fibers convert the output of a high-power semiconductor pump laser to a diffraction-limited output beam in simple, end-pumped fiber laser cavities. Inset shows refractive index profile typical of a cladding-pumped fiber.

The conventional optical fiber, single mode fiber, has only one effective wave-guiding property which is the fiber core. Owing to this, the pump light from the source should be coupled into the small core area to achieve efficient laser operation. Therefore, the laser diode needs to be single mode with high intensity output. The use of high pump power which is coupled directly to the doped fiber core will damage the threshold of the semiconductor material. To overcome the limitation, E. Snitzer et al introduced a double-clad fiber which can be coupled to the high pump power provided by the laser diode. Snitzer et al., (1988) use the available high-power multimode laser diodes of relatively low brightness and with the newly designed double-cladding (or double-clad) fibers. This fiber uses a cladding-pumping scheme by injecting the pump light to the fiber's cladding as shown in **Figure 2.18**.

Based on the figure, a second (outer) cladding is added with lower refractive index than that of the first (inner) cladding. This allows the injected pump light to be confined due to the TIR at the inner-outer cladding boundary. The large area of the inner cladding allows a larger fraction of the laser diode output power to be coupled to the fiber. The pump light travel in the first cladding overlaps with the doped core and gradually absorbed by it. The pump absorption is proportional to the ratio of the core area, A_{core} over the inner cladding area, A_{clad} (Muendel, 1996), A_{core}/A_{clad}. Thus, the core/cladding area ratio is very crucial in designing the double-clad fiber. Confined within the core area, the generated output has relatively high brightness and power. This is shown in **Figure 2.18 (b)** which depicts ratio of the area of cladding over the area of core of such fiber.

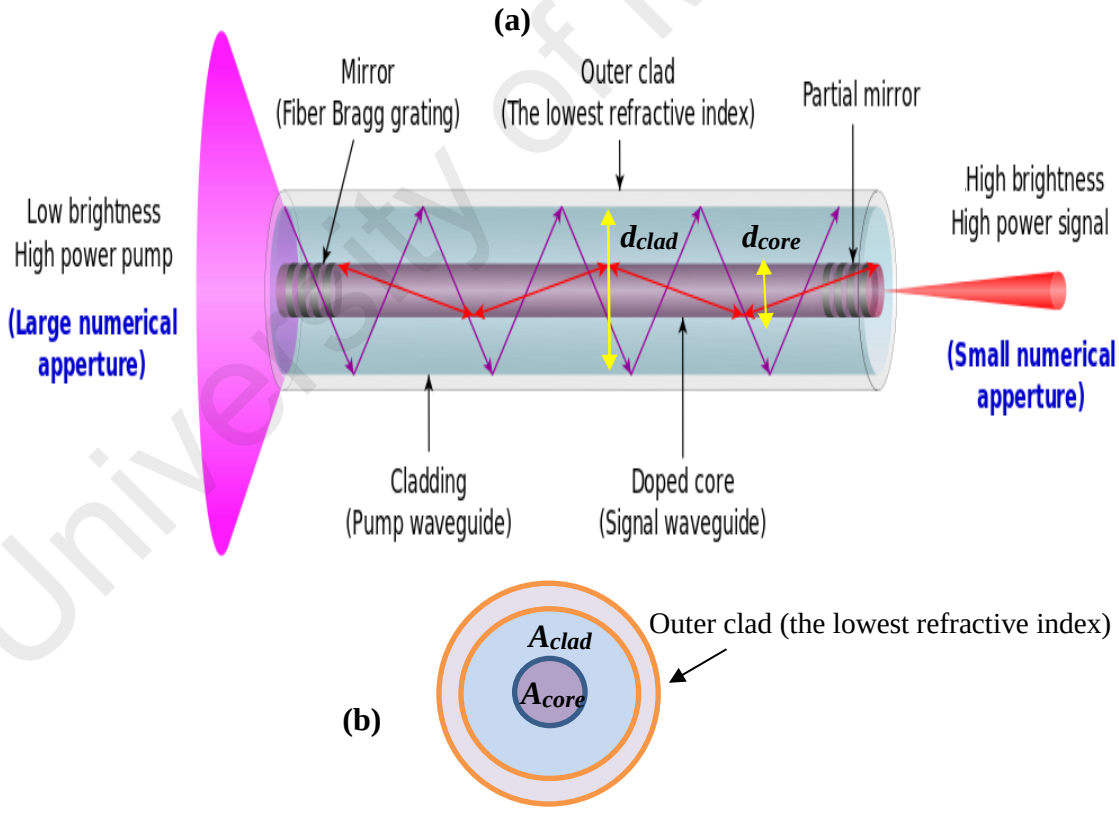

Figure 2.18: **(a)** Schematic drawing of a double-cladding fiber (source: Wikipedia 2016) and **(b)** cross-section of the double-cladding fiber with its area for cladding and core.

Apart from that, the cladding-pumping laser scheme exhibits high thermal tolerance for high power CW laser operation provided that certain parameters are optimized (Brown & Hoffman, 2001; Wang et al., 2004). However, (Lapointe et al., 2009) reported on the thermal degradation of double-clad optical fiber coatings which is known to be the major limiting factor for the operation of high power CW fiber lasers. Wang et. al proposed to overcome the limitation by decreasing the pump absorption and increasing the length of the fiber (Wang et al., 2004), however the laser will suffer from low efficiency due to the needs of higher pump absorption. In conclusion, by optimizing the combination of pump powers, pump absorption and fiber lengths, an acceptable laser performance can be achieved.

Another work proposed by Muendel (Muendel, 1996) is to design various shapes of inner cladding to enhance the power transfer from the pump to the doped core (Li et al., 2004; Liu & Ueda, 1996). The approaches taken were to offset the core of the fiber and to alter the geometry of the inner cladding. Therefore, provides significant difference in the pump absorption efficiency of the double-clad fiber compared to the conventional circular shaped inner cladding. The designed were based on the ray propagation in the fiber. There are two types of rays propagating in the inner cladding which are the meridional rays and skew rays. Meridional rays are rays that pass through the axis of the optical fiber, while skew rays travel through an optical fiber without passing through its axis (Muddu, 2003). Most of the pump signal propagates as helical rays in the inner cladding, therefore most of the skew rays miss the core and only the meridional rays overlap with the doped core. This limitation can be overcome by offsetting the core from the center of the inner cladding (Liu & Ueda, 1996) as in **Figure 2.19 (e)**.

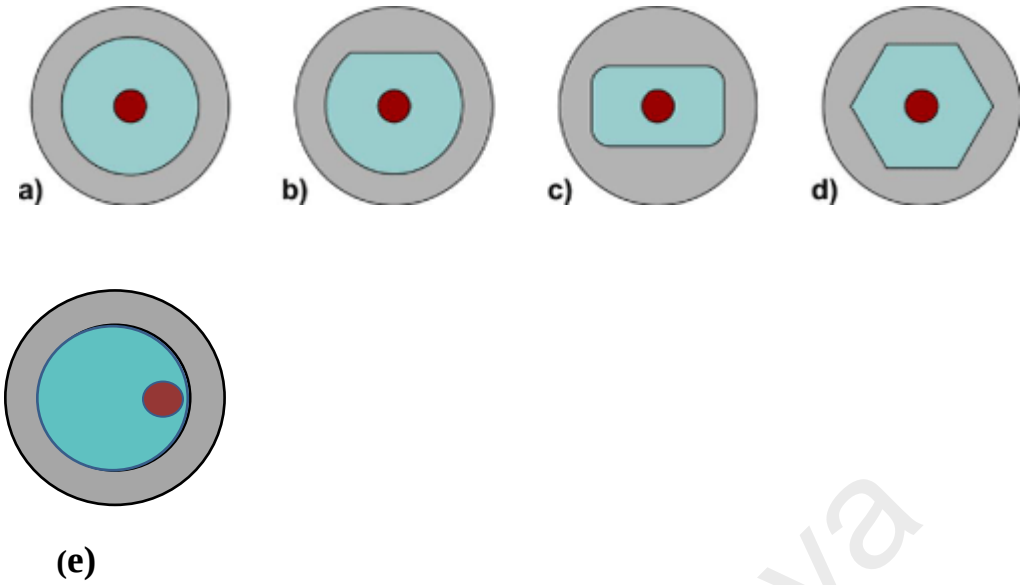

Figure 2.19: Various designs of inner cladding, double-clad fiber **(a)** centred core **(b)** D-shaped **(c)** rectangular **(d)** hexagonal **(e)** offset core (Digonnet, 2002).

The ratio of absorbable power to pump power is defined as;

$$\mu = \frac{P_a}{P_r} \tag{2-26}$$

For circular double-clad fiber;

$$\mu_1 = \frac{2}{\pi}\left[\frac{\rho}{R_0}\sqrt{1-\left(\frac{\rho}{R_0}\right)^2} + sin^{-1}\left(\frac{\rho}{R_0}\right)\right] \tag{2-27}$$

ρ and R_O are the radius of the core and first cladding respectively. And for off-set double clad fiber;

$$\mu_2 = \frac{2}{\pi}\left[\frac{\rho+P}{R_0}\sqrt{1-\left(\frac{\rho+P}{R_0}\right)^2} + sin^{-1}\left(\frac{\rho+P}{R_0}\right)\right] \tag{2-28}$$

where P is the off-set. Comparing μ_1 and μ_2, we can conclude that because of "P", we always have $\mu_2 > \mu_1$ and briefly, the larger the P the higher the absorption. But including the rectangular inner cladding with appropriate NA, we still get the maximum launched pump power into double cladd fibers compared to μ_2 and μ_1.

2.12 2D Nanomaterials Saturable Absorber

An ideal saturable absorber has a broadband absorption, ultrafast recovery time in picosecond (~ps), low saturation intensity, appropriate modulation depth, high damage threshold as well as cost- and time-efficient to make. Graphene oxide (GO) has a recovery time of ~1.5 ps when observed using 780 nm, 250-fs laser (Elim et al., 2003). The research on 2D nanomaterials are being studied intensively as result of discovery of graphene by Novoselov et al., to find the successor to graphene. It was discovered that 2D nanomaterials reveal different electronic, optical, thermal and mechanical properties from its 3D form (Novoselov et al., 2004).

In the field of optoelectronics, they can be used for photovoltaics, photodetection and photoluminescence. The existence of Pauli blocking property inside these 2D nanomaterials such transitionmetal dichalcogenides (TMDs enables them to be utilized as saturable absorbers to generate Q-switched and mode-locked lasers. Indeed, 2D nanomaterials such as transition metal dichalcogenides (TMDs) (Lieth & Terhell, 1977; Wang et al., 2012; Wilson & Yoffe, 1969), which has 60 different variations, has been utilized as saturable absorber to generate passive Q-switched and mode-locked fiber lasers (Huang & Luo, 2014; Luo et al., 2014; Zhang et al., 2014). Topological insulators such as Bi_2Te_3 and Sb_2Te_3 (Hasan & Kane, 2010; Khanikaev et al., 2013), which are a class of the 2D nanomaterials that only permits the flow of electrons on its surface, have

also has been successfully demonstrated to achieve Q-switched and mode-locked fiber lasers (Bonaccorso & Sun, 2014; Huang et al., 2014; Jia et al., 2015; Luo et al., 2014).

The emerging of 2D nanomaterials in industrial applications has started since 1960s (Savage, 1993). The evolving of 2D nanomaterials namely carbon nanotubes and graphene provide greater benefits owing to their extraordinary properties. These carbon nanostructures and graphene are significant for current technological and scientific revolution; nanotechnology. The 2D nanomaterials such as carbon-based 2D materials, silicate clays, transition metal dichalcogenides (TMDs), and transition metal oxides (TMOs) provide enhanced physical, chemical, and biological functionality owing to their uniform shapes, high surface-to-volume ratios, and surface charge. Their extreme thinness has been explored for pioneering works in fiber lasers system such as the 2D nanomaterials saturable absorber which respond rapidly to external signals such as laser.

2.12.1 Carbon Nanotubes

The carbon nanotubes (CNTs) was observed in 1991 by Iijima in the carbon soot of graphite electrodes during the arc discharge method (Ando & Iijima, 1993). CNTs can be formed by rolling the graphene sheet into a cylindrical nanostructure at specific discrete (chiral) angles. **Figure 2.20** shows the atomic structure of graphitic materials which consists of (a) 0D Fullerene, (b) 1D Carbon nanotubes (CNTs), (c) 3D Graphite and (d) single layer graphene (2D graphene). The terms graphene comes from the single atomic layer of graphite (Geim & Novoselov, 2007). The combination of the rolling angle and radius of the CNTs decide the nanotube properties. In CNTs, the bandgap is controlled by the diameter, which in turn defines the operating wavelength of the CNTs. According to the number of walls that form the nanotube, CNTs can be categorized as single-walled nanotubes (SWCNTs) or multi-walled nanotubes (MWCNTs). In the case of a MWCNT, concentric graphene sheets are stacked one on top of the other which then

form the large diameter of the outer tubes of MWCNTs. Iijima reveals the structure of these tubes using transmission electron microscopy (TEM) (Iijima, 1991).

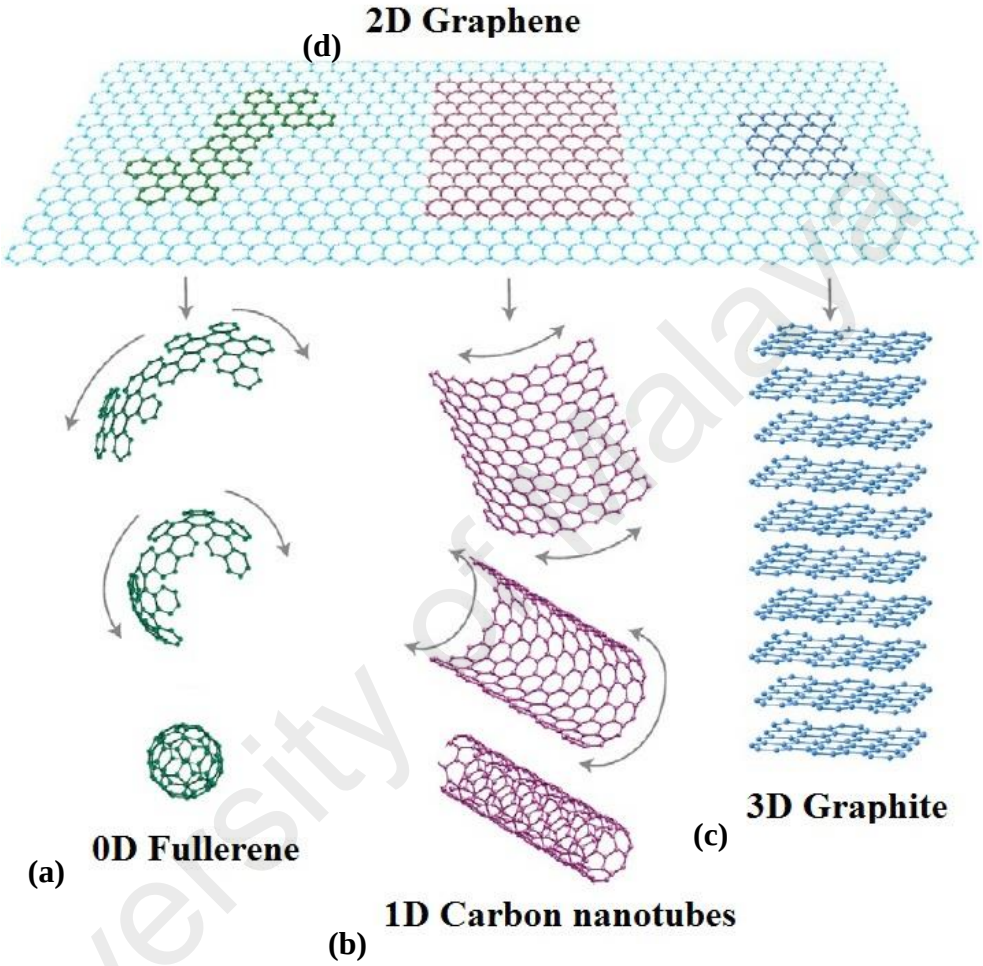

Figure 2.20: Basis of all graphitic forms. Graphene is a 2D building material for carbon materials of all other dimensionalities. It can be wrapped up into **(a)** 0D buckyballs, rolled into **(b)** 1D nanotubes or stacked into **(c)** 3D graphite (Geim & Novoselov, 2007).

Another important feature of MWCNTs is the rolled up diameter which are in the range of tens of nanometers and in some cases even more than 100 nm (Darabont et al.,

2005) as compared to SWCNTs which have a diameter of only up to 2 nm as depicted in **Figure 2.21**.

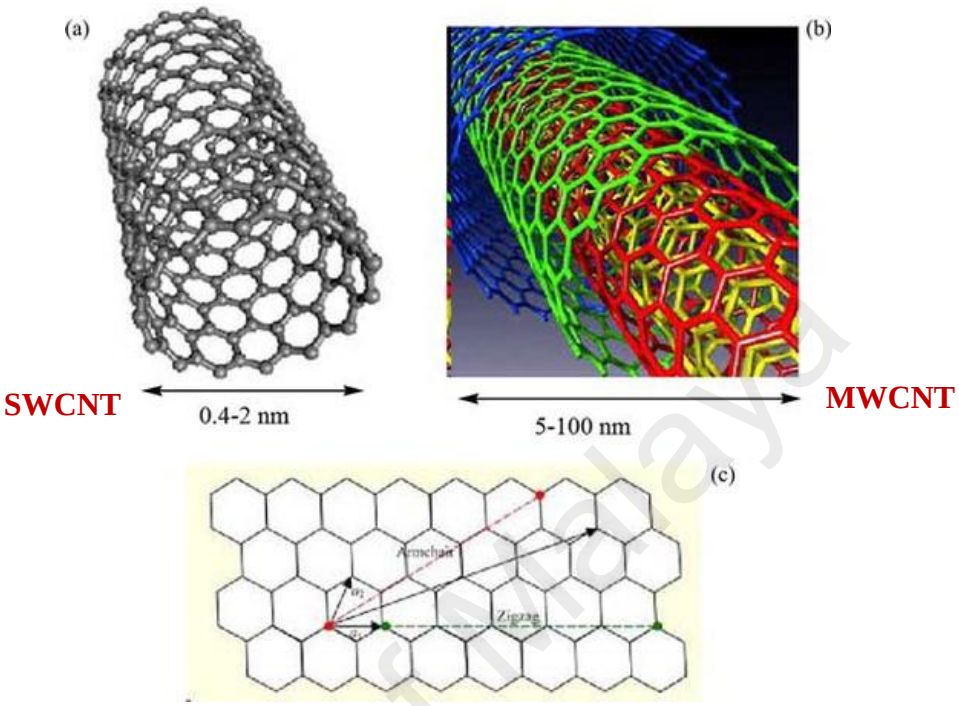

Figure 2.21: CNT structure arrangements **(a)** SWCNT **(b)** MWCNT **(c)** Structure arrangement of CNT layer.

Various methods have been implemented to integrate the SAs in the laser devices, for example free space arrangement, optical deposition in fiber ends and inside fiber, evanescent field using tapered fiber and sandwiching the SAs polymer composite between two fiber connectors (Sun et al., 2012). The latter is the most famous technique used so far. Apart from that, host polymer is another important material to incorporate in the fabrication of CNTs. The characteristic of the host polymer is usually stable against humidity or other environmental factors and laser irradiation (Booth, 1989). The wide range of host polymer used include polivinyl alcohol (PVA), poly-carbonate (PC), polyimide (PI), polymethyl methacrylate (PMMA), carboxymethyl cellulose (CMC) and many more (Hasan et al., 2009). Since the first demonstration of SWCNTs as SA in 2003, the performance of ultrafast laser has improved significantly.

2.12.2 Graphene

In 2004, Geim and Novoselov have discovered single layer graphene as depicted in **Figure 2.20 (d)** and found that the material does not exist in a free-state. A few-layer graphene and single layer graphene have been produced using scotch-tape method from graphite (Geim & Novoselov, 2007). The method is called mechanical exfoliation of graphite. The large-scale graphene production is called liquid-phase exfoliation (LPE) method, in which graphite flakes are dispersed in solvent, followed by ultrasonification and centrifugation to obtain dispersed solution of small flakes of few-layer and single-layer graphene (Hernandez et al., 2008). However, the most promising method for graphene fabrication is a chemical vapour deposition (CVD) method (Obraztsov et al., 2007). Graphene rapidly become a rising star due to its unique and valuable electronic properties (Geim & Novoselov, 2007). A few layer or single layer graphene can be determined by Raman spectroscopy measurement (Graf et al., 2007). Single layer graphene exhibits optical transmittance as high as 97.7 % with linear Dirac electron dispersion which enables broadband application (Bonaccorso et al., 2010).

Graphene has been used in many fields and its nonlinear optical absorption properties enable graphene to be used in photonic applications (Hasan et al., 2009). When a laser source is applied to the graphene, the electrons in the lower energy state (valence band) absorb the photon, hence higher electron energy state (conduction band) is occupied until further absorption is blocked, which is known as a Pauli blocking effect. This results in saturable absorption of graphene (Sun et al., 2010). Due to the ultrafast saturable absorption of graphene, it has been demonstrated to be a promising material as a saturable absorber in mode-locking to generate ultrashort laser pulses. The first reported mode-locked laser was in 2009 which incorporate graphene as a saturable absorber (Sun et al., 2010). Since then, graphene became a new SA material with ultrafast recovery time and operational wavelength independence.

Interestingly, to date there have been only three reports on TDFLS incorporating a graphene-based SA. **Table 2-1** summarizes the recent achievements in Tm-doped graphene-based lasers.

Table 2-1: Summary of the Reported TDFL with Graphene based SA

Reference	SA Type	Centre wavelength	Repetition rate	Pulse width	Output power
(Zhang et al., 2015)	LPE (PVA)	1942 nm	6.46 MHz	3.6 ps	2 mW
(Wang et al., 2013)	LPE (DMF)	1953 nm	16.94 MHz	1.52 μs	1.41 mW
(Sobon et al., 2013)	CVD (PMMA)	1884 nm	20.5 MHz	2.28 μs	1.35 mW

2.12.3 Graphene Oxide

An interest on graphene oxide (GO) (Stankovich et al., 2007) has exponentially risen, as documented by the yearly number of peer-reviewed works published on this topic, which have passed from a few units in 2007 to some thousands in 2013 (data taken from Scopus). GO is a two dimensional material. It is the oxidized form of graphene, with O functional groups decorating the sp^2 C basal plane (Stankovich et al., 2007). All its physical properties can be tuned from those of fully oxidized GO to, approximately, those of graphene by simply removing the functional groups from its surface. This process allows it to pass from an insulating material to a semi-metal. Due to the presence of the O functional groups, GO is also hydrophilic and it can be dispersed in water solution (Stankovich et al., 2007), contrary to graphene which is hydrophobic. The size of the GO flakes can be also tuned and varied from a few nm to mm (Su et al., 2009).

CHAPTER 3 : THULIUM-DOPED FIBER LASERS IN LINEAR AND RING CAVITY CONFIGURATION

3.1 Introduction

Laser systems operating in 2 μm "eye safe" wavelength region have gained steadily increasing interest in recent years since they offer exceptional advantages especially for free-space applications compared to the conventional systems that operate at shorter wavelengths. For instance, they are suitable for applications in LIDAR and gas sensing systems as well as in free-space optical communication (Cariou et al., 2006; Scholle et al., 2010). Strong water absorption in this wavelength range makes such lasers also very useful for medical applications. These 2 μm lasers can achieve a substantial heating of small areas and thus they allow for very precise cutting of biological tissue. The wavelength also overlaps with many absorption lines of several gas molecules such as hydrogen bromide (HBr) and carbon dioxide (CO_2), which creates the possibility of constructing cost-effective gas sensors. The development of 2 μm fiber laser can be realized based on radiative transition in thulium trivalent cation, Tm^{3+}. However, there are still many issues to be addressed such as low quantum efficiency of generated laser in high phonon energy glass host matrix such as silica-based glass fibers. Therefore, thulium-doped fibers (TDFs) normally employ low phonon energy glass hosts, for instance, fluoride glass, in which the up-conversion intensity is reported to be quite high in the ultraviolet region (Jackson & King, 1998). Nevertheless, since the fluoride host is a rather soft type of glass, it is very hard to draw optical fiber from the preform due to its lower melting temperature. Recently, the interest has shifted back to silica based host TDFs as the phonon energy of silica glass can be reduced by incorporating silica network modifiers like aluminum (Al) and germanium (Ge). Thus TDFs with modified silica host

have emerged as a promising gain medium for achieving an efficient TDFL (Jander & Brocklesby, 2004).

Recently, the development of thulium-doped optical fiber lasers (TDFL) operating at near 2000 nm has become an interesting topic for many researchers (Gumenyuk et al., 2011; Wu et al., 2007; Zhang et al., 2011b). This is attributed to the possibility of achieving laser of high efficiency, high output power, and retina safe in addition to specific applications plausible for this wavelength, such as for remote sensing and biomedical applications (Slobodtchikov et al., 2007). Thulium presents three major absorption bands in the infrared region from the ground state absorption (GSA) which are $^3H_6$ to $^3F_4$ (~1670 nm), $^3H_5$ (~1210 nm) and $^3H_4$ (~790 nm) (Moulton et al., 2009b). One of the advantages of thulium is the enormous bandwidth emission from $^3F_4 \rightarrow {}^3H_6$ transition which is close to 130 nm.

In this chapter, a study of newly fabricated graphene oxide which has a characteristic of the paper-based film. In addition to the discussion on the fabrication process of graphene oxide and pencil core, a thorough analysis on the performance of fiber laser has been investigated experimentally. Effect on the use of different pumping wavelength has also been investigated in terms of their ability to generate higher lasing efficiency as well as lower threshold power. The experiment is conducted to study the Q-switched and mode-locked TDFLs using 2D nanomaterials saturable absorber (SA) which are graphite i.e. pencil-core and home-made graphene oxide, respectively.

3.2 Working Principle of Thulium-Doped Fiber Lasers

Thulium (Tm) is a rare element with atomic number 69. Tm can be pumped at several different wavelength bands, which are located at 793 nm, 1210 nm, and 1560 nm regions. Silica-based thulium-doped fibers (TDFs) have a very broad emission spectrum, which ranging from 1800 nm to 2100 nm. The span is about 300 nm and thus it provides a wide flexibility in operating wavelength of the TDFL. This is due to the Tm ions interaction with the local crystal field, its energy levels Stark split into broad energy bands, which is an inhomogeneous broadening effect (Agger & Povlsen, 2006). The increased phonon energies due to temperature changes also contribute to this broadening (Svelto & Hanna, 1976). TDFL operating at around 2 μm region can be realized by laser diode pumping at the wavelength near 800 nm ($^3H_4$) and 1560 nm ($^3F_4$). The 2 μm laser can be obtained in a single doped TDF due to the energy transition between the $^3F_4 \rightarrow {}^3H_6$ states. The typical energy level diagram of the Tm^{3+} with possible laser transition and cross relaxation process is shown in **Figure 3.1**. The $^3H_6 \rightarrow {}^3F_4$ absorption band of silica TDF possesses an extremely broad line-width, close to 130 nm, it is one of the broadest in any of the trivalent rare earth (Digonnet, 2001). The pump band mostly used for $^3H_6 \rightarrow {}^3H_4$ transition is at about 800 nm, which exhibits no significant excited-state absorption (ESA). The $^3H_6 \rightarrow {}^3H_4$ transition is very broad, and it allows pumping at the strong peak near 790 nm with either AlGaAs laser diode or sapphire laser. One important feature of this transition is the cross-relaxation between Tm^{3+} pairs, which takes place when the Tm^{3+} concentration is sufficiently high (Tropper et al., 1991). As shown in **Figure 3.1**, the cross-relaxation process leads to energy transfer from a Tm^{3+} ion in the $^3H_4$ level (donor) to a neighbouring Tm^{3+} ion in the ground state (the acceptor). The latter is thus excited to the upper laser level ($^3F_4$ level), whereas the donor drops to the $^3F_4$ level, yielding two excited ions for one pump photon, or a quantum efficiency of 2 as shown in **Figure 3.1** (Moulton et al., 2009a).

The phenomenon of cross-relaxation can be used to produce an efficient 2 μm laser using a 800-nm pumping in conjunction with TDF, which has high Tm^{3+} concentration. Another pump band for Tm^{3+} is at 1560 nm, where lasing near 2 μm in the pure TDF also occurs between the $^3F_4$ and $^3H_6$ states. The spectral bandwidth of the TDF also covers a very large range from 1.7 – 2.1 μm.

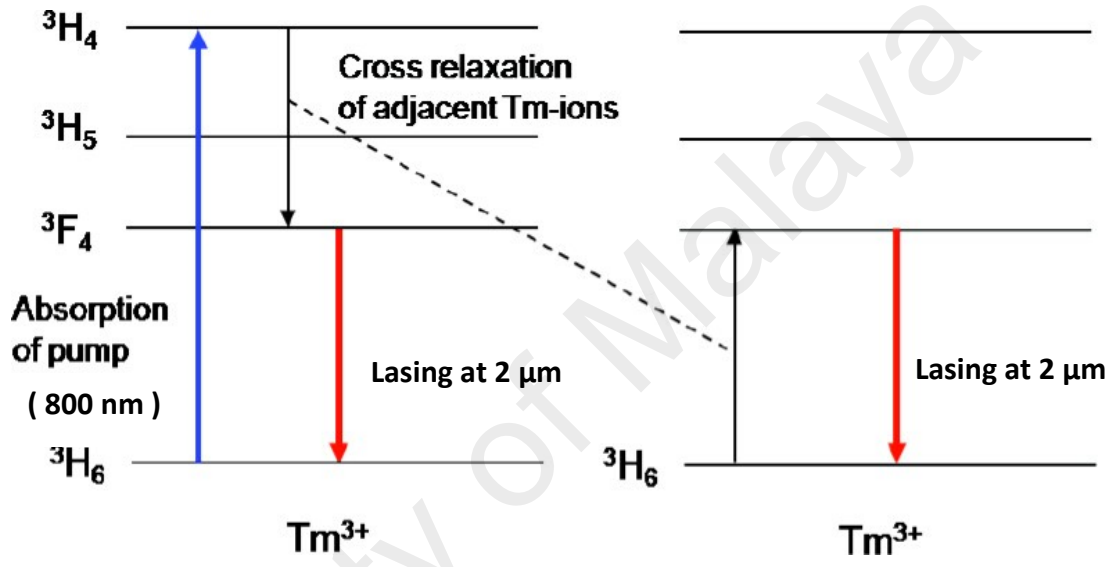

Figure 3.1: Energy level diagram showing cross-relaxation of excited Tm^{3+} into the metastable level.

3.3 Lasing Performance of Continuous Wave TDFL in Ring Cavity

In this section, the performance of continuous wave (CW) TDFL is investigated based on a commercial TDF (**Nufern SM-TSF-9/125**) with 800 nm pumping. **Figure 3.2** shows the experimental setup, which was carried out at the optimum active fiber length of 2 m. The TDF used has a core and cladding diameters of 9 μm and 125 μm, respectively with a numerical aperture of 0.15. It has a Tm^{3+} ion absorption of 27 dB/m at 793 nm.

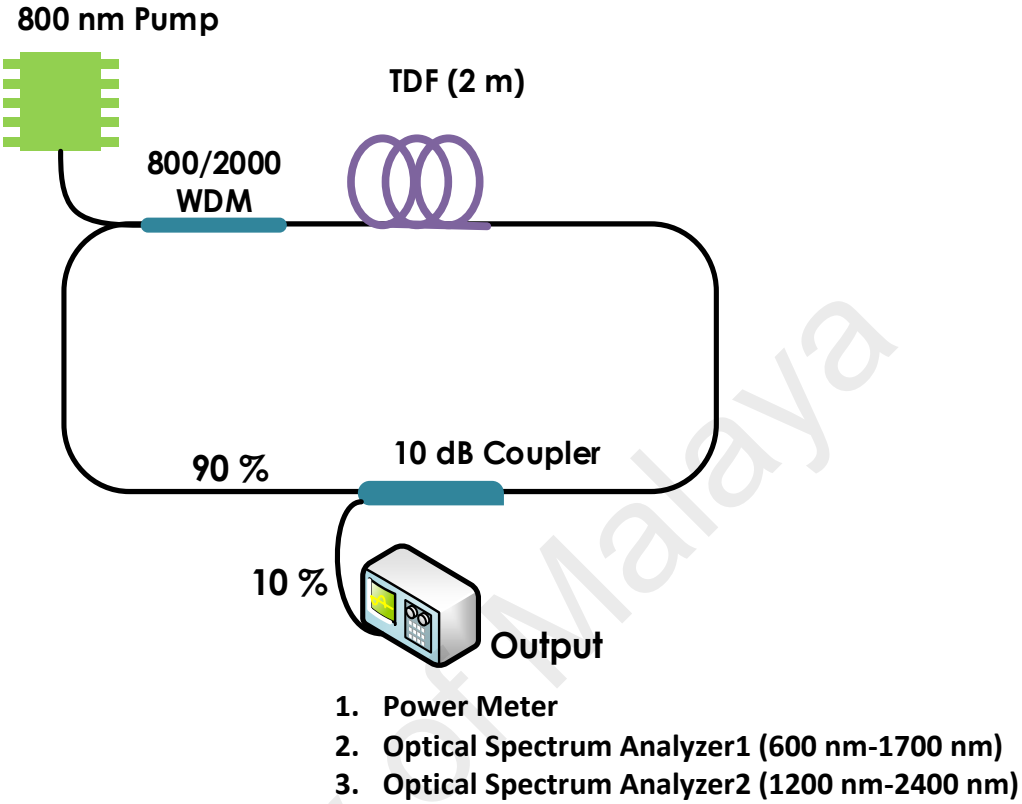

Figure 3.2: Experimental setup for the TDFL in a ring cavity configuration.

A 800-nm laser diode with the maximum output power of 182 mW is used as a pumping source for the proposed ring laser. It is launched into the active fiber via 800/2000 nm wavelength division multiplexer (WDM). The output laser is tapped out from a 10 % port of a 10 dB coupler. The remaining signal is channeled through the 90 % port of the 10 dB coupler where it will now come into contact with the 2000-nm port of the WDM, thereby completing the ring cavity. The 10 % port of the 10 dB coupler is connected to a digital power meter (**ThorLabs PM100D/S302C**), optical spectrum analyzer1 (600 nm-1700 nm) (OSA1: **Yokogawa AQ6370B**) and optical spectrum analyzer2 (1200 nm-2400 nm) (OSA2: **Yokogawa AQ6375**).

At first, the amplified spontaneous emission (ASE) was investigated for the TDFL using a 800-nm single-mode pumping scheme. In the experiment, TDF length was fixed at 2 m while the 800-nm pump power is fixed at 155.58 mW. The pump is launched into the fiber when the 10 dB coupler is removed from the cavity and the forward ASE is monitored using two OSAs i.e. OSA1 and OSA2 accordingly with different wavelength specification. **Figure 3.3** shows the spectrum of TDF where the residual pump is observed at the wavelength of 804.61 nm, while the 1614.09 nm line is a second order pump from the laser diode.

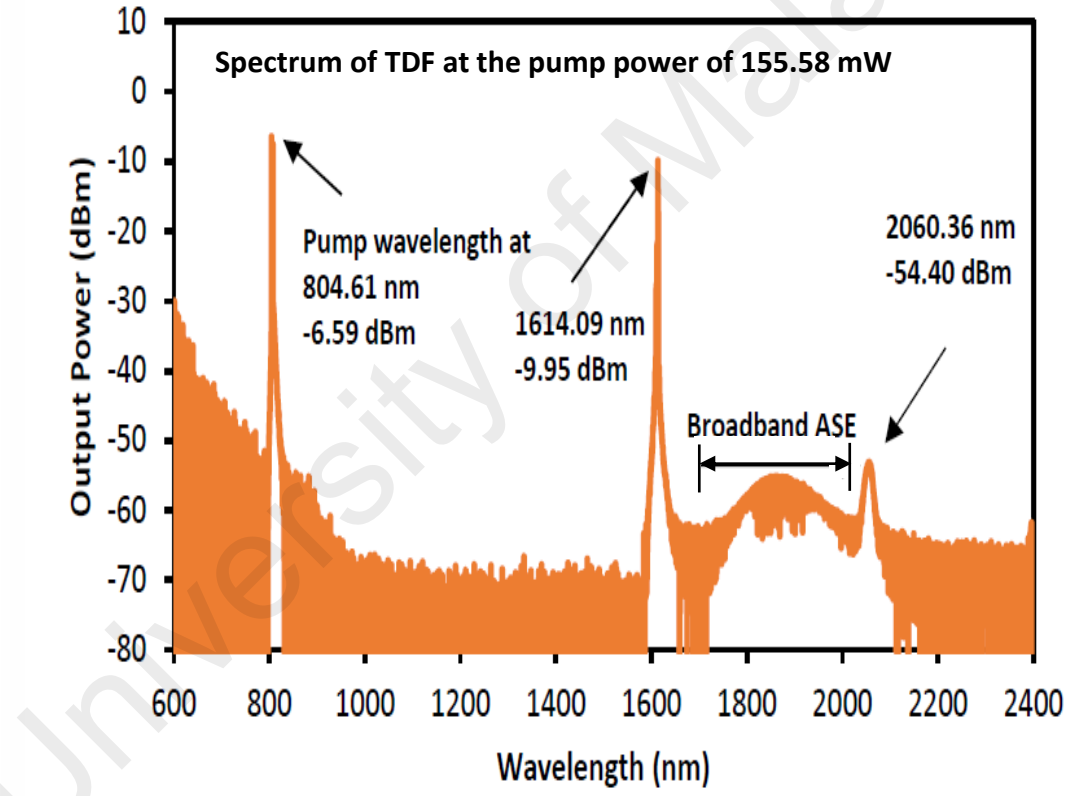

Figure 3.3: Spectrum of TDF at the pump power of 155.58 mW.

As seen in the figure, the TDF emits broadband ASE at a 1720 - 2010 nm region as pumped by the 800 nm photons. The peak emission is obtained at the centre wavelength of 1872 nm. It is also observed that a broad ASE peaking at 2060.36 nm is achieved by

the 800 nm pumped TDF. This is most probably due to the shorter wavelength TDF's ASE, which is absorbed and emits at around 2060 nm region. We could conclude that the broad ASE emission in the 1720 - 2010 nm region is achieved through the transition of a thulium ion from $^3F_4$ to $^3H_6$ level. **Figure 3.4 (a)** shows the lasing spectrum of the TDFL recorded by both OSA1 and OSA2 alternately when the 800-nm pump power was 182 mW.

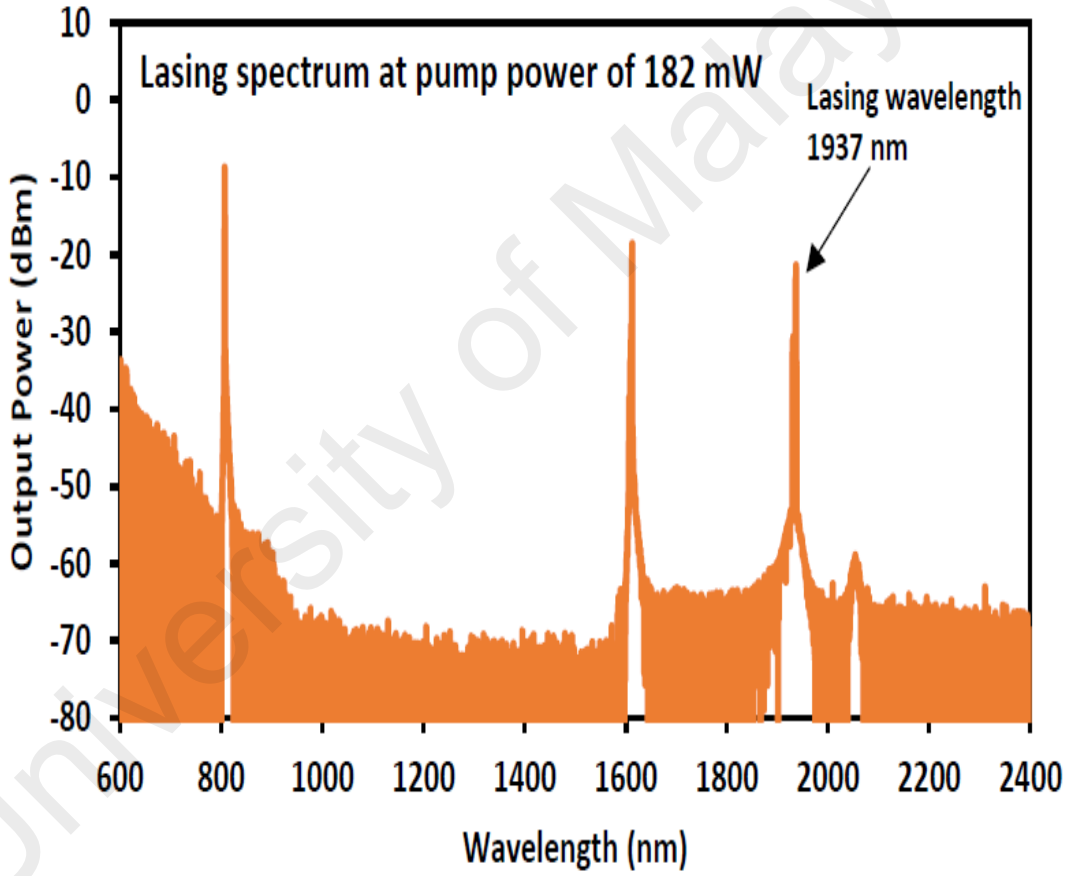

(a)

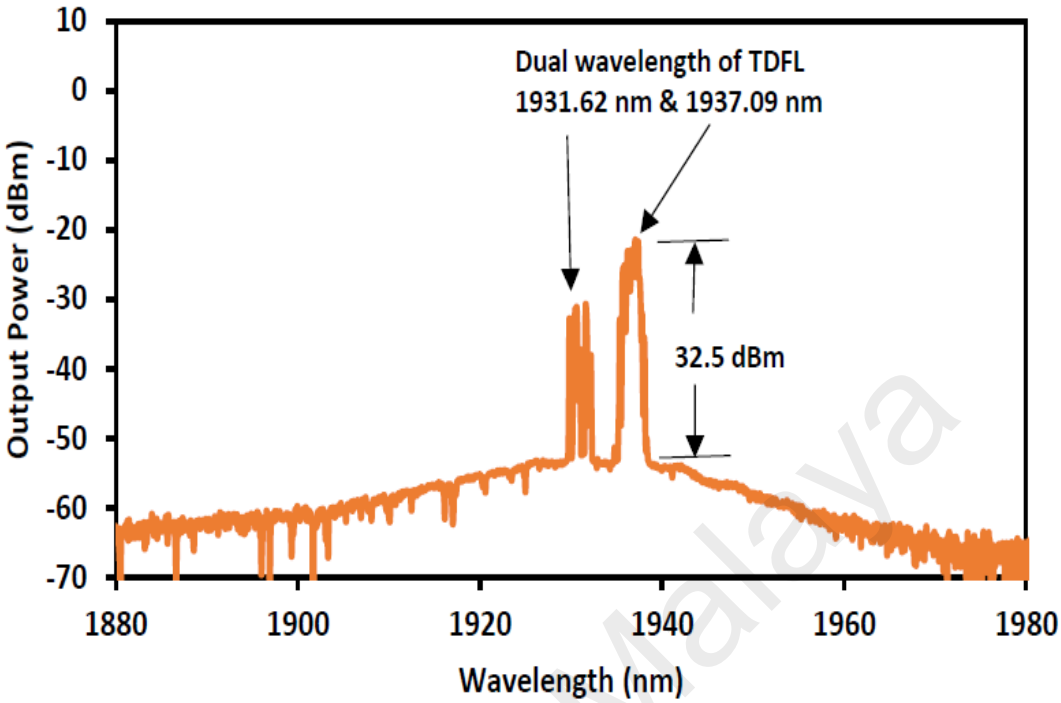

(b)

Figure 3.4: The lasing spectrum of TDFL at the pump power of 182 mW in a scanning range of **(a)** 600-2400 nm. **(b)** The enlarged lasing spectrum spanning within 1880 -1980 nm.

The TDFL produces dual-wavelength output operating at 1931.62 nm and 1937.09 nm with a signal-to-noise ratio of more than 30 dB as depicted in **Figure 3.4 (b)**. The 800-nm pumping allows only ground state absorption to contribute to the stimulated emission and lasing. In this process, Tm^{3+} ions absorb the 800 nm pump photons and are excited to upper laser level $^3H_4$, which causes population inversion between $^3H_6$ and $^3H_4$ level. As the Tm^{3+} ions drop back to the ground state they emit photons in the 2-µm region. On the other hand, the 800-nm pumping creates excitation of photons for the active Tm^{3+} ions. Thulium ions at the $^3H_6$ level absorb pump photons and excited the upper laser level of $^3H_4$. The excited ions are then transferred non-radiatively to the $^3F_4$ level before they relax at the $^3H_6$ level to emit photons in the 2-µm region.

The high thulium doping concentration may increase the possibility of Tm cross-relaxation to occur, by pumping Tm^{3+} ions with the 800 nm pump, the 'two for one' cross relaxation process may contribute to the population inversion at $^3F_4$ level. As a sufficient number of Tm^{3+} ions occupy the ground state, some of the neighbouring ions will absorb the emitted photons, which are the result of other Tm^{3+} ions going through the transition from $^3H_4$ to $^3F_4$ level. Consequently, two ions can be excited to $^3F_4$ level using only one pump photon and this enhances the emission in the 2-μm region.

Figure 3.5 shows the laser output power against the input pump power, which indicates that it increases linearly as the input power increased gradually. The slope efficiency of 16.11 % was obtained with the threshold pump power of 155.85 mW.

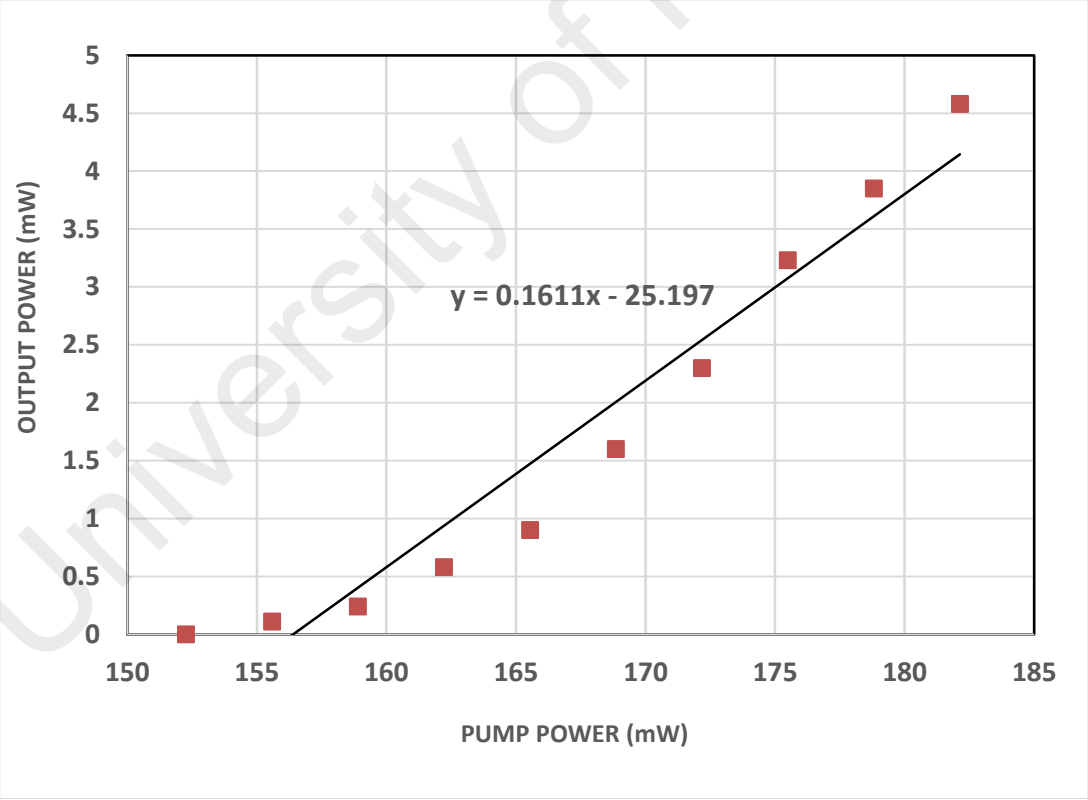

Figure 3.5: The performance of the output power of the TDFL.

The efficiency is relatively high due to a high thulium doping concentration in the gain medium, which supports the cross-relaxation process in the TDFL. Thus, the TDFL requires a smaller pump power to initiate lasing. The high thulium doping concentration in the TDF increases the cross-relaxation process such that the optimum length for lasing is comparatively short. To avoid clustering from a high concentration of rare-earth ion doping, aluminum is added as a host modifier to reduce phonon energy of the core glass in the fiber. This, in turn, increases the probability of radiative emission and improves lasing efficiency.

3.4 Multiwavelength Thulium-Doped Fiber Lasers

A multi-wavelength thulium doped fiber laser (TDFL) with a slope efficiency of 16.57 % is demonstrated using a linear cavity consisting of a broadband mirror and a flat cleaved fiber end in conjunction with 1552 nm pumping. The TDFL produces eleven lines within a wavelength range from 1895 to 1907 nm with a constant spacing of 1.2 nm and signal to noise ratio of more than 27 dB. The multi-wavelength TDFL is capable of generating pulses with a repetition rate of 11.62 MHz and average output power of 93 mW at the maximum pump power of 1100 mW. The proposed multi-wavelength TDFL is suitable for a multitude of real-world applications such as range-finding, medicine, and spectroscopy due to its ability to operate in the eye-safe region of 2-micron.

3.4.1 Introduction to Multiwavelength Fiber Lasers

Multiwavelength fiber lasers have attracted lots of interest in recent years due to their potential applications in wavelength division multiplexing (WDM) communication, precise spectroscopy and optical fiber sensing. There are many different methods to realize stable multiwavelength fiber laser operation, such as liquid nitrogen cooling

(Yamashita & Hotate, 1996), multiple fiber Bragg gratings (Liu et al., 2011), anisotropic gain effects (Chen et al., 2000; Chen et al., 2009; Hamzah et al., 2010), nonlinear optical loop mirror (Liu et al., 2012), four-wave mixing (FWM) (Han et al., 2006), comb filter (Sun et al., 2008) and nonlinear polarization rotation (NPR) (Feng et al., 2006; Zhang et al., 2008). In the past two decades, most of the previous investigations of multiwavelength fiber lasers focus on 1 and 1.5 μm band. Since 2 μm lasers have lots of applications in LIDAR, communication and atmospheric sensing, they have also attracted broad attention in recent years. However, there are few reports on tunable or multiwavelength fiber lasers near 2 μm up to now (Geng et al., 2011; Jusoh et al., 2014; Peng et al., 2013).

Usually, the NPR mechanism is used in passively mode-locked lasers to generate ultrashort pulse trains (Tiu et al., 2014). However, the lasers based on NPR effect can also work in another operating regime to produce the continuous wave multi-wavelength emission (Zheng et al., 2013). By adjusting the polarization in the ring-cavity, NPR can induce intensity-dependent loss (IDL) to alleviate mode competition caused by a homogeneous broadening in the gain medium. In this thesis, we proposed and experimentally demonstrated a multi-wavelength thulium-doped fiber laser operating at around 2 μm region based on NPR technique (effect). Since the TDF used in the cavity has a reasonably high nonlinearity, it produces sufficient NPR effect and four-wave mixing (FWM)-induced IDL effect in the laser cavity (Hisyam et al., 2016). In this case, the transmission term varies too fast with the power and thus allows multi-wavelengths to oscillate in the linear cavity. In this work, a high-reflectivity optical mirror is used as a reflector to reduce the threshold pump power while a 1552 nm single-mode fiber laser is used as a pump source.

3.4.2 Experimental Setup for Multiwavelength TDFL

Figure 3.6 shows the experimental setup of the multi-wavelength TDFL using a simple half-opened linear cavity, which is formed by the broadband mirror and an output coupler reflector. The 5-m long TDF is used as the gain medium of the fiber laser. It has a numerical aperture (NA) of 0.15, core and cladding diameters of 9 and 125 µm, respectively, loss of less than 0.2 dB/km at 1900 nm, and peak core absorption at 1180 and 793 nm are 9.3 and 27 dB/m, respectively. The TDF is pumped by a 1552-nm fiber laser via a wavelength division multiplexer (WDM, 1550/2000).

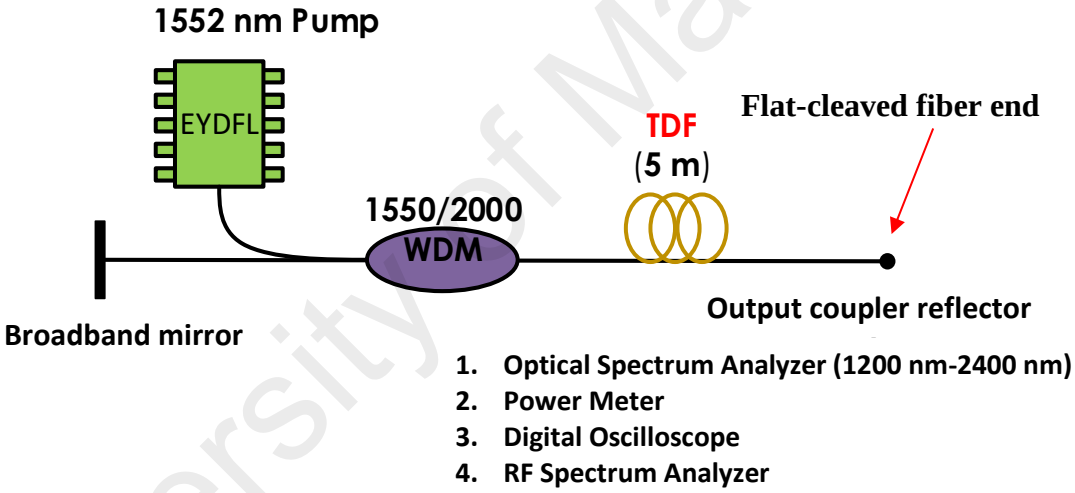

Figure 3.6: Experimental setup for the multi-wavelength TDFL.

The output coupler reflector is formed by the perpendicular cleaved fiber end, which has a 4 % Fresnel reflection. The multi-wavelength output spectrum and power of the TDFL are analyzed by using an optical spectrum analyzer (1200 nm-2400 nm) (OSA; **Yokogawa AQ6375**) with a resolution of 0.02 nm and optical power meter (OPM), respectively. The temporal characteristic of the laser is investigated using a 500 MHz digital oscilloscope and RF spectrum analyzer via a fast photodetector. The total cavity length is measured as 16.2 m which specify 2 times of a single trip length of 8.1 m.

The laser operation is supposed to be grounded on the TDF gain and the resonance between a broadband mirror and a 4 % Fresnel reflection from the perpendicular cleaved fiber end. When the TDF is pumped by a 1552 nm laser to generate population inversion of thulium ions, the emitted energy is then transferred to thulium ions to generate an amplified spontaneous emission (ASE) in 2-μm region via spontaneous and stimulated emission process. The ASE oscillates in the linear cavity to generate laser when the gain overcomes the total cavity loss. With increasing power of the pump, the multi-wavelength laser is generated due to the effect of the TDF birefringence, which induced round-trip phase variation in the linear laser cavity based on the nonlinear polarization rotation (NPR) effect. The NPR arises due to the high nonlinear effect in TDF and WDM devices. These effects cause the intracavity modulation in the linear cavity configuration which contributing the mode-locked effects.

3.4.3 Result and Discussion on Multiwavelength TDFL

The output spectrum of the proposed TDFL is recorded by an OSA and the result is shown in **Figure 3.7**. At the maximum 1552 nm pump power of 1100 mW, the output spectrum shows two peaks centered at 1552 and 1901.60 nm, which represents the residual pump and multi-wavelength laser respectively within the scanning wavelength from 1520 nm to 2000 nm as shown in **Figure 3.7 (a)**. The lasing peak and residual pump powers are obtained at -6.2 dBm and -24.4 dBm, respectively and thus the difference is 18.2 dB. The output power of the TDFL is measured to be 93 mW by the OPM at the pump power of 1100 mW. Based on the ratio between the peak laser power and the residual pump (18.2 dB), it is obtained that the measured output power is mostly contributed by the multi-wavelength laser. **Figure 3.7 (b)** shows the multi-wavelength laser spectrum, which is obtained within the wavelength region from 1888 nm to 1915 nm. As seen in **Figure 3.7 (b)**, eleven multi-wavelength output lines are obtained at a

range of 1895 and 1907 nm with a constant spacing of 1.2 nm. The lasing wavelength has a signal to noise ratio (SNR) of more than 27 dB with a 3 dB bandwidth of less than 0.1 nm. **Figure 3.7 (c)** shows the spectra of multi-wavelength TDFL at three different pump powers of 500, 800 and 1100 mW. As shown in the figure, the equal spacing of all spectra is maintained at 1.2 nm while the number of lines is increased from 7 to 11 as the pump power is increased from the threshold power of 500 mW to 1100 mW. The peak power of each line is also increased with the pump power.

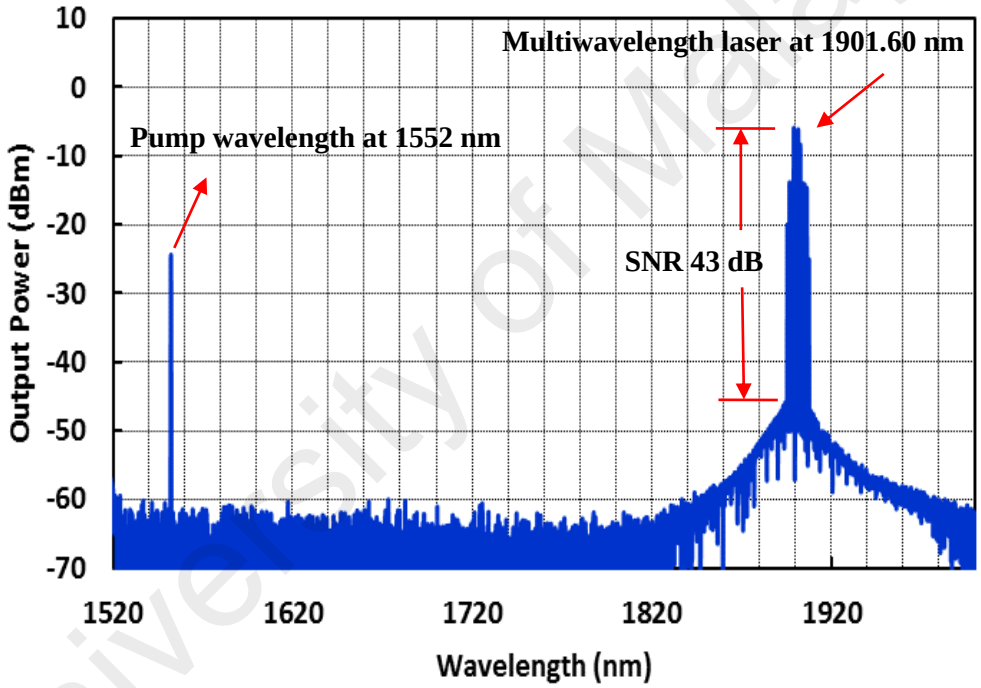

(a)

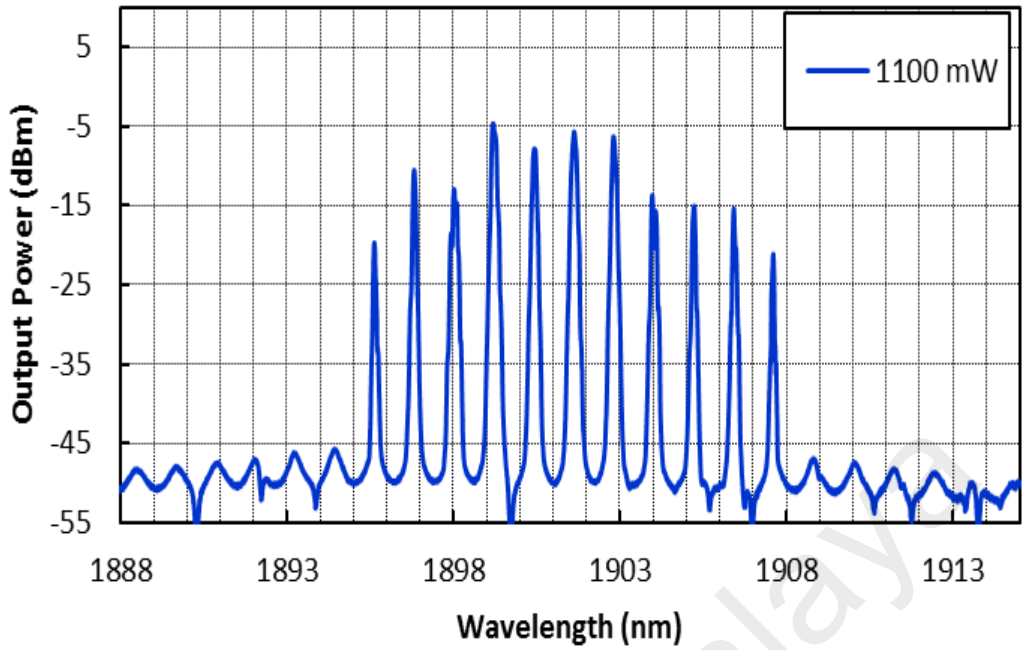

(b)

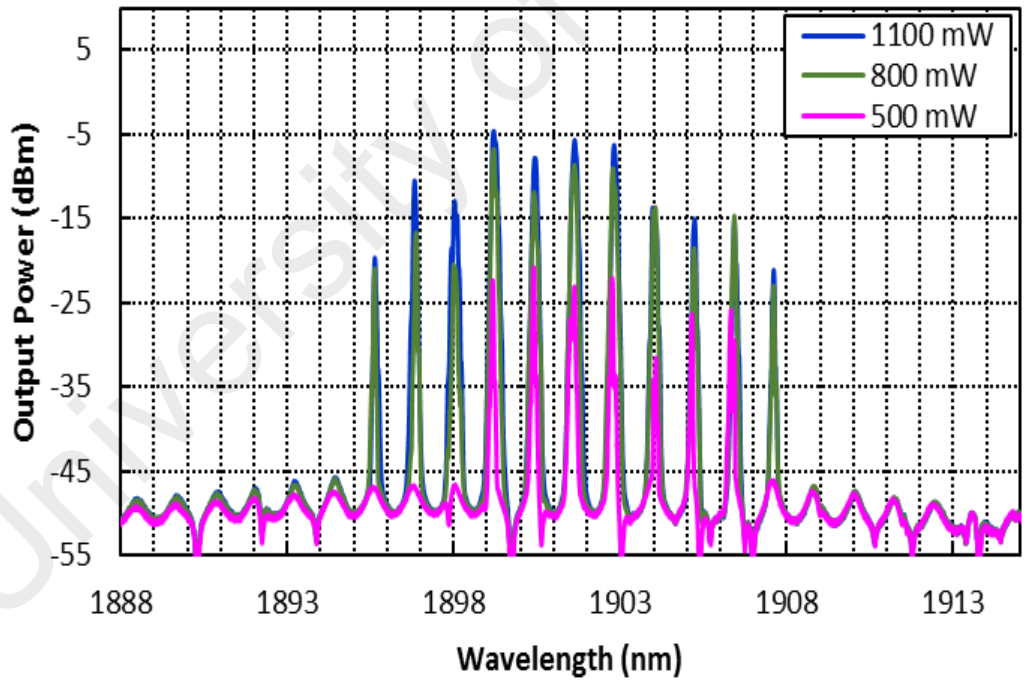

(c)

Figure 3.7: **(a)** Output spectrum of the TDFL at the pump power of 1100 mW. **(b)** The spectrum of multiwavelength TDFL spanning 1888-1915 nm. **(c)** Multiwavelength TDFL at three different pump powers.

Figure 3.8 shows the output power characteristic of the multi-wavelength laser against the 1552 nm pump power. As shown in **Figure 3.8**, the TDFL starts to lase at a threshold pump power of 500 mW to generate a laser operating around 1907 nm region. The output power of the laser is observed to increase linearly with the increment of single mode 1552 nm pump power up to 1100 mW. The slope efficiency of the multi–wavelength laser is measured to be around 16.57 %. For single mode TDFL system, this is the highest slope efficiency, which has been reported so far for the linear cavity configuration. At the single-mode pump power of 1100 mW, the multi-wavelength laser produces the maximum total output power of 93 mW.

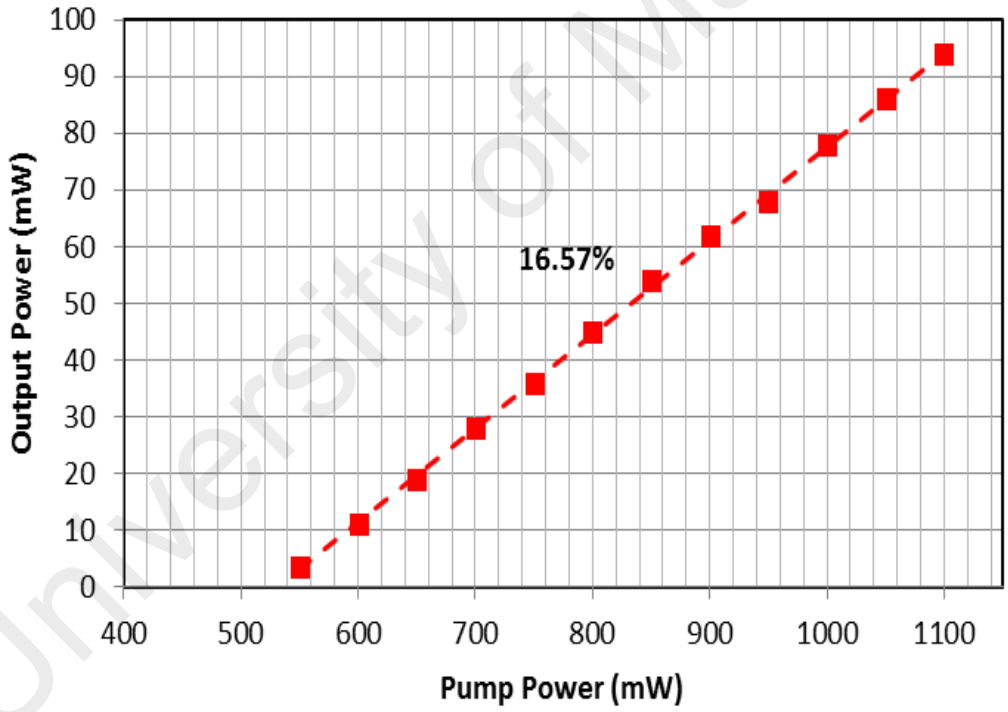

Figure 3.8: The output power of the multi-wavelength laser against the 1552 nm single mode pump power for the TDFL in the linear cavity configuration.

The output spectra of the TDFL is investigated within 60 minutes for a stability test at a maximum pump power of 1100 mW. The result is depicted in **Figure 3.9** which indicates a consistent multi-wavelength line with the same spacing is obtained within the period.

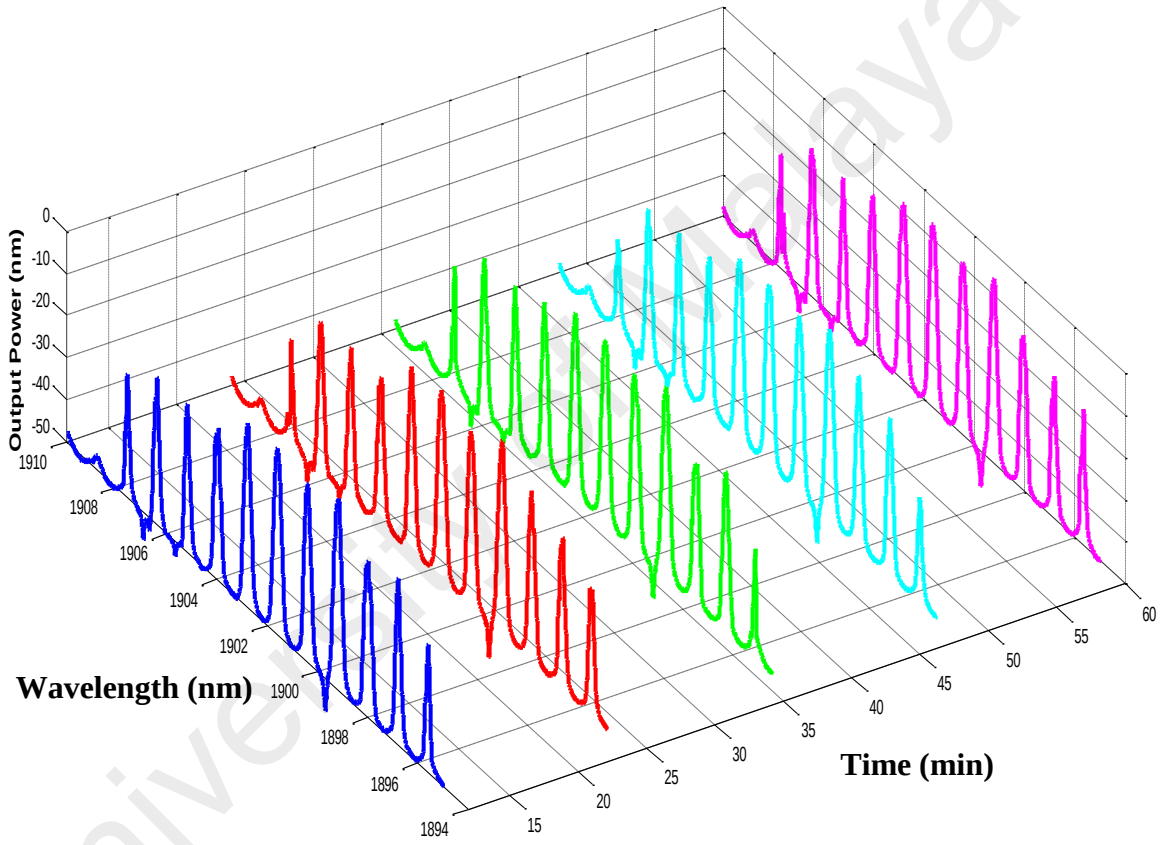

Figure 3.9: Stability of output spectrum within 60 minutes under the pump power of 1100 mW.

The temporal characteristic of the multi-wavelength laser is also investigated using a digital oscilloscope with the help of photo-detector. **Figure 3.10** shows the typical characteristic of the pulse train emitted from the TDFL at the maximum pump power of 1100 mW. The pulse train has a period of 86 ns with a pulse width less than 3 ns as

observed in the digital oscilloscope. At a time of 500 ns, a pulse reaches a voltage of 58 mV meanwhile the highest voltage of 62 mV for the pulse at 582 ns. In the figure, the negative voltage is the undershoot voltage occurs as a result of impedance mismatching in the digital oscilloscope.

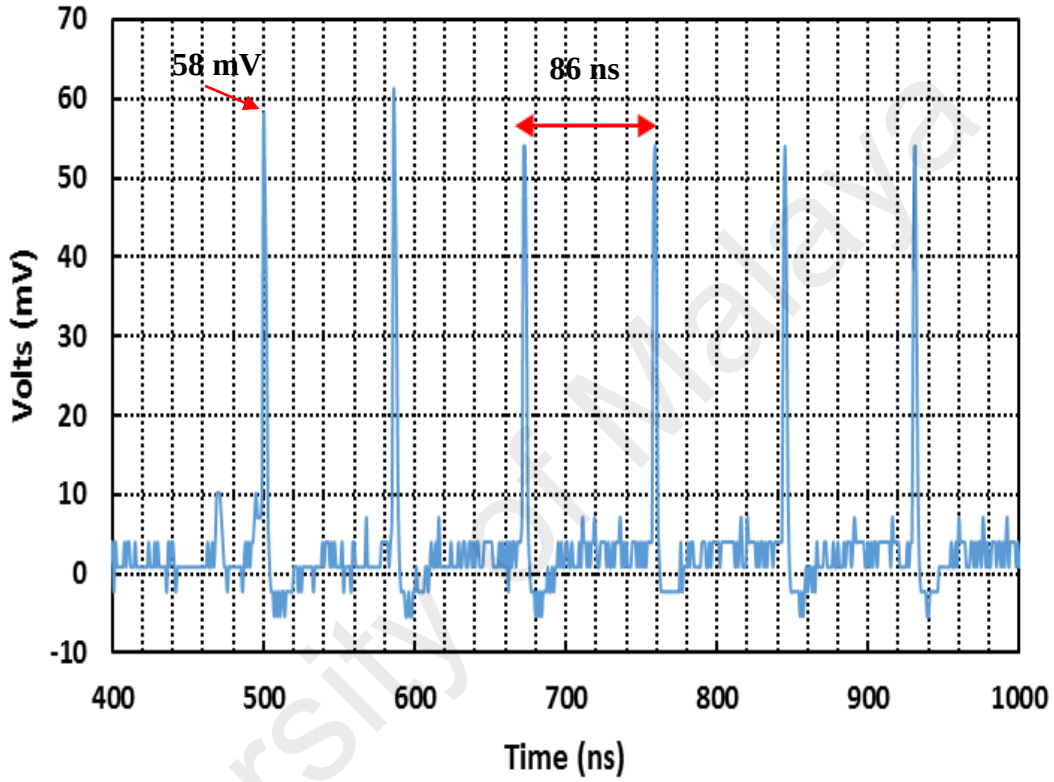

Figure 3.10: Pulse train of the TDFL at the pump power of 1100 mW.

The RF spectrum of the multi-wavelength laser is also recorded by RF spectrum analyzer as shown in **Figure 3.11**. It shows a pulse fundamental repetition rate of 11.62 MHz, which agree very well with a pulse period of 86 ns in **Figure 3.10** and corresponds to double trips cavity length of 16.2 m. The SNR of the RF spectrum is more than 36 dB, which indicates a stable mode-locking operation of the TDFL in the linear cavity. **Figure 3.11** shows the harmonic spectrum of the TDFL within 200 MHz spans. The mode-

locking operation is most probably due to the NPR effect in the linear laser cavity. The harmonic spectrum of the TDFL contains 22 pulses train for spanning from 0 to 200 MHz.

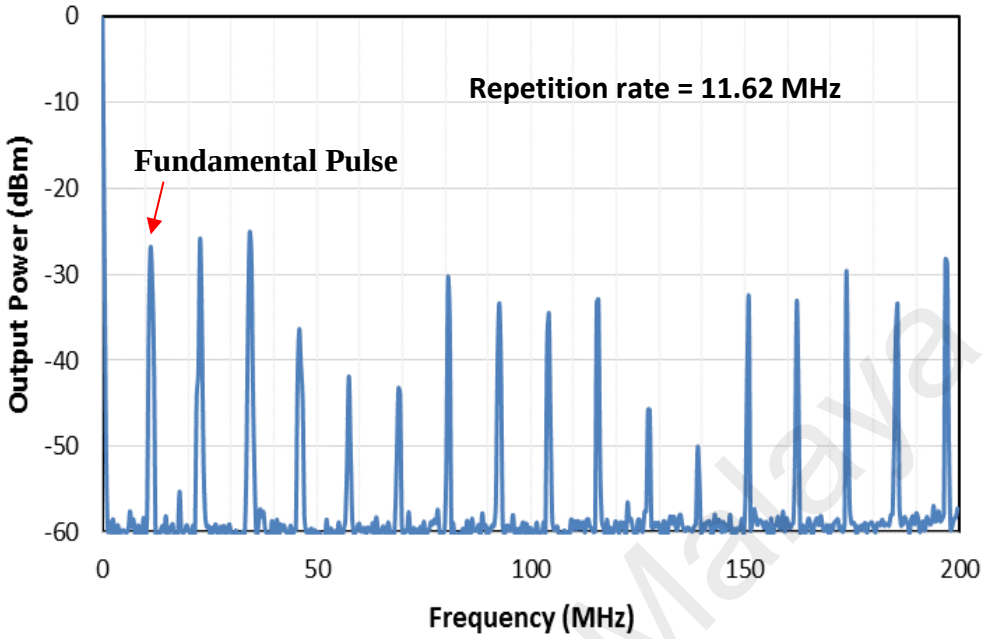

Figure 3.11: A harmonic spectrum within 200 MHz span of the TDFL at the pump power of 1100 mW.

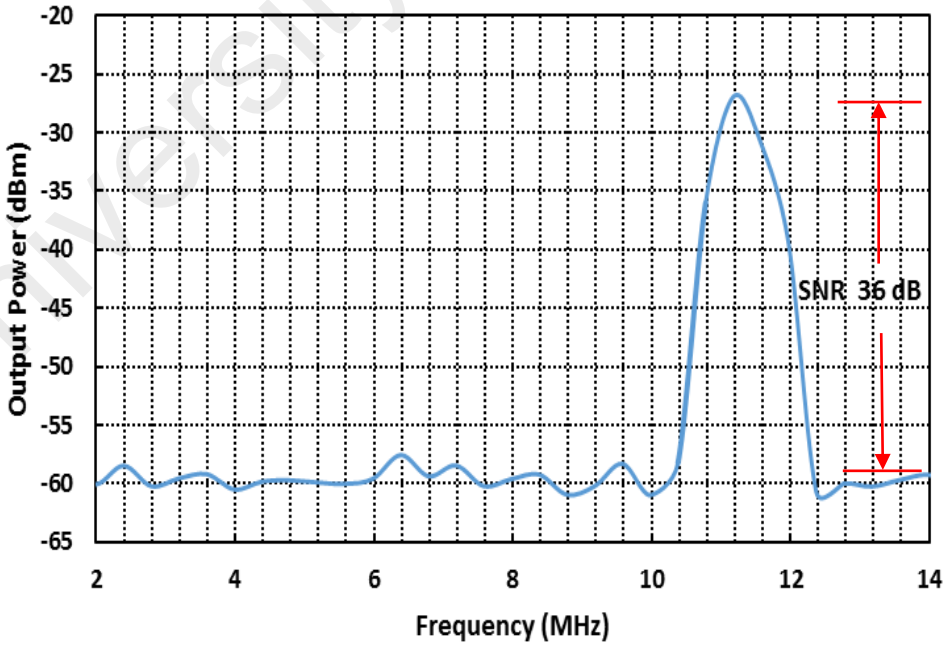

Figure 3.12: RF profile of the fundamental pulse of the TDFL spanning from 2 to 14 MHz.

3.5 Q-Switched TDFL Using Pencil Core Saturable Absorber

In this section, we demonstrated Q-switched thulium-doped fiber lasers (TDFL) using pencil-core flakes as saturable absorber (SA) for the first time. The pencil-core flakes originate from a mundane object, which is ready-available material, fast to prepare, and cost-effective. The SA was fabricated by exfoliating pencil-core flakes onto adhesive surface of a tape and then repeatedly folded over the tape until the flakes homogeneously deposited on the tape. A small piece of the tape is then sandwiched between two ferrules and incorporated in TDFL cavity for Q-switching pulse generation.

3.5.1 Introduction

Pulse fiber lasers have undergone tremendous development in the past few decades since they have quite different characteristics compared with continuous-wave lasers. The high peak power, controllable repetition rate, and pulse duration enable the pulse fiber laser to contribute significantly to laser development for practical applications, including material processing, LIDAR, laser communications, environmental detection, medical care, nonlinear frequency conversion, and laser acceleration (Creeden et al., 2009; Larsen et al., 2012; Pierce et al., 2001; Simakov et al., 2011). Q-switching is one of the approaches to realize the pulse fiber lasers, which are of great interest in recent years for the above-mentioned applications. In addition, Q-switched all-fiber lasers have advantages in terms of their flexibility, large accumulated one-trip gain, high beam quality, and intense power confined in mode field diameters of only a few micrometers. The Q-switching in all fiber lasers has been achieved by applying a mechanical force on highly dispersive fiber Bragg gratings. The mechanical force or vibration could be provided by piezoelectric actuators (Russo et al., 2002), magnetostrictive transducers (Pérez-Millán et al., 2005) or acousto-optics modulators (Delgado-Pinar et al., 2006).

Modulation of the Q-factor can also be realized in passive approaches using semiconductor saturable absorber mirrors (Wang et al., 2012) and solid-state saturable absorber fibers (Tsai et al., 2010). Recently, the search for alternative saturable absorber (SA) materials for passive Q-switching has intensified essentially as the alternative to the traditional SA. For instance, single-wall carbon nanotubes and graphene have emerged as new SA material with superior performance, such as wideband operation, mechanical and environmental robustness (Martinez & Sun, 2013). Graphene from graphite can be defined as single layer of two-dimensional (2D) carbon atoms densely packed into a hexagonal honeycomb structure, with a richness of photonic properties (Bonaccorso et al., 2010). Each layer of graphene only absorbs 2.3 % of incident light, transmitting around 97.7 %, and reflecting less than 0.1 %. These properties of graphene attract enormous interest especially for deployment as SA in passive mode-locked or Q-switched fiber laser (Ma et al., 2012; Saidin et al., 2014). Tremendous work on graphene can be seen since 2004 by Novoselov et al., (2004). The simplest of graphene creation is to use bulk graphite and exfoliate it into an individual panel. This conventional technique is known as mechanical cleavage or Scotch tape (Novoselov, 2011). The method remains popular in obtaining high-quality samples with surfaces are exceptionally clean. Graphite also can be exfoliated from the pencil-core. The pencil-core is made of graphite mixed with a clay binder. The various graphite pencil grades are achieved by altering the proportion of graphite to clay; the more the clay, the harder the pencil (Petroski, 1990). To date, pulse fiber lasers operating at 2 μm pulse have gained tremendous interest because of its exciting and promising applications in biomedical, manufacturing industries, material processing, and remote sensing (Grudinin, 2013). However, only a few works on the generation of Q-switched fiber lasers near 2 μm region have been reported (Saidin et al., 2014; Tang et al., 2014). For instance, Saidin et al. reported the

graphene SA from electrochemical exfoliation technique that can generate Q-switching pulse in 2 μm region (Saidin et al., 2014).

In this section, a Q-switched thulium-doped fiber laser (TDFL) is demonstrated using pencil-core flakes as SA for the first time. The pencil-core SA is fabricated using mechanical exfoliation technique of the pencil graphite. The SA is performed using the Raman spectroscopy to confirm the presence of graphene layer. The SA tape is attached to the fiber end ferrules for generating the TDFL in ring cavity configuration.

3.5.2 Preparation of Pencil Core Saturable Absorber

The pencil core saturable absorber (SA) sample is fabricated using the standard "mechanical exfoliation" technique as shown in **Figure 3.13**. This involves cleaving and crashing a pencil-core into flakes using a metal blade (**Figure 3.13 (a)**). The pencil core is 2B grade and made of graphite mixed with the clay binder. Then, the flakes are placed on Scotch tape before the tape is repeatedly folded over the flakes and opening it up again (**Figure 3.13 (b)**). This folding and opening process of the tape is repeated as many times as possible to harvest the graphite fragment. Once the tape is coated with a relatively thin layer of graphite, this process is stopped. As a result, the area (2.5 cm × 6 cm) of pencil-core flakes is formed and called as pencil-core tape (**Figure 3.13 (c)**). A small piece of pencil-core tape is then cut to be deposited onto the fiber end surface of the ferrule with index matching gel is used as holding agent (**Figure 3.13 (d)**).

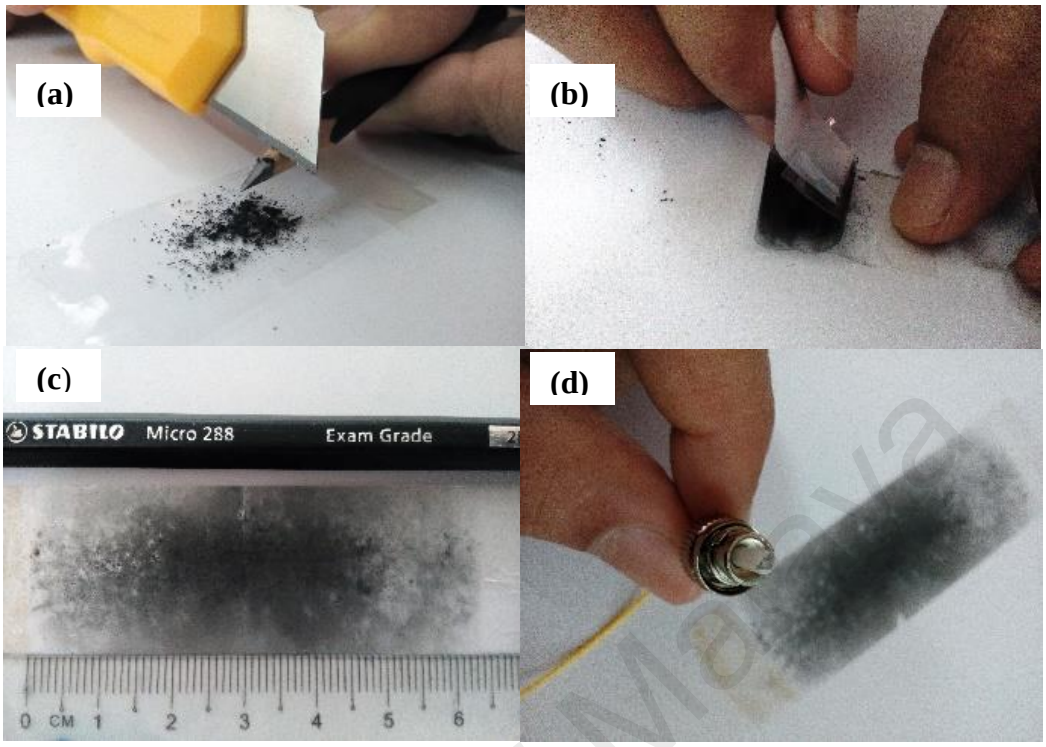

Figure 3.13: **(a)** Mechanical exfoliation from pencil core. **(b)** The pencil-core flakes are exfoliated onto the sticky surface of the tape. **(c)** The homogeneous pencil-core flakes layer is on the tape. **(d)** A small piece of pencil-core tape is cut and deposited onto the fiber end connector.

Raman spectroscopy (Raman microscope, **Renishaw**) is performed to confirm the presence of graphene layer on the surface of pencil-core tape using laser excitation at 514 nm with an exposure power of 10 mW as depicted by **Figure 3.14**. The **Figure 3.14** shows the measured Raman spectra in two different areas (A and B) with comparable intensity and three similar prominent peaks within 200 cm^{-1} – 3200 cm^{-1} of Raman Shift. As shown in **Figure 3.14**, both spectra at areas A and B reveal three prominent peaks; D at 1347.34 cm^{-1}, G at 1577.76 cm^{-1}, and 2D at 2707.23 cm^{-1}, which indicates the signature of the graphene layer.

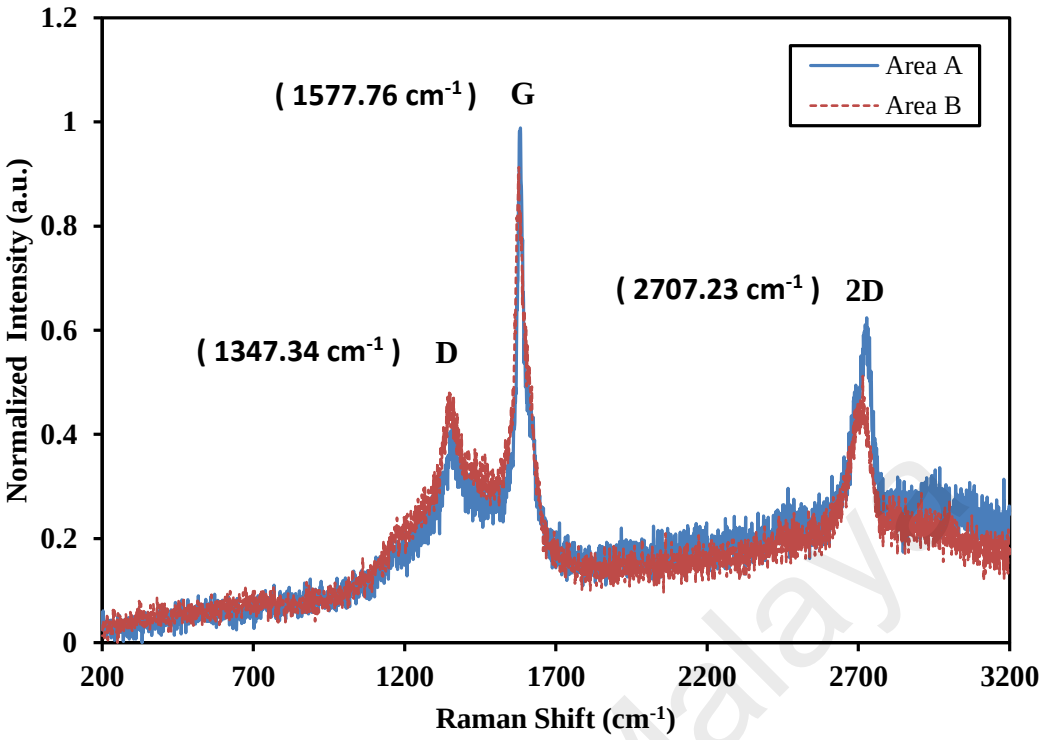

Figure 3.14: Raman spectrum of the pencil-core tape.

The G band contributes to an E_{2g} mode of graphite and is related to the in-plane vibration of the sp^2-bonded carbon atoms, whereas the D band is associated with the vibrations of the carbon atoms with the sp^3 electronic configuration of disordered graphite (Reich & Thomsen, 2004). The intensity ratio of the D and the G bands of the pencil core tape is about 0.42 and 0.57 for area A and B, respectively. Thus, this indicates the defect levels in the pencil core samples for two different areas are almost similar. However, the amount of the structural defects for both areas is not large since the D peak is not very broad. The intensity ratio between the G and the 2D peak can be used to determine the graphene layer (Ferrari, 2007). It was reported that single-layer graphene has a low-intensity ratio, usually lower than 0.5, whereas multi-layer graphene shows a higher intensity ratio (≥1) (Graf et al., 2007). The shape of the 2D peak can also be used to estimate the number of graphene layers. As the graphene layer increases, the full width half maximum (FWHM) of the 2D peak follows. The Raman spectroscopy reveals a broad

2D peak, which indicates that the graphene has a multi-layer structure. As shown in **Figure 3.14**, the FWHM of the 2D peak of both areas is obtained at 60 cm^{-1}. From the intensity ratio of the G and the 2D peaks and FWHM, it can be concluded that the number of graphene layers is highly oriented pyrolytic graphite (HOPG) (Ferrari et al., 2006; Graf et al., 2007).

3.5.3 Laser Configuration for Q-Switched TDFL in Ring Cavity

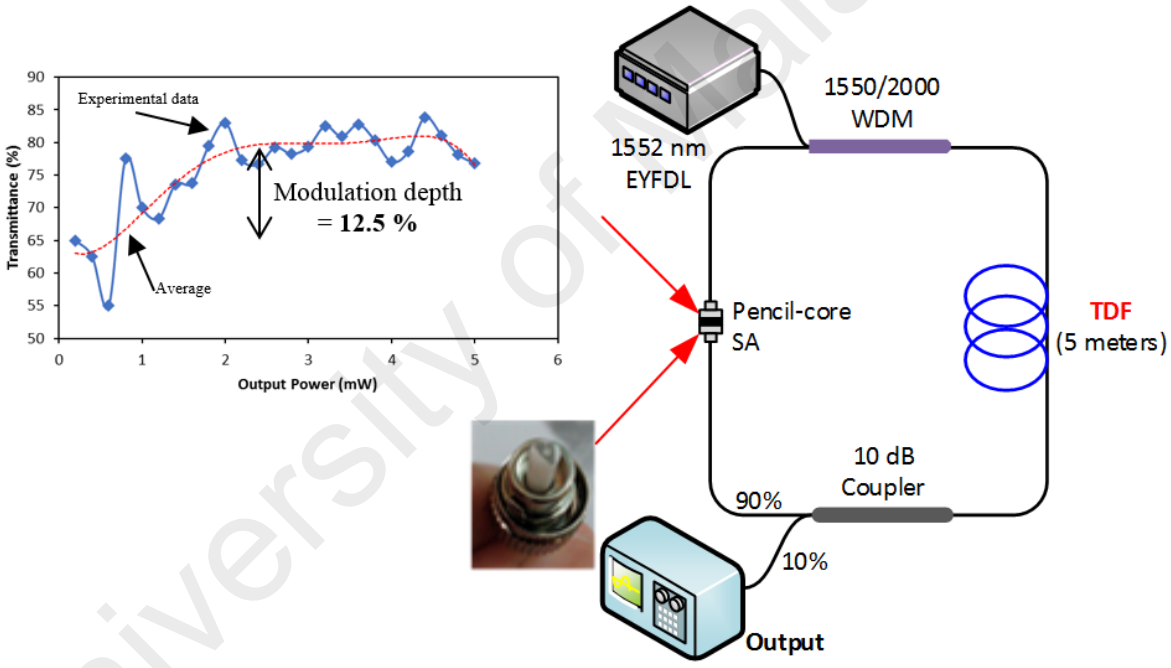

Figure 3.15: Schematic configuration of the Q-switched TDFL based on pencil-core SA. Inset shows the modulation depth of SA.

Figure 3.15 shows the schematic configuration of the proposed Q-switched TDFL, which uses the pencil core spectrum of the pencil-core tape flakes-based SA as a Q-switcher. The SA is fabricated by cutting a small part of the prepared tape (2 mm × 2 mm) and sandwiching it between two FC/PC fiber connectors, after depositing index-

matching gel onto the fiber end. The insertion loss of the SA is measured approximately 0.75 dB at 1940.41 nm. Inset of **Figure 3.15** shows the transmission characteristic of the SA, which indicates the modulation depth of about 12.5 %. In this experiment, a simple ring cavity is demonstrated in which a 5-m-long thulium-doped fiber (TDF) is forward pumped by a 1550-nm erbium–ytterbium co-doped fiber laser via 1550/2000 nm wavelength division multiplexer. The TDF used has the numerical aperture of 0.15, the core and cladding diameters of 9 and 125 μm, respectively, loss of less than 0.2 dB/km at 1900 nm, and peak core absorption at 1180 and 793 nm are 9.3 and 27 dB/m, respectively. The laser output was obtained via a 90/10 output coupler located between the TDF and SA, which tapped out about 10 % of the oscillating light from the ring cavity. The optical spectrum analyzer (OSA,**Yokogawa AQ6375**) is used for the spectral analysis of the Q-switched TDFL with a spectral resolution of 0.05 nm, whereas the 500 MHz oscilloscope (OSC**, LeCroy WaveJet 352A**) is used to observe the output pulse train of the Q-switched operation via a 7 GHz bandwidth InGaAs photodetector (**EOT ET-5010F**). The rise time for oscilloscope and photodetector is about 750 ps and less than 50 ps, respectively. The total cavity length of the ring resonator is measured to be approximately 10.87 m, comprising 5 m TDF and 5.87 m SMF-28 fiber.

3.5.4 Q-Switching Performance of TDFL in Ring Cavity

With the absence of the SA in the ring cavity, the TDFL produces a continuous-wave (CW) lasing as the 1552-nm pump power is increased above 190 mW. As the SA is inserted into the ring cavity, the laser starts to generate a Q-switching pulse train as the 1552-nm pump power is increased above the threshold value of 389 mW. A stable pulse train is obtained within the pump power region of 389–431 mW.

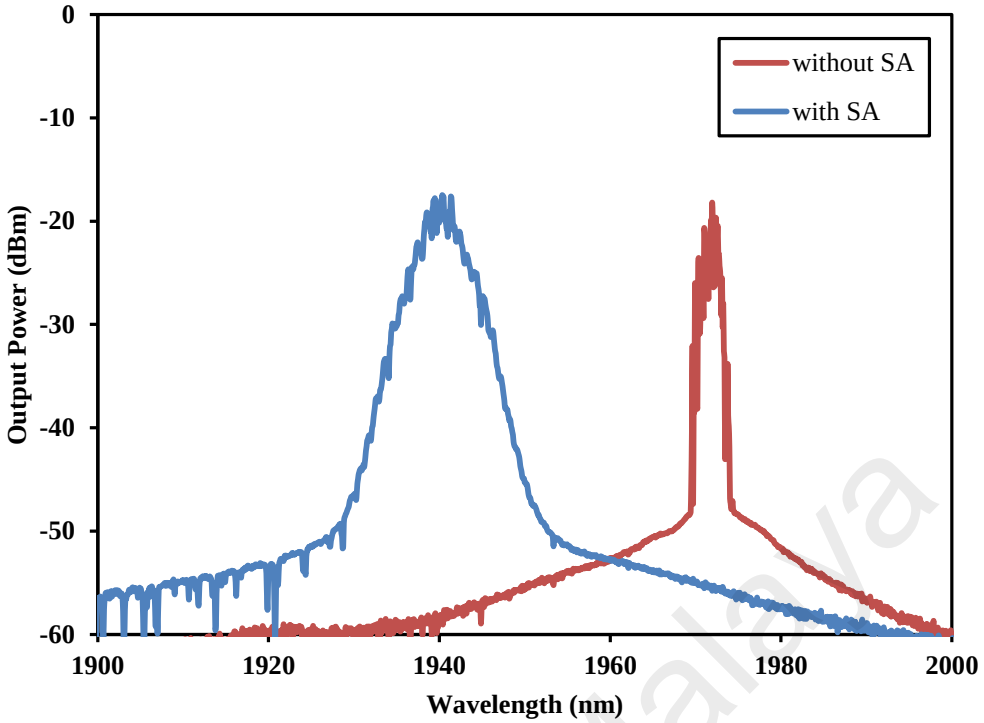

Figure 3.16: Spectral characteristics of TDFL with and without the pencil-core based SA at the 1552 nm pump power of 389 mW.

Figure 3.16 compares the output spectrum of the ring TDFL with and without the SA at the pump power of 389 mW. As shown in **Figure 3.16**, the CW laser operates approximately at 1971.94 nm with a 20 dB bandwidth of 3.6 nm and signal-to-noise ratio of about 30 dB. It is observed that the laser wavelength shifts to a shorter wavelength of 1940.41 nm, and the 20 dB bandwidth of the laser spectrum increases to 16 nm with the incorporation of the SA in the cavity. Compared to the CW laser, the threshold pump power of the Q-switched laser is slightly higher and the operating wavelength shifts to a shorter wavelength due to the insertion loss from the SA. As the loss in the cavity increases, the oscillating laser shifts toward the absorption wavelength for the TDF. Spectral broadening is also observed for the Q-switched laser due to the self-phase modulation (SPM) effect in the ring cavity.

Figure 3.17 (a) shows the typical pulse train of the Q-switched laser, which was obtained from the digital oscilloscope trace when the pump power is fixed at the threshold value of 389 mW. There is no distinct amplitude modulation in the entire Q-switched envelope in the spectrum, which leads to a knowledge that the self-mode locking effect on the Q-switching is weak. **Figure 3.17 (b)** shows the enlarged single envelope of the pulse train, which indicates the FWHM or pulse width of 6.70 µs. The average output power is measured to be about 0.60 mW at this pump power. The repetition rate is 14.95 kHz and thus the pulse energy is calculated to be approximately 40.13 nJ. The pulse energy could be improved by reducing the losses in the cavity. The highest voltage is 3.22 mV at 300 µs. In the figure, the negative voltage is the undershoot voltage occurs as a result of impedance mismatching in the digital oscilloscope.

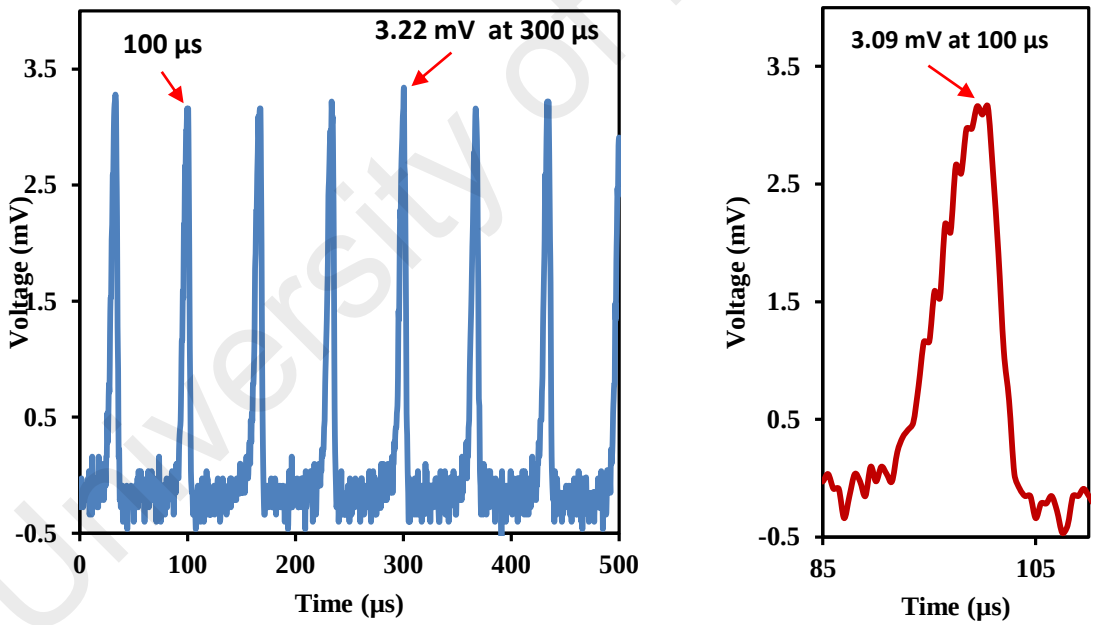

Figure 3.17: Typical oscilloscope trace at the 1552 nm pump power of 389 mW **(a)** pulse train with a repetition rate of 14.95 kHz and **(b)** The corresponding enlarged single pulse envelope of a fundamental pulse.

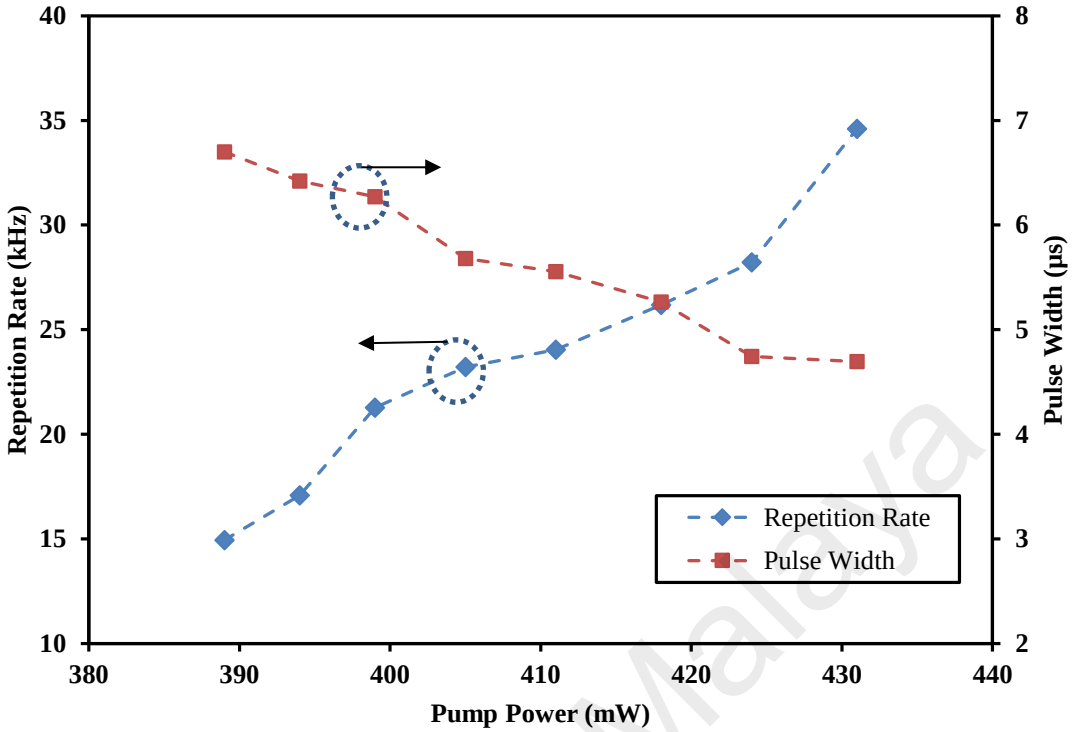

Figure 3.18: Repetition rate and the pulse width as a function of the pump power.

Figure 3.18 shows how the repetition rate and pulse width of the proposed Q-switched laser are related to the 1552-nm pump power. As the pump power increases from 389 to 431 mW, the repetition rate monotonically increases from 14.95 to 34.60 kHz while the pulse width is also detuned from 6.70 to 4.69 μs. This confirms that the constructed laser is working under passively Q-switching. Unlike passively mode-locking condition where the repetition rate of the output pulses is fixed corresponding to the cavity length (Ismail et al., 2014), the repetition rate of a Q-switched fiber laser can be varied with reference to the lifetime of gain medium as well as pump power. Since different pump powers induce different time required to replenish the extracted energy between two consecutive pulses, the detuning of repetition rate takes place.

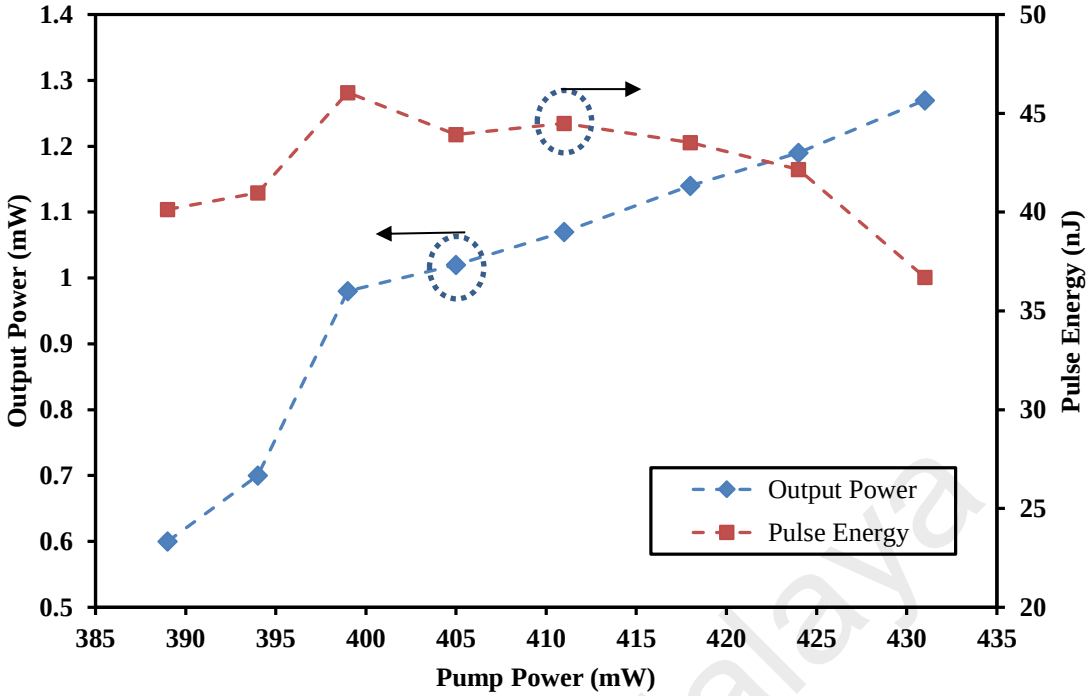

Figure 3.19: Output power and the pulse energy against pump power.

In the experiment, when more gain is provided to saturate the SA, both average output power, and pulse energy are found to increase monotonically with the increment of the pump power as shown in **Figure 3.19**. The output power of 1.27 mW, which corresponds to pulse energy of 36.71 nJ is achieved at the maximum pump power of 431 mW. The fiber laser shows a stable operation without significant degradation of the first reported deposited pencil-core as SA with such output pulse energy level. The obtained pulse energy in the experiment is found to be competitive to the previous reports using graphene-SA (Saidin et al., 2013; Tang et al., 2014). Although such pulse energy still cannot outperform that using convention semiconductor-based SA (Wang et al., 2014), further improvement for scaling up pulse energy is foreseeable with pencil-core SA for high damage threshold together with optimizing the cavity length and cavity loss.

3.5.5 Summary on Q-Switched TDFL

A Q-switched TDFL has been achieved using pencil-core based SA. The SA is fabricated by cleaving the pencil-core flakes onto adhesive surface of a tape, which is then repeatedly folded over to homogeneously distribute the graphite layer on the tape. A small piece of the tape, which is sandwiched in between two ferrules is incorporated in TDFL cavity to realize a stable Q-switching pulse train. The stable Q-switching pulse train is obtained as the 1552-nm pump power is increased above the threshold pump power of 389 mW. At this pump power, the pulse width and the repetition rate are obtained at 6.70 μs and 14.95 kHz, respectively. The highest pulse energy of 46.05 nJ is obtained at a repetition rate of 21.28 kHz when the output power is 0.98 mW. Given by the simplicity of preparing a pencil-core tape, this experiment proves that non-conductive pencil-core can be an alternative to existing graphene-based SA.

3.6 Mode-Locked Thulium-Doped Fiber Lasers Using Graphene Oxide Paper

In this section, we have successfully demonstrated passively mode-locked thulium-doped fiber laser (TDFL) based on a linear cavity configuration using a GO paper-based SA as a mode-locker. The paper -based GO was prepared using the modified Hummer's method. A simple all-fiber passive mode-locked thulium-doped fiber (TDF) linear cavity laser operating at 1901.5 nm with an incorporation of home-made graphene oxide paper-based saturable absorber is practically demonstrated. The TDF linear cavity laser generates mode-locking pulses at a threshold pump power of 540 mW. By varying the pump power from the threshold power to 1052 mW, pulse repetition rates remain constant at 82.4 MHz. At the maximum pump power of 1052 mW, the pulse width is estimated as 25 ps, whereas the pulse energy is calculated as 83.1 pJ.

3.6.1 Introduction

Ultrafast fiber lasers have attracted considerable attention from scientists and researchers due to their potential application in optical telecommunication, medicine, and materials processing (Lin et al., 2007). Among the different types of the ultrafast fiber laser, a passively mode-locked pulsed laser is highlighted for their compactness, reliability and low cost. Many methods had been proposed to generate passively mode-locked, such as nonlinear polarization rotation (NPR) (Tiu et al., 2014), nonlinear amplifying loop mirror (NALM) (Chernysheva, 2012), carbon nanotube (CNT) saturable absorber (SA) (Solodyankin, 2008), graphene SA (Tiu et al., 2014) and graphene oxide (GO) SA (Pan et al., 2016). Compare to artificial saturable absorber approaches (NPR and NALM), film-based SA (CNT, graphene and graphene oxide) perform a better environmental stability and independent to the polarization changes in the cavity. On the other hand, fiber lasers operating in 2 μm wavelength region have also attracted a great attention due to their numerous possible applications. For instance, 2 μm wavelength covers broad atmospheric transmission windows and an eye-safe region which are useful for free space telecommunications, hollow core fiber data transmission and laser radar (Henderson, 1993). Moreover, 2 μm wavelength lasers can be implemented as an instrument for non-invasive surgery (Hüttmann, 2005). Besides, 2 μm laser can also be used for air quality analysis based on the absorption lines of greenhouse gases (Bremer, 2013).

Current research is primarily focused on beyond graphene two-dimensional (2D) materials such as topological insulators (TIs) (Sotor et al., 2014), transition metal dichalcogenides (TMDs) (Li et al., 2015) and black phosphorus (Ismail et al., 2016) as a passive SA. Those materials have superior attributes, such as a mechanical and environmental robustness. However, it requires complex chemical process and limited

wideband operation (Das et al., 2015). So far, enormous research on graphene- based SAs have moved towards to mature technology which guarantee produces the SA with wideband absorption profile, stable pulse generation, and easy to handle. However, they still lack exploration in generating pulsed laser at 2-μm wavelength region. In this section, we have successfully demonstrated passively mode-locked TDFL based on a linear cavity configuration using a graphene oxide paper (GOP)-based SA as a phase-locker.

3.6.2 Preparation of Graphene Oxide Film

In this section, we prepared the GO using the modified Hummer's method. At first, the oxidation of graphite flakes was carried out by mixing sulfuric acid (H_2SO_4), phosphoric acid (H_3PO_4), graphite flakes and potassium permanganate ($KMnO_4$) using a magnetic stirrer. **Figure 3.20** shows the modified Hummer method for preparation of paper-based graphene oxide. The mixture was left for 3 days during the stirring process to allow the oxidation of graphite. The colour of the mixture changes from dark purplish green to dark brown. Later, an H_2O_2 solution was added to stop the oxidation process, and the colour of the mixture changes to bright yellow, indicating a high oxidation level of graphite. The graphite oxide formed was washed three times with 1 M of HCl aqueous solution and repeatedly with deionized water until a pH of 4–5 was achieved. The washing process was carried out using simple decantation of supernatant via a centrifugation technique. During the washing process with the deionized water, the graphite oxide experienced exfoliation, which resulted in the thickening of the graphene solution, forming a GO gel. The GO gel was then mixed again with deionized water to obtain graphene oxide flakes solution.

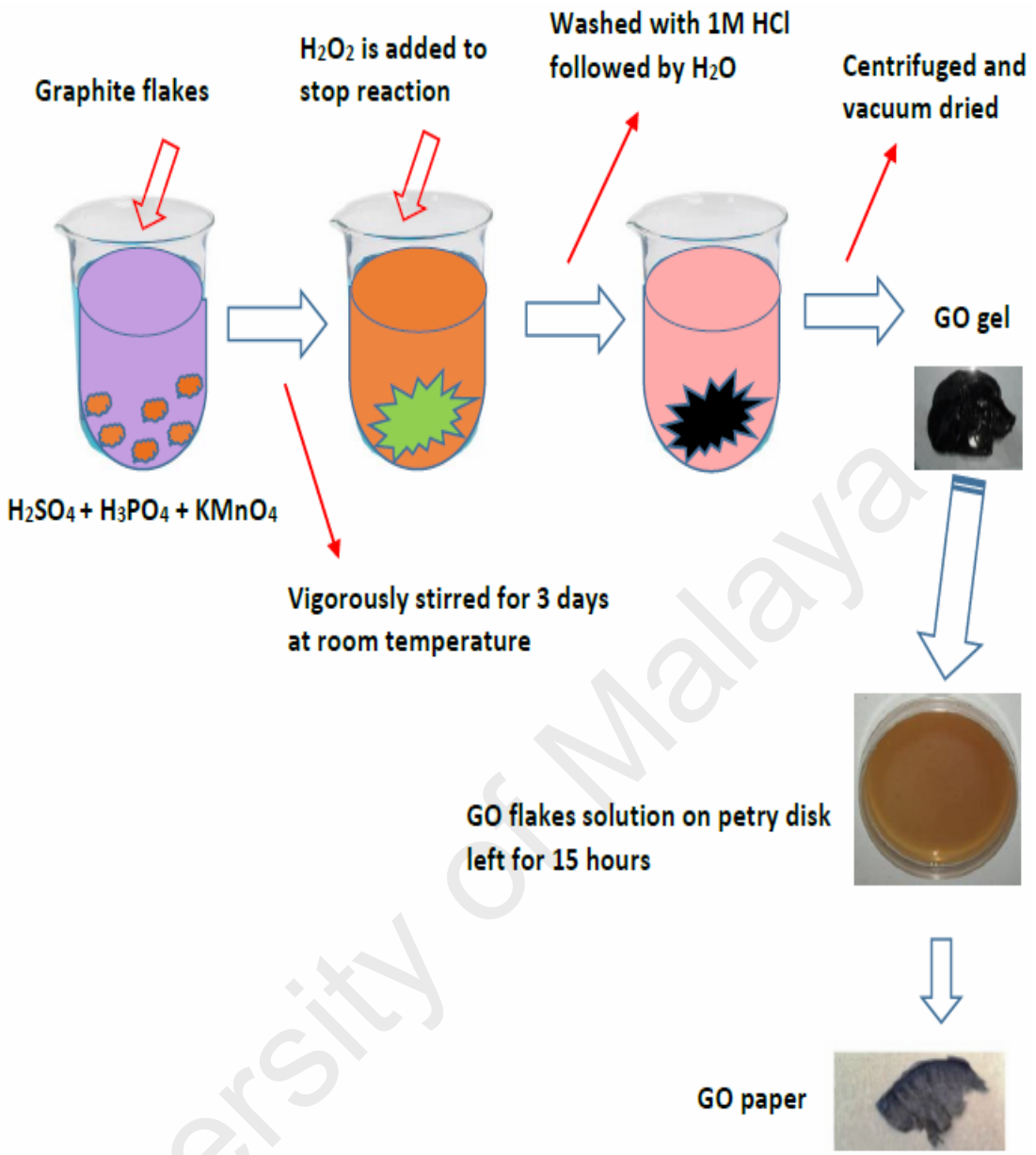

Figure 3.20: Preparation of graphene oxide film using modified Hummer's method.

The graphene oxide solution was thinly spread into a petry disk and left for 15 hours to make a paper-like material. A free-standing graphene oxide paper is obtained after drying. The fiber-type SA device was constructed by inserting a piece of the graphene oxide paper in between two ferrules. The SA device is labeled as a graphene oxide paper based saturable absorber (GOSA) in an experimental set-up.

Raman spectroscopy (Raman microscope, **Renishaw**) is performed to confirm the presence of graphene layer on the surface of GOP by using laser excitation at 514 nm with an exposure power of 10 mW. The detector was a charge-coupled device (CCD) camera. **Figure 3.21 (a)** shows the measured Raman spectrum with two similar prominent peaks within the Raman shift of 100 to 3200 cm^{-1}.

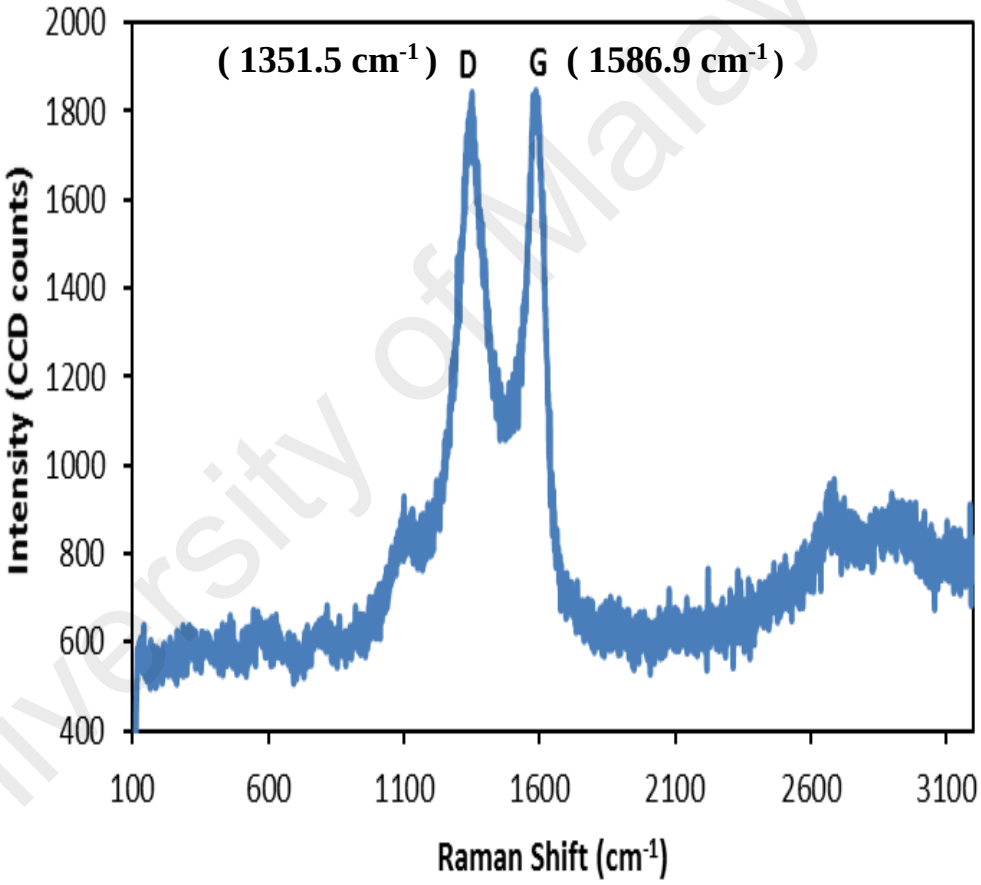

(a)

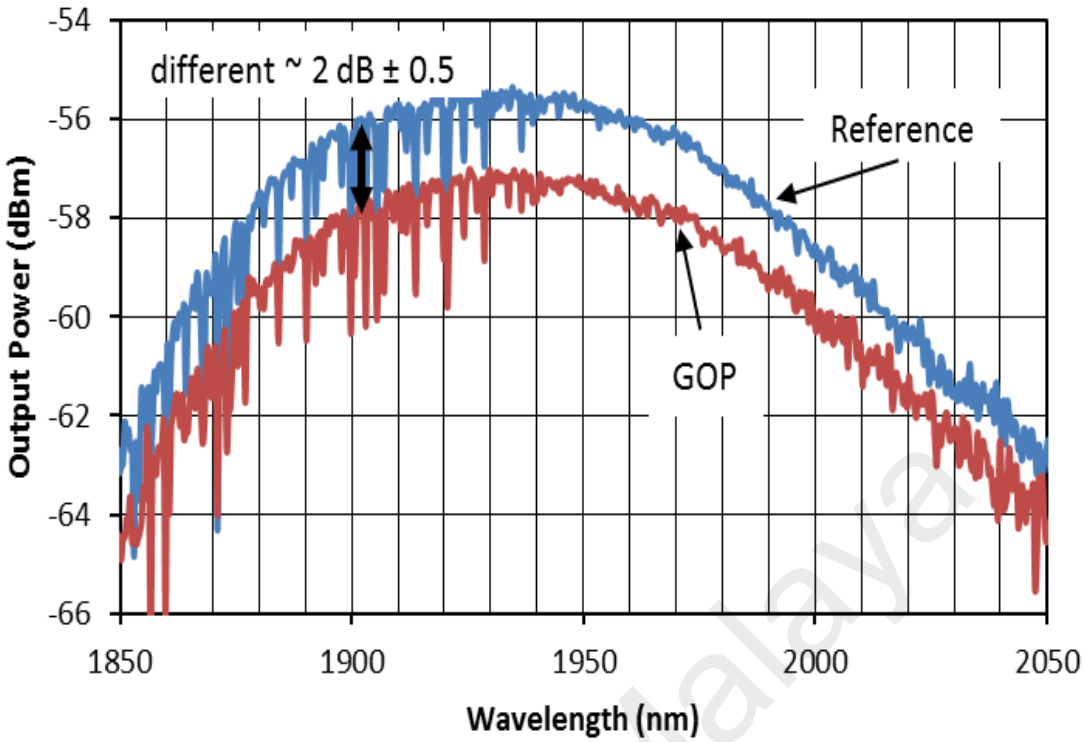

(b)

Figure 3.21: Material characterization of GOP **(a**) Raman spectrum. **(b)** Linear optical profile.

The Raman spectrum reveals two prominent peaks of GO film at 1351.5 cm^{-1} and 1586.9 cm^{-1}, which determine as D and G band, respectively. The G band contributes to an E_{2g} mode of graphite and is related to the in-plane vibration of the sp^2-bonded carbon atoms, whereas the D band is associated with the vibrations of the carbon atoms with the sp^3 electronic configuration of disordered graphite. The intensity ratio of D and G bands of the GOP is about 0.997 which indicates the defect levels of a sample. The amount of the structural defects for both areas is not large since the D peak is not too broad. In addition, slightly weak of D peak indicates a low density of defects and high crystallinity of the graphene. The insertion loss of the SA is measured to be around 2.6 dB at 1901 nm.

3.6.3 Experimental Set-up for Mode-Locked Thulium-Doped Fiber Lasers

The experimental set-up of the proposed mode-locked TDFL is illustrated in **Figure 3.22** which the linear resonator consists of a 5-m long TDF (**Nufern SM-TSF-9/125**) as the gain medium, wavelength division multiplexer (WDM), fiber Bragg grating (FBG), a circulator, a 200-m long single-mode fiber (SMF), GOSA, a polarization controller (PC) and a 10-dB output coupler. The TDF has a numerical aperture of 0.15, core and cladding diameters of 9 and 125 µm respectively, loss of less than 0.2 dB/km at 1900 nm, and peak core absorption at 1180 nm and 793 nm are 9.3 dB/m and 27 dB/m, respectively.

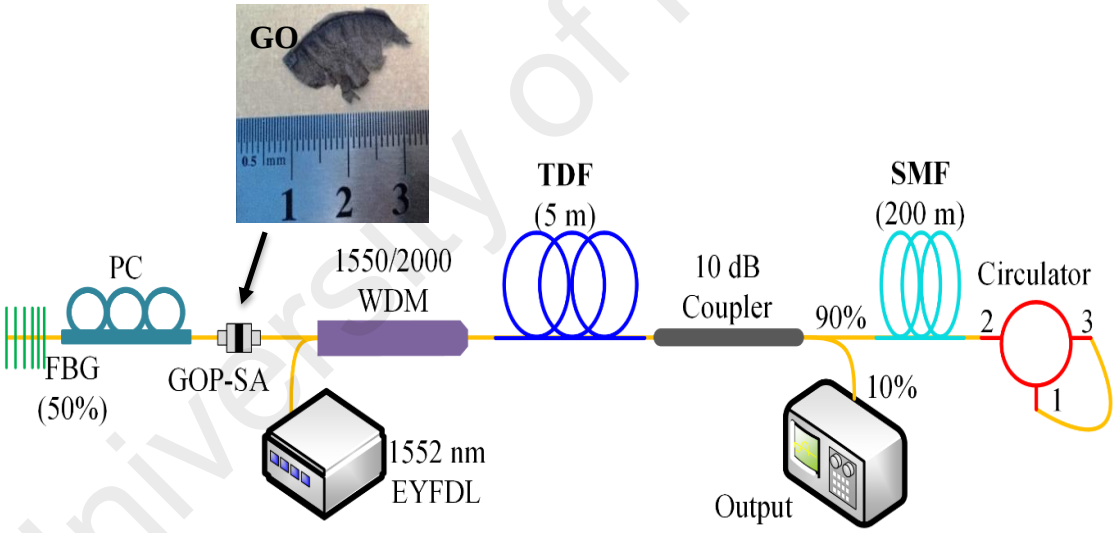

Figure 3.22: Schematic diagram of the proposed mode-locked thulium-doped fiber laser.

A 1552 nm erbium-ytterbium doped fiber laser (EYDFL) is used to pump the TDF via the WDM. To realize a linear cavity configuration, one end of the cavity is connected to FBG while another end is connected to port 2 of a circulator. Ports 3 and 1 of the

circulator are connected to allow the incoming light from port 2 to be reflected back. The FBG (**TeraXion**) operates in 2 μm region with 50 % reflectivity within 0.6 nm bandwidth at a peak wavelength of 1901.6 nm. The 200-m long SMF is incorporated to increase nonlinearity effect in the cavity. The GOSA is incorporated in the linear cavity to achieve the mode-locking operation. A PC is used to adjust the polarization state of the oscillating light. The laser light is extracted from the cavity by a 10-dB coupler which retains 90 % of the light in the cavity for continuous oscillation. An optical spectrum analyzer (OSA, **Yokogawa AQ6375**) with a wavelength resolution of 0.05 nm is used to capture the output laser spectrum while a 500 MHz oscilloscope (OSC, **LeCroy W325A**) in conjunction with a 7 GHz bandwidth photodetector (**EOT ET-5010F**) is used to detect the pulse train.

3.6.4 Performance of Mode-Locking TDFL in Linear Cavity

The oscillator started to operate at mode-locked regime after reaching the launched pump power of 540 mW. Mode-locking operating occurred with a wide pump power tuning range up to 1052 mW. **Figure 3.23 (a)** shows the output spectra of the mode-locked TDFL when the pump power is fixed at 1052 mW. After incorporating the GOP-SA into the cavity, we have obtained the pulsed lasing at 1901.6 nm according to the peak wavelength of FBG with 3dB-bandwidth spectral of 0.3 nm (24.87 GHz). The operating wavelength of the pulsed laser decreases in amplitude due to the increase of cavity loss with the incorporation of GOP-SA. The **Figure 3.23 (b**) shows a generated laser has more than 10 dB peak higher than a pump wavelength which confirms about 90 % of the output power is generated from the laser, not from the pump wavelength.

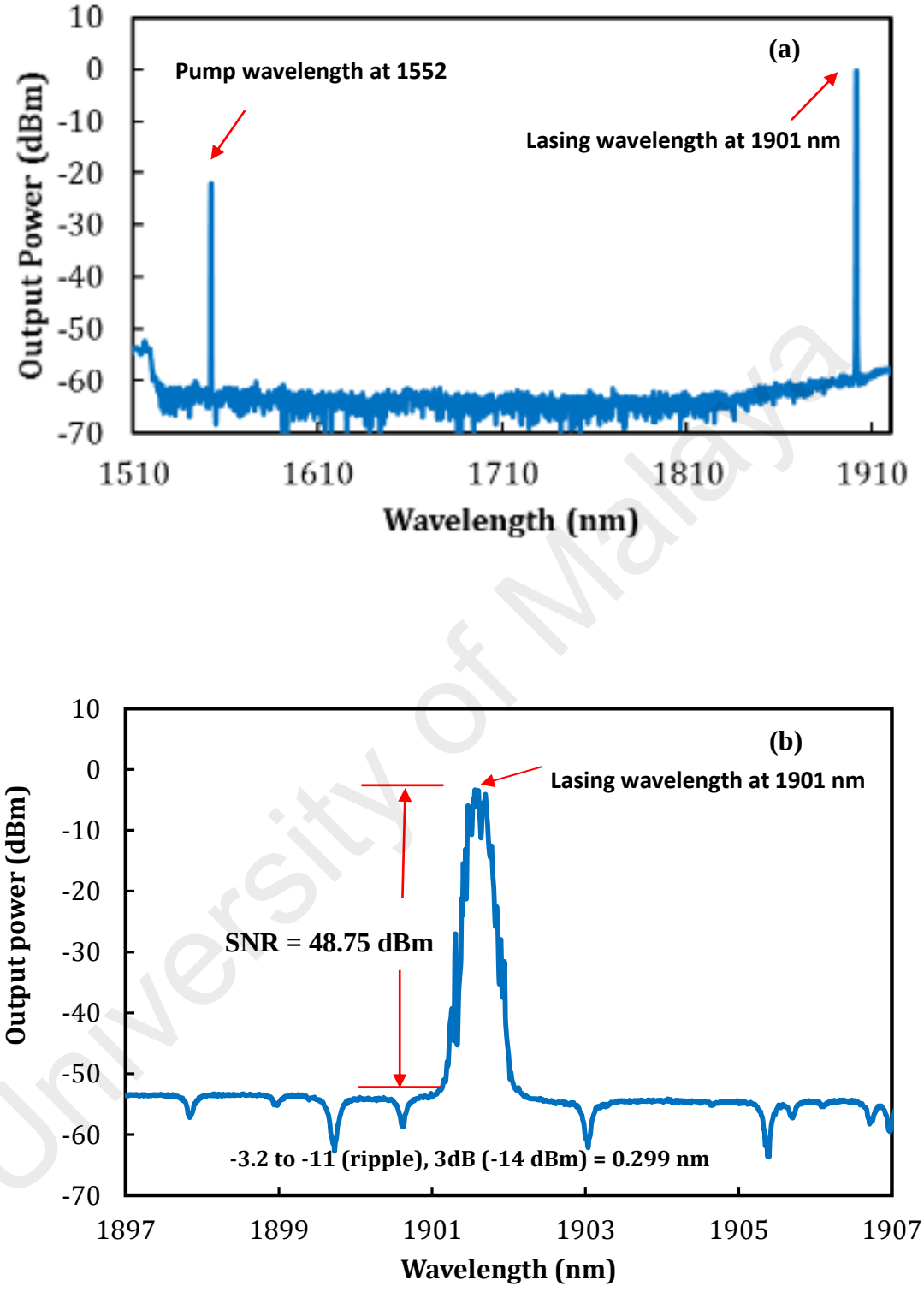

Figure 3.23: **(a)** Optical spectrum in a region of 1510 nm – 1920 nm. **(b)** The enlarged optical spectrum of mode-locked TDFL when the pump power is fixed at 1052 mW.

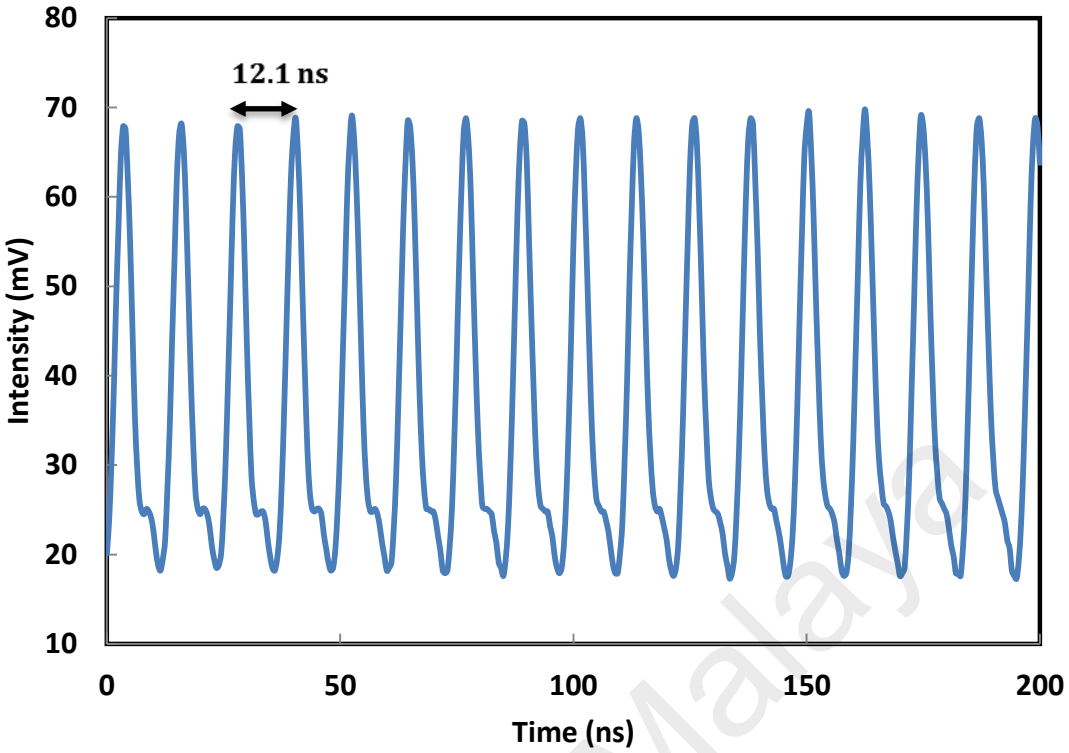

Figure 3.24: A stable mode-locked pulse train of the proposed TDFL in a linear cavity at the pump power of 1052 mW.

A stable mode-locked pulse train at the pump power of 1052 mW is observed as shown in **Figure 3.24**. Throughout the mode-locked tuning range, the pulse repetition rate remains constant at 82.5 MHz, which corresponded to pulse period of 12.1 ns. The oscilloscope trace shows a pulse width of 5.2 ns, which is much broader than actual pulse width. This actual pulse width can be measured by using an autocorrelator or mathematically calculated based on the time-bandwidth product (TBP). Thus, based on $sech^2$ pulse profile, the pulse width is estimated as minimum as 12.66 ps. It is impossible to have the pulse width less than 12.66 ps. If the cavity produces the soliton mode-locked lasers, the 3 dB spectral bandwidth may broaden with Kelly sidebands presence at both left and right of the center wavelength. Then, the ultrashort pulse width of femtoseconds or few-picoseconds will generate. As we remove the GOP-SA from the cavity, the oscilloscope trace disappears and no frequency presences in RF spectrum. This validates

the mode-locked regime due to the GOP-SA, not induced from Brillouin backscattering phenomena.

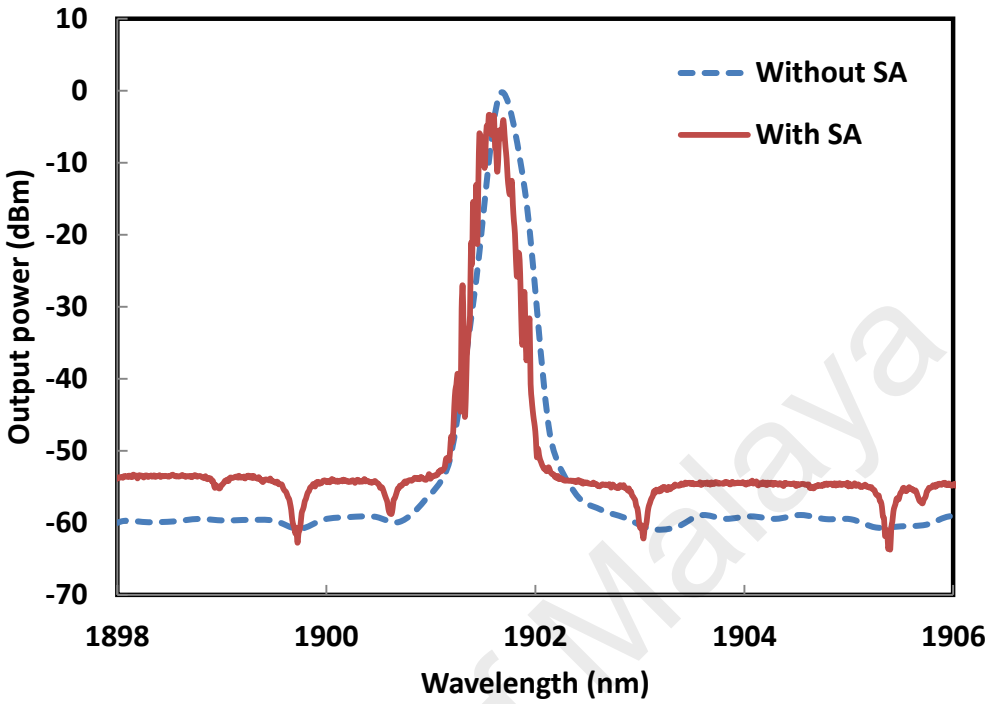

Figure 3.25: Optical spectrum with and without SA when the pump power is fixed at 1052 mW within the same optical resolution of 0.05 nm.

Figure 3.25 shows the output spectra of the TDFL with and without the SA when the pump power is fixed at 1052 mW. Without the SA, we observed the stable continuous wave (CW) operation of TDFL at 1901.7 nm. After incorporated the GOP-SA into the cavity, we have obtained the pulsed lasing slightly blue shifted to 1901.5 nm. The operating wavelength of the pulsed laser shifted to 1901.5 nm as well as a decrease in amplitude due to the increase of cavity loss with the incorporation of GOSA. To compensate for the loss, the laser operates at a shorter wavelength which exhibits a higher gain. Throughout the mode-locked tuning range, output power linearly increases with the increment of pump power. As the pump power increased from 540 mW to 1052 mW, the output power increased from 0.5 mW to 6.9 mW as shown in **Figure 3.26**. These indicate the cavity efficiency of 1.24 % as the TDFL operated in the mode-locked regime.

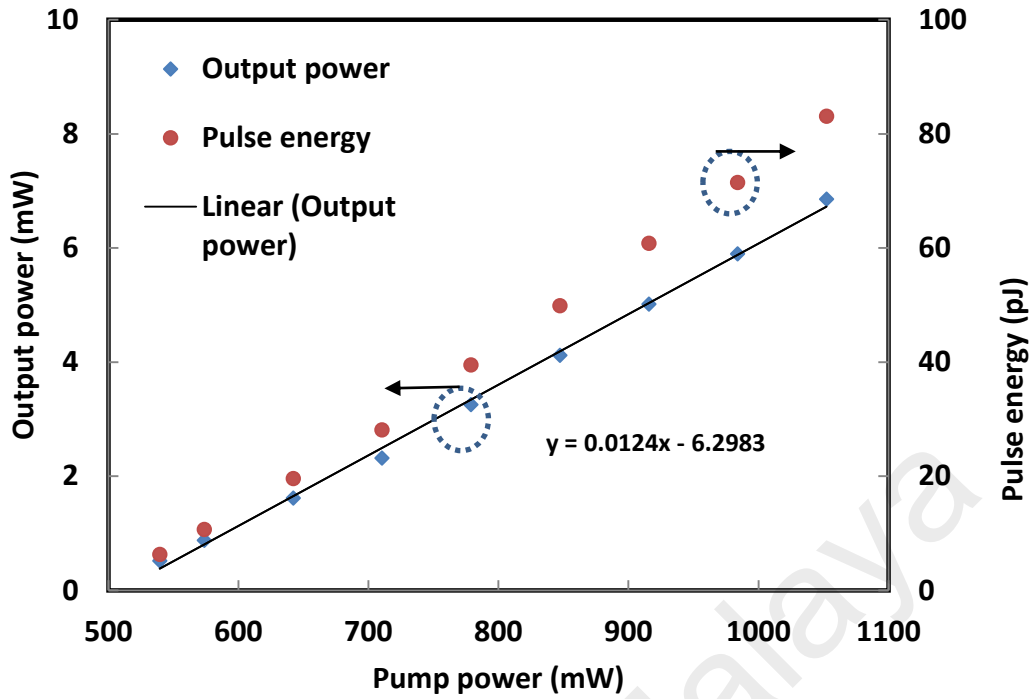

Figure 3.26: Output power and pulse energy of the proposed mode-locked TDFL against the pump power.

Due to the linear increment of output power against pump power, pulse energy exhibits directly proportional to pump power as well. In **Figure 3.26**, the pulse energy increased from 6.3 pJ to 83.1 pJ as the pump power increased from 540 mW to 1052 mW. The stability of the mode-locking operation is further studied with RF spectrum analyzer as shown in **Figure 3.27**. The obtained RF spectrum with 400 MHz spans corresponds to its time domain, which appropriated to the Fourier transform. A signal to noise ratio (SNR) of fundamental repetition rate is about more than 43 dB, where indicates an excellent stability of the mode-locking operation. As shown in the figure, the presence of the repetition rate amplitude is decreased until to 4^{th} harmonic, before it disappears. This validates the obtained pulse width will be narrowed as small as a picosecond, whereas the constant amplitude of repetition rate at every harmonic indicates the femtosecond pulse width size can be achieved (Hisyam et al., 2016; Sotor et al., 2015). Moreover, the

frequency separation of 82.5 MHz is well agreed upon the pulse repetition rate of 12.1 ns as shown in **Figure 3.24**.

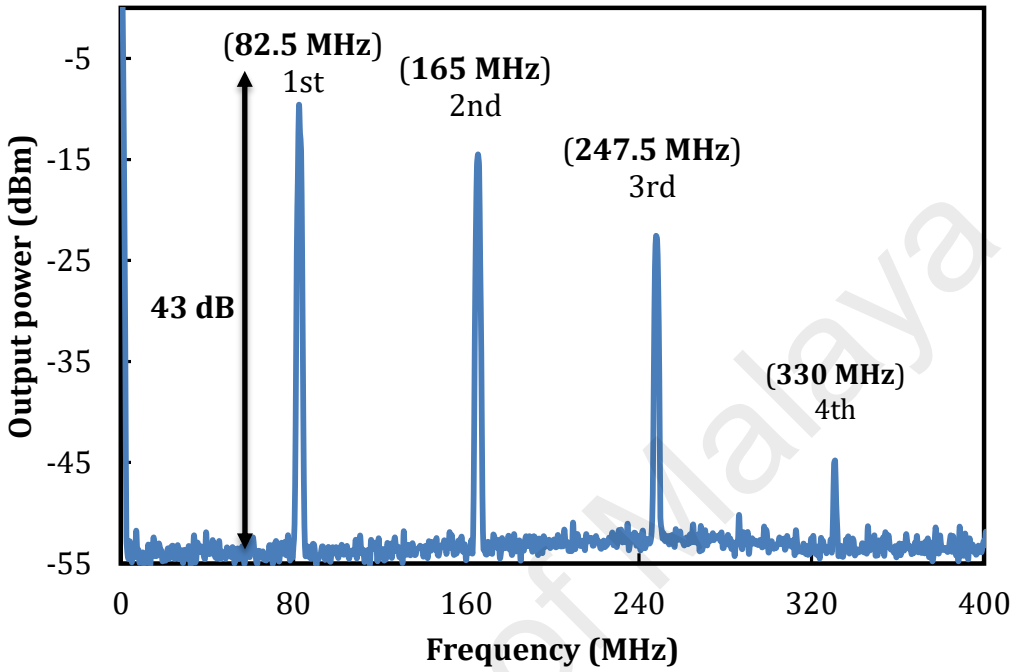

Figure 3.27: RF spectrum of the proposed mode-locked TDFL at the pump power of 1052 mW.

3.6.5 Summary on Mode-Locked TDFL

In summary, we have proposed and practically demonstrated the passive mode-locked TDF linear cavity laser operating at 1901.5 nm with an incorporation of a home-made GOP-SA. The TDFL generates a mode-locking pulse at a threshold pump power of 540 mW. By varying the pump power from the threshold power to 1052 mW, pulse repetition rates remain constant at 82.4 MHz. At the maximum pump power of 1052 mW, the pulse width is estimated as 25 ps, whereas the pulse energy is calculated as 83.1 pJ.

3.7 Conclusion for All TDFL Operations

Various TDFLs operating in multi-wavelength, Q-switching and mode-locking modes were successfully demonstrated. At first, the multi-wavelength TDFL operating in 2-micron region was demonstrated using a linear cavity consisting of a broadband mirror and a flat cleaved fiber end in conjunction with 1552 nm pumping. A 5-m long highly nonlinear TDF is used as a gain medium as well as to produce sufficient NPR and FWM-induced IDL effect in the laser cavity for both multi-wavelength and mode-locking operations. The TDFL achieved eleven output lines within a wavelength range from 1895 to 1907 nm with a constant spacing of 1.2 nm and signal to noise ratio of more than 27 dB at the maximum pump power of 1100 mW. The slope efficiency of the laser is 16.57 % with the maximum output power of 93 mW at the pump power of 1100 mW. In addition, the experimental results indicate that the proposed multi-wavelength fiber can also generate a stable pulse train with a repetition rate of 11.62 MHz. A Q-switched and mode-locked TDFLs have also been successfully demonstrated using 2D nanomaterials of carbon-based passive SA. A Q-switched TDFL has been achieved by using the pencil core-based SA. The SA is fabricated by cleaving the pencil core flakes onto adhesive surface of a tape, which is then repeatedly folded over to homogeneously distribute the graphite layer on the tape. A small piece of the tape, which is sandwiched in between two ferrules is incorporated in a TDFL cavity to realize a stable Q-switching pulse train. The stable Q-switching pulse train is obtained as the 1552 nm pump power is increased above the threshold pump power of 389 mW. At this pump power, the pulse width and the repetition rate are obtained at 6.70 μs and 14.95 kHz, respectively. The highest pulse energy of 46.05 nJ is obtained at a repetition rate of 21.28 kHz when the output power is 0.98 mW. Given by simplicity of preparing the pencil-core tape, this experiment proves that nonconductive pencil-core can be an alternative to existing graphene-based SA. A passively mode-locked TDFL was also proposed and practically demonstrated. The laser

employs the linear cavity configuration to operate at 1901.6 nm with an incorporation of a homemade GOP-SA. The TDFL generates a mode-locking pulse at a threshold pump power of 540 mW. By varying the pump power from the threshold power to 1052 mW, pulse repetition rates remain constant at 82.4 MHz. At the maximum pump power of 1052 mW, the pulse width is estimated as 12.66 ps, whereas the pulse energy is calculated as 83.1 pJ.

CHAPTER 4 : DEVELOPMENT OF THULIUM-YTTERBIUM CO-DOPED FIBER LASERS

4.1 Introduction

Thulium doped fiber lasers (TDFL) operating at near 1900 nm has obtained tremendous interest in the recent years due to the possibility of achieving laser of high output power, high efficiency and retina safe (Blackmon et al., 2012; Zen et al., 2013; Z. Zhang et al., 2011a). As discussed in the previous chapters, TDFL is also useful for specific applications plausible for this wavelength, such as for biomedical, remote sensing and sensor applications (De Young & Barnes, 2010; Fried et al., 2008). However, the quantum efficiency of the generated TDFLs is low when the active medium is produced in silica-based glass fibers, which have high phonon energy. Previously, thulium-doped fibers (TDFs) have been produced with low phonon energy fluoride glass hosts to achieve the optimum efficiency. However, the fluoride glass has a lower melting temperature and thus a special drawing tower is required for fabricating this type of soft glass fibers. Since the phonon energy of silica glass can be reduced by incorporating silica network modifiers like germanium (Ge) and aluminum (Al), there are also many works have been focused on producing silica based host TDFs. It is expected that TDFs with modified silica host can become a promising gain medium for achieving an efficient fiber laser operating at a wavelength near 1900 nm (Walsh & Barnes, 2004). A variety of pumping schemes operating at the wavelengths in the region of ~790, ~1200 and ~1600 nm have been explored for pumping the TDF.

However, high power laser diodes operating at these wavelengths are still costly and limited. An alternative approach to this is co-doping the fiber core with Yb^{3+} so that it can be pumped with a cheaper 980 nm laser diode. The quasi-resonant energy levels of Tm^{3+} with the excited Yb^{3+} level ($^2F_{5/2}$) allows possible $Yb^{3+} \rightarrow Tm^{3+}$ energy transfer which is similar to that in erbium-ytterbium co-doped fibers (EYDFs) (Pal et al., 2010). This opens a possibility of developing an efficient fiber laser operating near 2000 nm based on the 980-nm diode pumping.

On the other hand, pulsed fiber lasers have been extensively investigated in the past decade due to their superior performances for military and industrial applications, such as LIDAR sensing, nonlinear frequency conversion, and material processing. Most pulsed fiber lasers demonstrated so far are based on ytterbium- and erbium-doped fibers (Harun et al., 2012; Huang et al., 2009; Pan et al., 2007). For instance, Q-switched ytterbium-doped fiber lasers operating at 1-μm spectral region have been well-commercialized for material processing applications, such as marking, trimming, drilling and cutting (Huang et al., 2009; Pan et al., 2007). Recently, pulsed fiber lasers operating near 2000 nm are becoming emerging laser sources for scientific and industrial applications, because of their unique advantages in terms of eye-safe wavelength, and high absorption in greenhouse gases, liquid water, and most polycarbonate materials (Harun et al., 2013). Both active and passive techniques have been used to generate Q-switched and mode-locked fiber lasers near 2000 nm (Eichhorn & Jackson, 2007a; Harun et al., 2013; Ma et al., 2013; Sobon et al., 2013). In the previous chapter, a Q-switched and mode-locked TDFLs have been demonstrated using graphite based materials as a saturable absorber (SA).

Over the last few years, the carbon nanotubes (CNT) material has been widely used as a saturable absorber (SA) in various fiber laser cavity for both Q-switching and mode-locking applications (Harun et al., 2012; Harun et al., 2013; Martinez & Sun, 2013).

This is due to their inherent advantages, including fast recovery time, low saturation intensity, wide operating bandwidth and good compatibility with optical fibers. Recently, a new member of CNT family, multi-walled carbon nanotubes (MWCNTs) (Salavati-Niasari et al., 2010; Yu et al., 2013; Zhang et al., 2011) has also been widely investigated especially for nonlinear optics applications. The production cost of MWCNT material is about 50 % - 20 % of that of single-walled CNT material since the material growth does not need complicated techniques or special growing conditions (Zhang et al., 2011). Compared with single-walled CNTs, the MWCNTs have better thermal stability, higher mechanical strength as well as can absorb more photons per nanotube due to its higher mass density of the multi-walls (Ramadurai et al., 2008). Likewise, a graphene oxide (GO) was also proposed in recent years as SA especially in 1.5 μm region to make use of the merit of graphene material (Xu et al., 2012). The synthesis of GO is relatively easier than graphene (Stankovich et al., 2007) and it has excellent optical properties such as strong saturable absorption and ultrafast recovery time, which are comparable to that of graphene (He et al., 2012; Ismail et al., 2014; Loh et al., 2010; Wang et al., 2012; Xu et al., 2012).

In this chapter, the performance of a newly developed nano-engineering double-clad thulium-ytterbium co-doped fiber (TYDF) is investigated for both continuous wave (CW) and pulse laser operations. The proposed TYDF laser (TYDFL) operates in the wavelength region near 2000 nm based on energy transfer from $Yb^{3+} \rightarrow Tm^{3+}$ using a multimode pumping scheme at the wavelength ranging from 905 to 980 nm. This chapter is organized into seven sections. The next section discusses the working principle of the TYDFL. The third section explains in detail the fabrication of the TYDF. The lasing characteristic of the TYDFL is presented in the fourth section. In the fifth section, a Q-switched TYDFL is demonstrated using home-made MWCNTs-based SA. The SA is constructed by sandwiching a MWCNT-polyvinyl alcohol (MWCNT-PVA) film between

two fiber ferrules via a fiber connector. The soliton mode-locked TYDFL is then demonstrated in the sixth section using a commercially available GO paper SA. The seventh section concludes the finding of this work.

4.2 Working Principle of Thulium-Ytterbium Co-Doped Fiber Lasers

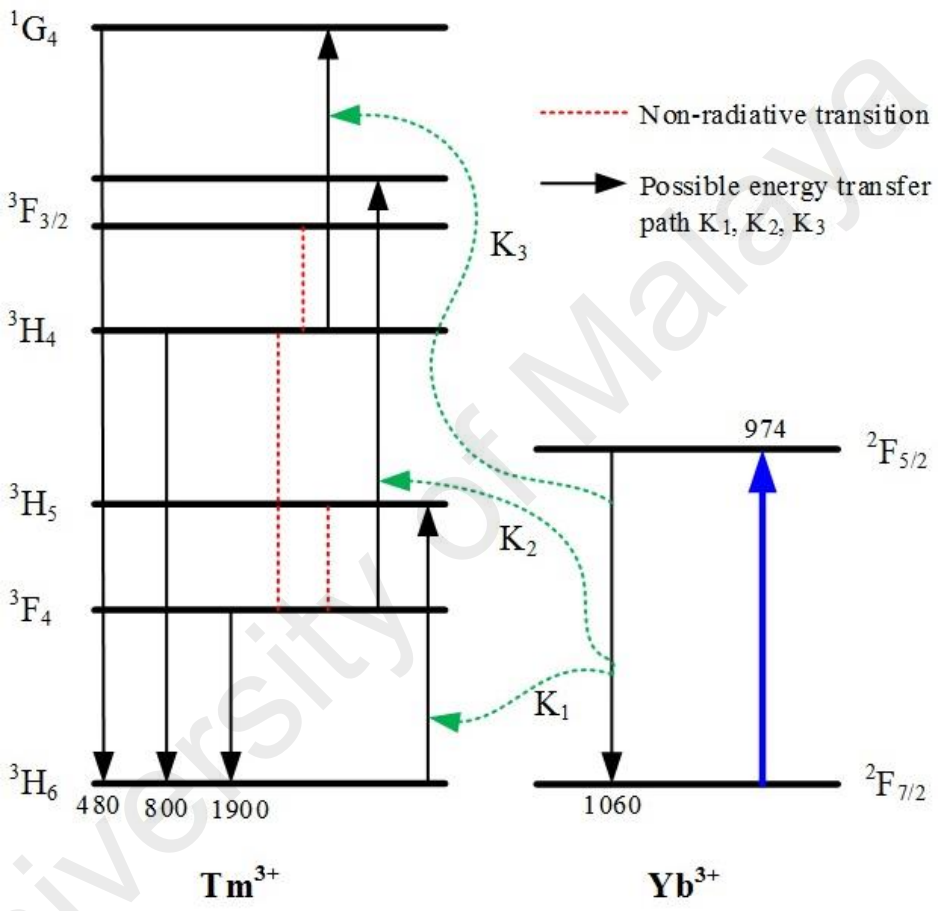

Figure 4.1: Energy diagram of TYDFL system. The lasing and pump wavelengths in nm.

Figure 4.1 shows the energy level diagram of the TYFL system in a silica host to explain its working principle. As illustrated in the figure, the strong resonance between the Yb^{3+} emission transition ($^2F_{5/2} \rightarrow {}^2F_{7/2}$) and the excited Tm^{3+} absorption ($^3F_4 \rightarrow {}^3F_2$) are obvious, which indicates a possible efficient energy transfer from Yb^{3+} to Tm^{3+} (Damanhuri et al., 2013). The lifetime of the $^3F_2$ level can be expected to be extremely

short because of the narrow energy gap between the $^3F_2$ and $^3F_3$. This signifies that energy transfer will not occur in the 'backward' direction. Similarly, the lifetimes of the $^3H_4$ and $^3H_5$ levels are sufficiently short and a multi-phonon decay allows the relaxation of a population inversion in the $^3F_2$ and $^3F_3$ levels to the $^3F_4$ level via the $^3H_4$ and $^3H_5$ levels. This population mechanism of $^3F_4$ level activates the radiative transition from $^3F_4 \rightarrow {}^3H_6$ and thus generating an amplified spontaneous emission (ASE) in the 1.9 µm wavelength region. However, it would be expected that there would be some initially excited Tm^{3+} to activate the above-mentioned energy transfer. Additionally, the quasi-resonant energy transfers from $^3H_6 \rightarrow {}^3H_5$ and $^3H_4 \rightarrow {}^1G_4$ also take place as soon as there is sufficient excited population of Tm^{3+}. This activates the radiative transition from $^1G_4 \rightarrow {}^3H_6$ and $^3H_4 \rightarrow {}^3H_6$, which produces 480 nm and 800 nm emissions simultaneously along with the 1.9 µm.

4.3 Fabrication and Characterization of Thulium-Ytterbium Co-Doped Fiber

Fabrication and characterization of the TYDF preform was fabricated using a modified chemical vapour deposition (MCVD) process in conjunction with solution doping technique (Halder et al., 2013). The core of the preform consists of a combination of alumino-silicate (SiO_2-Al_2O_3), yttrium alumino-silicate (SiO_2-Al_2O_3-Y_2O_3) and phosphor-silicate (SiO_2-P_2O_5) glasses, which were fabricated through the deposition of multiple porous layers at several deposition temperatures and various pre-sintering temperatures. In the MCVD process, a pure silica glass tube (with outer and inner diameters of 20 and 17 mm, respectively) was used for the deposition of several multiple porous un-sintered silicate soot layers while maintaining a suitable deposition temperature at around 1400–1450 °C. The deposited silica tube was then cut so that a suitable strength of dopant precursors can be doped in the glass using the solution doping technique. During the solution doping process, the deposited multiple un-sintered silicate

core layers are soaked with an alcoholic solution of a suitable strength of $YbCl_3.6H_2O$, $TmCl_3.6H_2O$, $AlCl_3.6H_2O$ and $YCl_3.6H_2O$ for about 45 minutes.

Then, the glass tube underwent hydration and oxidation processes at the temperature of around 950 °C. Sintering of the un-sintered layers was then performed by slowly increasing the temperature from 1500 to 2000 °C. Upon the completion of this process, the tube was slowly collapsed to transform it into an optical preform.

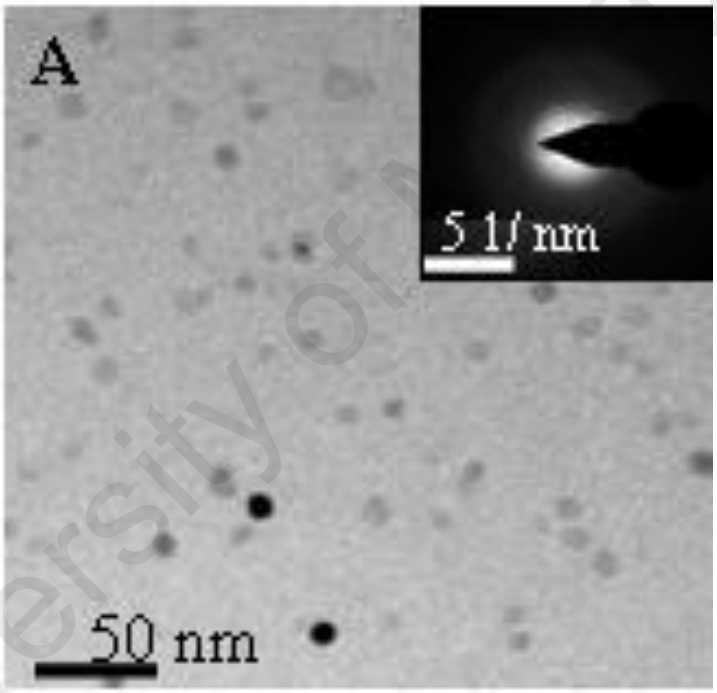

Figure 4.2: TEM image of the annealed Tm/Yb co-doped preform. The inset: Electron diffraction pattern.

After making of a preform, the annealing was done in a closed furnace at a temperature around 1400 °C for 3 hours with heating and cooling rate of 200 °C /min. During the annealing process, the core glass is phase separated into yttria-alumina along with Tm and Yb rich-nanoparticles having sizes 20-25 nm as observed from transmission

electron microscopy (TEM) analyses shown in **Figure 4.2**. The TEM image was also taken using thin film sampling technique at the active core of fiber samples. The size of nanoparticles, which was formed by yttria-alumino-silicate–rare earth (YAS-RE) phases decreases in the fiber as shown in **Figure 4.3 (A)**. This is due to the effect of a cooling during the drawing process. During the annealing process, the cooling of annealed preform is around 200 °C /min which very much slower than that of the cooling process at fiber drawing stage.

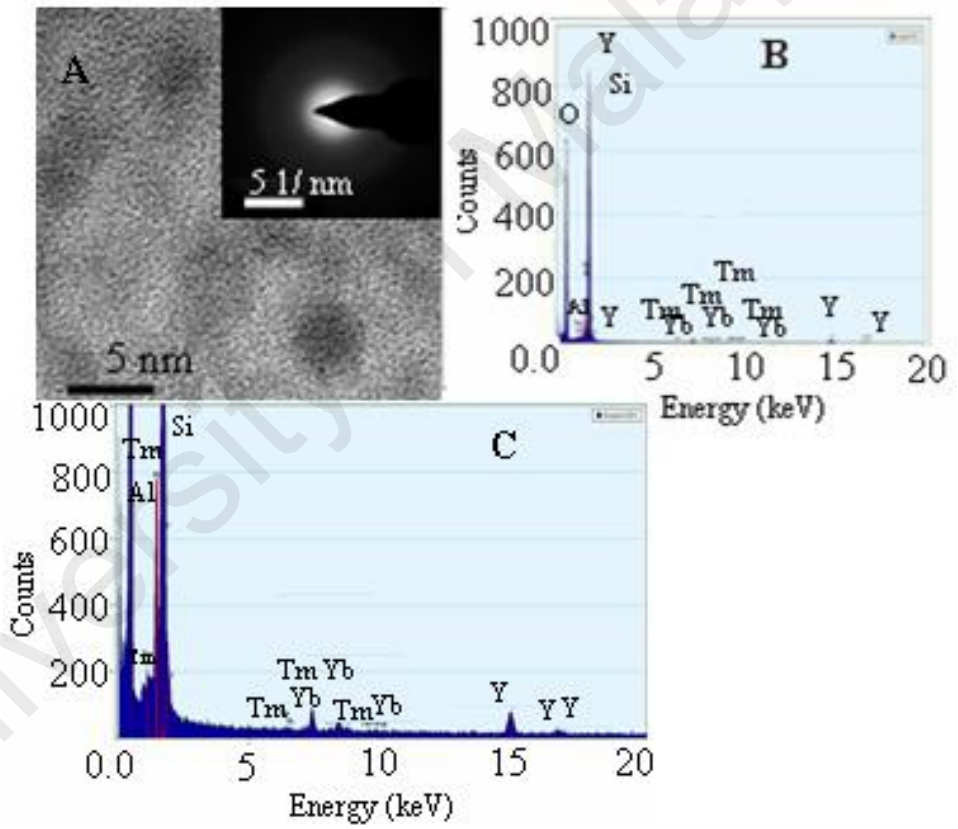

Figure 4.3: **(A)** TEM image of the fiber (Inset: Electron diffraction pattern) and EDX plot taken for **(B)** on the particles and **(C)** outside of black spots.

Thus, this slow cooling process allows sufficient time to grow up nano YAS-RE phases of 20-25 nm size into the silica glass matrix. At the time of fiber drawing, we melt the preform again at 2050 °C and cool the fiber rapidly by drawing the fiber at a spooling speed of 30 m/min. When the soft bare fiber with a significantly smaller diameter of 125 µm is exposed in air, they rapidly cooled down. To prevent the growth of YAS-RE phases into larger sizes, the maximum limit of the cooling time during fiber drawing should be around 1 minute. It is observed that this phase separation is a spontaneous process during cooling, thus the granular phase can grow only up to a reduced size i.e. 4.0 -5.0 nm into the matrix within this short time. Electron diffraction pattern shows amorphous nature of the particles. Energy dispersive X-ray (EDX) spectra taken on and out of the particles as shown in **Figure 4.3** clearly indicates that the nanoparticles are composed of yttria-alumina along with Tm and Yb rich phase-separated regions. The fabricated optical preform consists of Al_2O_3, Y_2O_3, Tm_2O_3 and Yb_2O_3 dopants with an average weight percentage of 5.5, 3.30, 0.70 and 4.0, respectively measured from an electron probe microanalyzer (EPMA). The composition of dopants in this fiber was optimized to allow the formation of smaller phase-separated nanoparticles of 3–5 nm, which functions to reduce the background loss of the fiber as well as to increase the energy transfer efficiency from Yb to Tm ions. The presence of Y_2O_3 and Al_2O_3 helps to decrease the phonon energy of silica glass and also prevent the clustering of Yb and Tm ions into the core glass matrix and thus increases the probability of radiative emission (Loghman-Estarki et al., 2013; Loghman-Estarki et al., 2015).

The fabricated circular preform is converted to octagonal shaped through grinding followed by polishing method. The fiber is then coated with a low refractive index (RI) polymer to ensure the robustness of the fiber. Such octagonal shaped low RI coated fiber is then drawn at a temperature of 2050 °C with an outer cladding diameter of 125 µm from such geometrically modified preform. The fabricated fiber consists of a dual-clad

structure where the multimode pump light is coupled into the inner cladding. As the pump light travels down the fiber in the inner cladding, the photons overlap with the core to get absorb by the Yb^{3+} ions dopants. The octagonal geometry of the cladding of the fabricated TYDF improves the pumping absorption efficiency since more pump photons are being directed into the core region.

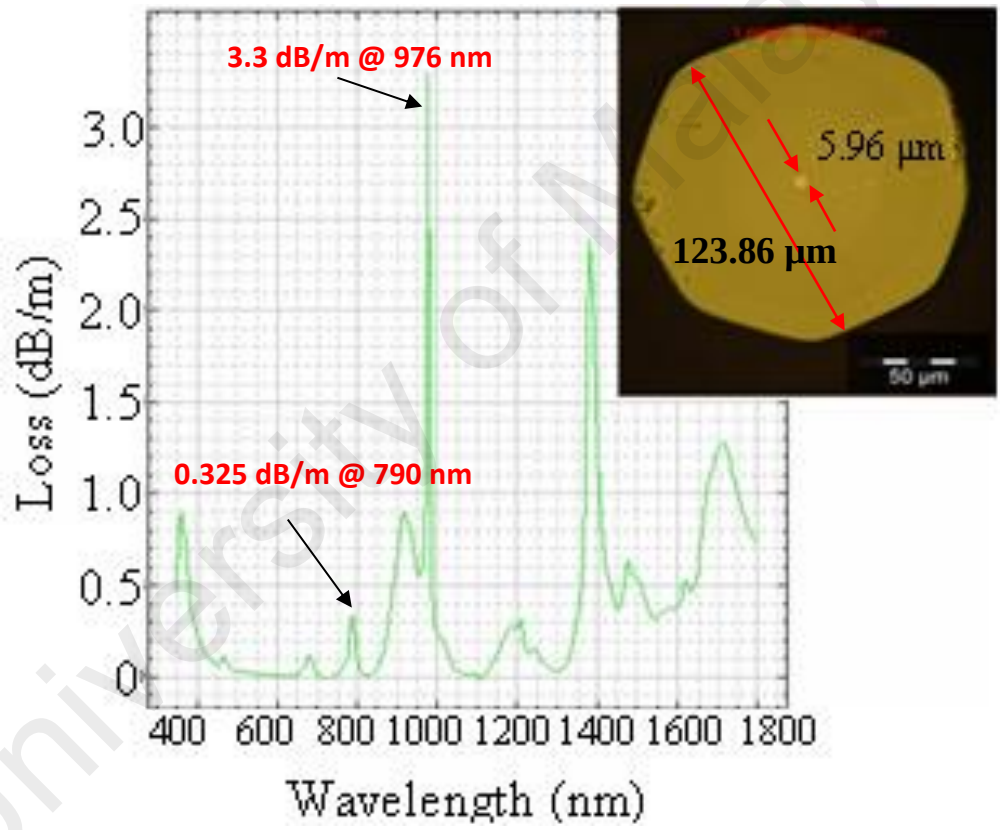

Figure 4.4: : Spectral attenuation curve of the newly developed octagonal shaped low RI coated fiber with its cladding absorption at 790 nm and 976 nm. The inset shows a microscopic cross-sectional view of the fiber.

The octagonal geometrical shape has more broken circular geometry (eight sides) and a symmetrical cross-section compared to the conventional hexagonal shape. The higher number of broken circular geometry could provide more pump absorption, which in turn increases the laser output power (Latiff et al., 2016). In addition, the more symmetrical cross-section in the octagonal geometry could provide a lower splicing loss.

The doping levels of Tm^{3+} and Yb^{3+} ions of the fabricated TYDF are 4.85 x 10^{19} ions/cc and 27.3 x 10^{19} ions/cc, respectively as measured using an EPMA. The cladding absorption loss curve of the octagonal shaped double-clad TYDF is measured and the spectrum is given in **Figure 4.4**. The cladding absorption of such fiber at 790 nm and 976 nm are found to be 0.325 and 3.3 dB/m respectively. The inset of **Figure 4.4** shows the microscopic view of fiber cross-section. It is shown the double-clad fiber has a core and an inner cladding diameters of 5.96 µm and 123.86 µm, respectively. NA of the TYDF is measured to be 0.23.

4.4 Lasing Characteristic of the TYDFL with Linear Configuration

At first, the lasing characteristic of the TYDFL is investigated based on linear configuration and multimode pumping. The experimental setup for the proposed TYDFL is shown in **Figure 4.5**. It uses the fabricated TYDF as the gain medium, which is pumped by a multimode laser diode via a multimode combiner (MMC). Both MMC input signal fiber end and TYDF end are perpendicularly cleaved to establish a Fabry–Perot laser cavity based on Fresnel reflection. The refractive index difference between the silica fiber and air provides about 4 % reflectivity which is sufficient to allow an oscillation in the linear setup. A multimode laser diode (MMLD) is used as the optical pump source which is coupled into the TYDF via the MMC. The output of the laser is routed to an optical spectrum analyzer (OSA) and power meter for spectral and power analysis, respectively.

The lasing performance is investigated for three different TYDF lengths; 5 m, 10 m and 15 m and pumping wavelengths; 905 nm, 927 nm, and 980 nm. This laser configuration contains no adjustable parts and its operation can only be controlled externally by the amount of the multimode pump power.

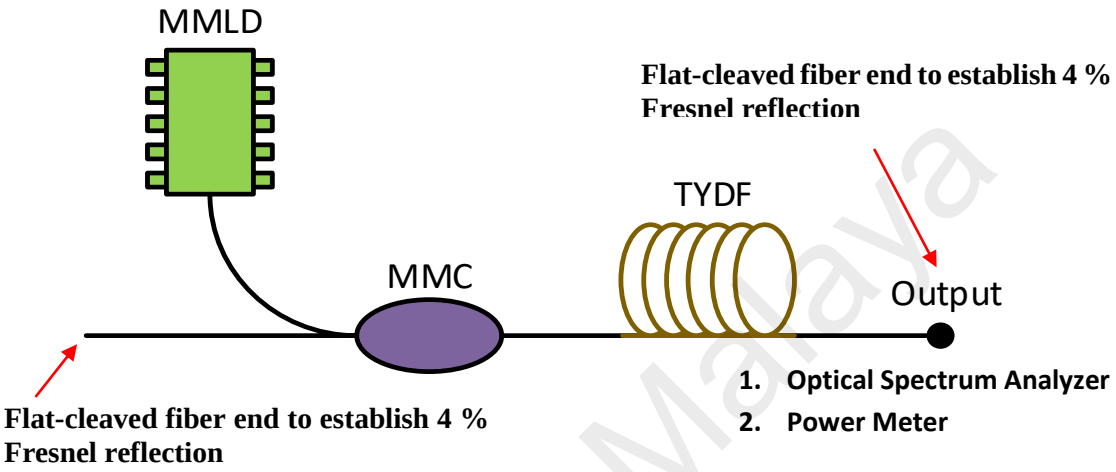

Figure 4.5: Experimental setup for investigating the lasing characteristic of the TYDFL in a linear cavity configuration.

Figure 4.6 shows the output spectra of the linear TYDFL when the gain medium length is varied from 5 to 15 m. In the experiment, the multimode 980 nm pump power is fixed at 1.0 W. As shown in the figure, the output spectrum moves to longer wavelength with the increase of the TYDF length. This is due to the absorbed 980 nm photons, which increases with the fiber lengths and thus the emitted photons are also increased. These photons are re-absorbed by the Tm^{3+} ion along the fiber length to emit ASE photons at a longer wavelength, which then oscillates in the linear cavity to generate the laser. As seen in **Figure 4.6**, the laser operates at a center wavelength of 1936.4 nm, 1958.6 nm and 1967.5 nm at TYDF length of 5 m, 10 m, and 15 m, respectively. A ripple is also observed at the region of the laser, which it most probably attributed to mode competition inside

the laser cavity. A sharp and narrow linewidth output spectrum is expected with the use of FBG or another wavelength selective filter in the cavity. The emission at 1540 nm region was also observed due to the energy transition from $^3H_4$ to $^3F_4$. As shown in **Figure 4.6**, emission from this transition occur at 1522, 1544 and 1559 nm with the TYDF lengths of 5, 10 and 15 m, respectively.

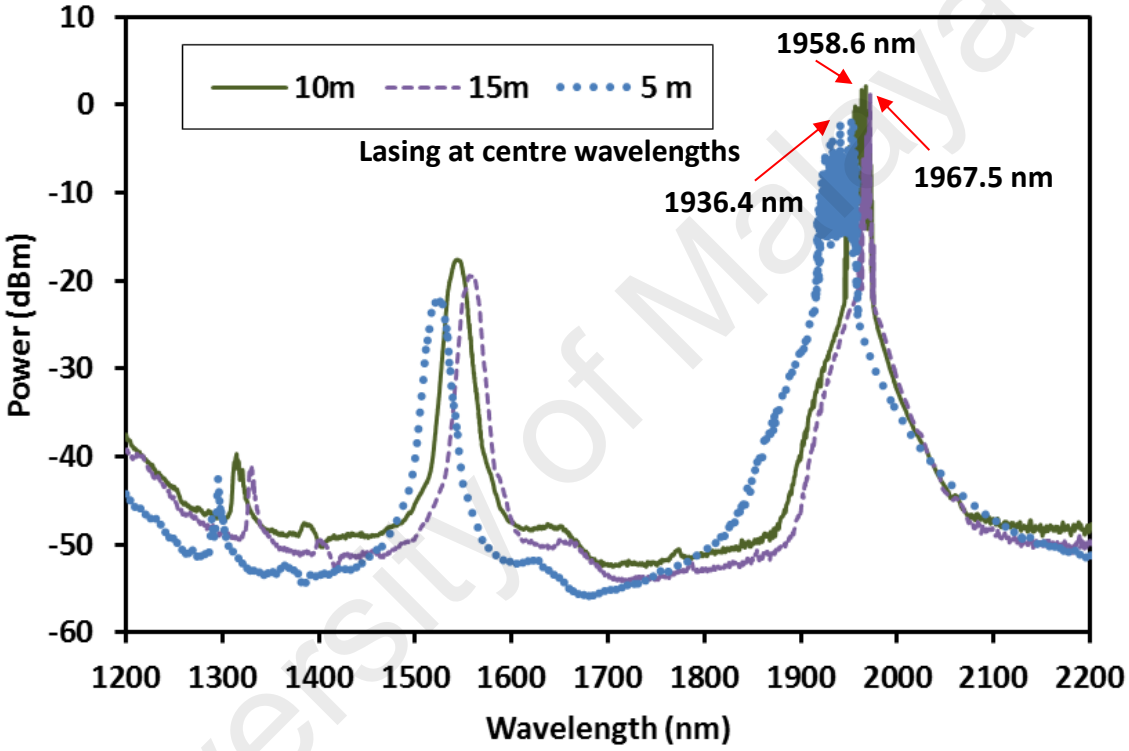

Figure 4.6: Spectra of the linear TYDFL with a 980 nm pumping and its lasing operate at centre wavelengths of 1936.4 nm, 1958.6 nm, and 1957.5 nm.

Then, we conduct an experiment to find the optimal pumping wavelength for the proposed TYDFL. **Figure 4.7** shows the relation between the laser output power and the multimode pump power when the TYDF length is fixed at 15 m. The experiment was carried out at three different pumping wavelengths of 905 nm, 927 nm and 980 nm.

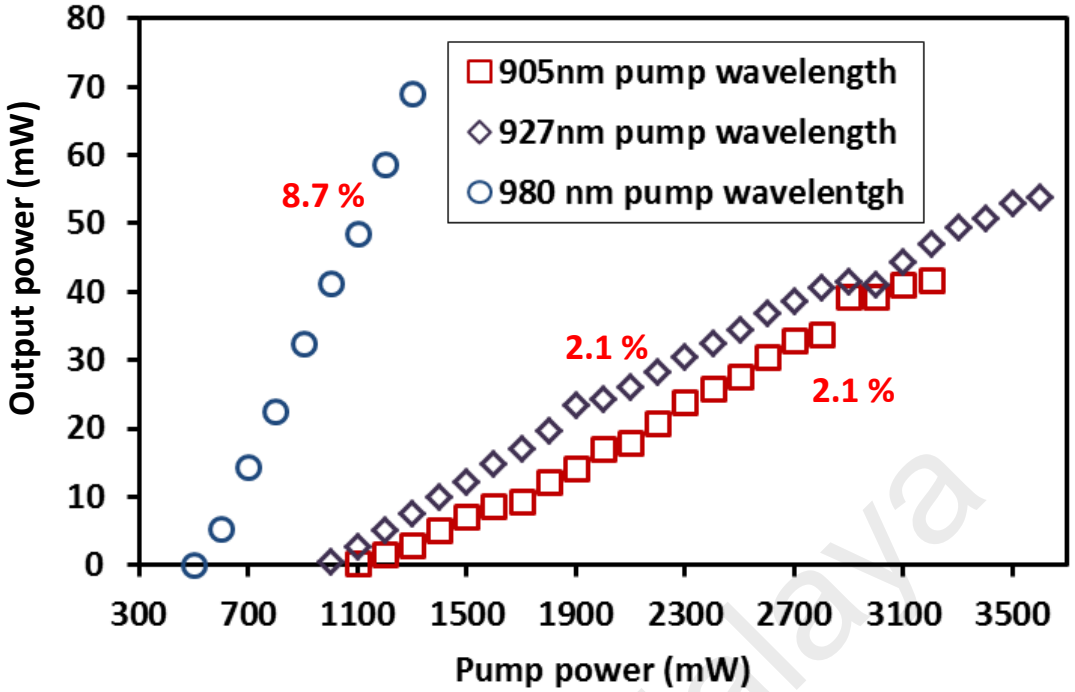

Figure 4.7: Output power against the multimode pump power at three different pumping wavelengths with its slope efficiencies for a 15 m length of TYDF.

It is observed that the output power of the TYDFL is linearly increased with the pump power. The slope efficiencies of 2.1 %, 2.1 %, and 8.7 % are obtained at the pumping wavelengths of 905 nm, 927 nm, and 980 nm, respectively. The highest efficiency is obtained at 980 nm pumping wavelength since it is closer to the peak absorption wavelength of the TYDF at 976 nm. It is also found that the threshold pump power is significantly lower at the optimum pump wavelength of 980 nm. We continue the experiment to find the optimal length of operation for the TYDFL.

Figure 4.8 shows the laser output power variation with the multimode pump power for three different fiber lengths when the pump wavelength is fixed at the 980 nm. The output power is linearly increased with the pump power with slope efficiencies of 6.4 %, 9.9 % and 8.7 % at the TYDF lengths of 5 m, 10 m, and 15 m, respectively.

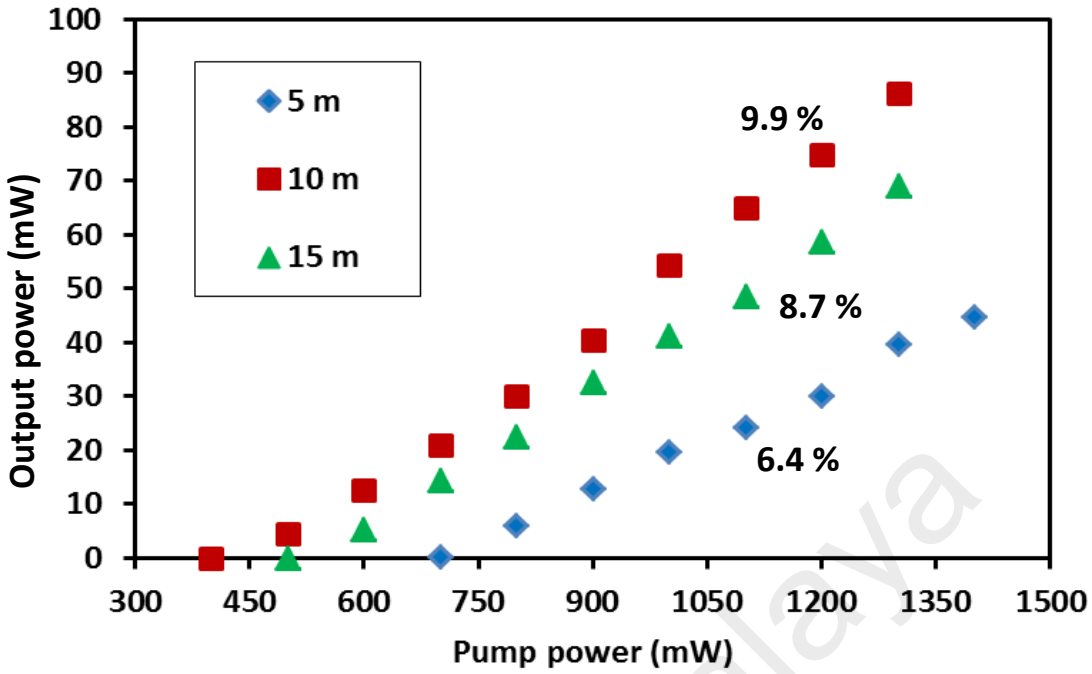

Figure 4.8: An output power of the proposed TYDFL against the 980 nm pump power at different TYDF lengths with its slope efficiencies.

The proposed laser operates based on the energy transfer from ytterbium ions into the thulium ions in the presence of 980 nm pump. As the pump photons are absorbed by the ytterbium ions, it excites the ion from a ground state $^2F_{7/2}$ to $^2F_{5/2}$ due to multiphonon-assisted anti-Stokes excitation process. As the ytterbium ion relaxes to the ground state, energy transfer process happens to neighbouring thulium ion. When the thulium ions in the ground state ($^3H_6$) absorb the donated photons, it got elevated to $^3H_5$ level before it irradiatively relaxes to $^3F_4$. Thulium ions that populate this state level drops to the ground state again generating the ASE in 1.95 µm region, which oscillates in the proposed linear cavity to generate the laser.

The threshold pump powers of the laser are obtained at 700 mW, 400 mW, and 500 mW for the TYDFL configured with 5 m, 10 m, and 15 m long TYDF, respectively

in a linear configuration. The maximum output powers are obtained at 39.7 mW, 86.3 mW, and 69.1 mW from 5 m, 10 m, and 15 m TYDF, respectively at the maximum pump power of 1. 3 W. It is found that the efficiency of the laser is the highest (9.9 %) at 10 m long TYDF and its threshold pump power of 400 mW, while a 15 m long TYDF provides the second lowest threshold pump power of 500 mW with a slope efficiency of 8.7 %. This indicates that the optimum length of the linear TYDFL is within 10 to 15 m. Compared to the conventional TYDFL, which is configured with D-shaped inner cladding (Damanhuri et al., 2013), the efficiency of the proposed TYDFL is significantly improved by employing the newly developed octagonal shaped TYDF.

4.5 Q-Switched TYDFL Using MWCNT-PVA Saturable Absorber

The key component of the proposed Q-switched fiber laser is the SA, which is fabricated by incorporating dispersed MWCNT embedded in a polymer film in between two pigtails. To match the TYDFL operating wavelength of 2-micron, we used commercial MWCNT with the purity of 99 %, a length of 1-2 μm and distributed diameter of 10-20 nm. At first, the MWCNT powder was dispersed in deionized (DI) water with the assistance of sodium dodecyl sulphate (SDS). The surfactant solution was prepared by dissolving 4 g of SDS in 400 ml DI water. Then, 250 mg of MWCNT was added to this solution before the mixed solution was sonicated for 60 minutes at 50 W to achieve the homogeneous dispersion. The homogeneous solution was then centrifuged at 1000 rpm to remove large particles so that a stable dispersed MWCNT suspension could be obtained. On the other hand, the MWCNT polymer composite was prepared by adding the dispersed suspension into a PVA solution by three-to-two ratio. The PVA solution was prepared by dissolving 1 g of PVA (M_w = 89×10^3 g/mol) in 120 ml of DI water. Then, the mixed solution is then sonicated for about one hour to obtain a homogeneous

MWCNT-PVA composite. It was then cast onto a glass petri-dish and left to dry at a room temperature for at least 12 hours to produce a thick film of around 50 µm.

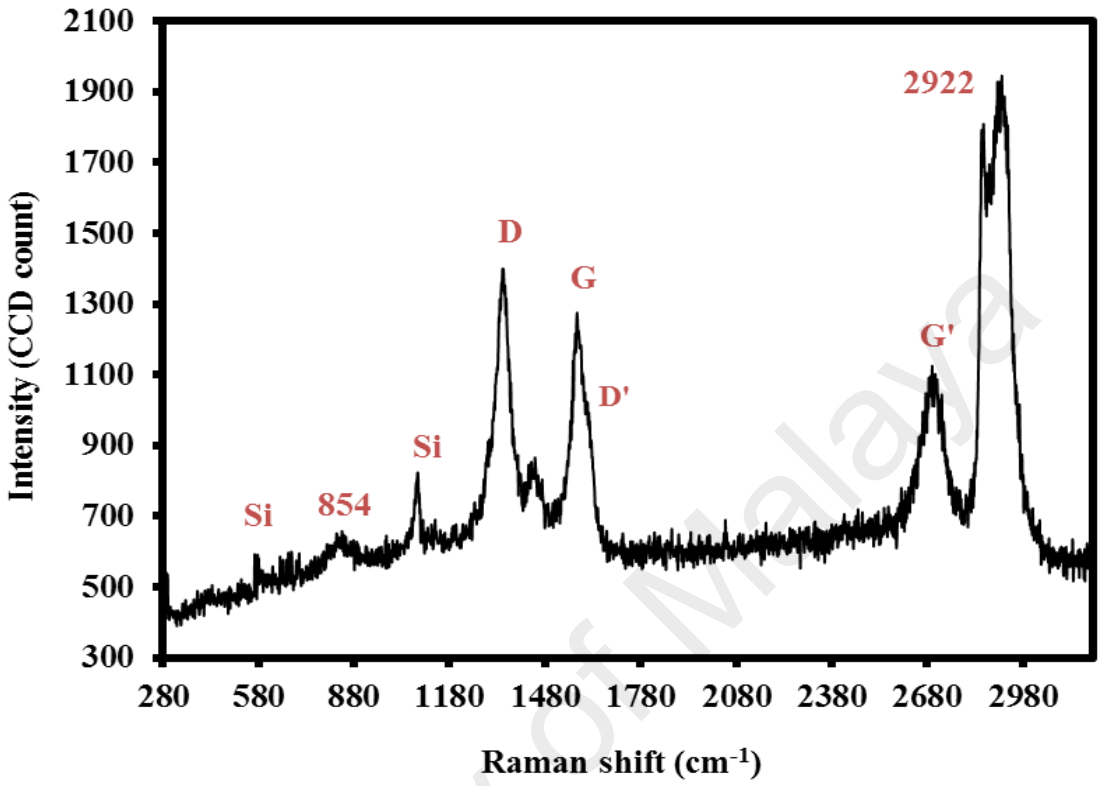

Figure 4.9: Raman spectrum obtained from the MWCNT embedded in PVA film.

It is observed that the spectrum bears a lot of similarity to graphene, which is not too surprising as the carbon nanotubes is simply a rolled up sheet of graphene. MWCNT has multi-layers of the graphene sheet wrapped around the core tube. In order to confirm the presence of MWCNT, Raman spectroscopy was performed on the polymer film sample using laser excitation at 532 nm. **Figure 4.9** shows the obtained Raman spectrum, which obviously indicates the distinct feature of the MWCNT.

We can obviously see well-defined G and G' bands at positions of 1580 cm^{-1} and 2705 cm^{-1}, respectively in the figure. The G band originates from in-plane tangential stretching of the carbon-bonds in the graphene sheet. We also observe a prominent band around 1350 cm^{-1}, which indicates that the carbon nanotubes are a multi-walled type. This

band is known as the D-band, which originates from a hybridized vibrational mode associated with graphene edges. The presence of strong D band indicates that the tubes has a multi-layer configuration with disorder structure. The D' band which is a weak shoulder of the G-band is also observed at 1613 cm^{-1}. This indicates that the carbon nanotubes have a double resonance feature induced by disorder and defect. In addition, others distinguishable features at 2920 cm-1, a small peak at 854 cm^{-1} and Si bands were also observed as shown in **Figure 4.9**. One important feature, a low energy radial breathing mode (RBB) at Raman shift of around 100 cm^{-1} to 400 cm^{-1}, which is usually observed in SWCNTs film is not seen in our spectrum. This is attributed to the MWCNT has multi-layers of the graphene sheet, which restricts the breathing mode.

The experimental setup of the proposed passively Q-switched ring TYDFL is shown in **Figure 4.10**. The ring resonator consists of a 5 m long of the newly fabricated TYDF, a multimode combiner (MMC), an isolator, a homemade MWCNT-PVA-based SA, and a 10 dB output coupler. The SA is fabricated by cutting a small part of the prepared MWCNT-PVA film and sandwiching it between two FC/PC fiber ferrules via a fiber connector. Index-matching gel was deposited onto the fiber ends to reduce the insertion loss up to around 3 dB at 1900 nm. The TYDF is pumped by a multimode laser diode operating at 980 nm via a MMC. The output of the laser is tapped through a 10 dB coupler while keeping 90 % of the light to oscillate in the laser ring cavity. The OSA is used for the spectral analysis whereas the oscilloscope is used to monitor the output pulse train of the Q-switched operation via a photo-detector. The cavity length is measured to be approximately 10 m. All components used in our experimental setup are polarization independent. No polarization controller (PC) was also included in the laser cavity as we had observed earlier that a PC did not improve our pulse stability.

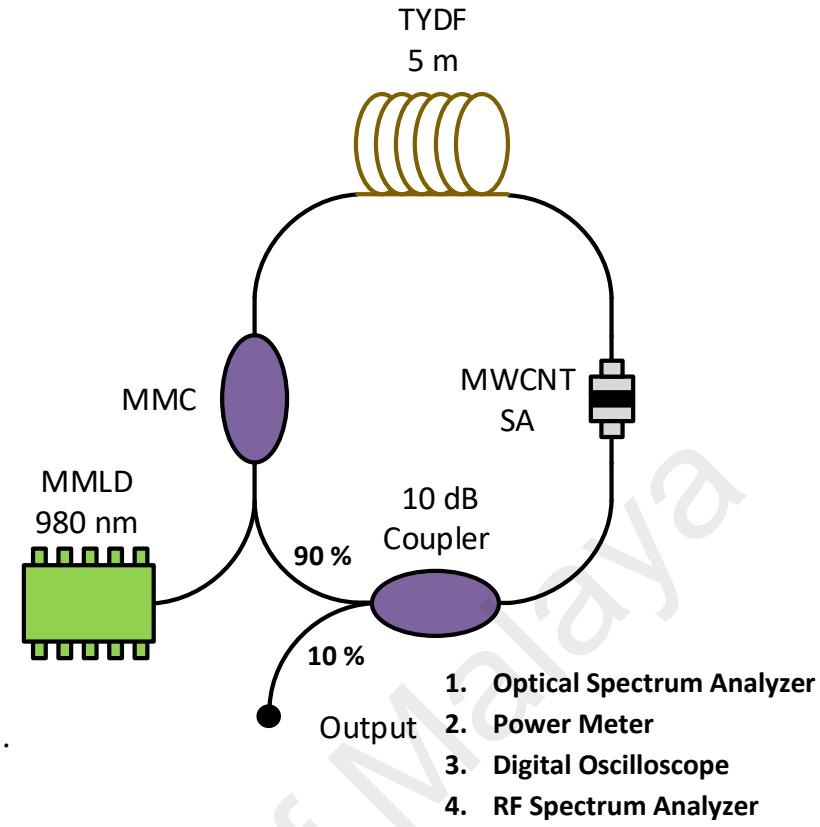

Figure 4.10: Configuration of the Q-switched TYDFL.

The Q-switching pulse train is obtained just by increasing the 980 nm pump power above 440 mW. A stable and self-starting Q- switched operation is maintained up to the pump power of 528 mW. It also observed that no Q-switched operation occurs without the MWCNTs SA incorporated in the ring cavity. This shows that the Q-switched operation is mainly induced by the SA. **Figure 4.11** compares the measured output spectra of the ring TYDFL with and without the SA in the cavity at the pump power of 440 mW. As seen in the figure, the Q-switched laser operates at a center wavelength of 1958 nm, which is slightly blue-shifted compared to that of the CW laser. The shifting of the central wavelength of the laser is most probably due to inhomogeneous broadening of TYDF and wavelength dependent of the MWCNTs loss. The spectral broadening is also observed due to the self-phase modulation effect in the ring cavity.

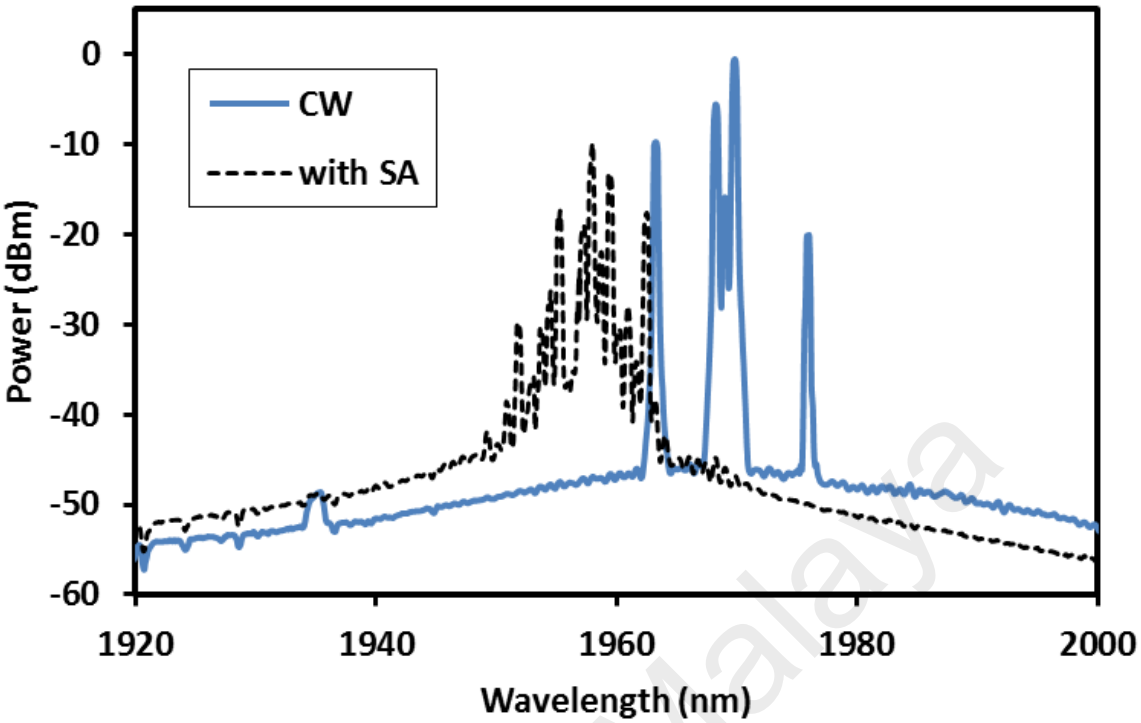

Figure 4.11: Output spectra of the TYDFL with and without SA at a fixed pump power of 440 mW.

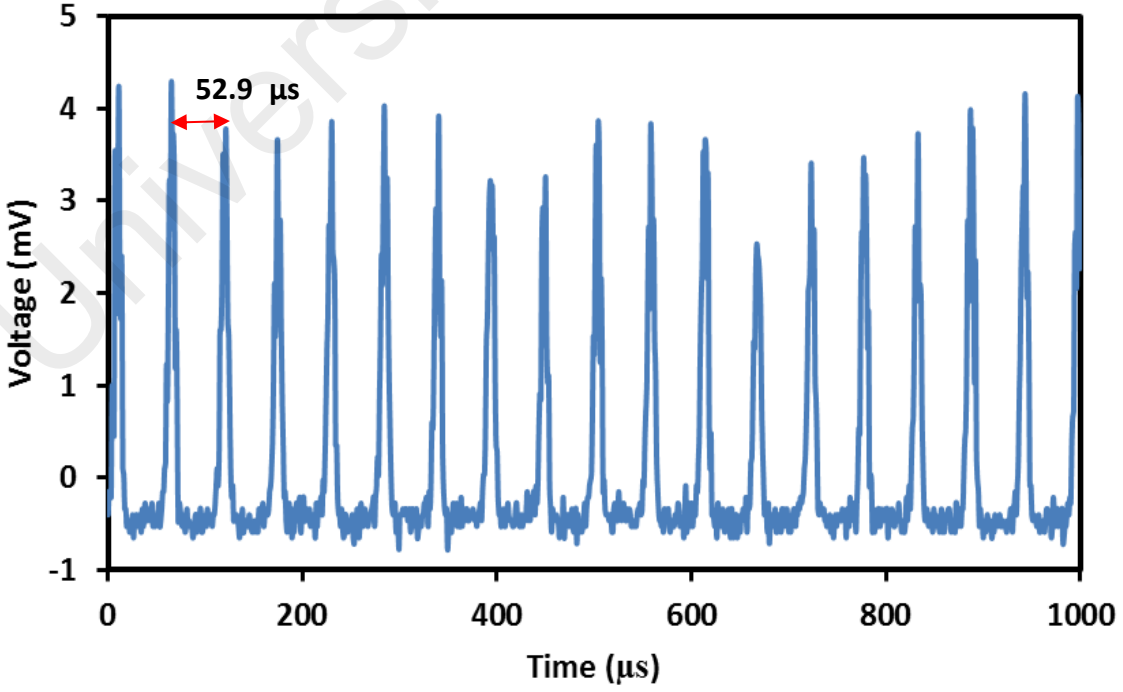

Figure 4.12: A typical pulse train from the TYDFL at a pump power of 440 mW.

Figure 4.12 shows the typical oscilloscope trace of the Q-switched pulse train at the threshold pump power of 440 mW. The spacing between two pulses is measured to be around 52.9 µs, which can be translated to pulse repetition rate of 18.9 kHz. The pulse width of a single pulse envelope is measured to be 7.94 µs. The highest voltage of 4.5 mV for the pulse train is obtained at 85 µs. In the figure, the negative voltage is the undershoot voltage occurs as a result of impedance mismatching in the digital oscilloscope.

Figure 4.13 shows how repetition rate and pulse width are related to the multimode pump power for the proposed Q-switched TYDFL. The pulse repetition rate of the laser was observed to increase almost linearly with the pump power, which agrees well with the passive Q-switching theory (Azooz et al., 2015). As shown in the figure, the pulse repetition rate can be tuned from 18.9 kHz to 35.1 kHz by varying the pump power from 440 to 528 mW.

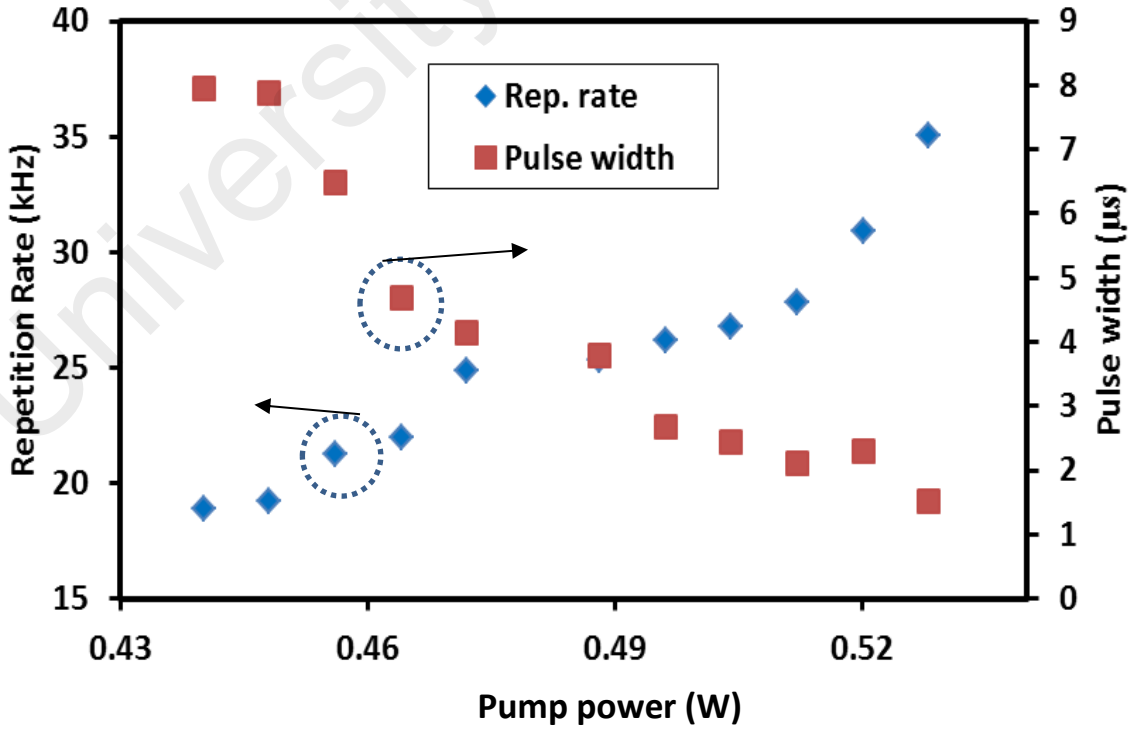

Figure 4.13: Repetition rate and pulse width as a function of the 980 nm pump power.

On the other hand, the pulse width decreases also almost linearly with the pump power. It reduces from 7. 94 μs to 1.52 μs as the pump power increases from 440 mW to 528 mW as shown in **Figure 4.13**. It should be noted that the Q-switching pulse disappears as the pump power is further increased above 528 mW.

Figure 4.14 shows the pulse energy of the TYDFL as a function of multimode pump power. As shown in the figure, the pulse energy fluctuates within 9.0 to 11.2 nJ as the 980 nm pump power increases from 440 to 528 mW. The maximum pulse energy of 11.2 nJ is obtained at 512 mW pump power.

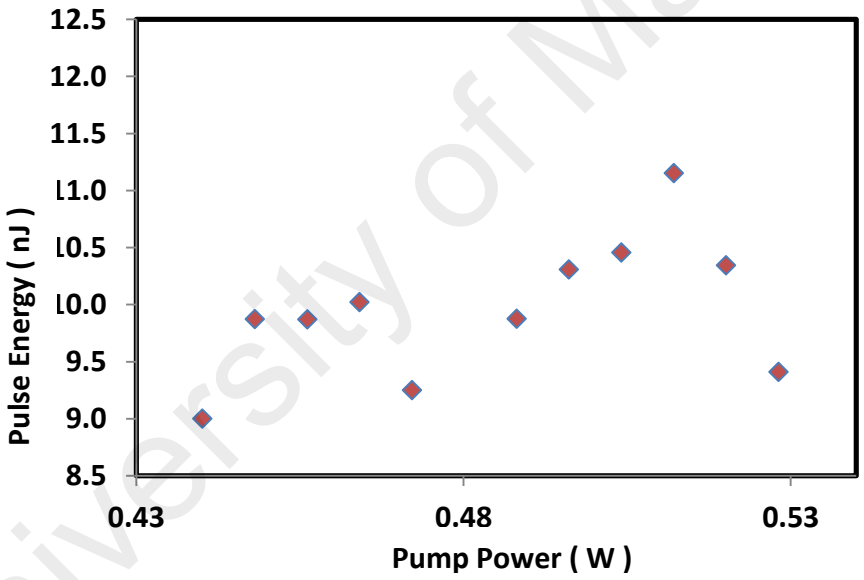

Figure 4.14: Pulse energy against the 980 nm pump power.

Figure 4.15 illustrates the RF spectrum of the Q-switched laser at 450 mW pump power. It shows that the laser operates at a repetition rate of 20 kHz with an optical signal to noise ratio (OSNR) of 42.2 dB. This indicates the high stability of the pulse train generated by the proposed Q-switched TYDFL.

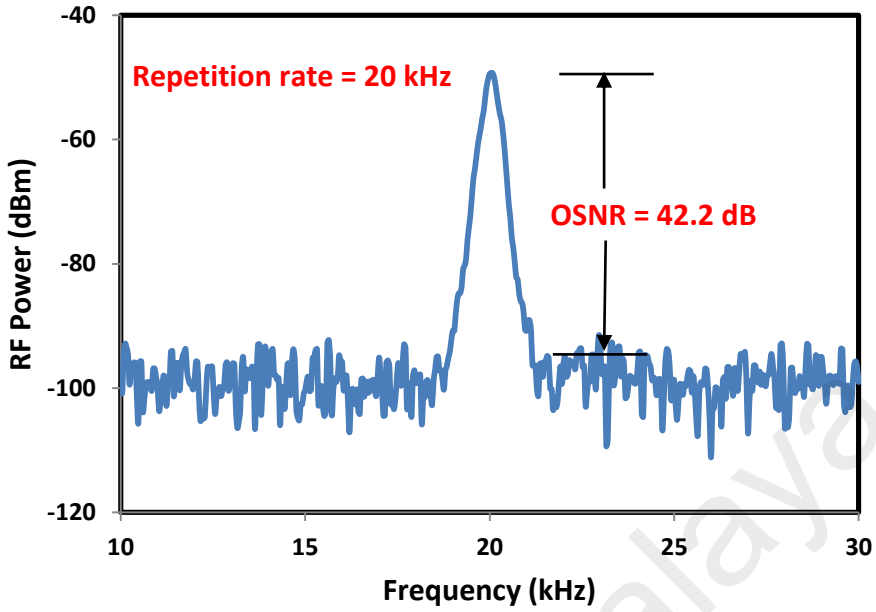

Figure 4.15: The RF spectrum of the Q-switched TYDFL at a pump power of 450 mW.

The Q-switching performance of the laser is expected to be improved by further optimization of the SA and laser cavity. These results indicate that MWCNTs has a big potential for superior Q-switching in 2-micron region. The fabrication of the MWCNTs based SA is also simple and thus the cost of the laser should be low. Therefore, it is suitable for applications in various fields such as environmental sensing, metrology, and biomedical diagnostics.

4.6 Mode-Locked TYDFL Using Graphene Oxide Paper

The graphene oxide (GO) paper can be prepared by mixing graphite oxide with water. The oxygen atoms of graphite oxide repel water molecules, thus, undergoing complete exfoliation in water, to produce colloidal suspensions with GO sheets. The colloidal suspensions were then filtered using a membrane to produce paper-like material

under a directional flow. In this work, the fiber-type GO-based SA device was assembled by sandwiching the commercial GO paper in between two fiber ferrules via a connector. It is then incorporated into a TYDFL cavity for a mode-locking application.

The configuration of the proposed laser is schematically shown in **Figure 4.16**, which consists of a 15-m long TYDF, a multi-mode coupler (MMC), a GO paper-based SA, and a 10 dB coupler in a ring configuration. A multimode laser diode operating at 905 nm was used to pump the TYDF through a MMC. A 10 dB coupler was used to tap out the laser output while allowing 90 % of the light to oscillate in the ring cavity. The cavity length was set at around 22.4 m so that the net cavity dispersion was anomalous for mode-locking.

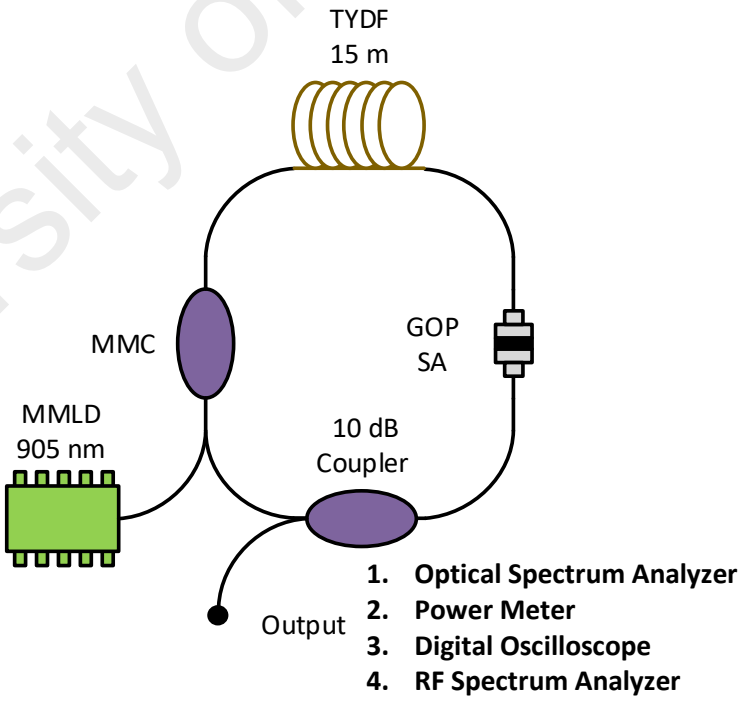

Figure 4.16: Experimental setup for the mode-locked TYDFL with a GO paper SA.

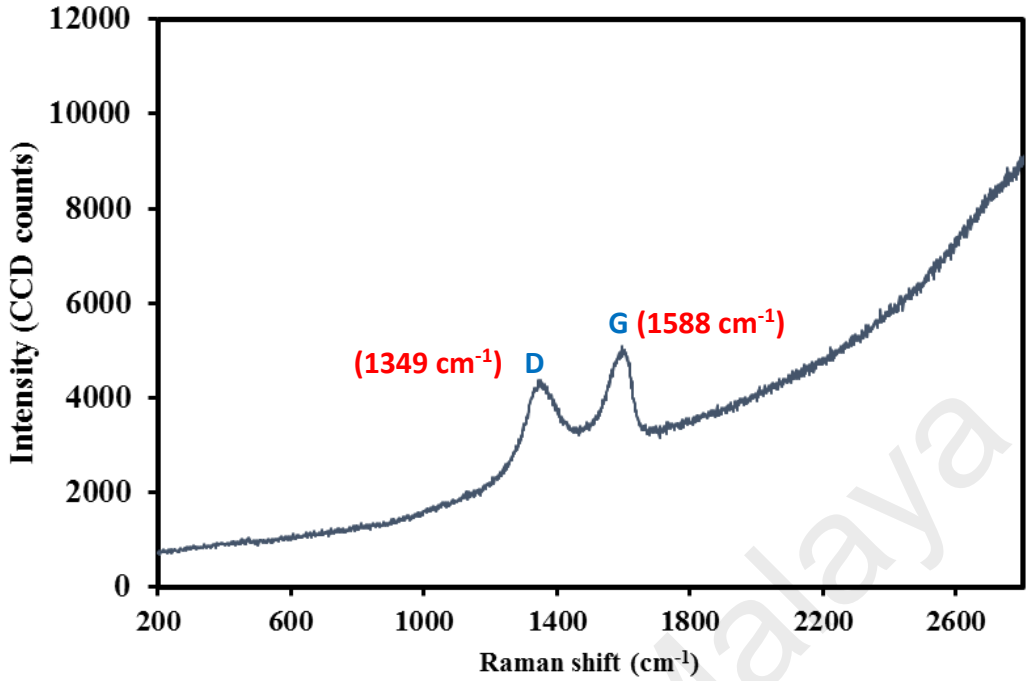

Figure 4.17: Raman spectrum of the GO paper showing D and G bands.

Figure 4.17 shows the result of the Raman spectroscopy on the GO paper used in the experiment. As seen in the figure, the Raman spectrum has two distinctive peaks at 1349 cm^{-1} and 1588 cm^{-1} that correspond to D-band and G-band respectively. This spectrum obviously indicates the distinct feature of the graphene. A mode-locking operation was self- started when pumping the TYDF at above the threshold pump power of 1.8 W. **Figure 4.18** shows the output spectra of the mode-locked TYDFL with and without the SA when the 905 nm multimode pump is fixed at 1.8 W. As illustrated in the figure, the operating wavelength of the TYDFL shifts from 1943.5 nm to 1942.0 nm with the insertion of SA into the cavity. The oscillating laser moves to a shorter wavelength region to acquire more gain for compensating the insertion loss of the SA.

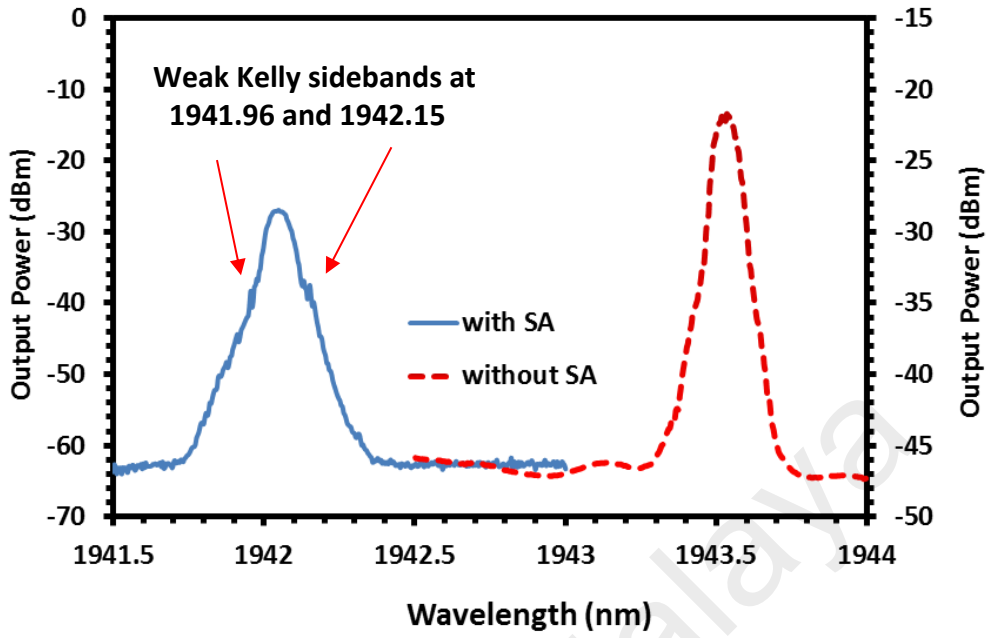

Figure 4.18: Output spectra for the TYDFL when the ring cavity is configured with and without SA.

As shown in the figure, weak Kelly sidebands are also observed at 1941.96 and 1942.15 nm, which confirms the presence of soliton in the proposed mode-locked TYDFL. This also proves that this mode-locked fiber laser is operating in anomalous dispersion regime. The laser cavity comprises of 15 m long TYDF and 7.4 m long SMF with estimated dispersions of -0.083 ps^2/m and -0.034 ps^2/m, respectively at an operating wavelength of 1942 nm. The total cavity dispersion (TCD) comprises of the fiber and the graphene material dispersion. Therefore, it is given by;

$$\text{TCD} = (D_{SMF} \times L_{SMF}) + (D_{TYDF} \times L_{TYDF}) + D_{graphene} \quad (4\text{-}1)$$

The material dispersion from graphene could be roughly deduced by;

$$D_{graphene} \approx -87 \times D_{SMF} = 2.958\ \text{ps}^2 \quad (4\text{-}2)$$

Assuming that D_{GO} is similar to $D_{graphene}$ and the output pulses of the soliton mode-locked laser possess a transform-limited, secant hyperbolic temporal shape, the soliton pulse width could be estimated through the following equation;

$$\Delta\lambda = \pm\lambda_o \sqrt{\frac{2}{cDL} - 0.0787\frac{{\lambda_o}^2}{(ct)^2}} \tag{4-3}$$

where $\Delta\lambda$ is the first order Kelly sideband separation, λ_o is the central wavelength, c is the light velocity in a vacuum, D is the average cavity dispersion parameter, L is the cavity length, and t is the soliton pulse width. Using experimentally observed parameters, including $\Delta\lambda$ = 0.1 nm, λ_o = 1942 nm and D = 1.46 ps^2, the pulse width is estimated to be around 1.1 ns. At the 905 nm multimode pump power of 1.8 W, the average output power was 0.13 mW, which corresponds to pulse energy of 5.8 pJ.

Figures 4.19 (a) and **(b)** show the typical pulse train and RF spectrum for the proposed mode-locked TYDFL when the 905 nm multimode pump power is fixed at 1.8 W. As shown in **Figure 4.19 (a)**, a pulse-to-pulse separation is measured to be around 44.8 ns, which corresponds to a repetition rate of around 22.32 MHz. The fundamental repetition rate is calculated as 8.6 MHz.

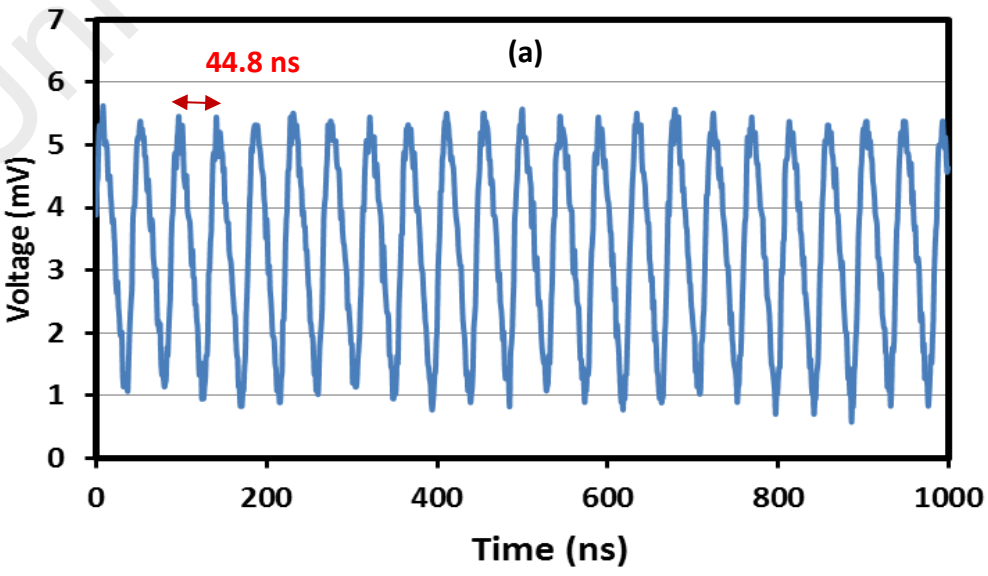

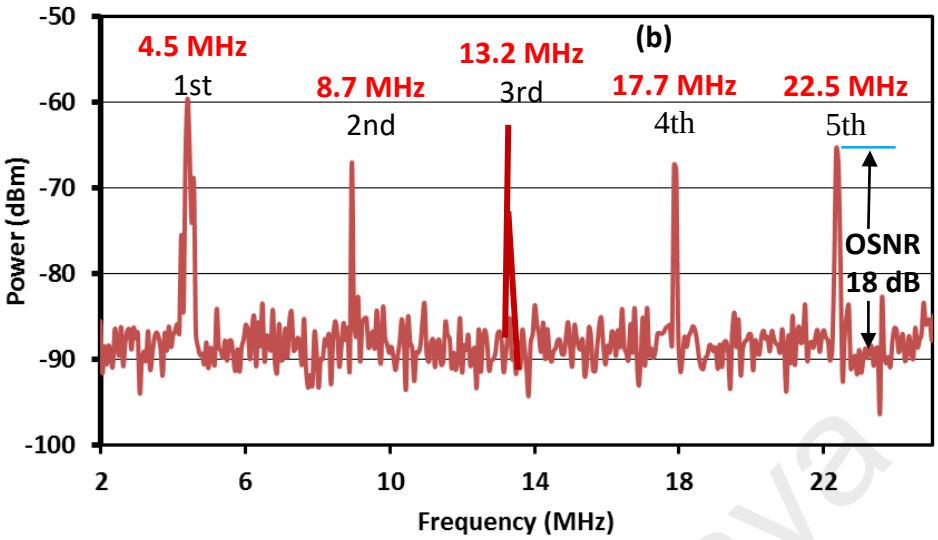

Figure 4.19: Mode-locking performance for the soliton mode-locked TYDFL **(a)** Typical pulse train **(b)** RF spectrum.

The repetition rate matches the fifth harmonic of the cavity roundtrip time with the cavity length of 22.4 m. This indicates the proposed GO paper SA exhibits sufficient saturable absorption, which is required to initiate the harmonic mode-locking operation. As seen in **Figure 4.19 (b)**, its fifth harmonic peak of the RF spectrum locates at the frequency of 22.5 MHz with an OSNR of 18 dB. This further confirms the feasibility of the mode-locking operation with the use of GO paper-based SA. However, the stability of the output pulse trains is still low based on the OSNR value. This is most probably due to the GO paper used, which is very sensitive to the polarization state of pulses. The use of polarization controller (PC) is expected to improve the OSNR of the laser. It is also observed that the output of the fiber laser was relatively stable during the measurement for half an hour.

4.7 Summary of TYDFL Operation

A new nano-engineering glass based octagonal shape double-clad TYDF with Tm^{3+} and Yb^{3+} ions doping levels of 4.85 x 10^{19} ions/cc and 27.3 x 10^{19} ions/cc, respectively was successfully evaluated for fiber laser application. With a linear configuration, the TYDFL operated at the center wavelength of 1936.4 nm, 1958.6 nm, and 1967.5 nm at TYDF lengths of 5 m, 10 m, and 15 m, respectively. The efficiency of the laser is the highest (9.9 %) at 10 m long TYDF and its threshold pump power of 400 mW, while a 15 m long TYDF provides the second lowest threshold pump power of 500 mW with a slope efficiency of 8.7 %. This indicates that the optimum length of the linear TYDFL is within 10 to 15 m. We have then demonstrated a Q-switched TYDFL operating in 1960 nm using MWCNT-PVA film-based SA. By varying the 980 nm multimode laser power from 440 to 528 mW, the pulse repetition rate increases from 18.9 to 35.1 kHz and the pulse duration reduces from 7. 94 to 1.52 μs. The maximum pulse energy of 11.2 nJ is obtained at the 980 nm multimode pump power of 512 mW. A soliton mode-locked TYDFL operating at 1942.0 nm was also demonstrated using a GO-based SA using the 905 nm multi-mode pump. The proposed laser produces the soliton pulse train with a repetition rate of 22.32 MHz, calculated pulse width of 1.1 ns, and calculated fundamental repetition rate of 8.6 MHz. The fifth harmonic peak of the RF spectrum locates at the frequency of 22.5 MHz with an OSNR of 18 dB. This further confirms the feasibility of the mode-locking operation with the use of GO paper-based SA.

CHAPTER 5 : CONTINUOUS WAVE, Q-SWITCHED AND MODE-LOCKED THULIUM-HOLMIUM CO-DOPED FIBER LASERS

5.1 Introduction

As discussed in the previous chapters, ultrafast fiber lasers operating in 2-micron regions are of great interest due to the various applications. They are demonstrated using a thulium-doped fiber (TDF) in Chapter 3 and thulium-ytterbium co-doped fiber (THDF) in Chapter 4. In addition to TDF and THDF, the 2-micron fiber lasers are also normally realized using holmium-doped fiber lasers. The holmium-doped fiber (HDF) has proved to be an attractive gain medium for the 2-micron lasers due to broad gain spectrum and high amplification factor (Scholle et al., 2010). The holmium laser operating at 2100 nm region was first demonstrated in 1965 (Johnson et al., 1965). The HDF offers a unique opportunity for operation at the long-wavelength edge of transparency of silica-based glass at ~2.15 μm (Kurkov et al., 2010). The existence of high power and high brightness pump lasers at around 1.12 -1.16 μm region, matching the absorption band of holmium-doped glass, allowed for demonstration of efficient holmium-doped silica fiber lasers (HDFL) (Jackson & Li, 2004; Kurkov et al., 2010; Kurkov et al., 2011). A Q-switched HDFL was also demonstrated with the pulse duration in the order of hundreds of nanoseconds (Sholokhov et al., 2011; Wu et al., 2009). However, ultrafast HDFL has not been demonstrated so far.

Due to the limited pump sources for the direct holmium ion pumping, co-doping is the best approach for developing holmium-based fiber laser systems. The thulium-holmium co-doped fiber lasers can be realized by laser diode pumping at a wavelength near 1.56 μm. The thulium-doped fiber laser is obtained through the ion transition between the $^3F_4$ - $^3H_6$ states when pumped at around 1.56 μm. The co-doping with

holmium ion allows for energy transfer from the thulium ion $^3F_4$ to the holmium ion $^5I_7$ state. The holmium ion transition of $^5I_7$ - $^5I_8$ generates lasing at the wavelengths near 2.1 μm (Oh et al., 1994). Until recently, there is still a lack of research work on generating pulsed all-fiber laser based on HDF or thulium-holmium co-doped fiber (THDF).

Recently, graphene, a single layer of carbon in a hexagonal lattice, has been intensively researched due to its wonderful optical properties (Bonaccorso et al., 2010). Graphene SA has been widely used as a broadband SA to passively Q-switch or mode lock the fiber laser or solid state laser, at different laser wavelengths ranging from 1 μm to 2 μm (Sotor et al., 2012; Wang et al., 2013). To date, many works have been reported on the integration of a graphene polyvinyl alcohol (PVA) SA into fiber laser system for ultra-short pulse generation. For instance, mode-locked erbium-doped fiber laser with a stable soliton-like pulse was achieved using a graphene from a CVD process (Sobon et al., 2013). In previous Chapters 3 and 4, mode-locked fiber lasers have been demonstrated using graphene oxide paper (GOP) as a SA in TDFL and TYDFL cavity, respectively. However, the GOP is easy to damage and cannot sustain a high temperature and thus it is not suitable for high power application.

In this chapter, a performance of continuous wave (CW), Q-switched and mode-locked thulium-holmium co-doped fiber lasers (THDFL) with 1552 nm pumping in ring configuration is investigated. Graphene oxide (GO) embedded in polyvinyl alcohol (PVA) film is used as a passive saturable absorber (SA) in generating Q-switched and mode-locked pulse train.

5.2 Working Principle of Thulium-Holmium Co-Doped Fiber Lasers

THDFL operation is based on energy transfer from Tm^{3+} to Ho^{3+} ions. **Figure 5.1** illustrates the complexity of energy transfer in Tm: Ho materials and displays some of the more important processes affecting Tm: Ho lasers. The main channel of energy transfer between Tm^{3+} and Ho^{3+} is the resonant transfer from the Tm $^3F_4$ to the Ho $^5I_7$, denoted by the process P_{28}. The reverse of this process is P_{71}, the backtransfer from the Ho $^5I_7$ to the Tm $^3F_4$. These energy transfer processes are illustrated in **Figure 5.2**.

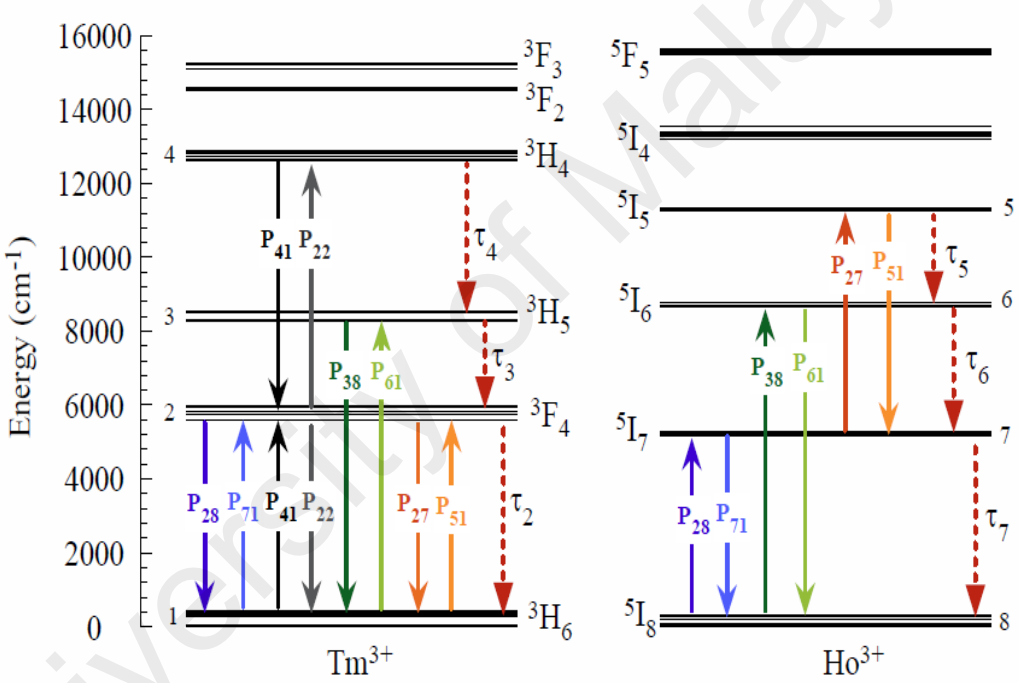

Figure 5.1: Energy level schematic of Tm-Ho energy transfer processes (Walsh, 2009).

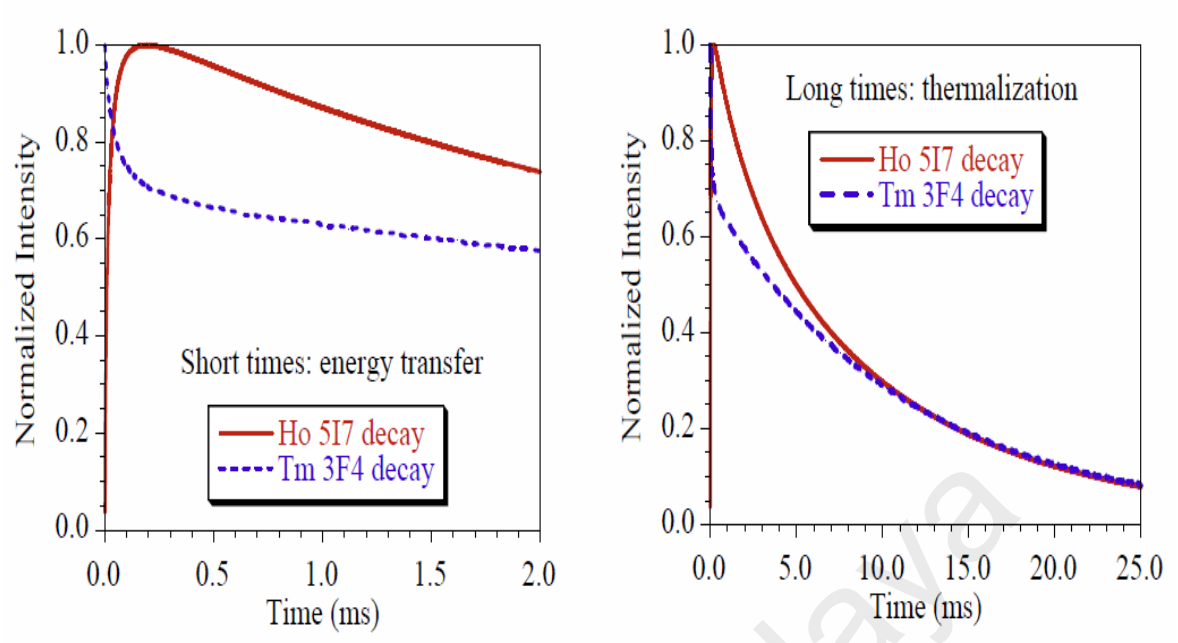

(a) **(b)**

Figure 5.2: Tm: Ho decay dynamics at **(a)** short and **(b)** long times after excitation of Tm $^3F_4$ (Walsh, 2009).

At early times after excitation of the Tm $^3F_4$ manifold, a sharp rise in Ho $^5I_7$ population as accompanied by a sharp decline in Tm $^3F_4$ population as shown in **Figure 5.2 (a)**. At long times after the pulse, the populations are thermalized and decay at the same rate as shown in **Figure 5.2 (b)**. The situation can be explained in the following way. After a pulse, the Tm^{3+} and Ho^{3+} ions have a certain amount of energy as a combined system and an agreement through Boltzmann statistics to maintain the distribution between the two. Even though the total amount of energy in the Tm $^3F_4$ and Ho $^5I_7$ manifolds is decreasing, the distribution between the two eventually reaches quasi-thermal equilibrium and the Tm^{3+} and Ho^{3+} ions decay at the same rate. By looking at the early parts of the decay curve, we can catch Tm^{3+} and Ho^{3+} in the act of sharing their energy. At later times they are still sharing energy, but have essentially become thermalized and each displays the same rate of decay. The energy transfer processes of

laser operation on the Ho $^5I_7 \rightarrow {}^5I_8$ transition at ~ 2 μm relies on two separate energy transfer processes. Excitation of the Tm $^3H_4$ is followed by cross relaxation, producing two excitations in the Tm $^3F_4$ for each pump photon. This is followed by direct energy transfer from the Tm $^3F_4$ to Ho $^5I_7$. It is a fairly efficient laser way of doing things, but there may be some advantages to using a Tm laser to pump Ho directly, rather than rely on the Tm – Ho energy sharing in co-doped Tm: Ho materials (Walsh, 2009).

In this study, the performance of fiber lasers with a thulium-holmium co-doped fiber (THDF) as the gain medium in a ring cavity configuration is investigated. The proposed lasers are a better choice than the conventional erbium-doped fiber lasers since they lase near 2 μm and have a broad bandwidth (1.7–2.1 μm) that can support short, high peak power pulses. Compared to a single doped holmium-doped fiber, the proposed laser is advantageous due to the use of 1552 nm pumping wavelength. The 1552 nm fiber laser is widely available and cheaper than 1.8 or 1.9 μm laser source.

5.3 Performances of Continuous Wave THDFL with 1552 nm Pumping

Lasing in a pure thulium-doped fiber (TDF) occurs between the $^3H_4 - {}^3H_6$ states when pumped at 1550 nm. The co-doping with holmium ions allows for energy transfer from the $^3H_4$ state of thulium ion to the $^5I_7$ state of holmium ions. This allows lasing on the $^5I_7 \rightarrow {}^5I_8$ transition of holmium ions (Ghisler et al., 1994; Oh et al., 1994) at wavelengths around or longer than 2-micron to occur, and thus increasing the laser's operating spectral bandwidth. THDFL can be pumped by a laser diode near 1550 nm instead of 1150 nm and emit light near the 2-micron region. In this section, the performance of a core-pumping THDFL is investigated.

The laser is based on a ring cavity using a commercial THDF as the gain medium. **Figure 5.3** shows the experimental setup for the THDFL, which the cavity consists of a section of the high concentration THDF as a gain medium, a 1550/2000 nm wavelength division multiplexer (WDM) and a 10 dB output coupler. A 1552 nm erbium-ytterbium co-doped fiber laser (EYDFL) with the maximum output power of around 1.2 W is coupled into the cavity through a WDM to pump a length of THDF (**Coractive TH512**). According to the manufacturer's specifications, the active fiber has Tm and Ho ions concentrations of 2900 and 400 ppm. wt., respectively with Tm/Ho ratio of 7.25 : 1. In general, it is believed that the greater Tm/Ho ratios may lower the lasing threshold. The large ratio will ensure that enough holmium ions will be sufficiently excited to exceed the transparency level of the laser transition for a given launched pump power. The output of the THDFL is tapped out from the 10 % port of the 10 dB coupler and its power and spectrum are characterized by a power meter and an optical spectrum analyzer (OSA) with a resolution of 0.015 nm, respectively.

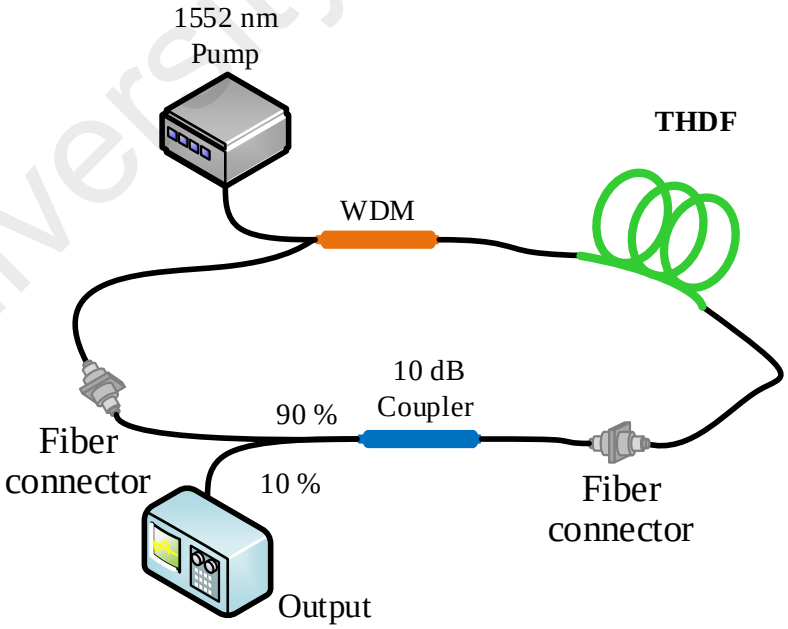

Figure 5.3: Configuration of the CW THDFL in a ring cavity.

Figure 5.4 shows the amplified spontaneous emission (ASE) spectra as the THDF is pumped by 1552 nm laser at various THDF lengths ranging from 1 to 5 m. In the experiment, the 1552 nm pump power is fixed at 500 mW and the ASE is measured after the THDF before it is connected to the 10 dB coupler. The ASE spectrum peaks at around 1900 nm and 2100 nm with 2 m and 5 m long THDF, respectively. This shows that 2 m and 5 m are the optimum lengths for generating photon based on thulium ions and holmium ions, respectively. Thulium ions operation at 1900 nm region is due to 1552 nm pumping while the generated ASE at 1900 nm is used to pump holmium ions to generate ASE at a longer wavelength region of 2100 nm. As the 1552 nm pump power increases, the ASE power in the ring cavity is also increased. The lasing starts as the pump power is increased above 650 mW. The operating wavelength of the laser is determined by the gain spectrum of the THDF which covers the wavelength region of 1790-2200 nm as well as the cavity loss.

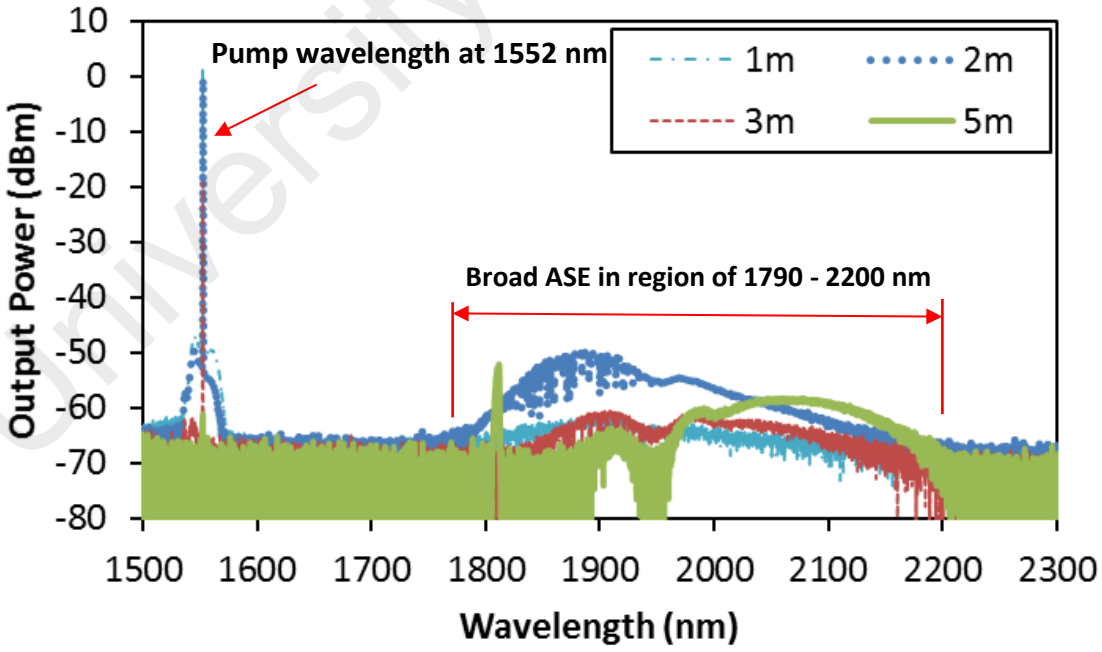

Figure 5.4: ASE spectra of at various THDF lengths as the active fiber is pumped by the 1552 nm laser.

The green spectra in **Figure 5.4** showed the spectrum of THDF for a length of 5 m. Moreover, the 1552 nm pump is highly absorbed by THDF and making the pumping wavelength for the green spectra almost disappeared. The spectra of the THDFL configured with 2 m and 5 m long THDF are shown in **Figure 5.5** when the pump power is fixed at 700 mW. The generated lasers peak at 1909 nm and 1983 nm when the THDF length is fixed at 2 m and 5 m, respectively. The 1909 nm lasing is due to Tm^{3+} ion transition ($^3H_4 \rightarrow {}^3H_6$) while the 1983 nm lasing is due to Ho^{3+} transition ($^5I_7 \rightarrow {}^5I_8$). At sufficient THDF length, energy transfer from Tm^{3+} to Ho^{3+} occurs and generates laser at the longer wavelength as shown in **Figure 5.5**. The optical signal to noise ratio (OSNR) is measured to be about 32 dB and 39 dB for 1909 nm and 1983 nm lasing respectively. The improved SNR is obtained at 1983 nm due to the longer active fiber used, which provides a higher Tm^{3+} and Ho^{3+} ions concentrations and thus enhances the population inversion in the gain medium.

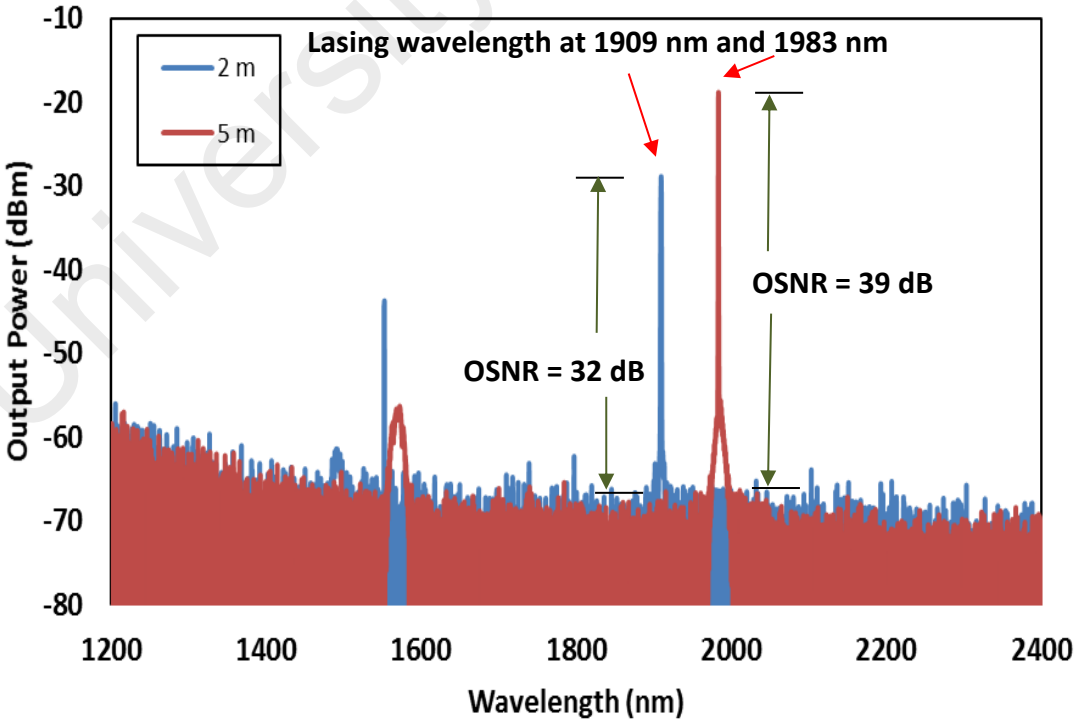

Figure 5.5: Output laser of the THDFL at pumping power of 700 mW.

The output power against the pump power is investigated for the THDFL performance at two different THDF lengths; 2 and 5 m. The result is summarized in **Figure 5.6**. It is observed that the THDFL demonstrates thulium and holmium ions operations at 1909 nm and 1983 nm as the gain medium length is fixed at 2 and 5 m long, respectively. As shown in the figure, lasing starts at a threshold pump power of 650 mW and the laser output increased linearly with launched pump power for both THDF lengths. A maximum output power of 31 mW was achieved at the pump power of 1100 mW for the THDFL configured with 5 m long gain medium, which operates at 1983 nm. The slope efficiencies of 2.15 % and 5.78 % are obtained for the 1909 nm and 1983 nm lasers, which are obtained at THDF lengths of 2 and 5 m respectively, as measured based on **Figure 5.6**.

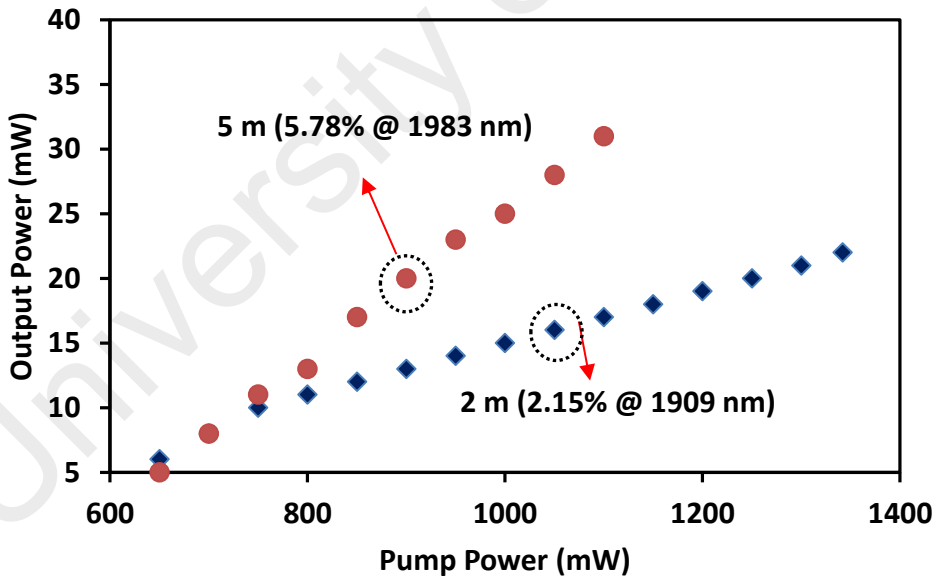

Figure 5.6: An output power of the CW THDFL against the pump power at two different active fiber lengths; 2 m and 5 m.

The slope efficiency of the laser increases with the longer fiber length due to the availability of higher active ions for population inversion and photon generation. The 1552 nm pump threshold of a laser is slightly smaller at 2 m since energy transfer is not required for generating 1909 nm laser. The efficiency of the proposed THDFL can be further improved by optimizing the resonator and the active fibers.

5.4 Fabrication and Characterization of Graphene Oxide PVA Film

Many fabrication methods and synthesis processes of graphene oxide currently involve tedious steps and long experimental time, especially in mixing, heating or cooling the reactants necessary for chemical oxidation. In this work, we prepared the GO using the simplified Hummer's method without any temperature control. Oxidation of graphite flakes was carried out by mixing sulfuric acid (H_2SO_4) and phosphoric acid (H_3PO_4) in a ratio of 320 ml and 80 ml respectively, graphite flakes and potassium permanganate (18 g), using a magnetic stirrer. After adding all the materials slowly, the one-pot mixture was left for stirring for 3 days to allow the oxidation of graphite. The colour of the mixture changes from dark purplish green to dark brown. Later, H_2O_2 solution was added to stop the oxidation process, and the colour of the mixture changes to bright yellow, indicating a high oxidation level of graphite. The graphite oxide formed was washed three times with 1 M of HCl aqueous solution and repeatedly with deionized water until a pH of 4–5 was achieved. The washing process was carried out using simple decantation of supernatant via a centrifugation technique with a centrifugation force of 10,000 g. During the washing process with deionized (DI) water, the graphite oxide experienced exfoliation, which resulted in the thickening of the graphene solution, forming a GO gel. The GO gel was then mixed with DI water to obtain graphene oxide flakes solution.

Then, we prepared a PVA solution by dissolving 1 g of PVA in 120 ml distilled water. Then we mixed the PVA solution with the centrifuged GO suspension at the ratio of 3:2 (in ml) to form the precursor and the mixture was stirred using an ultrasonic cleaner for about one hour. This step helped us get precursor with enough viscosity so that it could be easily used in forming a film. Finally, suitable amounts of precursor were spread thinly on the glass substrate, and let dry in an oven at a temperature of 56 °C to form the GO-PVA film, which is then used to construct a saturable absorber. The thickness of the film is about 50 µm.

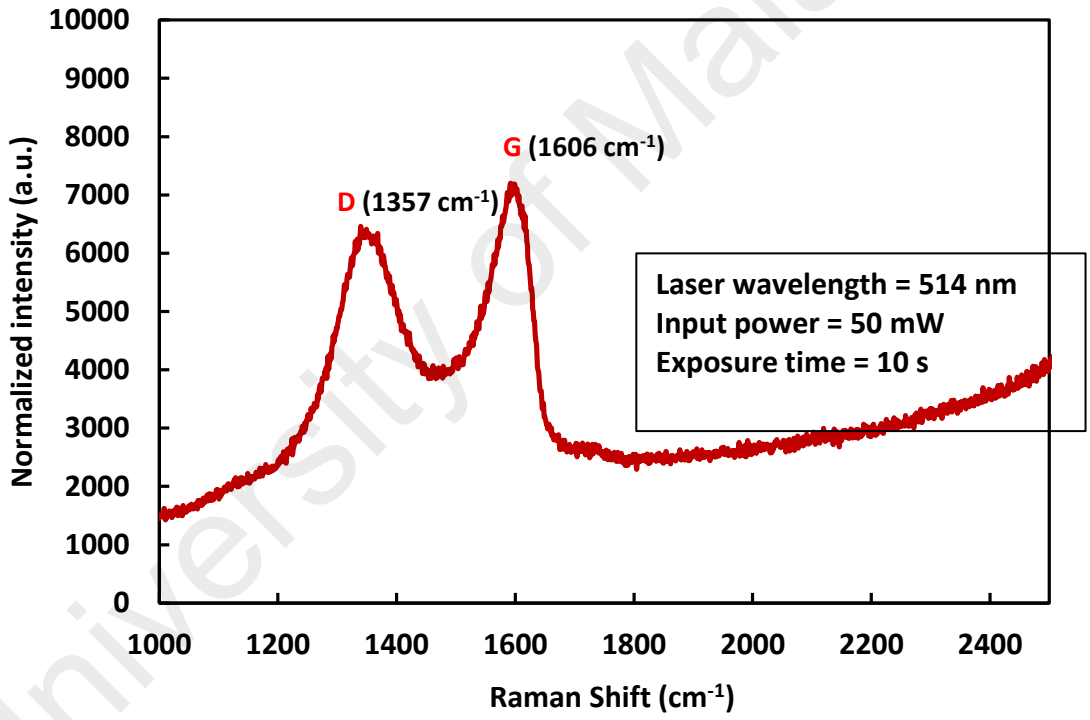

Figure 5.7: Raman spectrum of the fabricated GO-PVA film.

In order to check the existence of graphene element in the GO-PVA film, Raman spectroscopy measurement was performed on the sample. **Figure 5.7** shows the Raman spectrum, which was recorded by a spectrometer when a 514 nm beam of an argon ion laser is radiated on the GO-PVA film. As shown in **Figure 5.7**, there are two main peaks

at around 1357 cm^{-1} and 1606 cm^{-1}, the D, and the G, respectively, whereas Raman spectrum for pristine graphite/graphene should contain G peak only (Pei & Cheng, 2012).

The G peak originates from the in-plane vibration of sp^2 carbon atoms, it is due to the E_{2g} phonon at the Brillouin zone centre. The D peak indicates the presence of defects and disorder in the graphite/graphene structure. This mode arising from the doubly resonant disorder-induced mode. In this case, this is the result of oxygenation (O) of graphite to graphene oxide. Such structure contains covalently bonded oxygen functional groups, e.g. hydroxyl, epoxy, carbonyl, what destroy the network of conjugated double bonds. The D peak originates from the breathing modes of six-membered rings that are activated by defects (Eigler et al., 2012). The relative intensity ratio of both D and G peaks (I_D / I_G) is a measure of disorder degree and is inversely proportional to the average size of the sp^2 clusters which is 0.85. Although there is disordered cause by the O-incorporation that raise the D peak, however, the D peak is still relatively low due to the large GO sheets that close to the lateral size of few hundreds micron.

The nonlinear optical characteristic of the GO-PVA film was then investigated to confirm its saturable absorption. We used a transmission technique where a homemade mode-locked fiber laser operating at 1567 nm wavelength with 0.9 ps pulse width and 17.5 MHz repetition rate was used as a light source. The light is launched into the film and the transmitted power is recorded as a function of incident intensity. **Figure 5.8** shows the nonlinear saturable absorption for the GO-PVA film, which was obtained by varying the input laser power. In the figure, the experimental data are fitted according to the following simple two-level SA model:

$$T(I) = 1 - \alpha_s * exp\,(-I/I_{sat}) - \alpha_{ns} \quad (5.1)$$

where $T(I)$ is the transmission, α_s is the modulation depth, I is the input intensity, I_{sat} is the saturation intensity, and α_{ns} is the non-saturable absorption. As shown in **Figure 5.8**, the GO-PVA film based SA has the modulation depth or saturable absorption, non-saturable absorption, and saturation intensity of 11 %, 9 %, and 1.3 mW/cm^2, respectively.

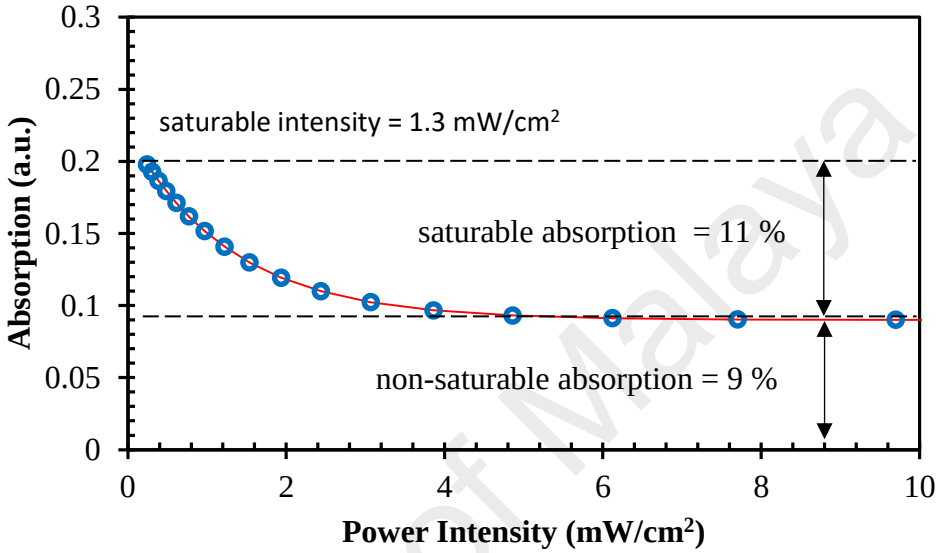

Figure 5.8: Nonlinear absorption characteristics for the fabricated GO-PVA film.

5.5 Q-Switched THDFL Using Graphene Oxide PVA Saturable Absorber

Q-switched fiber laser emitting at the eye-safe and water absorption region of around 2 μm are useful in many applications such as LiDAR, remote sensing, communication and medicine (Fermann & Hartl, 2013). Compared with the active technique, the passive approach is better in terms of simplicity, compactness, and flexibility of implementation (Wang et al., 2012). The passive Q-switching generation can be realized by using either an artificial saturable absorber (nonlinear polarization rotation, nonlinear optical loop mirror) or real saturable absorber (SA) techniques. Up to date, various real-SAs have been implemented such as semiconductor saturable absorber mirrors (SESAMs), two-dimensional (2D) materials (graphene, topological insulators,

transition-metal di-chalcogenides) and doped-fiber SA for Q-switching generation in various fiber lasers and cavities (Butler et al., 2013). However, the applications of SESAM are restricted due to their drawbacks such as complex optical alignments, environmental sensitivity, complicated fabrication and limited operating bandwidth. Among 2D nanomaterials, graphene is the most reliable material for SA applications.

In this section, we demonstrate an all-fiber THDFL that was core-pumped at 1552 nm and passively Q-switched at two wavelengths of 1910.7 and 1980.7 nm using a GO embedded in PVA film as a SA. Stable pulsing with a threshold pump power of 968 mW, a maximum repetition rate of 54.43 kHz, the highest pulse energy of 0.166 nJ and the smallest pulse width of 2.28 μs is obtained in a 12 m Q-switched resonator. **Figure 5.9** shows the configuration of the proposed Q-switched THDFL where the fabricated GO-PVA SA film is inserted in the laser cavity as a Q-switcher. It uses a 5 m long THDF, which was core-pumped by a laboratory-made 1552 nm fiber laser via fused wavelength division multiplexer (WDM). This pump providing a continues-wave pump power of up to 1.2 W. The THDF has a core and cladding diameters of 11.5 μm and 125 μm, a numerical aperture (NA) of 0.14 and thulium ion absorptions of 100 dB/m at 790 nm. The GO-PVA film was sandwiched between two fiber ferrules that have been applied with index matching gel to act as a passive Q-switcher in the cavity. After core-pumping up to 1.5 W pump power, it was observed that the GO-PVA film still can operate without any damage. The signal was coupled out using a 10 dB coupler which keeps 90 % of the light oscillating in the ring cavity for both spectral and temporal diagnostics. The output laser was tapped out from a 10 % port of the 10 dB coupler. The spectral characteristic was measured using an optical spectrum analyzer (OSA) which has a spectral resolution of 0.05 nm while the temporal characteristics were measured using a 500 MHz oscilloscope and a 7.8 GHz radio-frequency (RF) spectrum analyzer via a 7 GHz bandwidth InGaAs

photodetector. The rest of ring resonator comprises a 7 m SMF-28 fiber and thus the total cavity length is approximately 12 m.

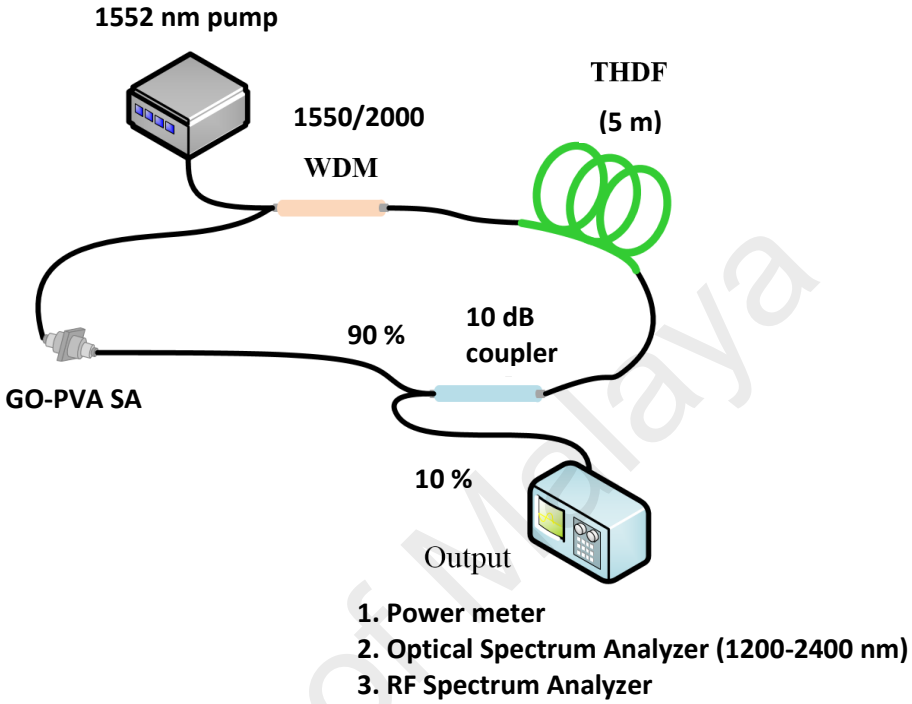

Figure 5.9: Laser configuration for THDFL in a ring cavity.

In the experiment, continuous wave (CW) laser was first generated at a pump power of around 900 mW. Then the laser transited to stable Q-switched pulses at the pump power of 968 mW where the operation was maintained up to the pump power of 1151 mW. The spectral characteristic of the Q-switched THDFL is shown in **Figure 5.10** at the pump power of 1077 mW. It indicates that the laser operates at two wavelengths of 1910.7 nm and 1980.7 nm with a 3 dB bandwidth of less than 0.1 nm. The generated lasers peak at 1910.7 nm and 1980.7 nm when the THDF length is fixed at 5 m. The 1910.7 nm lasing is due to Tm^{3+} ion transition ($^3H_4 \rightarrow {}^3H_6$) while the 1980.7 nm lasing is due to Ho^{3+} transition ($^5I_7 \rightarrow {}^5I_8$).

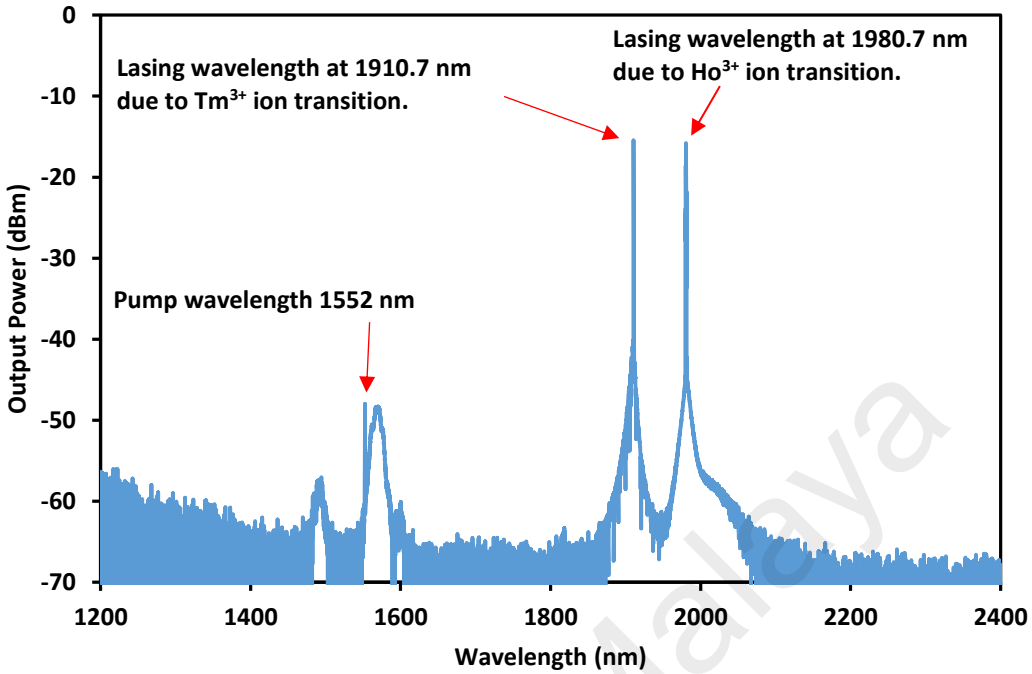

Figure 5.10: Optical spectrum of Q-switched THDFL with the GO-PVA SA at the pump power of 1077 mW.

The typical pulse train of the laser at the pump powers of 1151 mW is illustrated in **Figure 5.11**, which indicates the period of 18.4 μs without noticeable timing jitter. This corresponds to a pulse repetition rate of 54.34 kHz. The pulse width is approximately 2.44 μs, which is comparable to the values obtained by other SAs. To verify that the GO-PVA film was responsible for the Q-switching pulse generation for the laser, the film was removed from the setup. In this case, we observe no Q-switching pulse on the oscilloscope at any pump powers, which confirms the Q-switching operation was attributed to the SA.

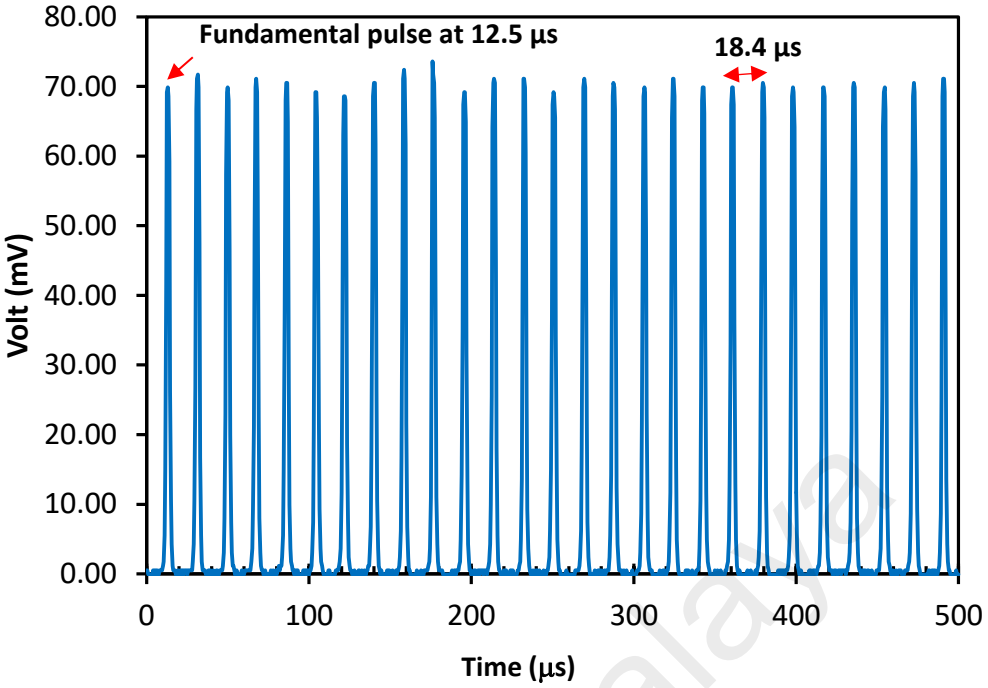

Figure 5.11: Typical oscilloscope trace of the Q-switched THDFL at the pump power of 1151 mW.

How the repetition rate and pulse width of the proposed Q-switched THDFL evolved with the variation of pump power are also investigated. The results are plotted in **Figure 5.12**, where the repetition rate of the Q-switching pulses is observed to monotonically increase from 30.22 to 54.43 kHz as the 1552 nm pump power is varied from 968 to 1151 mW. On the other hand, the pulse width is seen to fluctuate within 2.28 to 2.71 µs as the pump power is increased from 968 mW to 1151 mW. The smallest pulse width of 2.28 µs is obtained at the pump power of 1114 mW. The fluctuation is most probably due to the dual-wavelength operation. The pulse width could be further improved by either shortening the laser cavity or improving the SA film characteristics such as modulation depth. In addition, the average output power and the corresponding single-pulse energy of the laser are also investigated at various pump powers.

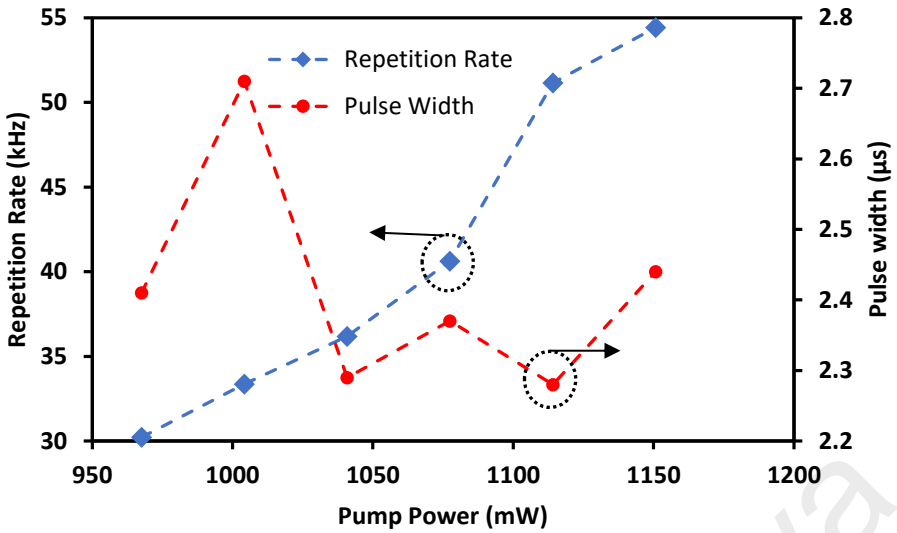

Figure 5.12: Repetition rate and pulse width of Q-switched THDFL at pump power within 968 mW to 1151 mW.

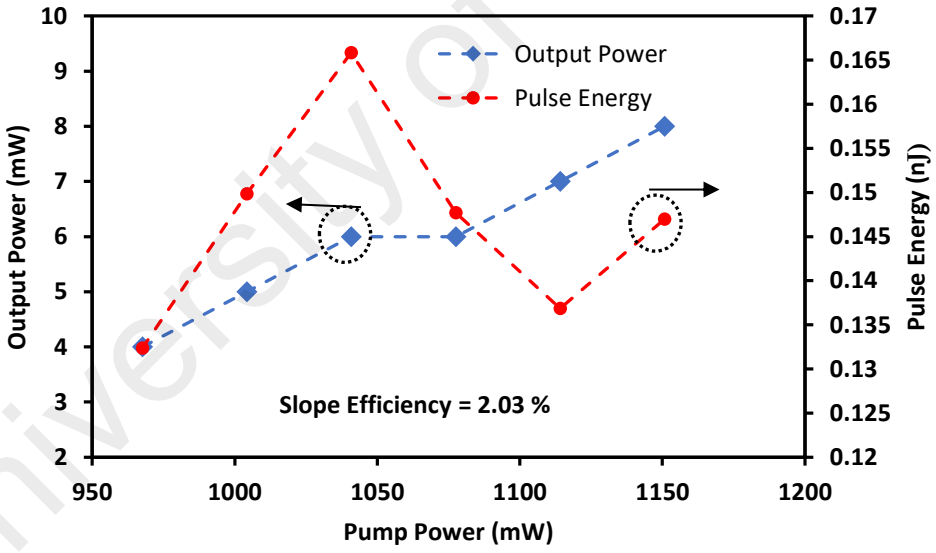

Figure 5.13: Output power and pulse energy of Q-switched THDFL at pump power within 968 mW to 1151 mW.

The results are plotted in **Figure 5.13** where the average output power increased from 4 to 8 mW as the 1552 nm pump power is varied from 968 to 1151 mW. The pulse energy also increased with the input pump increment. However, it suddenly dropped as the pump power exceeds 1041 mW before increases again as the pump power is further

increased above 1114 mW. The pulse energy fluctuation is attributed to the increase in noise level because of dual wavelength operation. The maximum pulse energy of 0.166 nJ is obtained at the pump power of 1041 mW.

Figure 5.14 shows the RF spectrum of the Q-switched THDFL at the pump power of 1004 mW, which was obtained within 600 kHz span. As illustrated in the figure, the fundamental repetition rate of the laser is 33.96 kHz which agrees with the pulse period of the oscilloscope trace. The signal-to-noise ratio of the RF spectrum is observed at 40 dB with the presence of harmonic peaks, which gradually decrease. This indicates the Q-switching operation has a broad pulse width (microseconds) and the frequency domain transformation corresponds to its time-domain. As the pump power above 1151 mW, the Q-switching operation would disappear. These results show that the GO-PVA material has a great potential for pulsed laser applications at 2-micron wavelength region.

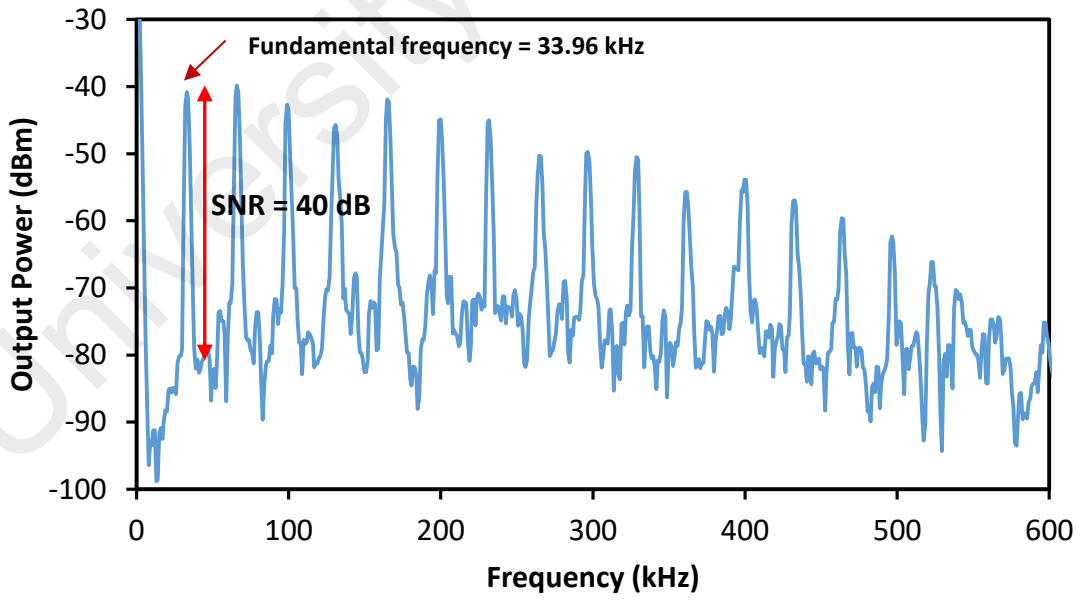

Figure 5.14: RF spectrum of Q-switched THDFL at the pump power of 1004 mW with showing the signal to noise ratio of 40 dB for the fundamental frequency.

5.6 Mode-Locked THDFL Using Graphene Oxide-PVA Saturable Absorber

Evolution of pulsed laser starts by using a dye gain medium in the 80s, and a decade later by the solid state gain medium. In the early 2000s, people start to move to the fiber gain medium in generating pulsed fiber laser due to high reliability and cost-efficient. Compare to the Q-switched fiber lasers, mode-locked fiber lasers have undergone tremendous research and development in a past few decades. The high peak power, high repetition rate, and ultra-short pulse duration enable a mode-locked fiber laser to contribute significantly for a wide area of applications. For instance, the mode-locked laser systems operating in the "eye safe" spectral range around 2-micron become a subject of growing interest and rapid development because of their increasing application requirements in free-space optical communication, LIDAR, military, medical surgery, material processing, etc (Fermann & Hartl, 2013; Fried et al., 2008).

In the previous section, Q-switched THDFL has been demonstrated using a newly developed GO embedded in PVA film as a SA. In this section, a mode-locked THDFL operating at 1979 nm is demonstrated by inserting the similar GO-PVA SA in a modified ring configuration. The mode-locked THDFL was generated by using the modified all-fiber ring cavity configuration in conjunction with GO-PVA based SA. The schematic diagram of the laser is shown in **Figure 5.15**. The laser cavity consists of 5 m long THDF as a gain medium, wavelength division multiplexer (WDM), 10 m long scandium-doped fiber (ScDF), an isolator, a 90:10 dB output coupler and SA. A 1552 nm EYDFL is used to pump the THDF via 1550/2000 nm fused WDM. The generated laser propagates in unidirectional and maintain its direction after passing through the isolator. The 10 m long ScDF was added in the cavity to gain sufficient nonlinearity effects for the mode-locked generation. The ScDF has a core composition of SiO_2-GeO_2-Sc_2O_3 with core diameter and NA of 7.5 μm and 0.12, respectively.

The group velocity dispersion (GVD, β_2) parameter for THDF is about -72.8 ps^2/km. Other fibers in the cavity are ScDF with -127 ps^2/km and a standard SMF with -80 ps^2/km, which constituted the rest of the ring. The total cavity length is around 17.3 m and the total net group delay dispersion (GDD) in the cavity is operates in anomalous dispersion condition of -1.818 ps^2. The fundamental repetition rate is calculated as 11 MHz.

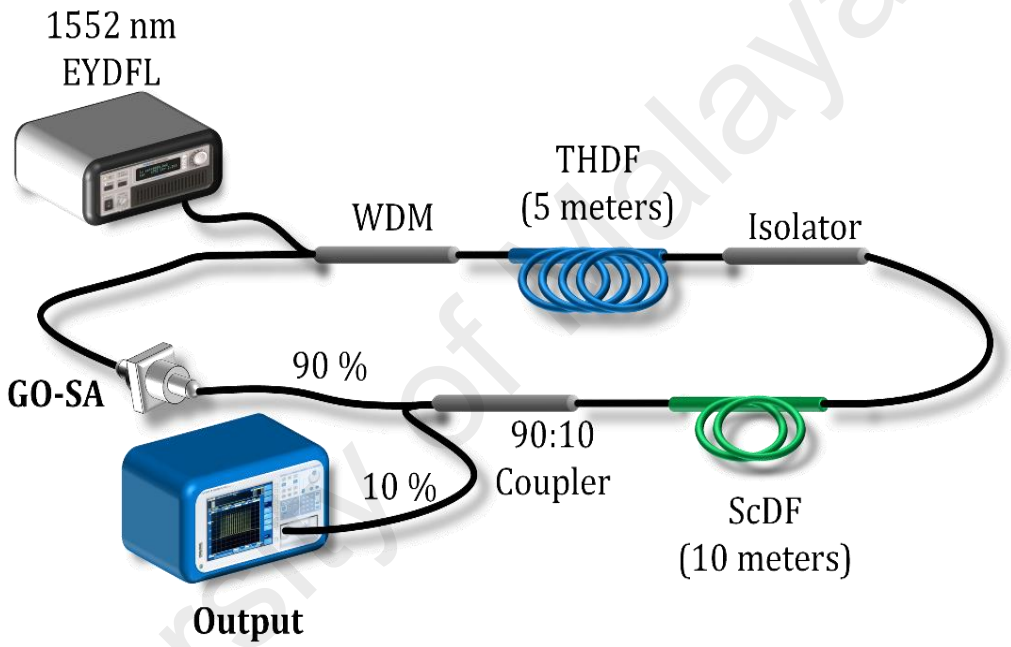

Figure 5.15: Schematic configuration of THDFL in a ring cavity with ScDF.

The mode-locked laser output was collected from 10 % port of the 90:10 output coupler while allowing the remaining of 90 % of the light to continuously oscillate in the cavity. With FC fiber adapter, the 1 mm x 1 mm GO-PVA film was sandwiched by two fiber ferrules to construct the SA device. Index matching gel was used as an adhesive and also as an element to fill the air-gap. Optical spectrum, pulse information and laser power of the proposed laser is measured by an optical spectrum analyzer (OSA), an oscilloscope

(OSC) combined with a 7 GHz photodetector and an optical power meter, respectively. The radio frequency (RF) spectrum is measured by a 7.8 GHz RF spectrum analyser (RFSA). The mode-locking performances were also investigated when the GO-PVA film removed from the cavity to eliminate the mode-locked mode. This can confirm the presence of mode-locked pulse train was owed to this film.

After the GO-PVA film is inserted in between two fiber ferrules and locked by a fiber adapter, the mode-locking performance of the laser is investigated by slowly increasing the pump power. It is observed that the mode-locked THDF lasers (THDFL) starts at the pump power of 1099 mW and continue stable until the maximum pump power of 1187 mW. The self-started mode-locking was obtained in the cavity is expected due to the high modulation depth of the SA.

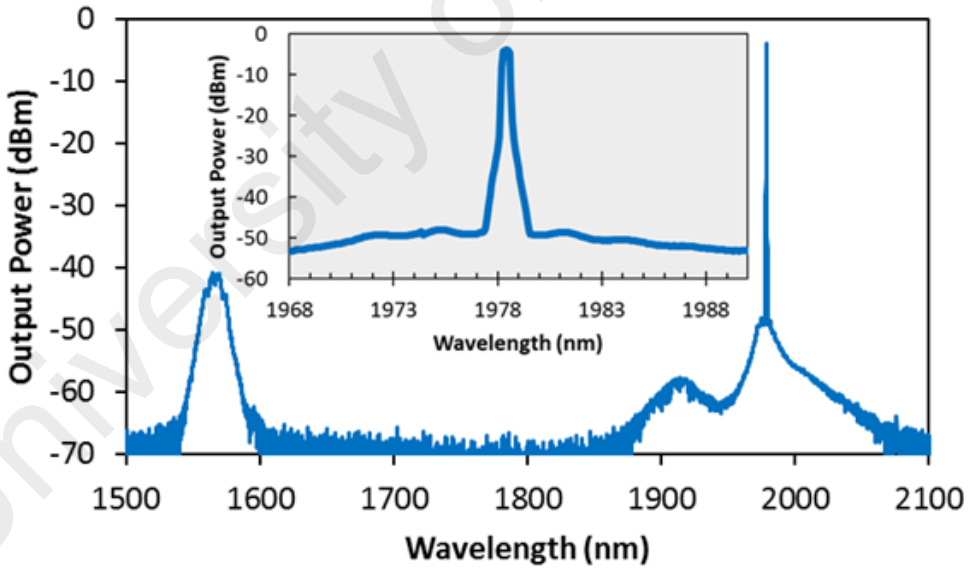

Figure 5.16: Output spectrum with GO-PVA SA at the pump power of 902 mW. The inset shows an enlarged image for pulsed output spectrum at the lasing wavelength of 1979 nm.

Figure 5.16 shows the output spectrum of THDFL in conjunction with GO-PVA SA at the pump power of 902 mW, and the inset is an enlarged image for pulsed output spectrum at lasing wavelength of 1979 nm with a narrow 3 dB spectral bandwidth of 0.4 nm. The measured average output power and the calculated single pulse energy against pump power are then investigated and the results are illustrated in **Figure 5.17**. As shown in the figure, both output power and pulse energy linearly increased with the pump power. It is obtained that the mode-locked THDFL has a slope efficiency of 2.67 %. At the maximum pump power of 1062 mW, the output power and the pulse energy are 15 mW and 1.66 nJ, respectively.

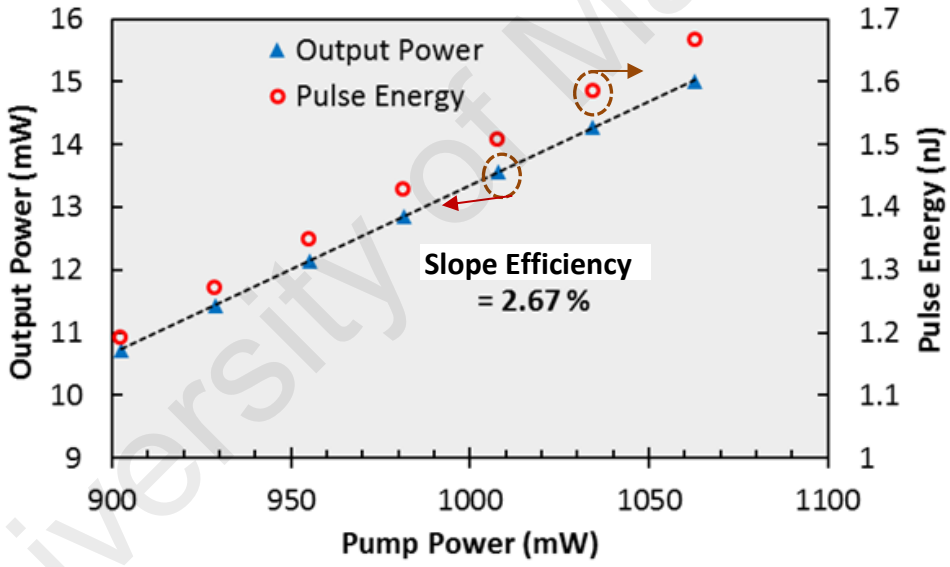

Figure 5.17: Output power and pulse energy obtained when the pump power is varied from 902 mW to 1062 mW.

Temporal characteristics are measured by using a digital oscilloscope and a RF spectrum analyzer via a photodetector. **Figures 5.18 (a)** and **(b)** show pulses train and frequency of the mode-locked lasers at the threshold of 900 mW and maximum pump power of 1060 mW, respectively. As shown in **Figure 5.18 (a)**, the pulse period of 112

ns is corresponded to a repetition rate of 9 MHz and remain stable until 1062 mW pump power. The repetition rate matched well with the fundamental cavity round trip frequency. However, we cannot measure the actual pulse width due to the equipment constraints.

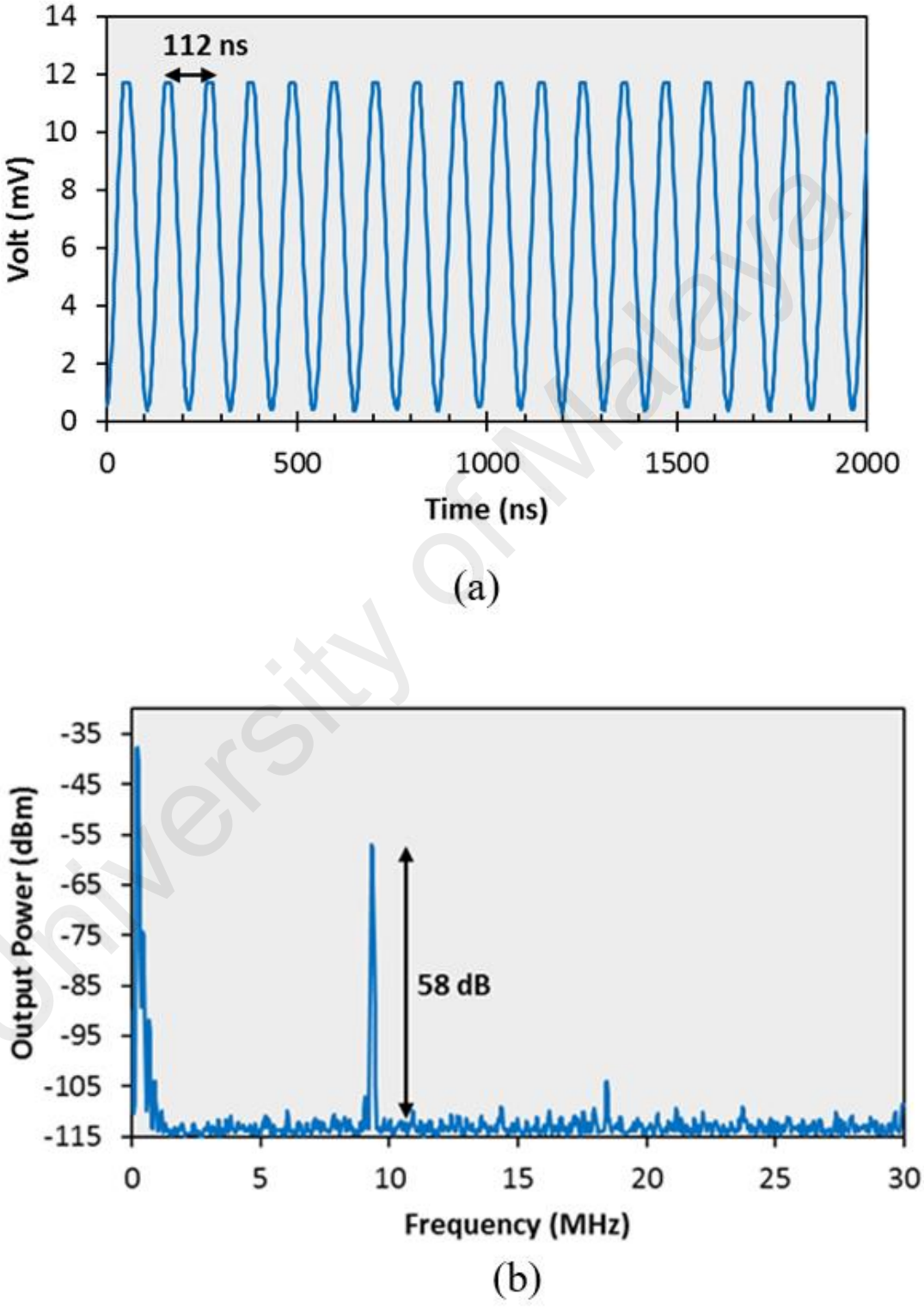

Figure 5.18: Temporal characteristics at the pump power of 1062 mW **(a)** the pulse train of the mode-locked THDFL **(b)** RF spectrum.

According to the $sech^2$ pulse profile with a time-bandwidth product (TBP) of 0.315, the minimum possible limit pulse width is calculated to be around 10.29 ps. This corresponds to the narrow pulse spectra as appears in the OSA (Kobtsev et al., 2011). **Figure 5.18 (b)** shows the RF spectrum confirms the presence of the repetition rate of 9 MHz in the mode-locked THDFL. The SNR is measured about 58 dB. With a single repetition rate appear in RFSA (frequency domain), this indicates the waveform in the OSC (time domain) is a cosine wave pattern which corresponds to the broad pulse width. The mode-locked operation will disappear as we remove a GO-PVA film in the cavity. Without ScDF, the cavity can only generate the Q-switched lasers.

5.7 Summary of THDFL Operations

CW, Q-switched and mode-locked THDFL have successfully demonstrated using THDF as a gain medium in conjunction with 1552 nm pumping. The lasers operate at around 1980 nm region with an efficiency of 5.78 % with the use of 5 m long gain medium due to Ho^{3+} transition ($^5I_7 \rightarrow {}^5I_8$). The GO-based SA film has been obtained by mixing the GO and PVA solution and dry it at the room temperature. The film has an absorption loss of 3.5 dB and a modulation depth of 11 %. It was incorporated into the THDFL cavity to passively generate a Q-switching and mode-locking pulse trains. The Q-switched laser produced a self-started pulse train with the repetition rate that can be tuned from 30.22 to 54.43 kHz as the 1552 nm pump power is increased from 968 to 1151 mW. At the maximum pump power of 1151 mW, the laser produced a Q-switching pulse train with repetition rate, pulse width, output power, and pulse energy of 54.43 kHz, 2.44 μs, 8 mW, and 0.146 nJ, respectively. By adding 10 m long ScDF inside the cavity, the mode-locked THDFL was realized. It generated a self-starting pulse train with the repetition rate of 9 MHz and an estimated minimum possible pulse width of 10.29 ps. At the maximum pump

power of 1062 mW, the mode-locked THDFL produced the output power and pulse energy of 15 mW and 1.66 nJ respectively. These results show GO has a great potential to be used as SA material for pulsed laser applications in the 2-micron region.

CHAPTER 6 : CONCLUSIONS AND FUTURE WORKS

6.1 Conclusions

This research work is devoted to the construction of fiber lasers that emit longer wavelength beams (in the spectral region of around 2 μm) utilizing thulium-doped and co-doped fiber for the improvement of lasing efficiency, pulse energy, pulse width, repetition rate and threshold pump power. The approach taken involves employing two different co-doping elements which are thulium-ytterbium co-doped fiber (TYDF) and thulium-holmium co-doped fiber (THDF) as the gain medium. Both fibers are a newly fabricated and a new commercial gain medium respectively, and their spectroscopic properties as well as energy transfer processes have been investigated. The research work carried out in the laboratory also involve fabrication of home-made 2D nanomaterials saturable absorber for the first time. In the Q-switched lasers, new implementation of 2D nanomaterials saturable absorber which are graphite (exfoliation of pencil-core), graphene oxide (GO) paper, GO polyvinyl alcohol (GO-PVA) and multi-walled carbon nanotubes (MWCNTs) have been proposed in conjunction with a commercial thulium-doped fiber (TDF), a newly fabricated TYDF and a commercial THDF as the gain medium. The proposed pulse laser performances are comparable to the reported published works.

We investigated the performance of the thulium-doped fiber (TDF) as the gain medium which is pumped by an 800 nm pump laser. Thulium-doped fiber lasers (TDFL) generated a broadband amplified spontaneous emission (ASE) across a wavelength range of 1820 - 2010 nm, with a threshold pump power of 155.58 mW. The TDFL is operating at dual wavelength of 1931.62 nm and 1937.09 nm with a signal-to-noise ratio (SNR) of more than 30 dB. The slope efficiency of TDFL which is 16.11 % relatively high due to

the high thulium doping concentration in the gain medium, which supports the cross-relaxation process in the TDFL. Thus, the TDFL requires a smaller pump power to initiate lasing. High thulium doping concentration in the TDF increases the cross-relaxation process such that the optimum length for lasing is comparatively short (Shamsudin et al., 2016).

The presence of graphene layer on the surface of GOP were performed by Raman spectroscopy using laser excitation at 514 nm with an exposure power of 10 mW. The Raman spectrum with two similar prominent peaks within the Raman shift of 100–3200 cm^{-1} and reveals two prominent peaks of GOP at 1351.5 $cm^{-1}$and 1586.9 cm^{-1}, which determine as D and G band, respectively. The G band contributes to an E_{2g} mode of graphite and is related to the in-plane vibration of the sp^2-bonded carbon atoms, whereas the D band is associated with the vibrations of the carbon atoms with sp^3 electronic configuration of disordered graphite. The intensity ratio of D and G bands of the GOP is about 0.997 which indicates the defect levels of sample. High intensity of D peak indicates the structural defects of GOP are high, and it is normal for chemical process of graphene flakes. The insertion loss of the GOP SA is measured to be around 2.6 dB at 1901.6 nm. The linear transmission measurement for GOP were performed by launching the homemade 2-μm amplified spontaneous emission (ASE) source and shows the fabricated GOP has a linear absorption of 2 dB ± 0.5 at 1901.6 nm.

The passive mode-locked TDF linear cavity laser operating at 1901.6 nm with an incorporation of a homemade GOP-SA. The TDFL generates mode-locking pulse at a threshold pump power of 540 mW. By varying the pump power from the threshold power to 1052 mW, pulse repetition rates remain constant at 82.4 MHz. At the maximum pump power of 1052 mW, the pulse width is estimated as 25 ps, whereas the pulse energy is calculated as 83.1 pJ.

A multi-wavelength thulium doped fiber laser (TDFL) with a slope efficiency of 16.57 % is demonstrated using a linear cavity consisting of a broadband mirror and a flat-cleaved fiber end in conjunction with 1552 nm pumping. The TDFL produces eleven lines within a wavelength range from 1895 to 1907 nm with a constant spacing of 1.2 nm and signal to noise ratio of more than 27 dB. The multi-wavelength TDFL is capable of generating pulses with a repetition rate of 11.62 MHz and average output power of 93 mW at the maximum pump power of 1100 mW. The proposed multi-wavelength TDFL is suitable for a multitude of real-world applications such as range-finding, medicine and spectroscopy due to its ability to operate in the eye-safe region of 2-micron.

We successfully demonstrated a new nano-engineering octagonal shape double-clad thulium-ytterbium co-doped fiber (TYDF) to provide an efficient lasing at 2000 nm region based on energy transfer from ytterbium to thulium ions. With a linear configuration, the TYDF laser (TYDFL) operates at the centre wavelength of 1936.4 nm, 1958.6 nm and 1967.5 nm at gain medium lengths of 5 m, 10 m and 15 m, respectively. The proposed laser produces the highest efficiency of 9.9 % and its lowest threshold pump power of 400 mW at 10 m long TYDF. The Q-switched laser operates at 1960 nm region is achieved by exploiting a multi-walled carbon nanotubes (MWCNTs) polymer composite film based saturable absorber (SA). The proposed TYDFL generates a stable pulse train with repetition rates and pulse widths ranging from 18.9 kHz to 35.1 kHz and 7.94 to 1.52 μs, respectively by varying the 980 nm multimode pump power from 440 mW to 528 mW. The maximum pulse energy of 11.2 nJ is obtained at the pump power of 512 mW. A higher performance Q switching is expected to be achieved with the optimization of the SA and laser cavity. A mode-locked TYDFL is also demonstrated using a fabricated graphene oxide (GO) paper as SA to operate at 1942.0 nm at a threshold pump power as low as 1.8 W using a 905 nm multi-mode pump power. The mode-locked TYDFL has a repetition rate of 22.32 MHz and calculated pulse-width of 1.1 ns.

In conclusion for TYDF, the enhancement of lasing performance has been identified in TYDF using three TYDF samples with different lengths i.e 5 m, 10 m and 15 m. The incorporation of active ytterbium ions in the gain medium helps increase the $^3F_4$ population and thus improves the efficiency of the laser through energy transfer processes without any degradation from up-conversion (UC). The experimental results reveal that a 10 m TYDF with has achieved higher efficiency of 9.9 %. This is attributed to the incorporation of Yb^{3+} ions in the gain medium which help to increase the $^3F_4$ population through energy transfer processes. TYDF which has the highest amount of active ytterbium and thulium concentrations exhibits the highest lasing efficiency. An efficient TYDFL with pumping at 980 nm wavelength in conjunction with cladding pumped technique was also demonstrated. Apart from that, the energy transfer processes can be optimized by modifying the dopants compositions thus increase the efficiency of stepwise energy transfer. By pumping the TYDF with an 980 nm pumping excitation, 2 energy transfer processes may occur which are cross relaxation and energy transfer from active Yb^{3+} to Tm^{3+} ions.

Due to the efficient energy transfer, a broadband amplified spontaneous emission (ASE) from THDF was proposed. The performance of continuous wave (CW), Q-switched and mode-locked thulium-holmium co-doped fiber lasers (THDFL) with 1552 nm pumping in ring configuration were investigated. Graphene oxide (GO) embedded in polyvinyl alcohol (PVA) film is used as a passive saturable absorber (SA) in generating Q-switched and mode-locked pulse train. The proposed THDFLis a better choice than the conventional erbium-doped fiber lasers since they lase near 2 μm and have a broad bandwidth (1.7-2.1 μm) that can support short, high peak power pulses. Compared to the singly doped holmium-doped fiber, the proposed laser is advantageous due to the use of 1552 nm pumping wavelength. The 1552 nm fiber laser is widely available and cheaper than 1.8 or 1.9 μm laser source. THDFL

configured with 5 m long gain medium, which operates at 1983 nm. The slope efficiencies of 2.15 % and 5.78 % are measured for the 1909 nm and 1983 nm lasers, which are obtained at THDF lengths of 2 and 5 m respectively. The slope efficiency of the laser increases with the longer fiber length due to the availability of higher active ions for population inversion and photon generation. The Q-switched laser produced a self-started pulses train with a repetition rate that can be tuned from 30.22 to 54.43 kHz as the 1552 nm pump power is increased from 968 to 1151 mW. At maximum pump power of 1151 mW, the laser produced a Q-switching pulse train with repetition rate, pulse width, output power, and pulse energy of 54.43 kHz, 2.44 μs, 8 mW, and 0.146 nJ, respectively. By adding 10 m long ScDF inside the cavity, a mode-locked THDFL was realized. It generated a self-starting pulse train with a repetition rate of 9 MHz and an estimated minimum possible pulse width of 10.29 ps. At the maximum pump power of 1062 mW, the mode-locked THDFL produced the output power and pulse energy of 15 mW and 1.66 nJ. These results show that the GO is a new potential SA material for pulsed laser applications in the 2-micron region.

The primary objectives focus on the development of CW, Q-switching and mode-locked fiber lasers at 2 μm region have been achieved. Even though several results are not as expected, the discussion and analysis of the performances have been carried out. The laser performances on the effect of co-doping ytterbium and holmium to the thulium ions have been investigated. Although TYDFL has been expected to give better lasing performance, several limiting factors have been identified to be the reason of poor lasing performance. The successful construction of a passively Q-switched fiber laser at the 2 μm region using in-house fabricated GOSA and MWCNTs as saturable absorber facilitates numerous applications in fiber communications and sensor. The findings in this work could be used in the future for the development of fiber lasers based sources for targeting new applications.

In this research works, we have successfully implemented and demonstrated various new configurations and techniques for realizing an all-fiber Q-switched fiber lasers. These lasers are based on commercial TDF, newly developed TYDF and THDF as the gain medium in conjunction with 800 nm, 980 nm and 1552 nm pumping. Two passive saturable absorbers; graphene and MWCNTs are developed and fabricated in-house to realize the Q-switching. The graphene oxide flakes are obtained via modified Hummer's method. In this method, the graphite are going process of oxidation electrolyte at room temperature and then mixed with the polymer to form a free standing film with a thickness of 50 µm.

On the other hand, the MWCNTs composite is prepared by mixing the MWCNTs homogeneous solution with a dilute polyvinyl alcohol (PVA) polymer solution before leaving it to dry at room temperature to produce a film. The fabricated SA is then attached to the end of fiber ferrule with the aid of index matching gel and connected with another clean fiber ferrule via FC/PC connector to construct the SA. The SA is incorporated in a ring TDFL and TYDFL to generate Q-switching pulse train. It is found that the MWCNTs-SA performs better than the GOSA. This is due to the better thermal management and the saturation fluence of the MWCNTs. To the best of our knowledge, this is the first reported Q-switched laser at 2 µm region using MWCNTs based SA.

6.2 Overall Numerical Conclusions

A comparison for the performance of Q-switched lasers is shown in **Table 6-1**.

Table 6-1: Performance comparison of the Q-switched laser of different gain mediums.

Gain media / Saturable Absorber	Pump wavelength	Maximum pump power	Highest repetition rate	smallest pulse width	Maximum pulse energy
TDFL / pencil-core	1552 nm	431 mW	34.60 kHz	4.69 μs	36.71 nJ
TYDFL / MWCNT-PVA	980 nm	528 mW	35.1 kHz	1.52 μs	11.2 nJ
THDFL / GO-PVA	1552 nm	1151 mW	54.43 kHz	2.28 μs	0.166 nJ

6.3 Future Works

Up to this point, all **three (3) objectives** of this thesis has been fulfilled and successfully implemented. However, the discussion can be further enhanced by establishing the cross-relaxation, energy transfer upconversion (ETU) and excited state absorption (ESA) measurement of the TDF, TYDF and THDF. These important parameters should be thoroughly studied by means of their respective level lifetime of the Tm^{3+}, active ytterbium ions and active holmium ions. The understanding of these effects and knowledge of the parameters can accurately describe the performance of the CW and pulsed laser. The performance of a fiber can be considerably impaired by undesired effects such as unsaturable absorption and ESA. Another important consideration which can be taken into account is the fabrication of the double-cladding TYDF. The TYDF cannot be pumped experimentally up to the kilowatt power level as usually reported in the literature, due to the fiber damage at the splicing point. The relatively high numerical aperture (NA) of the pumped cladding can be further designed to meet the high power applications.

The compact device such as array waveguide grating (AWG) which is used as a wavelength slicing mechanism may contribute to the multi-wavelength fiber laser generation. Another related field of interest to explore is the demonstration of the nonlinear effect such as Brillouin fiber laser (BFL) at the 2 μm region. The proposed Brillouin pump can be seeded by the THFL or TYDFL, provided that the laser can be tunable in several wavelength ranges which can be done by an external filter or a tunable bandpass filter. The realization of the fiber laser at 2 μm also enables some of the sensor-based experiments within the 2 μm region to be further studied. Since the 2 μm wavelength has strong absorption of water and biological tissue, the 2 μm fiber laser can be proposed as a source for incision of the tissue samples in an experiment which can be carried out in conjunction with Institute of Biological Science, Faculty of Science, University of Malaya.

In order to improve the pulse lasers, the average power and pulse energy of the nanosecond pulses can be further scaled up by using power amplifier stage. To realize this, a high pump power requirement which implies the use of a master oscillator/power amplifier (MOPA) can be designed. Apart from that, another method of implementing the pulse laser in 2-micron such as nonlinear polarization rotation (NPR) method can be further explored and the performance can be compared with the GOSA and MWCNTs based SA. The upgrading the Q-switched laser to mode-locked laser is crucial due to their femtosecond pulse laser generation which is widely used in most applications. The design of intracavity dispersion management of the laser needs to be comprehensively studied in order to achieve femtosecond pulse generation. The outcomes from this PhD thesis may provide a source of optimization for the next experiment in the future.

REFERENCES

Agger, S. D., & Povlsen, J. H. (2006). Emission and absorption cross section of thulium doped silica fibers. *Optics Express, 14*(1), 50-57.

Alcock, I., Ferguson, A., Hanna, D., & Tropper, A. (1986). Mode-locking of a neodymium-doped monomode fiber laser. *Electronics Letters, 22*(5), 268-269.

Alcock, I., Tropper, A., Ferguson, A., & Hanna, D. (1986). Q-switched operation of a neodymium-doped monomode fiber laser. *Electronics Letters, 22*(2), 84-85.

Allain, J., Monerie, M., & Poignant, H. (1989). Tunable CW lasing around 0.82, 1.48, 1.88 and 2.35 μm in thulium-doped fluorozirconate fiber. *Electronics Letters, 25*(24), 1660-1662.

Alvarez-Chavez, J., Offerhaus, H., Nilsson, J., Turner, P., Clarkson, W., & Richardson, D. (2000). High-energy, high-power ytterbium-doped Q-switched fiber laser. *Optics Letters, 25*(1), 37-39.

Ando, Y., & Iijima, S. (1993). Preparation of carbon nanotubes by arc-discharge evaporation. *Japanese Journal of Applied Physics Part 2 Letters, 32*, L107-L107.

Azooz, S., Harun, S., Ahmad, H., Halder, A., Paul, M. C., Pal, M., & Bhadra, S. K. (2015). Mode-Locked Thulium Ytterbium Co-Doped Fiber Laser with Graphene Oxide Paper Saturable Absorber. *Chinese Physics Letters, 32*(1), 014204.

Blackmon, R. L., Irby, P. B., & Fried, N. M. (2012). Enhanced thulium fiber laser lithotripsy using micro-pulse train modulation. *Journal of Biomedical Optics, 17*(2), 0280021-0280026.

Bonaccorso, F., & Sun, Z. (2014). Solution processing of graphene, topological insulators and other 2D crystals for ultrafast photonics. *Optical Materials Express, 4*(1), 63-78.

Bonaccorso, F., Sun, Z., Hasan, T., & Ferrari, A. (2010). Graphene photonics and optoelectronics. *Nature Photonics, 4*(9), 611-622.

Booth, B. L. (1989). Low loss channel waveguides in polymers. *Journal of Lightwave Technology, 7*(10), 1445-1453.

Bremer, K., Pal, A., Yao, S., Lewis, E., Sen, R., Sun, T., & Grattan, K. T. V. (2013). Sensitive detection of CO_2 implementing tunable thulium-doped all-fiber laser. *Applied Optics*, 52(17), 3957.

Brown, D. C., & Hoffman, H. J. (2001). Thermal, stress, and thermo-optic effects in high average power double-clad silica fiber lasers. *IEEE Journal of Quantum Electronics, 37*(2), 207-217.

Bünzli, J.-C. G., & Piguet, C. (2005). Taking advantage of luminescent lanthanide ions. *Chemical Society Reviews, 34*(12), 1048-1077.

Butler, S. Z., Hollen, S. M., Cao, L., Cui, Y., Gupta, J. A., Gutierrez, H. R., . . . Ismach, A. F. (2013). Progress, challenges, and opportunities in two-dimensional materials beyond graphene. *ACS Nano, 7*(4), 2898-2926.

Cariou, J.-P., Augere, B., & Valla, M. (2006). Laser source requirements for coherent lidars based on fiber technology. *Comptes Rendus Physique, 7*(2), 213-223.

Chen, Y.-F., Tsai, S., & Wang, S. (2000). High-power diode-pumped Q-switched and mode-locked Nd : YVO_4 laser with a Cr^{4+} : YAG saturable absorber. *Optics Letters, 25*(19), 1442-1444.

Chen, Z., Ma, S., & Dutta, N. (2009). Multiwavelength fiber ring laser based on a semiconductor and fiber gain medium. *Optics Express, 17*(3), 1234-1239.

Chernysheva, M. A., Krylov, A. A., Kryukov, P. G., & Dianov, E. M. (2012). Nonlinear amplifying loop-mirror-based mode-locked thulium-doped fiber laser. *IEEE Photonics Technology Letters*, 24(13), 1254.

Coté, G. L. (2001). Non-invasive and minimally-invasive optical monitoring technologies. *The Journal of Nutrition, 131*(5), 1596S-1604S.

Creeden, D., Budni, P. A., & Ketteridge, P. A. (2009). Pulsed Tm-doped fiber lasers for mid-IR frequency conversion. *SPIE LASE: Lasers and Applications in Science and Engineering (pp. 71950X-71950X). International Society for Optics and Photo,7195*: San Jose, California, USA: SPIE Publication.

Damanhuri, S. S. A., Halder, A., Paul, M. C., Ali, S. M. M., Saidin, N., Harun, S. W., . . . Bhadra, S. K. (2013). Effects of Yb/Tm concentration and pump wavelength on the performance of ytterbium-sensitized thulium-doped fiber laser. *IEEE Journal of Quantum Electronics, 49*(1), 95-99.

Darabont, A., Nemes-Incze, P., Kertész, K., Tapasztó, L., Koós, A., Osváth, Z., . . . Biró, L. (2005). Synthesis of carbon nanotubes by spray pyrolysis and their investigation by electron microscopy. *Journal of Optoelectronics and Advanced Materials, 7*(2), 631-636.

Das, S., Robinson, J. A., Dubey, M., Terrones, H., & Terrones, M. (2015). Beyond graphene: Progress in novel two-dimensional materials and van der Waals solids. *Annual Review of Materials Research, 45*, 1-27.

De Camargo, A., De Oliveira, S., De Sousa, D., Nunes, L., & Hewak, D. (2002). Spectroscopic properties and energy transfer parameters of Tm^{3+} ions in gallium lanthanum sulfide glass. *Journal of Physics: Condensed Matter, 14*(41), 9495.

De Young, R. J., & Barnes, N. P. (2010). Profiling atmospheric water vapor using a fiber laser lidar system. *Applied Optics, 49*(4), 562-567.

Delgado-Pinar, M., Zalvidea, D., Diez, A., Pérez-Millán, P., & Andres, M. (2006). Q-switching of an all-fiber laser by acousto-optic modulation of a fiber Bragg grating. *Optics Express, 14*(3), 1106-1112.

Digonnet, M. J. (2001). *Rare-earth-doped fiber lasers and amplifiers, revised and expanded*: New York, USA: CRC Press.

Digonnet, M. J. (2002). *Rare-Earth-Doped Fiber Lasers and Amplifiers, Revised and Expanded*: New York, USA: CRC Press.

Eichhorn, M., & Jackson, S. D. (2007a). High-pulse-energy actively Q-switched Tm^{3+}-doped silica 2 μm fiber laser pumped at 792 nm. *Optics Letters, 32*(19), 2780-2782.

Eichhorn, M., & Jackson, S. D. (2007b). High-pulse-energy actively Q-switched Tm^{3+}-doped silica 2 μm fiber laser pumped at 792 nm. *Optics Letters, 32*(19), 2780-2782.

Eigler, S., Dotzer, C., & Hirsch, A. (2012). Visualization of defect densities in reduced graphene oxide. *Carbon, 50*(10), 3666-3673.

Elim, H., Ji, W., Yuwono, A., Xue, J., & Wang, J. (2003). Ultrafast optical nonlinearity in poly (methylmethacrylate)-TiO_2 nanocomposites. *Applied Physics Letters, 82*(16), 2691-2693.

Fang, Q., Shi, W., Petersen, E., Kieu, K., Chavez-Pirson, A., & Peyghambarian, N. (2012). Half-mJ All-Fiber-Based Single-Frequency Nanosecond Pulsed Fiber Laser at 2- μm. *IEEE Photonics Technology Letters, 24*(5), 353-355.

Feng, X., Tam, H.Y., & Wai, P. (2006). Stable and uniform multiwavelength erbium-doped fiber laser using nonlinear polarization rotation. *Optics Express, 14*(18), 8205-8210.

Fermann, M. E., & Hartl, I. (2013). Ultrafast fiber lasers. *Nature Photonics, 7*(11), 868-874.

Ferrari, A., Meyer, J., Scardaci, V., Casiraghi, C., Lazzeri, M., Mauri, F., . . . Roth, S. (2006). Raman spectrum of graphene and graphene layers. *Physical Review Letters, 97*(18), 187401.

Ferrari, A. C. (2007). Raman spectroscopy of graphene and graphite: disorder, electron–phonon coupling, doping and nonadiabatic effects. *Solid State Communications, 143*(1), 47-57.

Fried, N. M., Lagoda, G. A., Scott, N. J., Su, L.-M., & Burnett, A. L. (2008). Non contact stimulation of the cavernous nerves in the rat prostate using a tunable-wavelength thulium fiber laser. *Journal of Endourology, 22*(3), 409-414.

Geim, A. K., & Novoselov, K. S. (2007). The rise of graphene. *Nature Materials, 6*(3), 183-191.

Geng, J., Wang, Q., Wang, J., Jiang, S., & Hsu, K. (2011). All-fiber wavelength-swept laser near 2 μm. *Optics Letters, 36*(19), 3771-3773.

Geusic, J., Marcos, H., & Van Uitert, L. (1964). Laser oscillations in Nd-doped yttrium aluminum, yttrium gallium and gadolinium garnets. *Applied Physics Letters, 4*(10), 182-184.

Ghisler, C., Lüthy, W., Weber, H., Morel, J., Woodtli, A., Dändliker, R., . . . Kotrotsios, G. (1994). A Tm^{3+} sensitized Ho^{3+} silica fiber laser at 2.04 μm pumped at 809 nm. *Optics Communications, 109*(3-4), 279-281.

Graf, D., Molitor, F., Ensslin, K., Stampfer, C., Jungen, A., Hierold, C., & Wirtz, L. (2007). Spatially resolved Raman spectroscopy of single-and few-layer graphene. *Nano Letters, 7*(2), 238-242.

Greinacher, E. (1980). History of rare earth applications, rare earth market today: overview. *Industrial Applications of Rare Earth Elements,* (pp 3-17): Essen, Germany: ACS Publication.

Grudinin, A. (2013). Fiber laser directions. *Nature Photonics, 7*(11), 846-847.

Gumenyuk, R., Vartiainen, I., Tuovinen, H., & Okhotnikov, O. G. (2011). Dissipative dispersion-managed soliton 2 μm thulium/holmium fiber laser. *Optics Letters, 36*(5), 609-611.

Halder, A., Paul, M. C., Harun, S. W., Bhadra, S. K., Bysakh, S., Das, S., & Pal, M. (2013). Visible and near infrared up-conversion luminescence in Yb^{3+} / Tm^{3+} co-doped yttria-alumino-silicate glass based optical fibers. *Journal of Luminescence, 143*, 393-401.

Hall, R. N., Fenner, G. E., Kingsley, J., Soltys, T., & Carlson, R. (1962). Coherent light emission from GaAs junctions. *Physical Review Letters, 9*(9), 366.

Hamzah, A., Harun, S., Huri, N., Lokman, A., Arof, H., Paul, M. C., . . . Ahmad, H. (2010). Multi-wavelength fiber laser with erbium doped zirconia fiber and semiconductor optical amplifier. *Optoelectronics and Advanced Materials-Rapid Communications, 4*(10), 1431-1434.

Han, Y.-G., Tran, T. V. A., & Lee, S. B. (2006). Wavelength-spacing tunable multiwavelength erbium-doped fiber laser based on four-wave mixing of dispersion-shifted fiber. *Optics Letters, 31*(6), 697-699.

Hanna, D., Percival, R., Perry, I., Smart, R., Suni, P., & Tropper, A. (1990). An Ytterbium-doped Monomode Fibre Laser: Broadly Tunable Operation from 1.010 μm to 1.162 μm and Three-level Operation at 974 nm. *Journal of Modern Optics, 37*(4), 517-525.

Hanna, D., Percival, R., Perry, I., Smart, R., Townsend, J., & Tropper, A. (1990). Frequency upconversion in Tm- and Yb: Tm-doped silica fibers. *Optics Communications, 78*(2), 187-194.

Hanna, D., Perry, I., Lincoln, J., & Townsend, J. (1990). A 1-Watt thulium-doped cw fibre laser operating at 2 μm. *Optics Communications, 80*(1), 52-56.

Harun, S., Ismail, M., Ahmad, F., Ismail, M., Nor, R., Zulkepely, N., & Ahmad, H. (2012). A Q-switched erbium-doped fiber laser with a carbon nanotube based saturable absorber. *Chinese Physics Letters, 29*(11), 114202.

Harun, S., Saidin, N., Zen, D., Ali, N., Ahmad, H., Ahmad, F., & Dimyati, K. (2013). Self-starting harmonic mode-locked thulium-doped fiber laser with carbon nanotubes saturable absorber. *Chinese Physics Letters, 30*(9), 094204.

Hasan, M. Z., & Kane, C. L. (2010). Colloquium: topological insulators. *Reviews of Modern Physics, 82*(4), 3045.

Hasan, T., Sun, Z., Wang, F., Bonaccorso, F., Tan, P. H., Rozhin, A. G., & Ferrari, A. C. (2009). Nanotube–polymer composites for ultrafast photonics. *Advanced Materials, 21*(38-39), 3874-3899.

He, X., Liu, Z.-B., Wang, D., Yang, M., Liao, C., & Zhao, X. (2012). Passively mode-locked fiber laser based on reduced graphene oxide on microfiber for ultra-wide-band doublet pulse generation. *Journal of Lightwave Technology, 30*(7), 984-989.

Hecht, J. (2010). Short history of laser development. *Optical Engineering, 49*(9), 091002-091023.

Henderson, S. W., Suni, P. J., Hale, C. P., Hannon, S., Magee, J. R., Bruns, D. L., & Yuen, E. H. (1993). Coherent laser radar at 2 μm using solid-state lasers. *IEEE Transactions on Geoscience and Remote Sensing, 31*(31), 34-15.

Herda, R., Kivistö, S., & Okhotnikov, O. G. (2008). Dynamic gain induced pulse shortening in Q-switched lasers. *Optics Letters, 33*(9), 1011-1013.

Hernandez, Y., Nicolosi, V., Lotya, M., Blighe, F. M., Sun, Z., De, S., . . . Gun'Ko, Y. K. (2008). High-yield production of graphene by liquid-phase exfoliation of graphite. *Nature Nanotechnology, 3*(9), 563-568.

Hisyam, M., Rusdi, M., Latiff, A., & Harun, S. (2016) Generation of Mode-locked Ytterbium doped fiber ring laser using few-layer black phosphorus as a saturable absorber. *IEEE Journal of Quantum Electronics, pp*(99), 1-1.

Hjelme, D. R., & Mickelson, A. R. (1992). Theory of timing jitter in actively mode-locked lasers. *IEEE Journal of Quantum Electronics, 28*(6), 1594-1606.

Huang, J., Huang, W., Zhuang, W., Su, K., Chen, Y., & Huang, K. (2009). High-pulse-energy, passively Q-switched Yb-doped fiber laser with AlGaInAs quantum wells as a saturable absorber. *Optics Letters, 34*(15), 2360-2362.

Huang, S.-L., Tsui, T.-Y., Wang, C.-H., & Kao, F.-J. (1999). Timing jitter reduction of a passively Q-switched laser. *Japanese Journal of Applied Physics, 38*(3A), L239.

Huang, Y., & Luo, Z. (2014). *Passively Q-switched linear-cavity erbium-doped fiber laser with few-layer TI: Bi_2Se_3 saturable absorber.* Paper presented at the Fiber-Based Technologies and Applications, (pp. FTh3D-5): Wuhan, China: Optical Society of America.

Huang, Y., Luo, Z., Li, Y., Zhong, M., Xu, B., Che, K., . . . Weng, J. (2014). Widely-tunable, passively Q-switched erbium-doped fiber laser with few-layer MoS_2 saturable absorber. *Optics Express, 22*(21), 25258-25266.

Hüttmann, G., Yao, C., & Endl, E. (2005). New concepts in laser medicine: towards a laser surgery with cellular precision. *Medical Laser Application, 2, 20*(22), 135-139.

Iijima, S. (1991). Helical microtubules of graphitic carbon. *Nature, 354*(6348), 56-58.

Ismail, E., Kadir, N., Latiff, A., Ahmad, H., & Harun, S. (2016). Black phosphorus crystal as a saturable absorber for both a Q-switched and mode-locked erbium-doped fiber laser. *RSC Advances, 6*(76), 72692-72697.

Ismail, M. A., Ahmad, H., & Harun, S. W. (2014). Soliton mode-locked erbium-doped fiber laser using non-conductive graphene oxide paper. *IEEE Journal of Quantum Electronics, 50*(2), 85-87.

Jackson, S., & Li, Y. (2004). High-power broadly tunable Ho^{3+}-doped silica fiber laser. *Electronics Letters, 40*(23), 1.

Jackson, S. D. (2003). Power scaling method for 2-μm diode-cladding-pumped Tm^{3+}-doped silica fiber lasers that uses Yb^{3+} codoping. *Optics Letters, 28*(22), 2192-2194.

Jackson, S. D. (2007). Passively Q-switched Tm^{3+}-doped silica fiber lasers. *Applied Optics, 46*(16), 3311-3317.

Jackson, S. D., & King, T. (1998). High-power diode-cladding-pumped Tm-doped silica fiber laser. *Optics Letters, 23*(18), 1462-1464.

James, C. (1911). Thulium I. 1. *Journal of the American Chemical Society, 33*(8), 1332-1344.

Jander, P., & Brocklesby, W. S. (2004). Spectroscopy of yttria-alumina-silica glass doped with thulium and erbium. *IEEE Journal of Quantum Electronics, 40*(5), 509-512.

Javan, A., Bennett Jr, W. R., & Herriott, D. R. (1961). Population inversion and continuous optical maser oscillation in a gas discharge containing a He-Ne mixture. *Physical Review Letters, 6*(3), 106.

Jeong, Y., Yoo, S., Coderaard, C., Nilsson, J., Sahu, J. K., Payne, D. N., . . . Harker, A. (2007). Erbium: ytterbium codoped large-core fiber laser with 297 W continuous-wave output power. *IEEE Journal of Selected Topics in Quantum Electronics, 13*(3), 573-579.

Jeong, Y. e., Sahu, J., Payne, D., & Nilsson, J. (2004). Ytterbium-doped large-core fiber laser with 1.36 kW continuous-wave output power. *Optics Express, 12*(25), 6088-6092.

Jia, F., Chen, H., Liu, P., Huang, Y., & Luo, Z. (2015). Nanosecond-Pulsed, Dual-Wavelength Passively Q-Switched c-Cut Nd : YVO_4 Laser Using a Few-Layer

Bi_2Se_3 Saturable Absorber. *IEEE Journal of Selected Topics in Quantum Electronics, 21*(1), 369-374.

Jiang, M., Ma, H., Ren, Z., Chen, X., Long, J., Qi, M., . . . Bai, J. (2013). A graphene Q-switched nanosecond Tm-doped fiber laser at 2 μm. *Laser Physics Letters, 10*(5), 055103.

Johnson, L., Geusic, J., & Van Uitert, L. (1965). Coherent oscillations from Tm^{3+}, Ho^{3+}, Yb^{3+} and Er^{3+} ions in yttrium aluminum garnet. *Applied Physics Letters, 7*(5), 127-129.

Johnson, L. F. (1962). Optical maser characteristics of Nd^{3+} in CaF_2. *Journal of Applied Physics, 33*(2), 756-756.

Jusoh, Z., Kasim, N., Munajat, Y., Ahmad, H., Harun, S., Halder, A., . . . Bhadra, S. K. (2014). New octagonal shape double-clad thulium-ytterbium co-doped fiber for generation of multi-wavelength and Q-switched lasers in 2 micron region. *Journal of Optoelectronics and Advanced Materials, 16*(7-8), 776-781.

Kafka, J., Hall, D., & Baer, T. (1989). Mode-locked erbium-doped fiber laser with soliton pulse shaping. *Optics Letters, 14*(22), 1269-1271.

Kao, K., & Hockham, G. A. (1966). *Dielectric-fiber surface waveguides for optical frequencies.* Paper presented at the Proceedings of the Institution of Electrical Engineers, *Vol. 113*(7), (pp. 1151-1158). London, United Kingdom: IET Digital Library.

Keller, U. (2003). Recent developments in compact ultrafast lasers. *Nature, 424*(6950), 831-838.

Keller, U. (2004). Ultrafast solid-state lasers. *Progress in Optics, 46*, 1-115.

Khanikaev, A. B., Mousavi, S. H., Tse, W.-K., Kargarian, M., MacDonald, A. H., & Shvets, G. (2013). Photonic topological insulators. *Nature Materials, 12*(3), 233-239.

Kobtsev, S., Kukarin, S., & Fedotov, Y. (2011). Mode-locked Yb-fiber laser with saturable absorber based on carbon nanotubes. *Laser Physics, 21*(2), 283-286.

Koester, C. J., & Snitzer, E. (1964). Amplification in a fiber laser. *Applied Optics, 3*(10), 1182-1186.

Kurkov, A. (2011). Q-switched all-fiber lasers with saturable absorbers. *Laser Physics Letters, 8*(5), 335.

Kurkov, A., Dvoyrin, V., & Marakulin, A. (2010). All-fiber 10 W holmium lasers pumped at λ= 1.15 μm. *Optics Letters, 35*(4), 490-492.

Kurkov, A. S., Sholokhov, E. M., Tsvetkov, V. B., Marakulin, A. V., Minashina, L., Medvedkov, O. I., & Kosolapov, A. F. (2011). Holmium fibre laser with record quantum efficiency. *Quantum Electronics, 41*(6), 492-494.

Lapointe, M. A., Chatigny, S., Piché, M., Cain-Skaff, M., & Maran, J. N. (2009, February). Thermal effects in high-power CW fiber lasers. In *Proc. SPIE Vol. 7195* (1) , p. 71951U).

Larsen, C., Noordegraaf, D., Hansen, K. P., Mattsson, K. E., & Bang, O. (2012). Photonic crystal fibers for supercontinuum generation pumped by a gain-switched CW fiber laser. *SPIE LASE: International Society for Optics and Photonics*, 82400L-82400L.

Latiff, A., Babar, I., Shamsudin, H., Paul, M., Halder, A., Das, S., . . . Harun, S. (2016). Highly Efficient Cladding Pumped Dual-Wavelength Thulium Ytterbium Co-Doped Fiber Laser. *Acta Physica Polonica, A., 130*(6), 1332-1335.

Layne, C., Lowdermilk, W., & Weber, M. (1975). Nonradiative relaxation of rare-earth ions in silicate laser glass. *IEEE Journal of Quantum Electronics, 11*, 798-799.

Layne, C., Lowdermilk, W., & Weber, M. J. (1977). Multiphonon relaxation of rare-earth ions in oxide glasses. *Physical Review B, 16*(1), 10.

Li, L., Jiang, S., Wang, Y., Wang, X., Duan, L., Mao, D., . . . Si, J. (2015). WS_2/fluorine mica (FM) saturable absorbers for all-normal-dispersion mode-locked fiber laser. *Optics Express, 23*(22), 28698-28706.

Li, Y., Jackson, S. D., & Fleming, S. (2004). High absorption and low splice loss properties of hexagonal double-clad fiber. *Photonics Technology Letters, IEEE, 16*(11), 2502-2504.

Lieth, R., & Terhell, J. (1977). Transition metal dichalcogenides *Preparation and crystal growth of materials with layered structures* (pp. 141-223): New York, USA: Springer Publisher.

Lin, J. H., Lin, K.-H., Hsu, C., Yang, W., & Hsieh, W. F. (2007). Supercontinuum generation in a microstructured optical fiber by picosecond self Q-switched mode-locked Nd : $GdVO_4$ laser. *Laser Physics Letters, 4*(6), 413.

Liu, A., & Ueda, K. (1996). The absorption characteristics of circular, offset, and rectangular double-clad fibers. *Optics Communications, 132*(5), 511-518.

Liu, X., Zhan, L., Luo, S., Gu, Z., Liu, J., Wang, Y., & Shen, Q. (2012). Multiwavelength erbium-doped fiber laser based on a nonlinear amplifying loop mirror assisted by un-pumped EDF. *Optics Express, 20*(7), 7088-7094.

Liu, X., Zhan, L., Luo, S., Wang, Y., & Shen, Q. (2011). Individually switchable and widely tunable multiwavelength erbium-doped fiber laser based on cascaded mismatching long-period fiber gratings. *Journal of Lightwave Technology, 29*(21), 3319-3326.

Loghman-Estarki, M. R., Edris, H., & Razavi, R. S. (2013). Large scale synthesis of non-transformable tetragonal Sc_2O_3, Y_2O_3 doped ZrO_2 nanopowders via the citric acid based gel method to obtain plasma sprayed coating. *Ceramics International, 39*(7), 7817-7829.

Loghman-Estarki, M. R., Nejati, M., Edris, H., Razavi, R. S., Jamali, H., & Pakseresht, A. H. (2015). Evaluation of hot corrosion behavior of plasma sprayed scandia and yttria co-stabilized nanostructured thermal barrier coatings in the presence of molten sulfate and vanadate salt. *Journal of the European Ceramic Society, 35*(2), 693-702.

Loh, K. P., Bao, Q., Eda, G., & Chhowalla, M. (2010). Graphene oxide as a chemically tunable platform for optical applications. *Nature Chemistry, 2*(12), 1015-1024.

Lu, B., Chen, H., Jiang, M., Chen, X., Ren, Z., & Bai, J. (2013). Graphene-based passive Q-switching for a 2 μm thulium-doped fiber laser. *Laser Physics, 23*(4), 045111.

Luo, Z., Liu, C., Huang, Y., Wu, D., Wu, J., Xu, H., . . . Weng, J. (2014). Topological-Insulator Passively Q-Switched Double-Clad Fiber Laser at 2 m Wavelength. *IEEE Journal of Selected Topics in Quantum Electronics, 20*(5), 1-8.

Ma, H., Wang, Y., Zhou, W., Long, J., Shen, D., & Wang, Y. (2013). A passively Q-switched thulium-doped fiber laser with single-walled carbon nanotubes. *Laser Physics, 23*(3), 035109.

Ma, J., Xie, G., Lv, P., Gao, W., Yuan, P., Qian, L., . . . Tang, D. (2012). Graphene mode-locked femtosecond laser at 2 μm wavelength. *Optics Letters, 37*(11), 2085-2087.

Maiman, T. H. (1960). Stimulated optical radiation in ruby. *Nature 187*, 493-494.

Martinez, A., & Sun, Z. (2013). Nanotube and graphene saturable absorbers for fibre lasers. *Nature Photonics, 7*(11), 842-845.

McClung, F., & Hellwarth, R. (1963). Characteristics of giant optical pulsations from ruby. *Proceedings of the IEEE, 51*(1), 46-53.

Mears, R. J., Reekie, L., Jauncey, I., & Payne, D. N. (1987). Low-noise erbium-doped fibre amplifier operating at 1.54 μm. *Electronics Letters, 23*(19), 1026-1028.

Mears, R. J., Reekie, L., Poole, S. B., & Payne, D. N. (1985). Neodymium-doped silica single-mode fibre lasers. *Electronics Letters, 21*(17), 738-740.

Milonni, P. W., & Eberly, J. H. (2010). *Laser Physics (2nd Edition)*. Hoboken, New Jersey, USA: Wiley.

Moulton, P. F. (1986). Spectroscopic and laser characteristics of Ti: Al_2O_3. *Journal of Optical Society of America B, 3*(1), 125-133.

Moulton, P. F., Rines, G., Slobodtchikov, E. V., Wall, K. F., Frith, G., Samson, B., & Carter, A. L. (2009a). Tm-doped fiber lasers: fundamentals and power scaling. *IEEE Journal of Selected Topics in Quantum Electronics, 15*(1), 85-92.

Moulton, P. F., Rines, G. A., Slobodtchikov, E. V., Wall, K. F., Frith, G., Samson, B., & Carter, A. L. (2009b). Tm-doped fiber lasers: fundamentals and power scaling. *IEEE Journal of Selected Topics in Quantum Electronics, 15*(1), 85-92.

Muddu, P. S. (2003). A Study of Image Transmission Through a Fiber-Optic Conduit and its Enhancement Using Digital Image Processing Techniques. (Doctoral dissertation, Florida State College of Engineering).

Muendel, M. H. (1996). *Optimal inner cladding shapes for double-clad fiber lasers*. Paper presented at the Lasers and Electro-Optics, 1996. Summaries of papers presented at the Conference on CLEO' 96.

Myslinski, P., Pan, X., Barnard, C. W., Chrostowski, J., Sullivan, B. T., & Bayon, J.-F. (1993). Q-switched thulium-doped fiber laser. *Optical Engineering, 32*(9), 2025-2030.

Nelson, L., Jones, D., Tamura, K., Haus, H., & Ippen, E. (1997). Ultrashort-pulse fiber ring lasers. *Applied Physics B: Lasers and Optics, 65*(2), 277-294.

Novoselov, K. (2011). Nobel lecture: graphene: materials in the flatland. *Reviews of Modern Physics, 83*(3), 837.

Novoselov, K. S., Geim, A. K., Morozov, S. V., Jiang, D., Zhang, Y., Dubonos, S. V., . . . Firsov, A. A. (2004). Electric field effect in atomically thin carbon films. S*cience, 306*(5696), 666-669.

Obraztsov, A., Obraztsova, E., Tyurnina, A., & Zolotukhin, A. (2007). Chemical vapor deposition of thin graphite films of nanometer thickness. *Carbon, 45*(10), 2017-2021.

Oh, K., Morse, T., Weber, P., Kilian, A., & Reinhart, L. (1994). Continuous-wave oscillation of thulium-sensitized holmium-doped silica fiber laser. *Optics Letters, 19*(4), 278-280.

Pal, A., Dhar, A., Das, S., Chen, S. Y., Sun, T., Sen, R., & Grattan, K. T. (2010). Ytterbium-sensitized Thulium-doped fiber laser in the near-IR with 980 nm pumping. *Optics Express, 18*(5), 5068-5074.

Pan, L., Utkin, I., & Fedosejevs, R. (2007). Passively Q-switched ytterbium-doped double-clad fiber laser with a Cr^{4+} : YAG saturable absorber. *IEEE Photonics Technology Letters, 19*(24), 1979-1981.

Pan, S.-D., Cui, L., Liu, J. Q., Teng, B., Kong, W. J., Liu, J. H., & Ge, X. H. (2016). 2.6 ps pulse from passively mode-locking Nd : $Gd_{0.64}Y_{0.36}VO_4$ laser based on graphene oxide. *Optik-International Journal for Light and Electron Optics, 127*(2), 673-676.

Panasenko, D., Polynkin, P., Polynkin, A., Moloney, J. V., Mansuripur, M., & Peyghambarian, N. (2006). Er-Yb femtosecond ring fiber oscillator with 1.1-W average power and GHz repetition rates. *Photonics Technology Letters, IEEE, 18*(7), 853-855.

Paschotta, R., Häring, R., Gini, E., Melchior, H., Keller, U., Offerhaus, H., & Richardson, D. (1999). Passively Q-switched 0.1 mJ fiber laser system at 1.53 μm. *Optics Letters, 24*(6), 388-390.

Pask, H., Carman, R. J., Hanna, D. C., Tropper, A. C., Mackechnie, C. J., Barber, P. R., & Dawes, J. M. (1995). Ytterbium-doped silica fiber lasers: versatile sources for the 1-1.2 μm region. *IEEE Journal of Selected Topics in Quantum Electronics,, 1*(1), 2-13.

Patel, C. K. N. (1964). Continuous-Wave Laser Action on Vibrational-Rotational Transitions of CO_2. *Physical Review, 136*(5A), A1187.

Pei, S., & Cheng, H.-M. (2012). The reduction of graphene oxide. *Carbon, 50*(9), 3210-3228.

Peng, W., Yan, F., Li, Q., Liu, S., Feng, T., Tan, S., & Feng, S. (2013). 1.94 μm switchable dual-wavelength Tm^{3+} fiber laser employing high-birefringence fiber Bragg grating. *Applied Optics, 52*(19), 4601-4607.

Pérez-Millán, P., Díez, A., Andrés, M., Zalvidea, D., & Duchowicz, R. (2005). Q-switched all-fiber laser based on magnetostriction modulation of a Bragg grating. *Optics Express, 13*(13), 5046-5051.

Peterka, P., Kašík, I., Dhar, A., Dussardier, B., & Blanc, W. (2011). Theoretical modeling of fiber laser at 810 nm based on thulium-doped silica fibers with enhanced $^3H_4$ level lifetime. *Optics Express, 19*(3), 2773-2781.

Petrin, R. R., Jani, M. G., Powell, R. C., & Kokta, M. (1992). Spectral dynamics of laser-pumped Y3Al5O12: Tm, Ho lasers. *Optical Materials, 1*(2), 111-124.

Petroski, H. (1990). To Engineer is Human (1985). *The Pencil: The History of Design and Circumstance*.

Pierce, M., Stu Jackson, P. G., & Dickinsona, B. (2001). Development and application of fibre lasers for medical applications. *Proceedings of SPIE Vol. 4253*, 145.

Po, H., Snitzer, E., Tumminelli, R., Zenteno, L., Hakimi, F., Cho, N., & Haw, T. (1989). *Double clad high brightness Nd fiber laser pumped by GaAlAs phased array.* Paper presented at the Optical Fiber Communication Conference (p. PD7). Optical Society of America.

Poole, S. B., Payne, D. N., Mears, R. J., Fermann, M. E., & Laming, R. (1986). Fabrication and characterization of low-loss optical fibers containing rare-earth ions. *Journal of Lightwave Technology, 4*(7), 870-876.

Ramadurai, K., Cromer, C. L., Lewis, L. A., Hurst, K. E., Dillon, A. C., Mahajan, R. L., & Lehman, J. H. (2008). High-performance carbon nanotube coatings for high-power laser radiometry. *Journal of Applied Physics, 103*(1), 013103.

Reich, S., & Thomsen, C. (2004). Raman spectroscopy of graphite. *Philosophical Transactions of the Royal Society of London A: Mathematical, Physical and Engineering Sciences, 362*(1824), 2271-2288.

Richards, B. D., Tsangb, Y. H., Binksb, D. J., Lousteaua, J., & Jhaa, A. (2008). CW and Q-switched 2.1 μm $Tm^{3+}/Ho^{3+}/Yb^{3+}$-triply-doped tellurite fiber lasers. In *Proc. of SPIE Vol* (Vol. 7111, pp. 711105-1).

Ruan, J., Dong, G., Liu, X., Zhang, Q., Chen, D., & Qiu, J. (2009). Enhanced broadband near-infrared emission and energy transfer in Bi-Tm-codoped germanate glasses for broadband optical amplification. *Optics Letters*, *34*(16), 2486-2488.

Russo, N., Duchowicz, R., Mora, J., Cruz, J., & Andrés, M. (2002). High-efficiency Q-switched erbium fiber laser using a Bragg grating-based modulator. *Optics Communications*, *210*(3), 361-366.

Saidin, N., Zen, D., Hamida, B. A., Khan, S., Ahmad, H., Dimyati, K., & Harun, S. W. (2013). A Q-switched thulium-doped fiber laser with a graphene thin film based saturable absorber. *Laser Physics*, *23*(11), 115102.

Saidin, N., Zen, D. I. M., Ahmad, F., Damanhuri, S. S. A., Ahmad, H., Dimyati, K., & Harun, S. W. (2014). Q-switched thulium-doped fibre laser operating at 1900 nm using multi-layered graphene based saturable absorber. *IET Optoelectronics*, *8*(4), 155-160.

Salavati-Niasari, M., Davar, F., & Bazarganipour, M. (2010). Synthesis, characterization and catalytic oxidation of para-xylene by a manganese (III) Schiff base complex on functionalized multi-wall carbon nanotubes (MWNTs). *Dalton Transactions*, *39*(31), 7330-7337.

Savage, G. (1993). Applications of Carbon-carbon composites. In *Carbon-Carbon Composites* (pp. 323-359). Springer Netherlands.

Schmidt, O., Rothhardt, J., Röser, F., Linke, S., Schreiber, T., Rademaker, K., . . . Salin, F. (2007). Millijoule pulse energy Q-switched short-length fiber laser. *Optics Letters*, *32*(11), 1551-1553.

Scholle, K., Lamrini, S., Koopmann, P., & Fuhrberg, P. (2010). 2 µm laser sources and their possible applications. In *Frontiers in Guided Wave Optics and Optoelectronics*. InTech Publisher.

Shamsudin, H., Latiff, A., Razak, N., Jusoh, Z., Ahmad, H., & Harun, S. (2016). Performance comparison of single-mode single-cladding thulium doped and thulium/holmium co-doped fiber lasers in ring cavity. *Journal of Optoelectronics and Advanced Materials*, *18*(9-10), 757-762.

Sholokhov, E., Marakulin, A., Kurkov, A., & Tsvetkov, V. (2011). All-fiber Q-switched holmium laser. *Laser Physics Letters*, *8*(5), 382-385.

Simakov, N., Hemming, A., Bennetts, S., & Haub, J. (2011). Efficient, polarised, gain-switched operation of a Tm-doped fibre laser. *Optics Express, 19(16)*, 14949-14954.

Slobodtchikov, E., Moulton, P. F., & Frith, G. (2007, January). Efficient, high-power, Tm-doped silica fiber laser. In *Advanced Solid-State Photonics* (p. MF2). Optical Society of America.

Snitzer, E., Po, H., Hakimi, F., Tumminelli, R., & McCollum, B. C. (1988, January). Double clad, offset core Nd fiber laser. In *Optical Fiber Sensors* (p. PD5). Optical Society of America.

Sobon, G., Sotor, J., Pasternak, I., Krajewska, A., Strupinski, W., & Abramski, K. M. (2013). Thulium-doped all-fiber laser mode-locked by CVD-graphene/PMMA saturable absorber. *Optics Express, 21*(10), 12797-12802.

Solodyankin, M. A., Obraztsova, E. D., Lobach, A. S., Chernov, A. I., Tausenev, A. V., Konov, V. I., & Dianov, E. M. (2008). Mode-locked 1.93 μm thulium fiber laser with a carbon nanotube absorber. *Optics Letters*, 33(12), 1336-1338.

Sorokin, P., & Lankard, J. (1966). Stimulated emission observed from an organic dye, chloro-aluminum phthalocyanine. *IBM Journal of Research and Development, 10*(2), 162-163.

Sotor, J., Sobon, G., & Abramski, K. M. (2012). Scalar soliton generation in all-polarization-maintaining, graphene mode-locked fiber laser. *Optics Letters, 37*(11), 2166-2168.

Sotor, J., Sobon, G., Macherzynski, W., & Abramski, K. (2014). Harmonically mode-locked Er-doped fiber laser based on a Sb_2Te_3 topological insulator saturable absorber. *Laser Physics Letters, 11*(5), 055102.

Sotor, J., Sobon, G., Macherzynski, W., Paletko, P., & Abramski, K. M. (2015). Black phosphorus saturable absorber for ultrashort pulse generation. *Applied Physics Letters, 107*(5), 051108.

Spühler, G., Paschotta, R., Fluck, R., Braun, B., Moser, M., Zhang, G., . . . Keller, U. (1999). Experimentally confirmed design guidelines for passively Q-switched microchip lasers using semiconductor saturable absorbers. *Journal of Optical Society of America B, 16*(3), 376-388.

Stankovich, S., Dikin, D. A., Piner, R. D., Kohlhaas, K. A., Kleinhammes, A., Jia, Y., . . . Ruoff, R. S. (2007). Synthesis of graphene-based nanosheets via chemical reduction of exfoliated graphite oxide. *Carbon, 45*(7), 1558-1565.

Stiles, E. (2009). New developments in IPG fiber laser technology. In *Proceedings of the 5th International Workshop on Fiber Lasers* (Vol. 2).

Su, C. Y., Xu, Y., Zhang, W., Zhao, J., Tang, X., Tsai, C. H., & Li, L. J. (2009). Electrical and spectroscopic characterizations of ultra-large reduced graphene oxide monolayers. *Chemistry of Materials, 21*(23), 5674-5680.

Sun, G., Moon, D. S., Lin, A., Han, W. T., & Chung, Y. (2008). Tunable multiwavelength fiber laser using a comb filter based on erbium-ytterbium co-doped polarization maintaining fiber loop mirror. *Optics Express, 16*(6), 3652-3658.

Sun, Z., Hasan, T., & Ferrari, A. (2012). Ultrafast lasers mode-locked by nanotubes and graphene. *Physica E: Low-Dimensional Systems and Nanostructures, 44*(6), 1082-1091.

Sun, Z., Hasan, T., Torrisi, F., Popa, D., Privitera, G., Wang, F., . . . Ferrari, A. C. (2010). Graphene Mode-Locked Ultrafast Laser. *ACS Nano, 4*(2), 803-810.

Sun, Z., Popa, D., Hasan, T., Torrisi, F., Wang, F., Kelleher, E. J., . . . Ferrari, A. C. (2010). A stable, wideband tunable, near transform-limited, graphene-mode-locked, ultrafast laser. *Nano Research, 3*(9), 653-660.

Svelto, O., & Hanna, D. C. (1998). *Principles of Lasers* (Vol. 4). New York, USA : Plenum Press.

Taher, M., Gebavi, H., Taccheo, S., Milanese, D., & Balda, R. (2011). Novel approach towards cross-relaxation energy transfer calculation applied on highly thulium doped tellurite glasses. *Optics Express, 19*(27), 26269-26274.

Taher, M., Gebavi, H., Taccheo, S., Milanese, D., & Balda, R. (2012). Novel calculation for cross-relaxation energy transfer parameter applied on thulium highly-doped tellurite glasses. In *Proc. SPIE* (*Vol. 8257*, p. 825707).

Tang, Y., Yu, X., Li, X., Yan, Z., & Wang, Q. J. (2014). High-power thulium fiber laser Q switched with single-layer graphene. *Optics Letters, 39*(3), 614-617.

Tao, M., Huang, Q., Yu, T., Yang, P., Chen, W., & Ye, X. (2013). A highly efficient 57? pm Tm-doped fiber laser with two multimode fiber Bragg gratings. *Laser Physics, 23*(7), 075111.

Tiu, Z. C., Ahmad, F., Tan, S. J., Ahmad, H., & Harun, S. W. (2014). Passive Q-switched Erbium-doped fiber laser with graphene–polyethylene oxide saturable absorber in three different gain media. *Indian Journal of Physics*, 88(87), 727-731.

Tiu, Z. C., Tan, S. J., Ahmad, H., & Harun, S. W. (2014). Dark pulse emission in nonlinear polarization rotation-based multiwavelength mode-locked erbium-doped fiber laser. *Chinese Optics Letters, 12*(11), 113202.

Tiu, Z. C., Tan, S. J., Zarei, A., Ahmad, H., & Harun, S. W. (2014). Nonlinear Polarization Rotation-Based Mode-Locked Erbium-Doped Fiber Laser with Three Switchable Operation States. *Chinese Physics Letters*, 31(39), 094206.

Tropper, A., Smart, R., Perry, I., Hanna, D., Lincoln, J., & Brocklesby, B. (1990). Thulium-doped silica fiber lasers. *SPIE Fibre Laser Sources and Amplifiers, 1373*, 152-157.

Tsai, T.-Y., & Birnbaum, M. (2000). Co^{2+} : ZnS and Co^{2+} : ZnSe saturable absorber Q switches. *Journal of Applied Physics, 87*(1), 25-29.

Tsai, T. Y., Fang, Y. C., & Hung, S. H. (2010). Passively Q-switched erbium all-fiber lasers by use of thulium-doped saturable-absorber fibers. *Optics Express, 18*(10), 10049-10054.

Wagner, D. J. (1999). New York, U.S.A: Rensselaer Polytechnic Institute.

Walsh, B., & Barnes, N. (2004). Comparison of Tm: ZBLAN and Tm: silica fiber lasers; spectroscopy and tunable pulsed laser operation around 1.9 μm. *Applied Physics B, 78*(3-4), 325-333.

Walsh, B. M. (2009). Review of Tm and Ho materials; spectroscopy and lasers. *Laser Physics, 19*(4), 855-866.

Wang, F., Torrisi, F., Jiang, Z., Popa, D., Hasan, T., Sun, Z., . . . Ferrari, A. C. (2012). Graphene passively Q-switched two-micron fiber lasers. *Paper presented at the Lasers and Electro-Optics (CLEO)*, (pp. JW2A-72), Conference on Science and Innovation: Optical Society of America.

Wang, H. Y., Xu, W. C., Luo, A. P., Dong, J.-L., Cao, W. J., & Wang, L. Y. (2012). Controllable dissipative soliton and Q-switched pulse emission in a normal dispersion fiber laser using SESAM and cavity loss tuning mechanism. *Optics Communications, 285*(7), 1905-1907.

Wang, M., Chen, C., Huang, C., & Chen, H. (2014). Passively Q-switched Er-doped fiber laser using a semiconductor saturable absorber mirror. *Optik-International Journal for Light and Electron Optics, 125*(9), 2154-2156.

Wang, Q., Teng, H., Zou, Y., Zhang, Z., Li, D., Wang, R., . . . Wei, Z. (2012). Graphene on SiC as a Q-switcher for a 2 μm laser. *Optics Letters, 37*(3), 395-397.

Wang, Q. H., Kalantar-Zadeh, K., Kis, A., Coleman, J. N., & Strano, M. S. (2012). Electronics and optoelectronics of two-dimensional transition metal dichalcogenides. *Nature Nanotechnology, 7*(11), 699-712.

Wang, Y., Qu, Z., Liu, J., & Tsang, Y. H. (2012). Graphene Oxide Absorbers for Watt-Level High-Power Passive Mode-Locked Nd: GdVO Laser Operating at 1 m. *Journal of Lightwave Technology, 30*(20), 3259-3262.

Wang, Y., Xu, C. Q., & Po, H. (2004). Thermal effects in kilowatt fiber lasers. *Photonics Technology Letters, IEEE, 16*(1), 63-65.

Wang, Z., Zhu, S.-E., Chen, Y., Wu, M., Zhao, C., Zhang, H., . . . Wen, S. (2013). Multilayer graphene for Q-switched mode-locking operation in an erbium-doped fiber laser. *Optics Communications, 300*, 17-21.

Wikipedia. (2016, July). *Wikipedia*. Retrieved from https://en.wikipedia.org/wiki/Optical_fiber#cite_note-Bhat-17

Wilson, J., & Yoffe, A. (1969). The transition metal dichalcogenides discussion and interpretation of the observed optical, electrical and structural properties. *Advances in Physics, 18*(73), 193-335.

Wu, J., Jiang, S., Qua, T., Kuwata-Gonokami, M., & Peyghambarian, N. (2005). 2 μm lasing from highly thulium doped tellurite glass microsphere. *Applied Physics Letters, 87*, 211118.

Wu, J., Yao, Z., Zong, J., & Jiang, S. (2007). Highly efficient high-power thulium-doped germanate glass fiber laser. *Optics Letters, 32*(6), 638-640.

Wu, K. S., Ottaway, D., Munch, J., Lancaster, D. G., Bennetts, S., & Jackson, S. D. (2009). Gain-switched holmium-doped fibre laser. *Optics Express, 17*(23), 20872-20877.

Xu, J., Liu, J., Wu, S., Yang, Q.-H., & Wang, P. (2012). Graphene oxide mode-locked femtosecond erbium-doped fiber lasers. *Optics Express, 20*(14), 15474-15480.

Xu, J., Wu, S., Li, H., Liu, J., Sun, R., Tan, F., . . . Wang, P. (2012). Dissipative soliton generation from a graphene oxide mode-locked Er-doped fiber laser. *Optics Express, 20*(21), 23653-23658.

Yamashita, S., & Hotate, K. (1996). Multiwavelength erbium-doped fibre laser using intracavity etalon and cooled by liquid nitrogen. *Electronics Letters, 32*(14), 1298-1299.

Yang, L. M., Walton, D., Nees, J., & Weber, W. (1996). Compact, high power, modelocked upconversion laser using a thulium-doped ZBLAN fiber. *Electronics Letters, 32*(7), 658-659.

Yu, H., Zhang, L., Wang, Y., Yan, S., Sun, W., Li, J., . . . Lin, X. (2013). Sub-100 ns solid-state laser Q-switched with double wall carbon nanotubes. *Optics Communications, 306*, 128-130.

Zayhowski, J., & Dill, C. (1994). Diode-pumped passively Q-switched picosecond microchip lasers. *Optics Letters, 19*(18), 1427-1429.

Zayhowski, J., & Dill, C. (1995). Coupled-cavity electro-optically Q-switched Nd: YVO_4 microchip lasers. *Optics Letters, 20*(7), 716-718.

Zayhowski, J. J., & Kelley, P. L. (1991). Optimization of Q-switched lasers. *IEEE Journal of Quantum Electronics, 27*(9), 2220-2225.

Zen, D., Saidin, N., Damanhuri, S., Harun, S., Ahmad, H., Ismail, M., . . . Das, S. (2013). Mode-locked thulium-bismuth co-doped fiber laser using graphene saturable absorber in ring cavity. *Applied Optics, 52*(6), 1226-1229.

Zhang, H., Lu, S., Zheng, J., Du, J., Wen, S., Tang, D., & Loh, K. (2014). Molybdenum disulfide (MoS_2) as a broadband saturable absorber for ultra-fast photonics. *Optics express, 22*(6), 7249-7260.

Zhang, L., Wang, Y., Yu, H., Sun, L., Hou, W., Lin, X., & Li, J. (2011). Passive mode-locked Nd : YVO_4 laser using a multi-walled carbon nanotube saturable absorber. *Laser Physics, 21*(8), 1382-1386.

Zhang, M., Howe, R. C., Woodward, R. I., Kelleher, E. J., Torrisi, F., Hu, G., . . . Hasan, T. (2015). Solution processed MoS_2-PVA composite for sub-bandgap mode-locking of a wideband tunable ultrafast Er : fiber laser. *Nano Research, 8*(5), 1522-1534.

Zhang, X., Hong, P., Bass, M., & Chai, B. (1995). Blue upconversion with excitation into Tm ions at 780 nm in Yb-and Tm-codoped fluoride crystals. *Physical Review B, 51*(14), 9298.

Zhang, Z., Boyland, A., Sahu, J., Clarkson, W., & Ibsen, M. (2011a). High-power single-frequency thulium-doped fiber DBR laser at 1943 nm. *IEEE Photonics Technology Letters*, *23*(7), 417-419.

Zhang, Z., Boyland, A., Sahu, J., Clarkson, W., & Ibsen, M. (2011b). High-power single-frequency thulium-doped fiber DBR laser at 1943 nm. *Photonics Technology Letters, IEEE*, *23*(7), 417-419.

Zhang, Z., Zhan, L., Xu, K., Wu, J., Xia, Y., & Lin, J. (2008). Multiwavelength fiber laser with fine adjustment, based on nonlinear polarization rotation and birefringence fiber filter. *Optics Letters*, *33*(4), 324-326.

Zheng, W., Ruan, S., Zhang, M., Liu, W., Zhang, Y., & Yang, X. (2013). Switchable multi-wavelength erbium-doped photonic crystal fiber laser based on nonlinear polarization rotation. *Optics & Laser Technology, 50*, 145-149.

Zhou, B., Lin, H., Chen, B., & Pun, E. Y. B. (2011). Superbroadband near-infrared emission in Tm-Bi codoped sodium-germanium-gallate glasses. *Optics Express, 19*(7), 6514-6523.

Zyskind, J., Mizrahi, V., DiGiovanni, D., & Sulhoff, J. (1992). Short single frequency erbium-doped fiber laser. *Electronics Letters, 28*(15), 1385-1387.

LIST OF PUBLICATIONS

Journal Publications

1. M.T. Ahmad, A.A. Latiff, **H. Shamsudin**, Z. Zakaria, H. Ahmad & S.W. Harun (2015). Wavelength-tunable thulium-doped fiber laser based on fiber Bragg grating stretching. *Journal of Optoelectronics and Advanced Materials-Rapid Communication*, Vol. 9, No. 5-6, p. 623 – 625.

2. A.A. Latiff, **H. Shamsudin**, H. Ahmad & S.W. Harun (2015). Q-switched thulium-doped fiber laser operating at 1940 nm region using pencil-core as saturable absorber. *Journal of Modern Optics*, vol.49, no.1, pp.1-10.

3. S.W. Harun, **H. Shamsudin**, H. Ahmad, A. Halder, M.C. Paul, M.Pal & S.K.Bhadra (2015). Development of CW and Pulsed Thulium-Ytterbium Fiber Laser Using Nano-Engineered Yttria-alumina-silica as gain medium in conjunction with cladding pumping technique. *Journal of Current Nanoscience, 30*(3), pp 1-10.

4. **H. Shamsudin**, A.A. Latiff, H. Ahmad & S.W. Harun (2016). Multi-wavelength Thulium-doped fiber laser operating at slope efficiency of 16.57% in linear cavity configuration. *Journal of Optoelectronics and Advance Material-Rapid Communication.*

5. A.A. Latiff, **H. Shamsudin**, N.S. Aziz, A.M. Hashim, N. Irawati, H. Ahmad & S. W. Harun (2016). Mode-Locked Generation in Thulium-doped Fiber Linear Cavity Lasers. *Optic-International Journal for Light and Electron Optics*, 127 (2016), pp 11119-11123.

6. A.A. Latiff, **H. Shamsudin**, Z.C. Tiu, H. Ahmad & S.W. Harun (2016). Switchable soliton mode-locked and multiwavelength operation in thulium-doped all-fiber ring laser. *Journal of Nonlinear Optical Physics & Materials*, 25(03) 1650034.

7. M.F.M.Rusdi, A.A. Latiff, M.B.M. Mahyudin, E. Hanafi, **H. Shamsudin**, K. Dimyati, & S.W. Harun (2016). Molydenum disulphide tape saturable absorber for mode-locked double clad ytterbium-doped all-fiber laser generation. *Chinese Physics Letter*, 33(11): 114201.

8. A.A. Latiff, N.A. Kadir, E.I. Ismail, **H. Shamsuddin,** H. Ahmad & S.W. Harun (2017). All-fiber dual-wavelength Q-switched and mode-locked EDFL by SMF-THDF-SMF structure as saturable absorber. *Optics Communications*, 389: pp 29–34.

9. A.A. Latiff, I.M. Babar, **H. Shamsudin**, H. Ahmad & S.W. Harun (2016). Highly Efficient Cladding-Pumped Dual-Wavelength Thulium-Ytterbium-Doped Fiber Laser.*Chinese Physics Letter*, Vol. 130: pp 1332-1335.

10. **H. Shamsudin**, A.A. Latiff, N.N.Razak, Z.Jusoh, H.Ahmad & S.W.Harun (2016) Performance comparison single-mode single-cladding thulium doped fiber and thulium/holmium co-doped fiber lasers in ring cavity. *Journal of Optoelectronics and Advanced Materials*, Vol.18, no.(9-10): pp 757-762.

Papers Presented at Conferences

1. A.A. Latiff, **H. Shamsudin**, Z.C. Tiu, S.W. Harun & H. Ahmad (2015). *Generation of coherent vector soliton mode-locked thulium-doped fiber ring laser.* Paper presented at 10th. International Symposium on Modern Optics and Its Applications, Bandung, Indonesia.

2. **H. Shamsudin**, A.A. Latiff, N.N. Razak, H. Ahmad & S.W. Harun (2015). *Ceneration of Passive Mode-Locked Thulium-doped fiber Laser Using Graphene Oxide paper-based Saturable Absorber.* Paper presented at 3rd. Malaysia Graphene and Carbon Nanotube Workshop 2015 (MGCW2015), Universiti Teknologi Malaysia, Kuala Lumpur, Malaysia.

APPENDIX

A selection of published papers in journal of ISI Web of Science as per requirement by the University of Malaya, Kuala Lumpur, Malaysia.

Development of CW and Pulsed Thulium Ytterbium Co-doped Fiber Lasers Using Nano-engineered Yttria-alimina-silica Based Gain Medium in Conjunction with Cladding Pumping Technique

Current Nanoscience, **12**(3): 299-308.

Author(s): S.W. Harun, **H. Shamsudin**, H. Ahmad, A. Halder, M.C. Paul, M. Pal and SK Bhadra.

Affiliation: Department of Electrical Engineering, Faculty of Engineering, University of Malaya, 50603 Kuala Lumpur, Malaysia., Fiber Optics and Photonics Division, Central Glass & Ceramic Research Institute, CSIR, Kolkata, India.

Abstract

Background: Pulsed fiber lasers operating near 1900 nm are becoming emerging laser sources for scientific and industrial applications, because of their unique advantages in terms of eye-safe wavelength, and high absorption in greenhouse gases, liquid water, and most polycarbonate materials. We develop new nanoengineering double-clad Thulium-Ytterbium co-doped fiber (TYDF) to provide an efficient lasing at 1950 nm region based on energy transfer from Ytterbium to Thulium ion. The performance of the TYDF is investigated for both continuous wave (CW) and pulse laser operations.

Methods: The TYDF is fabricated using a Modified Chemical Vapor Deposition (MCVD) process in conjunction with solution doping technique. The lasing characteristic of the TYDF laser (TYDFL) is investigated for both linear and ring configurations. The pulse generations are demonstrated using various passive saturable absorbers (SAs) such multiwalled carbon nanotubes (MWCNTs) and graphene oxide.

Results: With a linear configuration, the TYDFL operates at center wavelength of 1936.4 nm, 1958.6 nm and 1967.5 nm at gain medium lengths of 5 m, 10 m and 15 m, respectively. The proposed laser produces the highest efficiency of 9 .9 % at 10 m long TYDF and the lowest threshold pump power of 400 mW at a longer TYDF length of 15 m. The Q-switched laser operates at 1960 nm region is achieved by exploiting a MWCNTs embedded in polymer composite film as a SA. The proposed TYDFL generates a stable pulse train with repetition rates and pulse widths ranging from 18.9 to 35.1 kHz and 7.94 to 1.52 µs, respectively by varying the multimode 980 nm pump power from 440 mW to 528 mW. The maximum pulse energy of 11.2 nJ is obtained at the pump power of 512 mW. A higher performance Q switching is expected to be achieved with the optimization of the laser cavity and SA. A mode-locked TYDFL is also demonstrated using a graphene oxide (GO) based SA. The laser operates at 1942.0 nm with a threshold pump power as low as 1.8 W, a repetition rate of 22.32 MHz and calculated pulse duration of 1.1 ns.

Conclusion: The developed TYDF is capable for use in developing both CW and pulsed fiber laser in conjunction with cladding pumping technique.

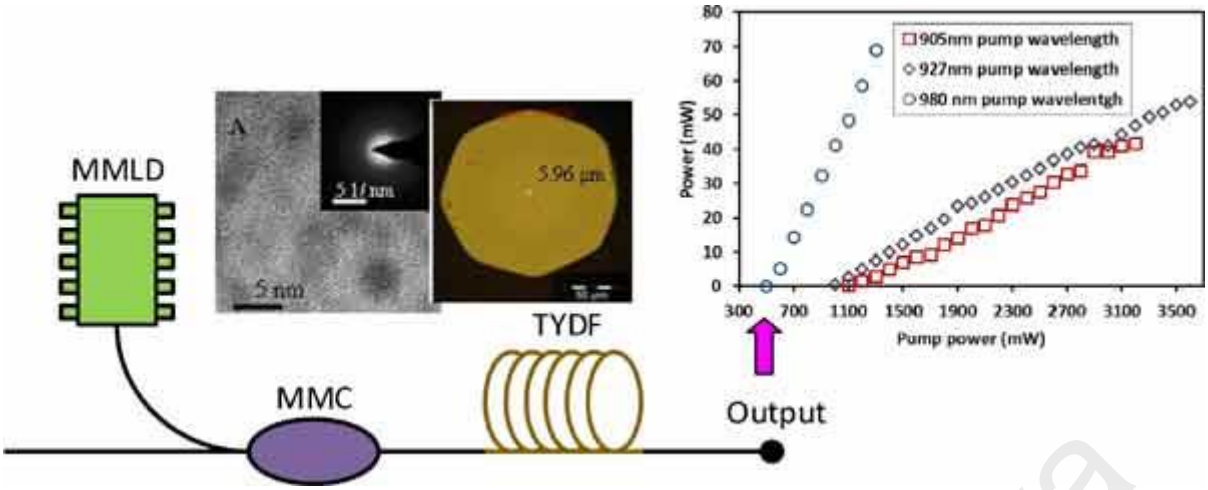

Keywords:

Graphene oxide, mode-locking, multi-walled carbon nanotubes, Q-switching, thulium ytterbium co-doped fiber.